Development and application of intestinal *in vitro* models to investigate the link between plastic particle toxicity, intestinal inflammation, and the NLRP3 inflammasome

Inaugural-Dissertation

zur Erlangung des Doktorgrades
der Mathematisch-Naturwissenschaftlichen Fakultät
der Heinrich-Heine-Universität Düsseldorf

vorgelegt von
Mathias Busch
aus Willich

Düsseldorf, März 2022

Aus dem IUF – Leibniz-Institut für umweltmedizinische Forschung

Gedruckt mit der Genehmigung der
Mathematisch-Naturwissenschaftlichen Fakultät der
Heinrich-Heine-Universität Düsseldorf

Berichterstatter:

1. Univ.-Prof. Dr. Jean Krutmann - IUF, Leibniz-Institut für Umweltmedizinische Forschung
2. Prof. Dr. Cornelia Monzel – Heinrich-Heine-Universität Düsseldorf

Tag der mündlichen Prüfung: 28.06.2022

Table of Contents

Danksagung

Mein besonderer Dank gilt meinem Doktorvater Univ.-Prof. Dr. Jean Krutmann für die Begutachtung meiner Dissertation, die Betreuung meiner Arbeit, sowie die Unterstützung bei der Aquirierung der Förderung für mein Promotionsprojekt. Weiterhin danke ich meiner Mentorin und Zweitgutachterin Prof. Dr. Cornelia Monzel für die Unterstützung während meiner Promotion und für die Begutachtung dieser Arbeit.

Darüberhinaus danke ich Dr. Roel Schins für die wertvolle Betreuung während meiner Promotion. Von der Unterstützung bei Förderungsanträgen, über fachliche Diskussionen, bis hin zur erfolgreichen Publikation meiner Ergebnisse, all dies wäre ohne die unersetzbare Unterstützung nicht gelungen.

Als nächstes möchte ich Dr. Catrin Albrecht und Dr. Angela Kämpfer für die großartige Unterstützung in der Anfangszeit meiner Promotion danken. Viele wichtige Diskussionen, Ratschläge und Hinweise haben einen wichtigen Beitrag zu meiner wissenschaftlichen Entwicklung geleistet.

Außerdem danken möchte Dr. Tina Wahle und Gerrit Bredeck für die enge Zusammenarbeit und hilfreiche Unterstützung bei wesentlichen Teilen meiner Arbeit.

Ebenfalls danken möchte ich den aktuellen und ehemaligen Mitgliedern der Arbeitsgruppe Schins „Partikel, Entzündung, Genomintegrität“: Adriana Sofranko, Gabriele Wick, Ion Tacu, Isabelle Masson, Lora Gerber, Giulia diLauro, Veronika Büttner, Andrea Boltendahl, Dr. Eleonora Scarcello und Janine Becht. Vielen Dank für die positive Arbeitsatmosphäre und die gegenseitige Unterstützung. Es war ein Vergnügen, sowohl das Labor als auch die Mittagspause mit euch zu teilen.

Weiterhin danke ich allen Co-Autoren und Kooperationspartnern für ihre Mitarbeit und Unterstützung meines Promotionsprojekts.

Zu guter Letzt danke ich meiner Frau Irina, sowie meinen Eltern Elmar und Birgit Busch für die seelische und finanzielle Unterstützung während meiner gesamten akademischen Ausbildung.

Abbreviations

°C	Degree Celsius
µg	Microgram
µl	Microliter
µm	Micrometer
µM	Micromolar
AB	Alcian Blue
Ag	Silver
$AgNO_3$	Silver nitrate
ANOVA	Analysis of variance
ASC	Apoptosis-associated speck-like protein
ATP	Adenosine triphosphate
BfR	Bundesinstitut für Risikobewertung
BMDM	Bone marrow-derived macrophages
BSA	Bovine serum albumin
C	Carbon
CASP1	Caspase-1
CD	Crohns disease
cm	Centimeter
cm^2	Square centimeter
cm^3	Cubic centimeter
CRISPR	Clustered regularly interspaced short palindromic repeats
Cu	Copper
CuO	Copper oxide
DAMP	Danger-associated molecular pattern
dH_2O	Deionized water
DLS	Dynamic light scattering
DMEM	Dulbecco's modified eagle medium
DMSO	Dimethyl sulfoxide
DNA	Desoxyribonucleic acid
DQ12	Dörentruper Quartz 12
DSS	Dextran sodium sulfate
EDTA	Ethylenediaminetetraacetic acid
EFSA	European food safety agency
ELISA	Enzyme-linked immunosorbent assay
ENM	Engineered nanomaterial
FACS	Fluorescence-activated cell sorting
FCS	Fetal calf serum
FT-IR	Fourier-transform-infrared
g	Gram
GALT	Gut-associated lymphoid tissue
GFP	Green fluorescent protein
GI	Gastrointestinal
GIT	Gastrointestinal tract
gRNA	Guide ribonucleic acid
GSDMD	Gasdermin D
H	Hydrogen
h	Hour
H_2SO_4	Sulfuric acid
HBSS	Hanks' balanced salt solution
HCl	Hydrochloric acid
HRMA	High resolution melt analysis
IATA	Integrated approach to testing and assessment
IBD	Inflammatory bowel disease
IFN	Interferon
IL	Interleukin
INT	Iodonitrotetrazolium chloride
ISDD	*In vitro* sedimentation, diffusion and dosimetry model
ITS	Integrative testing strategy
IUPAC	International union of pure and applied chemistry
K	Potassium
kHz	Kilohertz
kPa	Kilopascal
LANUV	Landesamt für Natur, Umwelt und Verbraucherschutz
LDH	Lactate dehydrogenase
LPS	Lipopolysaccharide
LRR	Leucine-rich repeat
M	Molar
mA	Milliampere
M-cells	Microfold-cells
ME	Mercaptoethanol
MEM	Minimum essential medium
MET-1	Microbial ecosystem therapeutic-1
mg	Milligram

min	Minutes
mJ	Millijoule
ml	Milliliter
mm	Millimeter
mM	Millimolar
MMS	Methyl methanesulfonate
MNP	Micro- and nanoplastics
MUC	Mucin
MWCNT	Multi-walled carbon nanotubes
NaCl	Sodium chloride
NAD	Nicotinamide adenine dinucleotide
$NaHCO_3$	Sodium bicarbonate
NaOH	Sodium hydroxide
NEAA	Non-essential amino acid
NF-κB	Nuclear factor kappa B
ng	Nanogram
NLRP3	NOD-, LRR- and pyrin domain-containing protein 3
nm	Nanometer
nM	Nanomolar
NM	Nanomaterial
NOD	Nucleotide-binding oligomerization domain
NP	Nanoparticle
ns	Nanosecond
NSAID	Non-steroidal antiinflammatory drug
O	Oxygen
P/S	Penicillin/Streptomycin
PA	Polyamide
Pa	Pascal
PA6	Polyamide 6
PAMP	Pathogen-associated molecular pattern
PAN	Polyacrylonitrile
PAS	Periodic acid-Schiff
PBMC	Peripheral blood mononuclear cell
PBS	Phosphate buffered saline
PCR	Polymerase chain reaction
PDI	Polysdispersity index
PE	Polyethylene
PES	Polyester
PET	Polyethylene terephthalate
PFA	Para-formaldehyde
pg	Picogram
pH	Potentia hydrogenii
pM	Picomolar
PMA	Phorbol-12-myristat-13-acetat
PMS	Phenazine methosulfate
PP	Polypropylene
PRR	Pattern recognition receptor
PS	Polystyrene
$PS\text{-}NH_2$	Amine-modified polystyrene
PTFE	Polytetrafluoroethylene
PVC	Polyvinyl chloride
PYD	Pyrin domain
QD	Quantum dot
qPCR	Quantitative polymerase chain reaction
qRT-PCR	Quantitative reverse transcription polymerase chain reaction
QSAR	Quantitative structure-activity relationship
R&D	Research & Development
RNA	Ribonucleic acid
ROS	Reactive oxygen species
RPMI	Roswell park memorial institute
s	Second
SD	Standard deviation
SEM	Scanning electron microscopy
SEM	Standard error of the mean
SiO_2	Silicon dioxide
SOP	Standard operating procedure
TEER	Transepithelial electrical resistance
TEM	Transmission electron microscopy
TiO_2	Titanium dioxide
TJ	Tight junction
TLR4	Toll-like receptor 4
TNF	Tumor necrosis factor
UC	Ulcerative colitis
UV	Ultraviolet
V	Volt
W	Watt
WST-1	Water-soluble tetrazolium 1

WT	Wildtype
ZnO	Zinc oxide
ZO-1	Zonula occludens 1
Ω	Ohm

Summary

The global environmental pollution with plastic waste has led to the contamination of entire ecosystems with plastic particles in micro- and nanometer range. As a consequence, drinking water and food has been shown to contain micro- and nanoplastics, leading to oral exposure in the human population.

The gastrointestinal tract (GIT) represents the first organ to come into contact with ingested plastic particles and could be a main target organ for particle-induced toxicity. Based on animal studies and *in vitro* experiments, the induction of pro-inflammatory reactions has been identified as one of the main adverse effects of micro- and nanoplastic particles in the GIT. As the NOD-, LRR- and pyrin domain-containing protein 3 (NLRP3) inflammasome has been shown to be involved in pro-inflammatory reactions after exposure to nanoparticles and fibers, it might also play a role plastic particle-mediated toxicity. Furthermore, NLRP3 is implicated in the pathogenesis of inflammatory bowel disease (IBD). This could imply a particular hazard coming from micro- and nanoplastics towards IBD-patients.

To investigate the link between plastic particle toxicity, intestinal inflammation and the NLRP3 inflammasome, advanced *in vitro* models of the healthy and inflamed intestine were developed, validated and applied to micro- and nanoplastic particles.

As a first step of this work, currently available *in vitro* models of the human intestine were described and strategies of varying complexity to study the intestinal effects of particles were reviewed. Based on the research questions of this thesis, an advanced triple culture model of the healthy and inflamed intestine (Caco-2/HT29-MTX-E12/THP-1) was chosen for the experimental work. In the first experimental study, it was observed that treatment with polyvinyl chloride particles caused increased levels of the pro-inflammatory cytokine IL-1β and a reduced number of epithelial cells in the inflamed model, but not the healthy one. These observations suggest a crucial role of the inflammation status during plastic particle-induced toxicity. In the second study, the triple culture model was spatially inverted in order to allow toxicological testing of buoyant plastic particles like polyethylene. Treatment with polyethylene particles induced cytotoxic effects as well as pro-inflammatory reactions in both healthy and inflamed state. A third study aimed at screening a large panel of different micro- and nanoplastics for NLRP3 activation in the macrophage-like cell line THP-1. It was found that, except for amine-modified polystyrene, none of the tested materials acted as a direct NLRP3 activator. However, polyethylene terephthalate particles induced an NLRP3-independent pro-inflammatory reaction. In the last study, the role of the NLRP3 inflammasome during intestinal inflammation was investigated in modified triple cultures using THP-1 knockout cell lines. The results suggest an important, adverse role of the NLRP3 inflammasome pathway during acute intestinal inflammation.

The studies described in this thesis suggest that plastic particle-induced toxicity can depend on both polymer type and intestinal inflammation status. Although plastic particles do not appear to directly activate the NLRP3 inflammasome, the extent of acute intestinal inflammation is dependent upon NLRP3 activation. Since, for some polymer types, toxic effects depend on the inflammation status, their toxicological potential could still be indirectly linked to activation of the NLRP3 inflammasome. These findings contribute to the general understanding of possible adverse effects caused by micro- and nanoplastics and might aid in future risk assessment regarding the oral uptake of plastic particles.

Furthermore, the approaches developed and validated in the framework of this thesis present a valuable addition to the existing portfolio of *in vitro* models used in toxicological, pharmacological, and immunological research.

Zusammenfassung

Die globale Umweltverschmutzung mit Plastikmüll hat zur Kontamination ganzer Ökosysteme mit Plastikpartikeln im Mikro- und Nanometerbereich geführt. Als Konsequenz konnte gezeigt werden, dass Trinkwasser und Lebensmittel Mikro- und Nanoplastik enthalten, was zur oralen Exposition der gesamten Bevölkerung führt.
Der Gastrointestinaltrakt (GIT) stellt das erste Organ dar, welches mit oral aufgenommenen Plastikpartikeln in Kontakt kommt und könnte eines der Haupt-Zielorgane für partikelinduzierte Toxizität sein. Basierend auf Tierstudien und *in vitro* Experimenten wurde das Auslösen von entzündlichen Reaktionen als ein wichtiger adverser Effekt durch Mikro- und Nanoplastikpartikel im GIT identifiziert. Da gezeigt werden konnte, dass das NOD-, LRR- and pyrin domain-containing protein 3 (NLRP3)-Inflammasom bei pro-inflammatorischen Effekten, ausgelöst durch Nanopartikel und Fasern, involviert ist, könnte es auch eine Rolle bei Plastik-induzierter Toxizität spielen. Darüberhinaus ist das NLRP3-Inflammasom an der Pathogenese von chronisch-entzündlichen Darmkrankheiten beteiligt, was eine spezielle Gefahr, ausgehend von Mikro- und Nanoplastik, für diese Patienten implizieren könnte.
Um die Verbindung zwischen der Toxizität von Plastikpartikeln, intestinaler Entzündung und dem NLRP3 Inflammasom zu untersuchen, wurden fortgeschrittene *in vitro* Modelle des gesunden und entzündeten Darms entwickelt, validiert und auf Mikro- und Nanoplastikpartikel angewendet.
Als erster Schritt dieser Arbeit wurden aktuell verfügbare *in vitro* Modelle des menschlichen Darms beschrieben und mögliche Teststrategien unterschiedlicher Komplexität zusammengefasst, um intestinale Effekte von Plastikpartikeln zu untersuchen. Basierend auf den Forschungsfragen dieser Dissertation wurde ein fortgeschrittenes Tripel-Kultur Modell des gesunden und entzündeten Darms (Caco-2/HT29-MTX-E12/THP-1) für die experimentellen Arbeiten ausgewählt. In der ersten experimentellen Studie wurde beobachtet, dass eine Behandlung des entzündeten Modells mit Polyvinylchloridpartikeln zu erhöhten Leveln des pro-inflammatorischen Zytokins IL-1β und einer reduzierten Anzahl an Epithelzellen führt. Diese Beobachtung lässt vermuten, dass der Entzündungsstatus eine wichtige Rolle bei plastikpartikelinduzierter Toxizität spielt. In der zweiten Studie wurde die Tripel-Kultur räumlich invertiert, sodass es möglich ist, nicht-sedimentierende Plastikpartikel, wie z.B. Polyethylen, toxikologisch zu untersuchen. Eine Behandlung mit Polyethylen führte zu zytotoxischen Effekten und pro-inflammatorischen Reaktionen sowohl im gesunden, als auch entzündeten Modell. Das Ziel einer dritten Studie war das Screening einer großen Auswahl an verschiedenen Mikro- und Nanoplastikpartikeln, um herauszufinden, ob die Partikel das NLRP3 Inflammasom in der makrophagenähnlichen Zelllinie THP-1 aktivieren. Außer amino-modifiziertem Polystyrol agierte keines der getesteten Materialien als direkter NLRP3-Aktivator. Trotzdem zeigten Polyethylen-Terephthalatpartikel NLRP3-unabhängiges, pro-inflammatorisches Potenzial. In der letzten Studie wurde die Rolle des NLRP3 Inflammasoms während intestinaler Entzündung mittels modifizierter Tripel-Kulturen (THP-1 knockout Zelllinien) untersucht. Die Ergebnisse sprechen für eine wichtige, schädliche Rolle des NLRP3 Inflammasom-Signalwegs während der Entzündung.
Die Studien in dieser Dissertation suggerieren, dass Plastikpartikelinduzierte Toxizität sowohl von Polymertyp, als auch von Entzündungsstatus abhängig ist. Obwohl Plastikpartikel das NLRP3 Inflammasom anscheinend nicht direkt aktivieren können, ist das Ausmaß der intestinalen Entzündung direkt vom NLRP3-Signalweg abhängig. Da die Toxizität einiger Polymertypen vom Entzündungsstatus abhängig ist, könnte ihr toxikologisches Potenzial indirekt mit dem NLRP3 Inflammasom verknüpft sein. Diese Erkenntnisse tragen zum grundsätzlichen Verständnis von möglichen adversen Effekten bei, die durch Plastikpartikel entstehen und könnten bei zukünftiger Risikobewertung hilfreich sein.
Die Ansätze, die im Rahmen dieser Dissertation entwickelt und validiert wurden, präsentieren einen wertvollen Beitrag zur existierenden Auswahl an *in vitro* Modellen, die in der toxikologischen, pharmakologischen und immunologischen Forschung genutzt werden können.

1. General Introduction

1.1 Micro- and nanoplastics in the environment

In 2002, Paul J. Crutzen introduced the term “Anthropocene” to the scientific community and proposed it as the title of the current geological epoch, in which mankind became one of the most important factors affecting the earth’s biological, geological, and atmospherical processes. This includes species extinction, climate change, the exploitation of natural resources, and pollution of the environment with man-made pollutants (Crutzen, 2002). Environmental pollution includes the release of greenhouse gases, persistent organic chemicals, and mismanaged plastic waste into nature.

Development and industrial-scale production of plastic started in the first half of the 20th century and has drastically increased ever since (Andrady and Neal, 2009). Global plastics production was at 367 million tons in 2020 (www.plasticseurope.org) and is predicted to reach 1800 million tons in 2050 (Ryan, 2015). The word “plastic” is derived from the Greek word *Plastikos*, meaning “capable of being shaped or molded” and is defined as the “Generic term used in the case of polymeric material that may contain other substances to improve performance and/or reduce costs” by the International Union of Pure and Applied Chemistry (IUPAC) (Vert *et al.*, 2012). Plastics are polymers of organic and either synthetic, semi-synthetic, or natural carbon-based compounds that may contain additives like pigments, fragrances, or plasticizers. The properties of different plastics are mainly defined by their polymer composition, leading to different preferred areas of application.

Despite being a blessing for humankind due to unique properties, like durability and low production costs, the excessive use of plastics in everyday life has a major downside: the increasing pollution of the environment with mismanaged plastic waste. About 10 % of discarded waste is plastic, which accumulates in the environment due to its excellent persistence (Barnes *et al.*, 2009). Eriksen and colleagues estimated that up to 250,000 metric tons of plastic waste are floating in the oceans alone (Eriksen *et al.*, 2014).

Although plastics are such a versatile material and generally resistant to degradation, environmental conditions can cause the degradation of plastic polymers into smaller fragments known as microplastics (Andrady, 2012). The term „microplastics“ describes a large, heterogenous group of plastic fragments of different chemical composition and different origin – for example, polyethylene (PE), polyester (PES), and polystyrene (PS) – with a size smaller than 5 mm (Vianello *et al.*, 2013). In this context, the term *micro* has its origin in the Greek word for “small”, and not in the metric scale prefix. Microplastics can be divided into two categories: primary particles, intentionally synthesized microparticles as found in cosmetics like peelings or toothpaste; and secondary particles, originating from degradation processes of larger plastic products (Duis and Coors, 2016).

There is evidence that the continuous degradation of plastic products also leads to particles in the nanometer range, leading to the introduction of the term “nanoplastics” in 2016 (Gigault *et al.*, 2016; Lambert and Wagner, 2016). Currently, there is no consensus on a definition of nanoplastics: while Gigault *et al.* (2018) and other authors proposed a size range of 1-1000 nm for the term nanoplastics, some researchers refer to the EU recommendation on the definition of a nanomaterial[1] (EFSA, 2016b). However, unlike intentionally engineered nanomaterials (ENMs), for example, silicon dioxide (SiO_2), titanium dioxide (TiO_2), or silver nanoparticles, nanoplastics are mainly the consequence of environmental degradation, lacking a consistent chemical composition as well as a uniform size range or size cut-off based on production-wise limits. Thus, it is indeed debatable whether nanoplastics should be defined independently from ENMs.

Exposure to ultraviolet (UV) light, mechanical abrasion, and oxidative processes have been identified as the driving forces behind abiotic degradation of plastic waste into smaller fragments (Andrady, 2012; Julienne *et al.*, 2019). Both PS and PE have been shown to be susceptible to photo-initiated oxidation (Gijsman *et al.*, 1999): the UV radiation breaks a C-H bond in the backbone of these polymers, thus creating a free radical. A subsequent reaction with oxygen leads to the formation of peroxy radicals and then ultimately to chain-scission, crosslinking, or the formation of oxygen-containing functional groups (Gewert *et al.*, 2015). The fragmentation leads to smaller particles, thus enlarging the surface per volume ratio, enabling a faster degradation rate due to higher susceptibility to further reactions. Lambert and Wagner (2016) demonstrated the generation of plastic nanoparticles through simple UV radiation of a disposable PS coffee cup lid. Hebner and Maurer-Jones (2020) generated microplastic particles from various polymer types by UV radiation followed by water movement, the same stressors any plastic waste item experiences when floating in the ocean. Fragmentation into micro- and nanoplastic particles happens predominantly by material breaks in the regions of low molecular weight and crystallinity (Astner *et al.*, 2019), while elevated temperatures have been shown to increase the degradation process (Andrady, 2011; Jakubowicz, 2003).

Although being a minor contribution to the global problem that is plastic pollution, intentionally engineered particles, also known as primary microplastics, play into the equation as well. In general, they are produced similarly to “traditional” engineered nanomaterials, in order to enhance a product’s property. The most commonly used form of primary microplastics is polymer microbeads in personal care products like peelings, toothpaste, or cosmetic glitter (Yurtsever, 2019). After use, these particles are usually rinsed off and end up in wastewater (Habib *et al.*, 2019; Miraj *et al.*, 2019).

[1] A natural, incidental or manufactured material containing particles, in an unbound state or as an aggregate or as an agglomerate and where, for 50 % or more of the particles in the number size distribution, one or more external dimensions is in the size range 1 nm - 100 nm. (Recommendation on the definition of a nanomaterial (2011/696/EU))

Some types of micro- and nanoplastic particles are neither intentionally produced, nor are they generated through continuous abiotic and biotic degradation processes of large plastic waste, as previously described. It is estimated that 5 – 38 % of global plastic waste in the environment are particles from car tires (Kole *et al.*, 2017; Ziajahromi *et al.*, 2019). Friction between the road and car tires causes the rubber of the tires to wear off over time. This generates rubber particles on the micro- and nanoscale that are released into the environment, contributing to the global accumulation of polymeric particles (Halle *et al.*, 2019; Yukioka *et al.*, 2019). Other sources include micro- and nanofibers released from synthetic textile products during laundry (Cesa *et al.*, 2019) and industrial production (Deng *et al.*, 2019), or ultrafine particle emissions from 3D printers (Stephens *et al.*, 2013).

A great number of studies could show the extent of contamination in different ecosystems with microplastics in recent years. Predominantly in samples associated with aquatic ecosystems, numerous studies from all around the world reported the occurrence of microplastic particles in the environment (Acosta-Coley and Olivero-Verbel, 2015; Anderson *et al.*, 2017; Lots *et al.*, 2017; Migwi *et al.*, 2020; Zhang *et al.*, 2019), even at highly remote places like the Arctic (Bergmann *et al.*, 2019), Antarctica (Waller *et al.*, 2017), or the Challenger Deep in the Pacific Ocean (Peng *et al.*, 2020), emphasizing the magnitude of microplastic pollution on the entire planet earth.

1.1.1 Human exposure to micro- and nanoplastics

Due to the ubiquity of micro- and nanoplastics in the environment, it can be assumed that humans are exposed to plastic particles. The most studied route of exposure is the oral route, as microplastic contamination can be directly quantified in water and food samples (Mintenig *et al.*, 2019; Oliveri Conti *et al.*, 2020). Numerous studies have reported the presence of plastic particles in drinking water of various sources (as reviewed by Marsden *et al.*, 2019). The most reported polymer types were polyethylene terephthalate (PET) and polypropylene (PP), while particle counts ranged from 0 to 10^4 particles per liter. Several studies showed the presence of microplastic particles in fish (as reviewed by Barboza *et al.*, 2018), and contamination with microplastics was also demonstrated in other foods and beverages like beer (Kosuth *et al.*, 2018), honey (Liebezeit and Liebezeit, 2015), milk (Kutralam-Muniasamy *et al.*, 2020), fruits and vegetables (Oliveri Conti *et al.*, 2020), and salt (Karami *et al.*, 2017). Cox and colleagues estimated the annual intake of plastics in adults to be between 39 000 and 52 000 particles via the diet alone (Cox *et al.*, 2019). In 2019, Schwabl *et al.* reported the presence of microplastic particles in human stool for the first time in healthy volunteers from Europe and Asia. Particles were of sizes ranging from 50 to 500 µm, while PP and PET were the polymers most commonly found (Schwabl *et al.*, 2019). However, the majority of studies quantifying plastic particle contamination only analyzed the presence of microplastics, as the detection of nanoplastics in

biological samples presents an enormous challenge and reliable, harmonized methodologies are not available yet (Cai *et al.*, 2021). Therefore, the real exposure of humans with plastic particles could be several orders of magnitude higher than estimated, as particles in the lower nanometer range have been neglected in studies quantifying plastic particles in food and water. Another route of microplastic exposure in humans is via inhalation of airborne particles and fibers. Studies reported the presence of microplastics in the atmosphere, with the prominent shape being fibers, presumably released from clothing made of synthetic textiles (Chen *et al.*, 2019; Wright *et al.*, 2019). Fibers found in in- or outdoor air were mainly in the size range between 50 and 250 µm (Dris *et al.*, 2017). Furthermore, construction workers are exposed to airborne ultrafine polyvinyl chloride (PVC) particles during welding of PVC (Jørgensen *et al.*, 2016) and thermal cutting of PS foam leads to aerosols containing particles between 20 and 220 nm (Zhang *et al.*, 2012). However, these exposures are profession-specific and do not apply to the general population. As a consequence of microplastics being present in ambient air, respirable plastic particles and fibers could be found in human lung tissue (Amato-Lourenço *et al.*, 2021), as well as in the sputum of patients with respiratory diseases (Huang *et al.*, 2022). Although inhaled microplastics naturally end up in the lung, the inhalation of plastic particles and fibers contributes to oral exposure as well. Via mucociliary clearance, inhaled particles trapped in mucus are transported along the airways to the pharynx, where they are eventually swallowed (Wanner *et al.*, 1996). In summary, although the actual exposure of humans to plastic particles is yet to be quantified, it can safely be assumed that the entire population is subject to constant oral uptake of micro- and nanoplastics. This assumption is further supported by the fact that plastic particles were found in human blood samples for the first time in 2022, although the route of uptake was not subject to investigation (Leslie *et al.*, 2022). The authors reported a mean concentration of 1.6 µg plastics (particles > 700 nm) per ml blood and found PET, PE and PS to be the most abundant polymers.

1.1.2 Toxicological effects of micro- and nanoplastics after oral exposure

Since the problems associated with microplastic pollution have only recently been acknowledged, toxicological effects of plastic particles remain largely unknown. National (Bundesinstitut für Risikobewertung, BfR) as well as international (European Food Safety Authority, EFSA) authorities are currently dealing with the problems of microplastic pollution. Despite increasing recognition and concern, only limited information about possible health risks is available. The EFSA declared the impossibility of a reasonable risk assessment and encouraged scientific research on the topic in 2016 (EFSA, 2016a).

The polymers, which the plastics particles consist of, are generally regarded as non-toxic and biologically inert, qualifying plastic items for numerous applications in various sectors. For instance, plastics are used as food and beverage packaging, medical devices and body

implants such as joint replacements or stents. However, based on toxicological data of engineered nanomaterials, small plastic particles might pose a threat to human health (Wright and Kelly, 2017), due to new physical properties that arise from the small size, like the enlarged surface area and the ability to enter cells (Behzadi *et al.*, 2017).

The majority of available studies regarding microplastic effects are of ecotoxicological nature and investigate uptake and effects of plastic particles in invertebrate or lower vertebrate model organisms, like waterflea (*Daphnia magna*) (Imhof *et al.*, 2017), zebrafish (*Danio rerio*) (Jin *et al.*, 2018; Lei *et al.*, 2018) and nematodes (*Caenorhabditis elegans*) (Lei *et al.*, 2018). These studies indicate that damage of intestinal tissue and triggering of stress reactions might play a major role in the toxicity of plastic particles. Lei *et al.* (2018) described this for several common types of plastics (polyamide (PA), PE, PVC, and PS).

Studies in higher vertebrate models, such as mice and rats, reported dysbiosis and inflammation of the gut after oral micro- and nanoplastic uptake (Choi *et al.*, 2021; Jin *et al.*, 2019; Li *et al.*, 2019; Lu *et al.*, 2018). Further effects observed in rodents after oral microplastic exposure include metabolic disorders (Lu *et al.*, 2018; Luo *et al.*, 2019), liver damage (Deng *et al.*, 2017; Mu *et al.*, 2021), and reproductive toxicity (Wei *et al.*, 2022; Xie *et al.*, 2019).

For the most part, *in vitro* experiments in mammalian cell lines do not report direct cytotoxicity, but the uptake and/or translocation of plastic particles (Cortés *et al.*, 2020; Domenech *et al.*, 2020), pro-inflammatory reactions (Chen *et al.*, 2021b; Forte *et al.*, 2016) and the induction of oxidative stress (Schirinzi *et al.*, 2017). Oxidative stress and the generation of reactive oxygen species (ROS) are closely connected to the development of chronic inflammatory diseases and the associated risk of cancer development (Reuter *et al.*, 2010).

Although toxicological effects have been observed in various organs, the intestine appears to be one of the main target organs after oral exposure to micro- and nanoplastics, as similar intestinal effects have been reported in zebrafish, mouse, and *in vitro* models. In the majority of studies, the observed effects were related to inflammatory processes.

1.2 Intestinal inflammation

1.2.1 Anatomy and functions of the gastrointestinal tract

The gastrointestinal tract (GIT) is the canal from the mouth to the anus, functioning as the main digestive system in humans. It consists of the esophagus, stomach, small and large intestine and covers multiple functions, such as transport and digestion of food, absorption of nutrients, and excretion of feces (Cheng *et al.*, 2010). Ingested food, ground up into chyme in the mouth, is swallowed, and reaches the stomach via the esophagus. In the stomach, the chyme is sterilized by hydrochloric acid and churned by contractions, while proteins are broken down into polypeptides by proteases (Soybel, 2005). Through the pylorus, the chyme reaches the small intestine, which consists of the three parts duodenum, jejunum, and ileum. The main

function of the small intestine is the digestion of food and absorption of nutrients in the form of macromolecules (Campbell *et al.*, 2019). The epithelial layer of the small intestine consists of alternating villi and crypts, enlarging the surface available for nutrient absorption (Kiela and Ghishan, 2016). The presence of microvilli on enterocytes, so-called brush borders, increases the intestinal surface even further (Shiner and Birbeck, 1961). In the colon, also called large intestine, water and electrolytes are resorbed. Regarding the structure, small and large intestine are similar for the most part, despite the different functions (Azzouz and Sharma, 2021). Ultimately, feces is excreted through the rectum (Moran and Jackson, 1992).

The intestinal epithelium is permanently in contact with foreign matter, including toxic or carcinogenic compounds and particles. Therefore, the proliferation and replacement rate of epithelial cells in the intestine is rather high. At the bottom of the crypts, stem cells are constantly dividing, generating new epithelial cells that migrate to the top of the villi and ultimately undergo apoptosis and shed into the lumen (Potten, 1998). The enterocyte turnover in humans is estimated to be 3.5 days (Darwich *et al.*, 2014).

Enterocytes, the main intestinal cell type, form a selective barrier in the intestine. They restrict the passage of potential toxins while absorbing nutrients using specific transporter enzymes located on the apical membranes (Ferraris and Diamond, 1989). The paracellular pathway in the epithelium is controlled by the enterocytes through a continuous tight junction network (Assimakopoulos *et al.*, 2011). Another cell type found in the intestinal epithelium are mucus-producing goblet cells. The portion of goblet cells varies along the intestinal tract, ranging from 24 % in the distal colon to 10 % in the small intestine (Lozoya-Agullo *et al.*, 2017). The mucus produced and secreted by these goblet cells predominantly consists of glycosylated mucin proteins (Pelaseyed *et al.*, 2014). It is a defense mechanism against pathogens that functions by reducing the interaction of bacteria with the epithelial cells (Hansson, 2012). Furthermore, gut-associated lymphoid tissue (GALT) can be found in the epithelial layer of the intestine. GALT is composed of the Peyer's patches, mesenteric lymph nodes, leukocytes, and specialized epithelial cells called Microfold (M-) cells (Lorenz and Newberry, 2004; Powell *et al.*, 2010). M-cells are an important part of the intestinal immune system, capable of transcytosis of macromolecules and particles to the lymphoid follicles (Kimura, 2018).

Macrophages, a highly important cell type of the innate immune system, can be found below the epithelium in the *lamina propria* (Nagashima *et al.*, 1996). The main tasks of intestinal macrophages are phagocytosis and degradation of foreign materials, pathogens, and dead or tumor cells. Macrophages are able to produce and secrete high amounts of cytokines, making them a key player in inflammatory processes (Hirayama *et al.*, 2017).

1.2.2 Inflammatory bowel disease

The inflammatory bowel diseases (IBD) Crohn's disease (CD) and ulcerative colitis (UC) are characterized by a chronically inflamed intestine. Between 1990 and 2017, the global number of cases rose from 3.7 million to 6.8 million, marking a strong increase of 85 % (Alatab *et al.*, 2020). The precise etiology of IBD remains unknown, but the interplay between genetic susceptibility and environmental risk factors is thought to be of high importance (Leso *et al.*, 2015).

Genome-wide association studies identified a large number of IBD-associated susceptibility gene loci (Jostins *et al.*, 2012). These include single nucleotide polymorphisms in receptor proteins associated to the intestinal microbiome (Ogura *et al.*, 2001), proteins related to autophagy (Hampe *et al.*, 2007), or interleukins (IL) and their receptors (Anderson *et al.*, 2011; Brand, 2009; Duerr *et al.*, 2006; Tremelling *et al.*, 2007). Environmental factors that have been found to contribute to the pathogenesis of IBD are smoking (Bernstein *et al.*, 2006), use of drugs, especially antibiotics (Shaw *et al.*, 2010), stress (Bitton *et al.*, 2008), and ambient air pollution (Ananthakrishnan *et al.*, 2011). Diet, as well as its direct effect on the microbiome, is thought to be an important factor as well (Knight-Sepulveda *et al.*, 2015; Wu *et al.*, 2013). Differences in the microbial composition have been found in IBD patients when compared to healthy controls (Joossens *et al.*, 2011). While originally being labeled a "modern western disease", both the incidence and prevalence of IBD are rising in other parts of the world, as western lifestyle and diet are progressively being adopted in developing countries (Loftus, 2004; Rizzello *et al.*, 2019).

The most common clinical symptoms of IBD are diarrhea, fatigue, abdominal pain, and blood in stool (Singh *et al.*, 2011). Patients suffering from IBD typically experience active and inactive (remission) disease phases (Zallot and Peyrin-Biroulet, 2013), with specific stressors being responsible for entering the next active phase (Singh *et al.*, 2011).

The disturbance of intestinal homeostasis, leading to the relapsing inflammation found in IBD, is characterized by a variety of cellular features. Although the initiating factors are poorly understood, studies found that IBD-patients exhibit an impaired intestinal barrier (Maloy and Powrie, 2011), as well as different mucin expression and secretion compared to healthy individuals (Furr *et al.*, 2010; Sheng *et al.*, 2011; Yamamoto-Furusho *et al.*, 2015). This defective barrier leads to increased contact between the epithelium and bacteria, triggering a reaction of the immune system (Johansson *et al.*, 2014), leading to an increased expression and release of pro-inflammatory cytokines (Neurath, 2014; Shioya *et al.*, 2007; Singh *et al.*, 2016). For example, enterocytes can directly secrete IL-8 as a response to bacterial entry, to attract macrophages (Eckmann *et al.*, 1993). Phagocytosis and destruction of pathogens by macrophages lead to an immediate innate cellular immune response, characterized by the release of other cytokines like tumor necrosis factor-alpha (TNF-α) (Janeway *et al.*, 2001;

Pathmakanthan, 2000). TNF-α is able to promote apoptosis and further dysfunction of the epithelial barrier (van Antwerp *et al.*, 1998; Wang *et al.*, 2005; Wang *et al.*, 2006), leading to a vicious cycle of continuous inflammatory responses. This chronic state of inflammation can induce oxidative DNA damage (Pereira *et al.*, 2016), which ultimately increases the risk for colon cancer (Meira *et al.*, 2008).

So far, treatment of IBD is exclusively symptomatic, as it is currently not medically curable and the underlying causes of the disease are unknown (Mowat *et al.*, 2011). Common medical therapy includes treatment with anti-inflammatory steroids like prednisone (D'Haens *et al.*, 2011). Further options are immunosuppressive drugs like budesonide (Elitsur *et al.*, 1998), and TNF-inhibitors (Nielsen and Ainsworth, 2013). Due to the involvement of the NOD-, LRR- and pyrin domain-containing protein 3 (NLRP3) inflammasome complex in many inflammatory processes, targeting this specific inflammasome for the treatment of IBD is also considered in current research (Perera *et al.*, 2017).

1.3 The NLRP3 Inflammasome

The NLRP3 inflammasome, a multiprotein complex located in the cytosol, plays an important role in both inflammatory bowel diseases and inflammation-related particle effects (He *et al.*, 2016; Schroder and Tschopp, 2010; Zhen and Zhang, 2019). The main consequence of NLRP3 activation is the release of the pro-inflammatory cytokines IL-1β and IL-18, important early mediators of several immunological reactions (He *et al.*, 2016).

The release of IL-1β and IL-18 requires two steps: priming of the inflammasome and subsequent activation of the inflammasome (Wagatsuma and Nakase, 2020). The priming step is necessary to induce the expression of inactive NLRP3, pro-IL-1β, and pro-IL-18, the immature forms of IL-1β and IL-18. Priming is facilitated through Nuclear factor-kappa B (NF-κB), a cytosolic transcription factor activated by danger-associated molecular patterns (DAMPS) or pathogen-associated molecular patterns (PAMPs) (e.g. lipopolysaccharide (LPS) or TNF) binding to pattern recognition receptors (PRRs), such as the Toll-like receptor 4 (TLR4) (McKee and Coll, 2020).

The activation step of the NLRP3 inflammasome can be induced by a variety of different stimuli. DAMPs and PAMPs, such as nigericin or extracellular adenosine triphosphate (ATP), but also particles like TiO_2 or SiO_2, can trigger intracellular events that lead to NLRP3 activation (Baron *et al.*, 2015). These events include rupture of lysosomes, efflux of potassium (K^+) ions, or mitochondrial damage leading to the production of ROS. In the event of activation, NLRP3 oligomerizes and the pyrin domain recruits apoptosis-associated speck-like protein (ASC), which in turn recruits pro-caspase-1, the inactive form of caspase-1. After recruitment, pro-caspase-1 autocatalytically cleaves itself, leading to the active caspase-1. Caspase-1 is capable of cleaving its substrates pro-IL-1β and pro-IL-18, causing the release of mature IL-

1β and IL-18 (Lopez-Castejon and Brough, 2011). Furthermore, caspase-1 is able to cleave Gasdermin D (GSDMD), which forms pores in cell membranes, leading to a specific type of cell death called pyroptosis (Vince and Silke, 2016). Released IL-1β and IL-18 start subsequent pro-inflammatory cascades to promote tissue inflammation including recruitment of immune cells.

It has been shown that the NLRP3 inflammasome is involved in particle-induced inflammatory reactions. Inflammation and fibrosis in the lung after inhalation of crystalline silica or asbestos fibers have been shown to be NLRP3 dependent (Cassel *et al.*, 2008; Dostert *et al.*, 2008; Palomäki *et al.*, 2011). Furthermore, TiO_2 nanoparticles worsened colitis in mice via the NLRP3 inflammasome pathway (Ruiz *et al.*, 2017). Nano-scale TiO_2 and SiO_2 are able to activate the inflammasome in THP-1 cells and bone marrow-derived macrophages (Baron *et al.*, 2015; Kolling *et al.*, 2020). Lunov *et al.* demonstrated the activation of NLRP3 in human macrophages by amine-modified PS nanoparticles *in vitro* (Lunov *et al.*, 2011), while unmodified PS microplastics have been shown to activate the NLRP3 inflammasome *in vivo* in the liver (Mu *et al.*, 2021), ovaries (Hou *et al.*, 2021) and heart (Wei *et al.*, 2021) after oral uptake.

Furthermore, it has been reported that the activation of NLRP3 is implicated in the pathogenesis and progression of IBD (Shao *et al.*, 2019). Single nucleotide polymorphisms in the *NLRP3* gene have been associated with higher susceptibility towards UC (Hanaei *et al.*, 2018; Zhang *et al.*, 2014). Furthermore, NLRP3 inhibitors are currently discussed as potential IBD treatments (Perera *et al.*, 2017). For example, inhibition of the NLRP3 inflammasome by application of cardamonin has been reported to alleviate colitis symptoms in mice (Wang *et al.*, 2018). However, none of the NLRP3 inhibitors tested in (pre-)clinical trials have been approved for human treatment yet (Chen *et al.*, 2021a).

Interestingly, the exact role of the NLRP3 inflammasome in IBD is a controversial topic, as a number of *in vivo* studies reported contrasting results. On the one hand, a clear harmful role was reported by authors after comparing dextran sodium sulfate (DSS)-induced colitis in WT and *Nlrp3*$^{-/-}$ mice (Bauer *et al.*, 2010; Elinav *et al.*, 2011). On the other hand, researchers observed a protective role of NLRP3 in similarly designed studies (Allen *et al.*, 2010; Hirota *et al.*, 2011). The specific function of the NLRP3 inflammasome appears to be quite complex and is thought to be dependent on a number of factors including the microbiome (Bauer *et al.*, 2012), location in the tissue (Song-Zhao *et al.*, 2014; Zaki *et al.*, 2010) and how the inflammation is induced (Zhen and Zhang, 2019).

1.4 Aim of this thesis

The ubiquity of micro- and nanoplastic particles in drinking water and food leads to oral exposure of the human population (Marsden *et al.*, 2019; Oliveri Conti *et al.*, 2020). Based on toxicological data of engineered nanomaterials, potential human health hazards originating from ingested micro- and nanoplastic particles are currently discussed (Yee *et al.*, 2021). The gastrointestinal tract represents the first organ to come into contact with ingested particulate matter and has been identified as a possible target for plastic particle toxicity in recent animal studies (Lei *et al.*, 2018; Li *et al.*, 2019). An important factor regarding the toxicity of particles, in general, seems to be the activation of the inflammasome via the NLRP3 signaling pathway (Baron *et al.*, 2015; Lunov *et al.*, 2011). In addition, a link between the NLRP3 inflammasome and the pathogenesis of IBD has been demonstrated (Bauer *et al.*, 2012), although the exact role of NLRP3 in IBD is not completely clear yet (Zhen and Zhang, 2019). This could imply a particular hazard of plastic particles towards IBD-affected patients. To investigate these topics while considering the 3Rs – Reduction, Replacement and Refinement of animal use – (Russell and Burch, 1992), the development and application of models of human organs, as well as models of human diseases that do not involve animal experiments, is highly encouraged.

The **aim of this thesis** was to develop and apply advanced *in vitro* models of the intestine to investigate the link between plastic particle toxicity and intestinal inflammation, as well as the role of the NLRP3 inflammasome in both.

In **Chapter 2**, the current literature was reviewed regarding intestinal *in vitro* models and testing strategies for particle research. Currently available models, as well as additional strategies allowing realistic experimental conditions were put into perspective. **Chapter 3** describes the use of an established triple-culture model of the healthy and inflamed intestine to investigate toxicologically relevant effects of PS and PVC particles depending on the health status. Cytotoxicity, DNA damage, barrier integrity, mucus distribution, and release of pro-inflammatory cytokines were assessed after particle exposure. In **Chapter 4**, the triple-culture model was modified to allow investigation of buoyant plastic particles with a density of less than 1 g/cm³. The features of this spatially inverted transwell model were compared to the original using the enterotoxic compound diclofenac. Subsequently, PE model particles were applied and toxicologically relevant endpoints were assessed. In **Chapter 5**, THP-1 cells were established as a screening tool for NLRP3 inflammasome activation by plastic particles. Using CRISPR[2]/Cas gene editing technology, THP-1 *NLRP3*$^{-/-}$ cells were generated and the pro-inflammatory and cytotoxic effects of a large panel of model micro- and nanoplastic particles

[2] The acronym CRISPR stands for Clustered Regularly Interspaced Short Palindromic Repeats

were assessed in wildtype (WT) and knockout cells. This tool was validated by applying well-studied engineered nanomaterials and comparing the outcome to previously published data. In **Chapter 6**, the role of the NLRP3 inflammasome in acute intestinal inflammation was investigated by incorporating the THP-1 knockout cells into the *in vitro* triple culture model of the healthy and inflamed intestine and comparing the inflammatory parameters to the WT model. To establish a link to *in vivo* knockout models, the results were compared to data obtained from intestinal tissue explants from WT and *Nlrp3*$^{-/-}$ mice.

1.5 References

Acosta-Coley, I., Olivero-Verbel, J., 2015. Microplastic resin pellets on an urban tropical beach in Colombia. Environ. Monit. Assess. 187 (7), 435. doi:10.1007/s10661-015-4602-7.

Alatab, S., Sepanlou, S.G., Ikuta, K., Vahedi, H., Bisignano, C., Safiri, S., Sadeghi, A., Nixon, M.R., Abdoli, A., Abolhassani, H., Alipour, V., Almadi, M.A.H., Almasi-Hashiani, A., Anushiravani, A., Arabloo, J., Atique, S., Awasthi, A., Badawi, A., Baig, A.A.A., Bhala, N., Bijani, A., Biondi, A., Borzì, A.M., Burke, K.E., Carvalho, F., Daryani, A., Dubey, M., Eftekhari, A., Fernandes, E., Fernandes, J.C., Fischer, F., Haj-Mirzaian, A., Haj-Mirzaian, A., Hasanzadeh, A., Hashemian, M., Hay, S.I., Hoang, C.L., Househ, M., Ilesanmi, O.S., Jafari Balalami, N., James, S.L., Kengne, A.P., Malekzadeh, M.M., Merat, S., Meretoja, T.J., Mestrovic, T., Mirrakhimov, E.M., Mirzaei, H., Mohammad, K.A., Mokdad, A.H., Monasta, L., Negoi, I., Nguyen, T.H., Nguyen, C.T., Pourshams, A., Poustchi, H., Rabiee, M., Rabiee, N., Ramezanzadeh, K., Rawaf, D.L., Rawaf, S., Rezaei, N., Robinson, S.R., Ronfani, L., Saxena, S., Sepehrimanesh, M., Shaikh, M.A., Sharafi, Z., Sharif, M., Siabani, S., Sima, A.R., Singh, J.A., Soheili, A., Sotoudehmanesh, R., Suleria, H.A.R., Tesfay, B.E., Tran, B., Tsoi, D., Vacante, M., Wondmieneh, A.B., Zarghi, A., Zhang, Z.-J., Dirac, M., Malekzadeh, R., Naghavi, M., 2020. The global, regional, and national burden of inflammatory bowel disease in 195 countries and territories, 1990–2017: a systematic analysis for the Global Burden of Disease Study 2017. Lancet Gastroenterol. Hepatol. 5 (1), 17–30. doi:10.1016/S2468-1253(19)30333-4.

Allen, I.C., TeKippe, E.M., Woodford, R.-M.T., Uronis, J.M., Holl, E.K., Rogers, A.B., Herfarth, H.H., Jobin, C., Ting, J.P.-Y., 2010. The NLRP3 inflammasome functions as a negative regulator of tumorigenesis during colitis-associated cancer. J. Exp. Med. 207 (5), 1045–1056. doi:10.1084/jem.20100050.

Amato-Lourenço, L.F., Carvalho-Oliveira, R., Júnior, G.R., Dos Santos Galvão, L., Ando, R.A., Mauad, T., 2021. Presence of airborne microplastics in human lung tissue. J. Hazard. Mater. 416, 126124. doi:10.1016/j.jhazmat.2021.126124.

Ananthakrishnan, A.N., McGinley, E.L., Binion, D.G., Saeian, K., 2011. Ambient air pollution correlates with hospitalizations for inflammatory bowel disease: an ecologic analysis. Inflamm. Bowel Dis. 17 (5), 1138–1145. doi:10.1002/ibd.21455.

Anderson, C.A., Boucher, G., Lees, C.W., Franke, A., D'Amato, M., Taylor, K.D., Lee, J.C., Goyette, P., Imielinski, M., Latiano, A., Lagacé, C., Scott, R., Amininejad, L., Bumpstead, S., Baidoo, L., Baldassano, R.N., Barclay, M., Bayless, T.M., Brand, S., Büning, C., Colombel, J.-F., Denson, L.A., Vos, M. de, Dubinsky, M., Edwards, C., Ellinghaus, D., Fehrmann, R.S.N., Floyd, J.A.B., Florin, T., Franchimont, D., Franke, L., Georges, M., Glas, J., Glazer, N.L., Guthery, S.L., Haritunians, T., Hayward, N.K., Hugot, J.-P., Jobin, G., Laukens, D., Lawrance, I., Lémann, M., Levine, A., Libioulle, C., Louis, E., McGovern, D.P., Milla, M., Montgomery, G.W., Morley, K.I., Mowat, C., Ng, A., Newman, W., Ophoff, R.A., Papi, L., Palmieri, O., Peyrin-Biroulet, L., Panés, J., Phillips, A., Prescott, N.J., Proctor, D.D., Roberts, R., Russell, R., Rutgeerts, P., Sanderson, J., Sans, M., Schumm, P., Seibold, F., Sharma, Y., Simms, L.A., Seielstad, M., Steinhart, A.H., Targan, S.R., van den Berg, L.H., Vatn, M., Verspaget, H., Walters, T., Wijmenga, C., Wilson, D.C., Westra, H.-J., Xavier, R.J., Zhao, Z.Z., Ponsioen, C.Y., Andersen, V., Torkvist, L., Gazouli, M., Anagnou, N.P., Karlsen, T.H., Kupcinskas, L., Sventoraityte, J., Mansfield, J.C., Kugathasan, S., Silverberg, M.S., Halfvarson, J., Rotter, J.I., Mathew, C.G., Griffiths, A.M., Gearry, R., Ahmad, T., Brant, S.R., Chamaillard, M., Satsangi, J., Cho, J.H., Schreiber, S., Daly, M.J., Barrett, J.C., Parkes, M., Annese, V., Hakonarson, H., Radford-Smith, G., Duerr, R.H., Vermeire, S., Weersma, R.K., Rioux, J.D., 2011. Meta-analysis identifies 29 additional ulcerative colitis risk loci, increasing the number of confirmed associations to 47. Nat. Genet. 43 (3), 246–252. doi:10.1038/ng.764.

Anderson, P.J., Warrack, S., Langen, V., Challis, J.K., Hanson, M.L., Rennie, M.D., 2017. Microplastic contamination in Lake Winnipeg, Canada. Environ. Pollut. 225, 223–231. doi:10.1016/j.envpol.2017.02.072.

Andrady, A.L., 2011. Microplastics in the marine environment. Mar. Pollut. Bull. 62 (8), 1596–1605. doi:10.1016/j.marpolbul.2011.05.030.

Andrady, A.L., 2012. Biodegradation of Plastics: Monitoring what Happens, in: Brewis, D., Briggs, D., Pritchard, G. (Eds.), Plastics Additives. An A-Z reference, vol. 1. Springer Netherlands, Dordrecht, pp. 32–40.

Andrady, A.L., Neal, M.A., 2009. Applications and societal benefits of plastics. Philos. Trans. R. Soc. Lond. B Biol. Sci. 364 (1526), 1977–1984. doi:10.1098/rstb.2008.0304.

Assimakopoulos, S.F., Papageorgiou, I., Charonis, A., 2011. Enterocytes' tight junctions: From molecules to diseases. World J. Gastrointest. Pathophysiol. 2 (6), 123–137. doi:10.4291/wjgp.v2.i6.123.

Astner, A.F., Hayes, D.G., O'Neill, H., Evans, B.R., Pingali, S.V., Urban, V.S., Young, T.M., 2019. Mechanical formation of micro- and nano-plastic materials for environmental studies in agricultural ecosystems. Sci. Total Environ. 685, 1097–1106. doi:10.1016/j.scitotenv.2019.06.241.

Azzouz, L.L., Sharma, S., 2021. StatPearls: Physiology, Large Intestine, Treasure Island (FL).

Barboza, L.G.A., Dick Vethaak, A., Lavorante, B.R.B.O., Lundebye, A.-K., Guilhermino, L., 2018. Marine microplastic debris: An emerging issue for food security, food safety and human health. Mar. Pollut. Bull. 133, 336–348. doi:10.1016/j.marpolbul.2018.05.047.

Barnes, D.K.A., Galgani, F., Thompson, R.C., Barlaz, M., 2009. Accumulation and fragmentation of plastic debris in global environments. Philos. Trans. R. Soc. Lond. B Biol. Sci. 364 (1526), 1985–1998. doi:10.1098/rstb.2008.0205.

Baron, L., Gombault, A., Fanny, M., Villeret, B., Savigny, F., Guillou, N., Panek, C., Le Bert, M., Lagente, V., Rassendren, F., Riteau, N., Couillin, I., 2015. The NLRP3 inflammasome is activated by nanoparticles through ATP, ADP and adenosine. Cell Death Dis. 6, e1629. doi:10.1038/cddis.2014.576.

Bauer, C., Duewell, P., Lehr, H.-A., Endres, S., Schnurr, M., 2012. Protective and aggravating effects of Nlrp3 inflammasome activation in IBD models: influence of genetic and environmental factors. Dig. Dis. 30(suppl 1), 82–90. doi:10.1159/000341681.

Bauer, C., Duewell, P., Mayer, C., Lehr, H.A., Fitzgerald, K.A., Dauer, M., Tschopp, J., Endres, S., Latz, E., Schnurr, M., 2010. Colitis induced in mice with dextran sulfate sodium (DSS) is mediated by the NLRP3 inflammasome. Gut 59 (9), 1192–1199. doi:10.1136/gut.2009.197822.

Behzadi, S., Serpooshan, V., Tao, W., Hamaly, M.A., Alkawareek, M.Y., Dreaden, E.C., Brown, D., Alkilany, A.M., Farokhzad, O.C., Mahmoudi, M., 2017. Cellular uptake of nanoparticles: journey inside the cell. Chem. Soc. Rev. 46 (14), 4218–4244. doi:10.1039/c6cs00636a.

Bergmann, M., Mützel, S., Primpke, S., Tekman, M.B., Trachsel, J., Gerdts, G., 2019. White and wonderful? Microplastics prevail in snow from the Alps to the Arctic. Sci. Adv. 5 (8). doi:10.1126/sciadv.aax1157.

Bernstein, C.N., Rawsthorne, P., Cheang, M., Blanchard, J.F., 2006. A population-based case control study of potential risk factors for IBD. Am. J. Gastroenterol. 101 (5), 993–1002. doi:10.1111/j.1572-0241.2006.00381.x.

Bitton, A., Dobkin, P.L., Edwardes, M.D., Sewitch, M.J., Meddings, J.B., Rawal, S., Cohen, A., Vermeire, S., Dufresne, L., Franchimont, D., Wild, G.E., 2008. Predicting relapse in Crohn's disease: a biopsychosocial model. Gut 57 (10), 1386–1392. doi:10.1136/gut.2007.134817.

Brand, S., 2009. Crohn's disease: Th1, Th17 or both? The change of a paradigm: new immunological and genetic insights implicate Th17 cells in the pathogenesis of Crohn's disease. Gut 58 (8), 1152–1167. doi:10.1136/gut.2008.163667.

Cai, H., Xu, E.G., Du, F., Li, R., Liu, J., Shi, H., 2021. Analysis of environmental nanoplastics: Progress and challenges. Chem. Eng. J. 410, 128208. doi:10.1016/j.cej.2020.128208.
Campbell, J., Berry, J., Liang, Y., 2019. Anatomy and Physiology of the Small Intestine, in: , Shackelford's Surgery of the Alimentary Tract, 2 Volume Set. Elsevier, pp. 817–841.
Cassel, S., Eisenbarth, S., Iyer, S., Sadler, J., Colegio, O., Tephly, L., Carter, A., Rothman, P., Flavell, R., Sutterwala, F., 2008. The Nalp3 inflammasome is essential for the development of silicosis. Proc. Natl. Acad. Sci. 26 (105), 9035–9040. doi:10.1073/pnas.0803933105.
Cesa, F.S., Turra, A., Checon, H.H., Leonardi, B., Baruque-Ramos, J., 2019. Laundering and textile parameters influence fibers release in household washings. Environ. Pollut., 113553. doi:10.1016/j.envpol.2019.113553.
Chen, G., Feng, Q., Wang, J., 2019. Mini-review of microplastics in the atmosphere and their risks to humans. Sci. Total Environ., 135504. doi:10.1016/j.scitotenv.2019.135504.
Chen, Q.-L., Yin, H.-R., He, Q.-Y., Wang, Y., 2021a. Targeting the NLRP3 inflammasome as new therapeutic avenue for inflammatory bowel disease. Biomed. Pharmacother. 138, 111442. doi:10.1016/j.biopha.2021.111442.
Chen, Y.-C., Chen, K.-F., Lin, K.-Y.A., Chen, J.-K., Jiang, X.-Y., Lin, C.-H., 2021b. The nephrotoxic potential of polystyrene microplastics at realistic environmental concentrations. J. Hazard. Mater., 127871. doi:10.1016/j.jhazmat.2021.127871.
Cheng, L.K., O'Grady, G., Du, P., Egbuji, J.U., Windsor, J.A., Pullan, A.J., 2010. Gastrointestinal system. Wiley Interdiscip. Rev. Syst. Biol. Med. 2 (1), 65–79. doi:10.1002/wsbm.19.
Choi, Y.J., Park, J.W., Lim, Y., Seo, S., Hwang, D.Y., 2021. In vivo impact assessment of orally administered polystyrene nanoplastics: biodistribution, toxicity, and inflammatory response in mice. Nanotoxicology, 1–19. doi:10.1080/17435390.2021.1996650.
Cortés, C., Domenech, J., Salazar, M., Pastor, S., Marcos, R., Hernández, A., 2020. Nanoplastics as a potential environmental health factor: effects of polystyrene nanoparticles on human intestinal epithelial Caco-2 cells. Environ. Sci.: Nano 7 (1), 272–285. doi:10.1039/C9EN00523D.
Cox, K.D., Covernton, G.A., Davies, H.L., Dower, J.F., Juanes, F., Dudas, S.E., 2019. Human Consumption of Microplastics. Environ. Sci. Technol. 53 (12), 7068–7074. doi:10.1021/acs.est.9b01517.
Crutzen, P.J., 2002. Geology of mankind: "The Anthropocene". Nature 415, 23. doi:10.1038/415023a.
Darwich, A.S., Aslam, U., Ashcroft, D.M., Rostami-Hodjegan, A., 2014. Meta-analysis of the turnover of intestinal epithelia in preclinical animal species and humans. Drug Metab. Dispos. 42 (12), 2016–2022. doi:10.1124/dmd.114.058404.
Deng, H., Wei, R., Luo, W., Hu, L., Li, B., Di, Y., Shi, H., 2019. Microplastic pollution in water and sediment in a textile industrial area. Environ. Pollut. 258, 113658. doi:10.1016/j.envpol.2019.113658.
Deng, Y., Zhang, Y., Lemos, B., Ren, H., 2017. Tissue accumulation of microplastics in mice and biomarker responses suggest widespread health risks of exposure. Sci. Rep. 7, 46687. doi:10.1038/srep46687.
D'Haens, G.R., Panaccione, R., Higgins, P.D.R., Vermeire, S., Gassull, M., Chowers, Y., Hanauer, S.B., Herfarth, H., Hommes, D.W., Kamm, M., Löfberg, R., Quary, A., Sands, B., Sood, A., Watermeyer, G., Watermayer, G., Lashner, B., Lémann, M., Plevy, S., Reinisch, W., Schreiber, S., Siegel, C., Targan, S., Watanabe, M., Feagan, B., Sandborn, W.J., Colombel, J.F., Travis, S., 2011. The London Position Statement of the World Congress of Gastroenterology on Biological Therapy for IBD with the European Crohn's and Colitis Organization: when to start, when to stop, which drug to choose, and how to predict response? Am. J. Gastroenterol. 106 (2), 199-212. doi:10.1038/ajg.2010.392.

Domenech, J., Hernández, A., Rubio, L., Marcos, R., Cortés, C., 2020. Interactions of polystyrene nanoplastics with in vitro models of the human intestinal barrier. Arch. Toxicol. 94 (9), 2997–3012. doi:10.1007/s00204-020-02805-3.

Dostert, C., Pétrilli, V., van Bruggen, R., Steele, C., Mossman, B.T., Tschopp, J., 2008. Innate immune activation through Nalp3 inflammasome sensing of asbestos and silica. Science 320 (5876), 674–677. doi:10.1126/science.1156995.

Dris, R., Gasperi, J., Mirande, C., Mandin, C., Guerrouache M, Langlois, V., Tassin, B., 2017. A first overview of textile fibers, including microplastics, in indoor and outdoor environments. Environ. Pollut. 221, 453–458. doi:10.1016/j.envpol.2016.12.013.

Duerr, R.H., Taylor, K.D., Brant, S.R., Rioux, J.D., Silverberg, M.S., Daly, M.J., Steinhart, A.H., Abraham, C., Regueiro, M., Griffiths, A., Dassopoulos, T., Bitton, A., Yang, H., Targan, S., Datta, L.W., Kistner, E.O., Schumm, L.P., Lee, A.T., Gregersen, P.K., Barmada, M.M., Rotter, J.I., Nicolae, D.L., Cho, J.H., 2006. A genome-wide association study identifies IL23R as an inflammatory bowel disease gene. Science 314 (5804), 1461–1463. doi:10.1126/science.1135245.

Duis, K., Coors, A., 2016. Microplastics in the aquatic and terrestrial environment: Sources (with a specific focus on personal care products), fate and effects. Environ. Sci. Eur. 28 (1), 2. doi:10.1186/s12302-015-0069-y.

Eckmann, L., Kagnoff, M.F., Fierer, J., 1993. Epithelial Cells Secrete the Chemokine Interleukin-8 in Response to Bacterial Entry. Infect. Immun. 61 (11), 4569–4574. doi:10.1128/iai.61.11.4569-4574.1993.

EFSA, 2016a. Presence of microplastics and nanoplastics in food, with particular focus on seafood. EFSA J. 14 (6), 1462. doi:10.2903/j.efsa.2016.4501.

EFSA, 2016b. Re-evaluation of titanium dioxide (E 171) as a food additive. EFSA J. 14 (9), e04545. doi:10.2903/j.efsa.2016.4545.

Elinav, E., Strowig, T., Kau, A.L., Henao-Mejia, J., Thaiss, C.A., Booth, C.J., Peaper, D.R., Bertin, J., Eisenbarth, S.C., Gordon, J.I., Flavell, R.A., 2011. NLRP6 inflammasome regulates colonic microbial ecology and risk for colitis. Cell 145 (5), 745–757. doi:10.1016/j.cell.2011.04.022.

Elitsur, Y., Lichtman, S.N., Neace, C., Dosescu, J., Moshier, J.A., 1998. Immunosuppressive effect of budesonide on human lamina propria lymphocytes. Immunopharmacology 38 (3), 279–285. doi:10.1016/S0162-3109(97)00090-8.

Eriksen, M., Lebreton L C M, Carson H S, Thiel M, Moore C J, Borerro J C, Galgani F, Ryan P G, Reisser J, 2014. Plastic Pollution in the World's Oceans: More than 5 Trillion Plastic Pieces Weighing over 250,000 Tons Afloat at Sea. PLoS One 9 (12), e111913. doi:10.1371/journal.pone.0111913.

Ferraris, R.P., Diamond, J.M., 1989. Specific regulation of intestinal nutrient transporters by their dietary substrates. Annual review of physiology 51, 125–141. doi:10.1146/annurev.ph.51.030189.001013.

Forte, M., Iachetta, G., Tussellino, M., Carotenuto, R., Prisco, M., Falco, M. de, Laforgia, V., Valiante, S., 2016. Polystyrene nanoparticles internalization in human gastric adenocarcinoma cells. Toxicol. In Vitro 31, 126–136. doi:10.1016/j.tiv.2015.11.006.

Furr, A.E., Ranganathan, S., Finn, O.J., 2010. Aberrant expression of MUC1 mucin in pediatric inflammatory bowel disease. Pediatr. Dev. Pathol. 13 (1), 24–31. doi:10.2350/08-06-0479.1.

Gewert, B., Plassmann, M.M., MacLeod, M., 2015. Pathways for degradation of plastic polymers floating in the marine environment. Environ. Sci. Process. Impacts 17 (9), 1513–1521. doi:10.1039/c5em00207a.

Gigault, J., Pedrono, B., Maxit, B., Ter Halle, A., 2016. Marine plastic litter: the unanalyzed nano-fraction. Environ. Sci. Nano 3 (2), 346–350. doi:10.1039/C6EN00008H.

Gigault, J., Ter Halle, A., Baudrimont, M., Pascal, P.-Y., Gauffre, F., Phi, T.-L., El Hadri, H., Grassl, B., Reynaud, S., 2018. Current opinion: What is a nanoplastic? Environ. Pollut. 235, 1030–1034. doi:10.1016/j.envpol.2018.01.024.

Gijsman, P., Meijers, G., Vitarelli, G., 1999. Comparison of the UV-degrations chemistry of polypropylene, polyethylene, polyamide 6 and polybutylene terephthalate. Polym. Degrad. Stab. (65), 433–441. doi:10.1016/S0141-3910(99)00033-6.

Habib, R.Z., Salim Abdoon, M.M., Al Meqbaali, R.M., Ghebremedhin, F., Elkashlan, M., Kittaneh, W.F., Cherupurakal, N., Mourad, A.-H.I., Thiemann, T., Al Kindi, R., 2019. Analysis of microbeads in cosmetic products in the United Arab Emirates. Environ. Pollut. 258, 113831. doi:10.1016/j.envpol.2019.113831.

Halle, L.L., Palmqvist, A., Kampmann, K., Khan, F.R., 2019. Ecotoxicology of micronized tire rubber: Past, present and future considerations. Sci. Total Environ., 135694. doi:10.1016/j.scitotenv.2019.135694.

Hampe, J., Franke, A., Rosenstiel, P., Till, A., Teuber, M., Huse, K., Albrecht, M., Mayr, G., La Vega, F.M. de, Briggs, J., Günther, S., Prescott, N.J., Onnie, C.M., Häsler, R., Sipos, B., Fölsch, U.R., Lengauer, T., Platzer, M., Mathew, C.G., Krawczak, M., Schreiber, S., 2007. A genome-wide association scan of nonsynonymous SNPs identifies a susceptibility variant for Crohn disease in ATG16L1. Nat. Genet. 39 (2), 207–211. doi:10.1038/ng1954.

Hanaei, S., Sadr, M., Rezaei, A., Shahkarami, S., Ebrahimi Daryani, N., Bidoki, A.Z., Rezaei, N., 2018. Association of NLRP3 single nucleotide polymorphisms with ulcerative colitis: A case-control study. Clin. Res. Hepatol. Gastroenterol. 42 (3), 269–275. doi:10.1016/j.clinre.2017.09.003.

Hansson, G.C., 2012. Role of mucus layers in gut infection and inflammation. Curr. Opin. Microbiol. 15 (1), 57–62. doi:10.1016/j.mib.2011.11.002.

He, Y., Hara, H., Núñez, G., 2016. Mechanism and Regulation of NLRP3 Inflammasome Activation. Trends Biochem. Sci. 41 (12), 1012–1021. doi:10.1016/j.tibs.2016.09.002.

Hebner, T.S., Maurer-Jones, M.A., 2020. Characterizing microplastic size and morphology of photodegraded polymers placed in simulated moving water conditions. Environ. Sci. Process. Impacts 22 (2), 398–407. doi:10.1039/c9em00475k.

Hirayama, D., Iida, T., Nakase, H., 2017. The Phagocytic Function of Macrophage-Enforcing Innate Immunity and Tissue Homeostasis. Int. J. Mol. Sci. 19 (1), 92. doi:10.3390/ijms19010092.

Hirota, S.A., Ng, J., Lueng, A., Khajah, M., Parhar, K., Li, Y., Lam, V., Potentier, M.S., Ng, K., Bawa, M., McCafferty, D.-M., Rioux, K.P., Ghosh, S., Xavier, R.J., Colgan, S.P., Tschopp, J., Muruve, D., MacDonald, J.A., Beck, P.L., 2011. NLRP3 inflammasome plays a key role in the regulation of intestinal homeostasis. Inflamm. Bowel Dis. 17 (6), 1359–1372. doi:10.1002/ibd.21478.

Hou, J., Lei, Z., Cui, L., Hou, Y., Yang, L., An, R., Wang, Q., Li, S., Zhang, H., Zhang, L., 2021. Polystyrene microplastics lead to pyroptosis and apoptosis of ovarian granulosa cells via NLRP3/Caspase-1 signaling pathway in rats. Ecotoxicol. Environ. Saf. 212, 112012. doi:10.1016/j.ecoenv.2021.112012.

Huang, S., Huang, X., Bi, R., Guo, Q., Yu, X., Zeng, Q., Huang, Z., Liu, T., Wu, H., Chen, Y., Xu, J., Wu, Y., Guo, P., 2022. Detection and Analysis of Microplastics in Human Sputum. Environ. Sci. Technol. doi:10.1021/acs.est.1c03859.

Imhof, H.K., Rusek, J., Thiel, M., Wolinska, J., Laforsch, C., 2017. Do microplastic particles affect Daphnia magna at the morphological, life history and molecular level? PLoS One 12 (11), e0187590. doi:10.1371/journal.pone.0187590.

Jakubowicz, I., 2003. Evaluation of degradability of biodegradable polyethylene (PE). Polym. Degrad. Stab. 80 (1), 39–43. doi:10.1016/S0141-3910(02)00380-4.

Janeway, C.A., Travers, P., Walport, M., 2001. Immunobiology: The Immune System in Health and Disease. 5th edition. New York: Garland Science.

Jin, Y., Lu, L., Tu, W., Luo, T., Fu, Z., 2019. Impacts of polystyrene microplastic on the gut barrier, microbiota and metabolism of mice. Sci. Total Environ. 649, 308–317. doi:10.1016/j.scitotenv.2018.08.353.

Jin, Y., Xia, J., Pan, Z., Yang, J., Wang, W., Fu, Z., 2018. Polystyrene microplastics induce microbiota dysbiosis and inflammation in the gut of adult zebrafish. Environ. Pollut. 235, 322–329. doi:10.1016/j.envpol.2017.12.088.

Johansson, M.E.V., Gustafsson, J.K., Holmen-Larsson, J., Jabbar, K.S., Xia, L., Xu, H., Ghishan, F.K., Carvalho, F.A., Gewirtz, A.T., Sjövall, H., Hansson, G.C., 2014. Bacteria penetrate the normally impenetrable inner colon mucus layer in both murine colitis models and patients with ulcerative colitis. Gut 63, 281–291. doi:10.1136/gutjnl-2012-303207.

Joossens, M., Huys, G., Cnockaert, M., Preter, V. de, Verbeke, K., Rutgeerts, P., Vandamme, P., Vermeire, S., 2011. Dysbiosis of the faecal microbiota in patients with Crohn's disease and their unaffected relatives. Gut 60 (5), 631–637. doi:10.1136/gut.2010.223263.

Jørgensen, R.B., Buhagen, M., Føreland, S., 2016. Personal exposure to ultrafine particles from PVC welding and concrete work during tunnel rehabilitation. Occup. Environ. Med. 73 (7), 467–473. doi:10.1136/oemed-2015-103411.

Jostins, L., Ripke, S., Weersma, R.K., Duerr, R.H., McGovern, D.P., Hui, K.Y., Lee, J.C., Schumm, L.P., Sharma, Y., Anderson, C.A., Essers, J., Mitrovic, M., Ning, K., Cleynen, I., Theatre, E., Spain, S.L., Raychaudhuri, S., Goyette, P., Wei, Z., Abraham, C., Achkar, J.-P., Ahmad, T., Amininejad, L., Ananthakrishnan, A.N., Andersen, V., Andrews, J.M., Baidoo, L., Balschun, T., Bampton, P.A., Bitton, A., Boucher, G., Brand, S., Büning, C., Cohain, A., Cichon, S., D'Amato, M., Jong, D. de, Devaney, K.L., Dubinsky, M., Edwards, C., Ellinghaus, D., Ferguson, L.R., Franchimont, D., Fransen, K., Gearry, R., Georges, M., Gieger, C., Glas, J., Haritunians, T., Hart, A., Hawkey, C., Hedl, M., Hu, X., Karlsen, T.H., Kupcinskas, L., Kugathasan, S., Latiano, A., Laukens, D., Lawrance, I.C., Lees, C.W., Louis, E., Mahy, G., Mansfield, J., Morgan, A.R., Mowat, C., Newman, W., Palmieri, O., Ponsioen, C.Y., Potocnik, U., Prescott, N.J., Regueiro, M., Rotter, J.I., Russell, R.K., Sanderson, J.D., Sans, M., Satsangi, J., Schreiber, S., Simms, L.A., Sventoraityte, J., Targan, S.R., Taylor, K.D., Tremelling, M., Verspaget, H.W., Vos, M. de, Wijmenga, C., Wilson, D.C., Winkelmann, J., Xavier, R.J., Zeissig, S., Zhang, B., Zhang, C.K., Zhao, H., Silverberg, M.S., Annese, V., Hakonarson, H., Brant, S.R., Radford-Smith, G., Mathew, C.G., Rioux, J.D., Schadt, E.E., Daly, M.J., Franke, A., Parkes, M., Vermeire, S., Barrett, J.C., Cho, J.H., 2012. Host-microbe interactions have shaped the genetic architecture of inflammatory bowel disease. Nature 491 (7422), 119–124. doi:10.1038/nature11582.

Julienne, F., Delorme, N., Lagarde, F., 2019. From macroplastics to microplastics: Role of water in the fragmentation of polyethylene. Chemosphere 236, 124409. doi:10.1016/j.chemosphere.2019.124409.

Karami, A., Golieskardi, A., Keong Choo, C., Larat, V., Galloway, T.S., Salamatinia, B., 2017. The presence of microplastics in commercial salts from different countries. Sci. Rep. 7, 46173. doi:10.1038/srep46173.

Kiela, P.R., Ghishan, F.K., 2016. Physiology of Intestinal Absorption and Secretion. Best Pract. Res. Clin. Gastroenterol. 30 (2), 145–159. doi:10.1016/j.bpg.2016.02.007.

Kimura, S., 2018. Molecular insights into the mechanisms of M-cell differentiation and transcytosis in the mucosa-associated lymphoid tissues. Anat. Sci. Int. 93 (1), 23–34. doi:10.1007/s12565-017-0418-6.

Knight-Sepulveda, K., Kais, S., Santaolalla, R., Abreu, M.T., 2015. Diet and Inflammatory Bowel Disease. Gastroenterol. Hepatol. 11 (8), 511–520.

Kole, P.J., Löhr, A.J., van Belleghem, F.G.A.J., Ragas, A.M.J., 2017. Wear and Tear of Tyres: A Stealthy Source of Microplastics in the Environment. Int. J. Environ. Res. Public Health 14 (10). doi:10.3390/ijerph14101265.

Kolling, J., Tigges, J., Hellack, B., Albrecht, C., Schins, R.P.F., 2020. Evaluation of the NLRP3 Inflammasome Activating Effects of a Large Panel of TiO2 Nanomaterials in Macrophages. Nanomaterials 10 (9), 1876. doi:10.3390/nano10091876.

Kosuth, M., Mason, S.A., Wattenberg, E.V., 2018. Anthropogenic contamination of tap water, beer, and sea salt. PLoS One 13 (4), e0194970. doi:10.1371/journal.pone.0194970.

Kutralam-Muniasamy, G., Pérez-Guevara, F., Elizalde-Martínez, I., Shruti V C, 2020. Branded milks – Are they immune from microplastics contamination? Sci. Total Environ. 714, 136823. doi:10.1016/j.scitotenv.2020.136823.

Lambert, S., Wagner, M., 2016. Characterisation of nanoplastics during the degradation of polystyrene. Chemosphere 145, 265–268. doi:10.1016/j.chemosphere.2015.11.078.

Lei, L., Wu, S., Lu, S., Liu, M., Song, Y., Fu, Z., Shi, H., Raley-Susman, K.M., He, D., 2018. Microplastic particles cause intestinal damage and other adverse effects in zebrafish Danio rerio and nematode Caenorhabditis elegans. Sci. Total Environ. 619-620, 1–8. doi:10.1016/j.scitotenv.2017.11.103.

Leslie, H.A., van Velzen, M.J.M., Brandsma, S.H., Vethaak, D., Garcia-Vallejo, J.J., Lamoree, M.H., 2022. Discovery and quantification of plastic particle pollution in human blood. Environ. Int. 107199. doi:10.1016/j.envint.2022.107199

Leso, V., Ricciardi, W., Iavicoli, I., 2015. Occupational risk factors in inflammatory bowel disease. Eur. Rev. Med. Pharmacol. Sci. 19 (15), 2838–2851.

Li, B., Ding, Y., Cheng, X., Sheng, D., Xu, Z., Rong, Q., Wu, Y., Zhao, H., Ji, X., Zhang, Y., 2019. Polyethylene microplastics affect the distribution of gut microbiota and inflammation development in mice. Chemosphere 244, 125492. doi:10.1016/j.chemosphere.2019.125492.

Liebezeit, G., Liebezeit, E., 2015. Origin of Synthetic Particles in Honeys. Pol. J. Food Nutr. Sci. 65 (2), 143–147. doi:10.1515/pjfns-2015-0025.

Loftus, E.V., 2004. Clinical epidemiology of inflammatory bowel disease: Incidence, prevalence, and environmental influences. Gastroenterology 126 (6), 1504–1517. doi:10.1053/j.gastro.2004.01.063.

Lopez-Castejon, G., Brough, D., 2011. Understanding the mechanism of IL-1β secretion. Cytokine Growth Factor Rev. 22 (4), 189–195. doi:10.1016/j.cytogfr.2011.10.001.

Lorenz, R.G., Newberry, R.D., 2004. Isolated lymphoid follicles can function as sites for induction of mucosal immune responses. Ann. N Y Acad. Sci. 1029, 44–57. doi:10.1196/annals.1309.006.

Lots, F.A.E., Behrens, P., Vijver, M.G., Horton, A.A., Bosker, T., 2017. A large-scale investigation of microplastic contamination: Abundance and characteristics of microplastics in European beach sediment. Mar. Pollut. Bull. 123 (1-2), 219–226. doi:10.1016/j.marpolbul.2017.08.057.

Lozoya-Agullo, I., Araújo, F., González-Álvarez, I., Merino-Sanjuán, M., González-Álvarez, M., Bermejo, M., Sarmento, B., 2017. Usefulness of Caco-2/HT29-MTX and Caco-2/HT29-MTX/Raji B Coculture Models To Predict Intestinal and Colonic Permeability Compared to Caco-2 Monoculture. Mol. Pharm. 14 (4), 1264–1270. doi:10.1021/acs.molpharmaceut.6b01165.

Lu, L., Wan, Z., Luo, T., Fu, Z., Jin, Y., 2018. Polystyrene microplastics induce gut microbiota dysbiosis and hepatic lipid metabolism disorder in mice. Sci. Total Environ. 631-632, 449–458. doi:10.1016/j.scitotenv.2018.03.051.

Lunov, O., Syrovets, T., Loos, C., Nienhaus, G.U., Mailänder, V., Landfester, K., Rouis, M., Simmet, T., 2011. Amino-functionalized polystyrene nanoparticles activate the NLRP3 inflammasome in human macrophages. ACS Nano 5 (12), 9648–9657. doi:10.1021/nn203596e.

Luo, T., Zhang, Y., Wang, C., Wang, X., Zhou, J., Shen, M., Zhao, Y., Fu, Z., Jin, Y., 2019. Maternal exposure to different sizes of polystyrene microplastics during gestation causes

metabolic disorders in their offspring. Environ. Pollut. 255 (Pt 1), 113122. doi:10.1016/j.envpol.2019.113122.
Maloy, K.J., Powrie, F., 2011. Intestinal homeostasis and its breakdown in inflammatory bowel disease. Nature 474 (7351), 298–306. doi:10.1038/nature10208.
Marsden, P., Koelmans, A.A., Bourdon-Lacombe, J., Gouin, T., Anglada, L.D., Cunliffe, D., Jarvis, P., Fawell, J., France, J.D., 2019. Microplastics in drinking water. World Health Organization, Geneva.
McKee, C.M., Coll, R.C., 2020. NLRP3 inflammasome priming: A riddle wrapped in a mystery inside an enigma. J. Leukoc. Biol. 108 (3), 937–952. doi:10.1002/JLB.3MR0720-513R.
Meira, L.B., Bugni, J.M., Green, S.L., Lee, C.-W., Pang, B., Borenshtein, D., Rickman, B.H., Rogers, A.B., Moroski-Erkul, C.A., McFaline, J.L., Schauer, D.B., Dedon, P.C., Fox, J.G., Samson, L.D., 2008. DNA damage induced by chronic inflammation contributes to colon carcinogenesis in mice. J. Clin. Invest. 118 (7), 2516–2525. doi:10.1172/JCI35073.
Migwi, F.K., Ogunah, J.A., Kiratu, J.M., 2020. Occurrence and Spatial Distribution of Microplastics in the surface Waters of Lake Naivasha, Kenya. Environ. Toxicol. Chem. doi:10.1002/etc.4677.
Mintenig, S.M., Löder, M.G.J., Primpke, S., Gerdts, G., 2019. Low numbers of microplastics detected in drinking water from ground water sources. Sci. Total Environ. 648, 631–635. doi:10.1016/j.scitotenv.2018.08.178.
Miraj, S.S., Parveen, N., Zedan, H.S., 2019. Plastic microbeads: small yet mighty concerning. Int. J. Environ. Health. Res., 1–17. doi:10.1080/09603123.2019.1689233.
Moran, B.J., Jackson, A.A., 1992. Function of the human colon. Br. J. Surg. 79, 1132–1137. doi:10.1002/bjs.1800791106.
Mowat, C., Cole, A., Windsor, A., Ahmad, T., Arnott, I., Driscoll, R., Mitton, S., Orchard, T., Rutter, M., Younge, L., Lees, C., Ho, G.-T., Satsangi, J., Bloom, S., 2011. Guidelines for the management of inflammatory bowel disease in adults. Gut 60 (5), 571–607. doi:10.1136/gut.2010.224154.
Mu, Y., Sun, J., Li, Z., Zhang, W., Liu, Z., Li, C., Peng, C., Cui, G., Shao, H., Du, Z., 2021. Activation of pyroptosis and ferroptosis is involved in the hepatotoxicity induced by polystyrene microplastics in mice. Chemosphere 291(Pt 2), 132944. doi:10.1016/j.chemosphere.2021.132944.
Nagashima, R., Maeda, K., Imai, Y., Takahashi, T., 1996. Lamina propria macrophages in the human gastrointestinal mucosa: their distribution, immunohistological phenotype, and function. J. Histochem. Cytochem. 44 (7), 721–731. doi:10.1177/44.7.8675993.
Neurath, M.F., 2014. Cytokines in inflammatory bowel disease. Nat. Rev. Immunol. 14 (5), 329–342. doi:10.1038/nri3661.
Nielsen, O.H., Ainsworth, M.A., 2013. Tumor necrosis factor inhibitors for inflammatory bowel disease. N. Engl. J. Med. 369 (8), 754–762. doi:10.1056/NEJMct1209614.
Ogura, Y., Bonen, D.K., Inohara, N., Nicolae, D.L., Chen, F.F., Ramos, R., Britton, H., Moran, T., Karaliuskas, R., Duerr, R.H., Achkar, J.P., Brant, S.R., Bayless, T.M., Kirschner, B.S., Hanauer, S.B., Nuñez, G., Cho, J.H., 2001. A frameshift mutation in NOD2 associated with susceptibility to Crohn's disease. Nature 411 (6837), 603–606. doi:10.1038/35079114.
Oliveri Conti, G., Ferrante, M., Banni, M., Favara, C., Nicolosi, I., Cristaldi, A., Fiore, M., Zuccarello, P., 2020. Micro- and nano-plastics in edible fruit and vegetables. The first diet risks assessment for the general population. Environ. Res. 187, 109677. doi:10.1016/j.envres.2020.109677.
Palomäki, J., Välimäki, E., Sund, J., Vippola, M., Clausen, P.A., Jensen, K.A., Savolainen, K., Matikainen, S., Alenius, H., 2011. Long, needle-like carbon nanotubes and asbestos activate the NLRP3 inflammasome through a similar mechanism. ACS Nano 5 (9), 6861–6870. doi:10.1021/nn200595c.
Pathmakanthan, S., 2000. A lay doctor's guide to the inflammatory process in the gastrointestinal tract. Postgrad. Med. J. 76 (900), 611–617. doi:10.1136/pmj.76.900.611.

Pelaseyed, T., Bergström, J.H., Gustafsson, J.K., Ermund, A., Birchenough, G.M.H., Schütte, A., van der Post, S., Svensson, F., Rodríguez-Piñeiro, A.M., Nyström, E.E.L., Wising, C., Johansson, M.E.V., Hansson, G.C., 2014. The mucus and mucins of the goblet cells and enterocytes provide the first defense line of the gastrointestinal tract and interact with the immune system. Immunol. Rev. 260 (1), 8–20. doi:10.1111/imr.12182.

Peng, G., Bellerby, R., Zhang, F., Sun, X., Li, D., 2020. The ocean's ultimate trashcan: Hadal trenches as major depositories for plastic pollution. Water Res. 168, 115121. doi:10.1016/j.watres.2019.115121.

Pereira, C., Coelho, R., Grácio, D., Dias, C., Silva, M., Peixoto, A., Lopes, P., Costa, C., Teixeira, J.P., Macedo, G., Magro, F., 2016. DNA Damage and Oxidative DNA Damage in Inflammatory Bowel Disease. J. Crohns Colitis 10 (11), 1316–1323. doi:10.1093/ecco-jcc/jjw088.

Perera, A.P., Kunde, D., Eri, R., 2017. NLRP3 Inhibitors as Potential Therapeutic Agents for Treatment of Inflammatory Bowel Disease. CPD 23 (16). doi:10.2174/1381612823666170201162414.

Potten, C.S., 1998. Stem cells in gastrointestinal epithelium: numbers, characteristics and death. Philos. Trans. R. Soc. Lond. B Biol. Sci. 353 (1370), 821–830. doi:10.1098/rstb.1998.0246.

Powell, J.J., Faria, N., Thomas-McKay, E., Pele, L.C., 2010. Origin and fate of dietary nanoparticles and microparticles in the gastrointestinal tract. J. Autoimmun. 34 (3), 226-233. doi:10.1016/j.jaut.2009.11.006.

Reuter, S., Gupta, S.C., Chaturvedi, M.M., Aggarwal, B.B., 2010. Oxidative stress, inflammation, and cancer: How are they linked? Free Radic. Biol. Med. 49 (11), 1603–1616. doi:10.1016/j.freeradbiomed.2010.09.006.

Rizzello, F., Spisni, E., Giovanardi, E., Imbesi, V., Salice, M., Alvisi, P., Valerii, M.C., Gionchetti, P., 2019. Implications of the Westernized Diet in the Onset and Progression of IBD. Nutrients 11 (5). doi:10.3390/nu11051033.

Ruiz, P.A., Morón, B., Becker, H.M., Lang, S., Atrott, K., Spalinger, M.R., Scharl, M., Wojtal, K.A., Fischbeck-Terhalle, A., Frey-Wagner, I., Hausmann, M., Kraemer, T., Rogler, G., 2017. Titanium dioxide nanoparticles exacerbate DSS-induced colitis: role of the NLRP3 inflammasome. Gut 66 (7), 1216–1224. doi:10.1136/gutjnl-2015-310297.

Russell, W.M.S., Burch, R.L., 1992. The principles of humane experimental technique, Special ed. ed. UFAW, Potters Bar, 238 pp.

Ryan, P.G., 2015. A Brief History of Marine Litter Research, in: Bergmann, M., Gutow, L., Klages, M. (Eds.), Marine Anthropogenic Litter, vol. 22. Springer International Publishing, Cham, pp. 58–74.

Schirinzi, G.F., Pérez-Pomeda, I., Sanchís, J., Rossini, C., Farré, M., Barceló, D., 2017. Cytotoxic effects of commonly used nanomaterials and microplastics on cerebral and epithelial human cells. Environ. Res. 159, 579–587. doi:10.1016/j.envres.2017.08.043.

Schroder, K., Tschopp, J., 2010. The inflammasomes. Cell 140 (6), 821–832. doi:10.1016/j.cell.2010.01.040.

Schwabl, P., Köppel, S., Königshofer, P., Bucsics, T., Trauner, M., Reiberger, T., Liebmann, B., 2019. Detection of Various Microplastics in Human Stool: A Prospective Case Series. Ann. Intern. Med. 171 (7), 453–457. doi:10.7326/M19-0618.

Shao, B.-Z., Wang, S.-L., Pan, P., Yao, J., Wu, K., Li, Z.-S., Bai, Y., Linghu, E.-Q., 2019. Targeting NLRP3 Inflammasome in Inflammatory Bowel Disease: Putting out the Fire of Inflammation. Inflammation 42 (4), 1147–1159. doi:10.1007/s10753-019-01008-y.

Shaw, S.Y., Blanchard, J.F., Bernstein, C.N., 2010. Association between the use of antibiotics in the first year of life and pediatric inflammatory bowel disease. Am. J. Gastroenterol. 105 (12), 2687–2692. doi:10.1038/ajg.2010.398.

Sheng, Y.H., Lourie, R., Lindén, S.K., Jeffery, P.L., Roche, D., Tran, T.V., Png, C.W., Waterhouse, N., Sutton, P., Florin, T.H.J., McGuckin, M.A., 2011. The MUC13 cell-surface

mucin protects against intestinal inflammation by inhibiting epithelial cell apoptosis. Gut 60 (12), 1661–1670. doi:10.1136/gut.2011.239194.
Shiner, M., Birbeck, M.S.C., 1961. The microvilli of the small intestinal surface epithelium in coeliac disease and in idiopathic steatorrhoea. Gut 2 (3), 277–284. doi:10.1136/gut.2.3.277.
Shioya, M., Nishida, A., Yagi, Y., Ogawa, A., Tsujikawa, T., Kim-Mitsuyama, S., Takayanagi, A., Shimizu, N., Fujiyama, Y., Andoh, A., 2007. Epithelial overexpression of interleukin-32alpha in inflammatory bowel disease. Clin. Exp. Immunol. 149 (3), 480–486. doi:10.1111/j.1365-2249.2007.03439.x.
Singh, S., Blanchard, A., Walker, J.R., Graff, L.A., Miller, N., Bernstein, C.N., 2011. Common symptoms and stressors among individuals with inflammatory bowel diseases. Clin. Gastroenterol. Hepatol. 9 (9), 769–775. doi:10.1016/j.cgh.2011.05.016.
Singh, U.P., Singh, N.P., Murphy, E.A., Price, R.L., Fayad, R., Nagarkatti, M., Nagarkatti, P.S., 2016. Chemokine and cytokine levels in inflammatory bowel disease patients. Cytokine 77, 44–49. doi:10.1016/j.cyto.2015.10.008.
Song-Zhao, G.X., Srinivasan, N., Pott, J., Baban, D., Frankel, G., Maloy, K.J., 2014. Nlrp3 activation in the intestinal epithelium protects against a mucosal pathogen. Mucosal Immunol. 7 (4), 763–774. doi:10.1038/mi.2013.94.
Soybel, D.I., 2005. Anatomy and physiology of the stomach. Surg. Clin. North Am. 85 (5), 875-94, v. doi:10.1016/j.suc.2005.05.009.
Stephens, B., Azimi, P., El Orch, Z., Ramos, T., 2013. Ultrafine particle emissions from desktop 3D printers. Atmos. Environ. 79, 334–339. doi:10.1016/j.atmosenv.2013.06.050.
Tremelling, M., Cummings, F., Fisher, S.A., Mansfield, J., Gwilliam, R., Keniry, A., Nimmo, E.R., Drummond, H., Onnie, C.M., Prescott, N.J., Sanderson, J., Bredin, F., Berzuini, C., Forbes, A., Lewis, C.M., Cardon, L., Deloukas, P., Jewell, D., Mathew, C.G., Parkes, M., Satsangi, J., 2007. IL23R variation determines susceptibility but not disease phenotype in inflammatory bowel disease. Gastroenterology 132 (5), 1657–1664. doi:10.1053/j.gastro.2007.02.051.
van Antwerp, D.J., Martin, S.J., Verma, I.M., Green, D.R., 1998. Inhibition of TNF-induced apoptosis by NF-κB. Trends Cell Biol. 8 (3), 107–111. doi:10.1016/S0962-8924(97)01215-4.
Vert, M., Doi, Y., Hellwich, K.-H., Hess, M., Hodge, P., Kubisa, P., Rinaudo, M., Schué, F., 2012. Terminology for biorelated polymers and applications (IUPAC Recommendations 2012). Pure Appl. Chem. 84 (2), 377–410. doi:10.1351/PAC-REC-10-12-04.
Vianello, A., Boldrin, A., Guerriero, P., Moschino, V., Rella, R., Sturaro, A., Da Ros, L., 2013. Microplastic particles in sediments of Lagoon of Venice, Italy: First observations on occurrence, spatial patterns and identification. Estuar. Coast Shelf Sci. 130, 54–61. doi:10.1016/j.ecss.2013.03.022.
Vince, J.E., Silke, J., 2016. The intersection of cell death and inflammasome activation. Cell. Mol. Life Sci. 73 (11-12), 2349–2367. doi:10.1007/s00018-016-2205-2.
Wagatsuma, K., Nakase, H., 2020. Contradictory Effects of NLRP3 Inflammasome Regulatory Mechanisms in Colitis. Int. J. Mol. Sci. 21 (21), 8145. doi:10.3390/ijms21218145.
Waller, C.L., Griffiths, H.J., Waluda, C.M., Thorpe, S.E., Loaiza, I., Moreno, B., Pacherres, C.O., Hughes, K.A., 2017. Microplastics in the Antarctic marine system: An emerging area of research. Sci. Total Environ. 598, 220–227. doi:10.1016/j.scitotenv.2017.03.283.
Wang, F., Graham, W.V., Wang, Y., Witkowski, E.D., Schwarz, B.T., Turner, J.R., 2005. Interferon-gamma and Tumor Necrosis Factor-alpha Synergize to Induce Intestinal Epithelial Barrier Dysfunction by Up-Regulating Myosin Light Chain Kinase Expression. Am. J. Pathol. 166 (2), 409–419. doi:10.1016/S0002-9440(10)62264-X.
Wang, F., Schwarz, B.T., Graham, W.V., Wang, Y., Su, L., Clayburgh, D.R., Abraham, C., Turner, J.R., 2006. IFN-gamma-induced TNFR2 Upregulation is Required for TNF-

dependent Intestinal Epithelial Barrier Dysfunction. Gastroenterology 131 (4), 1153–1163. doi:10.1053/j.gastro.2006.08.022.
Wang, K., Lv, Q., Miao, Y., Qiao, S., Dai, Y., Wei, Z., 2018. Cardamonin, a natural flavone, alleviates inflammatory bowel disease by the inhibition of NLRP3 inflammasome activation via an AhR/Nrf2/NQO1 pathway. Biochem. Pharmacol. 155, 494–509. doi:10.1016/j.bcp.2018.07.039.
Wanner, A., Salathé, M., O'Riordan, T.G., 1996. Mucociliary clearance in the airways. Am. J. Respir. Crit. Care Med. 154 (6 Pt 1), 1868–1902. doi:10.1164/ajrccm.154.6.8970383.
Wei, J., Wang, X., Liu, Q., Zhou, N., Zhu, S., Li, Z., Li, X., Yao, J., Zhang, L., 2021. The impact of polystyrene microplastics on cardiomyocytes pyroptosis through NLRP3/Caspase-1 signaling pathway and oxidative stress in Wistar rats. Environ. Toxicol., 1–10. doi:10.1002/tox.23095.
Wei, Z., Wang, Y., Wang, S., Xie, J., Han, Q., Chen, M., 2022. Comparing the effects of polystyrene microplastics exposure on reproduction and fertility in male and female mice. Toxicology 465, 153059. doi:10.1016/j.tox.2021.153059.
Wright, S.L., Kelly, F.J., 2017. Plastic and Human Health: A Micro Issue? Environ. Sci. Technol. 51 (12), 6634–6647. doi:10.1021/acs.est.7b00423.
Wright, S.L., Ulke, J., Font, A., Chan, K.L.A., Kelly, F.J., 2019. Atmospheric microplastic deposition in an urban environment and an evaluation of transport. Environ. Int., 105411. doi:10.1016/j.envint.2019.105411.
Wu, G.D., Bushmanc, F.D., Lewis, J.D., 2013. Diet, the human gut microbiota, and IBD. Anaerobe 24, 117–120. doi:10.1016/j.anaerobe.2013.03.011.
Xie, X., Deng, T., Duan, J., Xie, J., Yuan, J., Chen, M., 2019. Exposure to polystyrene microplastics causes reproductive toxicity through oxidative stress and activation of the p38 MAPK signaling pathway. Ecotoxicol. Environ. Saf. 190, 110133. doi:10.1016/j.ecoenv.2019.110133.
Yamamoto-Furusho, J.K., Ascaño-Gutiérrez, I., Furuzawa-Carballeda, J., Fonseca-Camarillo, G., 2015. Differential Expression of MUC12, MUC16, and MUC20 in Patients with Active and Remission Ulcerative Colitis. Mediators. Inflamm. 2015, 659018. doi:10.1155/2015/659018.
Yee, M.S.-L., Hii, L.-W., Looi, C.K., Lim, W.-M., Wong, S.-F., Kok, Y.-Y., Tan, B.-K., Wong, C.-Y., Leong, C.-O., 2021. Impact of Microplastics and Nanoplastics on Human Health. Nanomaterials 11 (2). doi:10.3390/nano11020496.
Yukioka, S., Tanaka, S., Nabetani, Y., Suzuki, Y., Ushijima, T., Fujii, S., Takada, H., van Tran, Q., Singh, S., 2019. Occurrence and characteristics of microplastics in surface road dust in Kusatsu (Japan), Da Nang (Vietnam), and Kathmandu (Nepal). Environ. Pollut., 113447. doi:10.1016/j.envpol.2019.113447.
Yurtsever, M., 2019. Tiny, shiny, and colorful microplastics: Are regular glitters a significant source of microplastics? Mar. Pollut. Bull. 146, 678–682. doi:10.1016/j.marpolbul.2019.07.009.
Zaki, M.H., Boyd, K.L., Vogel, P., Kastan, M.B., Lamkanfi, M., Kanneganti, T.-D., 2010. The NLRP3 inflammasome protects against loss of epithelial integrity and mortality during experimental colitis. Immunity 32 (3), 379–391. doi:10.1016/j.immuni.2010.03.003.
Zallot, C., Peyrin-Biroulet, L., 2013. Deep Remission in Inflammatory Bowel Disease: Looking Beyond Symptoms. Curr. Gastroenterol. Rep. 15 (3). doi:10.1007/s11894-013-0315-7.
Zhang, D., Cui, Y., Zhou, H., Jin, C., Yu, X., Xu, Y., Li, Y., Zhang, C., 2019. Microplastic pollution in water, sediment, and fish from artificial reefs around the Ma'an Archipelago, Shengsi, China. Sci. Total Environ. 703, 134768. doi:10.1016/j.scitotenv.2019.134768.
Zhang, H., Kuo, Y.-Y., Gerecke, A.C., Wang, J., 2012. Co-release of hexabromocyclododecane (HBCD) and Nano- and microparticles from thermal cutting of polystyrene foams. Environ. Sci. Technol. 46 (20), 10990–10996. doi:10.1021/es302559v.

Zhang, H., Wang, Z., Lu, X., Wang, Y., Zhong, J., Liu, J., 2014. NLRP3 gene is associated with ulcerative colitis (UC), but not Crohn's disease (CD), in Chinese Han population. Inflamm. Res. 63 (12), 979–985. doi:10.1007/s00011-014-0774-9.

Zhen, Y., Zhang, H., 2019. NLRP3 Inflammasome and Inflammatory Bowel Disease. Front. Immunol. 10, 276. doi:10.3389/fimmu.2019.00276.

Ziajahromi, S., Drapper, D., Hornbuckle, A., Rintoul, L., Leusch, F.D.L., 2019. Microplastic pollution in a stormwater floating treatment wetland: Detection of tyre particles in sediment. Sci. Total Environ. 713, 136356. doi:10.1016/j.scitotenv.2019.136356.

2. Advanced *In Vitro* Testing Strategies and Models of the Intestine for Nanosafety Research

Angela A. M. Kämpfer[a], Mathias Busch[a], Roel P. F. Schins[a]

[a] *IUF – Leibniz-Research Institute for Environmental Medicine, Auf'm Hennekamp 50, 40225 Düsseldorf, Germany*

Chemical Research in Toxicology, 2020, 33 (5), 1163-1178

DOI: 10.1021/acs.chemrestox.0c00079

Author contribution: The author of this dissertation was involved in planning, writing and reviewing of the manuscript, with particular focus on the section "relevant aspects for the development of intestinal *in vitro* systems". Relative contribution: 30 %.

2.1 Abstract

There is growing concern about the potential adverse effects of oral exposure to engineered nanomaterials (ENM). Recent years have witnessed major developments in and advancement of intestinal *in vitro* models for nanosafety evaluation. The present paper reviews the key factors that should be considered for inclusion in nonanimal alternative testing approaches to reliably reflect the *in vivo* dynamics of the physicochemical properties of ENM as well the intestinal physiology and morphology. Currently available models range from simple cell line-based monocultures to advanced 3D systems and organoids. In addition, *in vitro* approaches exist to replicate the mucous barrier, digestive processes, luminal flow, peristalsis, and interactions of ENM with the intestinal microbiota. However, while the inclusion of a multitude of individual factors/components of particle (pre)treatment, exposure approach, and cell model approximates *in vivo*-like conditions, such increasing complexity inevitably affects the system's robustness and reproducibility. The selection of the individual modules to build the *in vitro* testing strategy should be driven and justified by the specific purpose of the study and, not least, the intended or actual application of the investigated ENM. Studies that address health hazards of ingested ENM likely require different approaches than research efforts to unravel the fundamental interactions or toxicity mechanisms of ENM in the intestine. Advanced reliable and robust *in vitro* models of the intestine, especially when combined in an integrated testing approach, offer great potential to further improve the field of nanosafety research.

2.2 The intestine as target organ for ENM: Lessons from the lung

The exposure of the general public to particles – including ENM – is undisputable but the intestine has been relatively neglected as a toxicologically relevant target organ. Concerns about the possible adverse health implications of nanoparticles were initially restricted to the respiratory tract, originating from observations in rodent studies where ultrafine particles of specific chemical composition (e.g. TiO_2 and carbon black) showed considerably stronger pulmonary toxicity than their larger size counterparts, when compared on an equal mass-dose basis.[1] Combined with the growing consensus that nanosize particles from industrial, traffic and domestic combustion sources are the most harmful constituents of ambient air pollution[2,3], this triggered the initiation and rapid expansion of nanosafety research.[4] It furthermore explains, why *in vivo* and *in vitro* research predominantly has focused on elaborating the potential health risks of inhalation exposure to engineered nanomaterials (ENM). However, pioneering studies that addressed the abundance of exogenous (nano-size) particles in the intestine and especially their potential implications in gastrointestinal disease[5,6], have stimulated experimental and regulatory toxicologists to address the hazards of ingested ENM.

With the exception of aerosol therapy as nanomedical application[7], pulmonary exposure to particles is largely unintentional, in contrast to oral exposure. Particles, including ENM, can reach the intestine upon deliberate administration in pharmaceuticals, neutraceuticals, food products and consumer products like toothpaste[8–10], or incidentally, e.g. as contaminant within a product.[11–13] Due to the increasing variety of applications and materials, the quantification of the overall uptake of ENM is challenging. The previously estimated number of 10^{12}-10^{13} particles per day in humans[14–16] is likely exceeded today as the exposure to ENM has increased drastically since then. Previous studies estimated these particle numbers based on an oral intake of up to 5.4 mg/day TiO_2 and 35 mg/day silicate microparticles.[14,15] In 2017, the European Food Safety Authority (EFSA) calculated a mean exposure of 63-189 mg/day for adults as part of the re-evaluation of food-grade TiO_2 (E171).[17] In the context of silica, both Dekkers *et al.*[18] and EFSA[19] estimated the dietary exposure to food-grade SiO_2 (E551) alone at 9.4 and 0.9-27 mg/kg bw/day, respectively. However, current knowledge about qualitative and quantitative intestinal exposure to incidentally present materials, to particles swallowed after mucociliary clearance[20,21] and following biliary excretion[22–24] is still poor.

Toxicological investigations with ENM have demonstrated that their adverse effects strongly depend on their physico-chemical properties, including solubility, (agglomerate) size, shape and surface reactivity.[25–28] The impact of the modification of such properties on the toxicokinetics and toxicodynamics of ENM in biological systems is nowadays well recognised.[29] In relation to inhalation exposure, the effects of lung lining fluid on translocation and toxicity has been revealed for various ENM.[30–32] Within the gastrointestinal tract, ENM are

subject to much more complex environments and processes that potentially impact their physico-chemical properties and thereby affect their interactions with toxicologically relevant target cells. Hence, the qualitative and quantitative contribution of specific particle properties to the toxicity of a given type of ENM may strongly differ between lung and intestine. The ongoing advancement of *in vitro* testing models for the lung has strongly benefited from the availability of *in vivo* (toxicokinetic and toxicodynamic) data for several types of micro- and nano-size particles. Compared to this, *in vivo* data on the abundance, the cellular localisation and adverse effects of ENM in the intestine are rather scarce. Future research initiatives into this direction, as recently pleaded by da Silva *et al.*[16], will contribute to the development and validation of advanced *in vitro* models of the intestine. **Figure 2.1** schematically depicts the major parameters that can affect the characteristics and bioavailability of ENM throughout the oro-gastrointestinal passage. Approaches to address these factors in *in vitro* nanosafety testing will be discussed in more detail in Section 2.4.

Upon oral exposure, the majority of ingested particles that are not dissolved continues to travel along within the chyme and will be excreted with undigested food components. A small proportion of ingested particles may be retained for longer time in the intestine, i.e. up to several days as indicated by pioneering studies in rodents for nanomedical drug delivery applications.[33] The rate of barrier passage of potentially harmful nanoparticles *in vivo* is typically low.[34–37] This has been an important argument for the relative neglect of addressing the oral exposure route in nanosafety research, when compared to oral drug delivery research. However, with the rising interest and introduction of nanotechnological applications in the food sector, e.g. towards safer production and packaging, to increase shelf-life, and to improve nutritional properties, calls for state-of-the-art nanosafety testing strategies for ingested ENM grew stronger.[38,39]

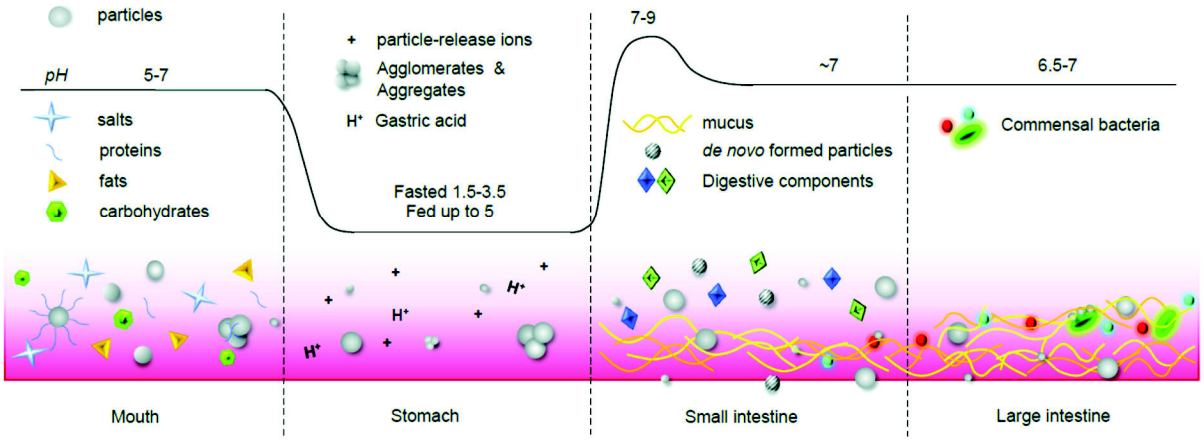

Figure 2.1 Parameters affecting the physico-chemical properties and availability of particles throughout the oro-gastrointestinal passage. Upon oral exposure, particles are subject to a range of factors that can affect their physico-chemical properties and, thereby, their behaviour in biological systems. A majority of particles is ingested within or in combination with food products. Food components such as fats, proteins, carbohydrates and salts strongly impact the agglomeration and dissolution of ENM. The following passage through the stomach and small intestine is characterised by significant pH changes – from pH 2 to 9, respectively. Acidic pH conditions can cause both aggregation or dissolution of particles. The dissolution of ENM can result in the formation of smaller structures with the same chemical composition as the original particles, the release of ionic material or non-soluble degradation products. During this passage also the de novo formation of nanoparticulate structures from ions and salts occurs. In the small intestine, ENM can be entrapped in the mucus barrier which to large extent prevents the interaction with and uptake into the epithelium. In addition to food ingredients, digestive components, e.g. enzymes, bile acid and micelles, can interfere with ENM and again impact their physico-chemical properties. In both the small and large intestine, the microbiota is a major factor that requires consideration in ENM hazard assessment. Throughout the GI-passage, only a minute fraction of particles is absorbed across the intestinal barrier. Hence, the large majority of ingested ENM continues to travel along the intestine within the chyme and is eventually excreted. This implies that locally concentrated amounts of ENM can be in contact with the microbiota for an extended period of time. Depending on ENM properties these interactions might have adverse effects on the microbial community which could result in an overall reduction or a compositional shift of the microbial community.

2.3 *In vitro* testing approaches for ENM: from the lung to the intestine

To a large extent, *in vitro* testing strategies for intestinal ENM exposure were initially based on, or at least inspired by, lung research. Herein, *in vitro* models composed of lung epithelial cells and macrophages were used to complement or to replace animal exposure studies that address effects of inhaled particles. In the context of key differences between these respective organs, the adequacy of a direct translatory approach needs to be considered. This concerns the specific characteristics of the *in vitro* model as well as the method of application of the ENM to the test system. In principle, two options are available for approaching *in vitro* testing of ENM in the intestine:

(1) Application of already well-established protocols and experimental approaches that align with those originally developed for pulmonary toxicity testing.

(2) Development and advancement of specific protocols that mimic organ- and/or exposure-specific features for ingested particles.

The first-mentioned “one protocol for all” approach implies that all factors are treated the same way regardless of the investigated material and organ. This includes the pre-exposure treatment of the ENM, the dosing strategy as well as the *in vitro* model design. Such approaches have already proven successful in nanosafety research. Over the past decade various standard operating procedures (SOPs) have been developed in large scale (inter)national research projects regarding the physico-chemical characterisation of ENM and their controlled suspension into cell culture media.[40–42] This has resulted in improved assay validity, reliability and (intra- and inter-laboratory) reproducibility to the benefit of ENM hazard ranking and grouping.[43] In these orchestrated approaches increasing attention has been focused on the identification of potential assay artefacts or interferences, and on the development of strategies to tackle or, at least, factor them in.[44,45] Specifically, in the field of inhalation toxicology, these exercises have strongly contributed to the stepwise unravelling of relevant cell signalling cascades that are activated following interactions between ENM and cells of the pulmonary tissues.[25] Furthermore, this supported the development of nanotoxicology-specific structure-activity relationship research approaches (i.e. “nano-QSAR”).[46] In the context of inhalation exposure and toxic responses in the respiratory tract, the usefulness of harmonised protocols and SOPs has been supported by the comparative evaluation of ENM-induced effects *in vitro* and *in vivo*.[41,47,48]

However, concerns have been expressed regarding the appropriateness of these standardised ENM testing protocols for the investigation of other target organs, including the intestine. This especially holds true in exercises aiming to directly compare hazards of an individual or a group

of ENM in different organs or tissues.[32] Accordingly, nanotoxicology research has witnessed major advancements in the development of organ-specific *in vitro* models and testing protocols. For instance, the importance of protein corona formation dynamics on nanoparticles in biological environments[49,50] has resulted in adaptations of dispersion protocols to better represent organ specificity, e.g. by addition of lung surfactant to *in vitro* lung models or serum to *in vitro* models that address organ toxicity of blood-borne ENM. Major progress has also been achieved in the development of advanced organ-mimicking *in vitro* 3D models and exposure approaches, at least in part driven by the endorsement of non-animal alternative testing in nanotoxicology.[51,52] For the lung, elaborate air-liquid interphase systems have been developed to avoid ENM-testing in suspension, as well as multi-cell type human airway reconstructing 3D tissue models.[53–56] Similarly, there is ongoing development of highly complex models for other organs such as skin and liver[57] that may be a benefit for nanosafety research. In the following sections, major advances in *in vitro* models and testing approaches for the intestine are presented in the context of their benefits and limitations for nanosafety research.

2.4 Advanced *in vitro* models for the intestine

The intestine is a complex, highly interactive environment comprising different epithelium-associated cell types with distinct tasks as well as various cell types with immuno-active functions (**Figure 2.2**). The mucus layer lining the luminal side of the epithelium provides the living environment for the microbiota[58], which should rightfully be described and treated as organ in itself. With the complexity of the digestive processes and the diversity of the intestinal tissue in mind, research has increasingly focused on the inclusion of physiologically relevant factors and the development of more complex intestinal models. Such approaches include:

1) replication of relevant parameters, e.g. digestive processes, the mucus barrier and the (three-dimensional) intestinal architecture,
2) incorporation of mechanical stimulation to account for peristalsis and luminal flow
3) the use of multicellular systems including intestinal organoids
4) mimicking the interactions and cross-talk with other organs (e.g. interconnected multi-organ models) and, most recently,
5) the inclusion of the microbiome.

The next section is divided in two complementary parts. The first segment expands on the individual parameters that are deemed relevant for an intestinal testing strategy as well as available models to address them. The second part focuses on applications of relevant models,

cell-free as well as cell-based, in the context of ENM testing. For reasons of conciseness, approaches using animal-derived cells were not considered.

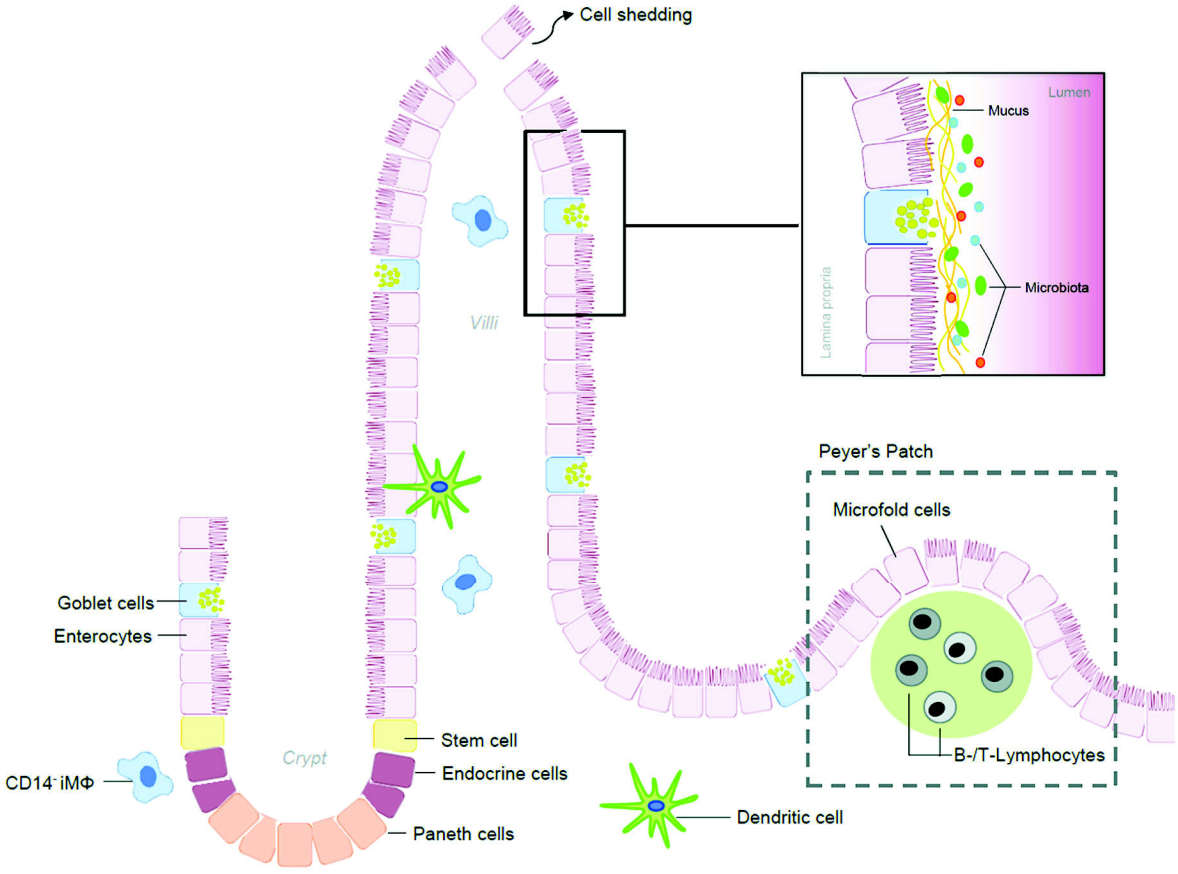

Figure 2.2 Schematic description of the major structures of the human intestine. The major epithelial cell types of the intestine – enterocytes, goblet cells, Paneth cells, endocrine cells, and stem cells – have highly distinct and specialised task profiles. Enterocytes are the most abundant cell type and are responsible for the general integrity of the intestinal barrier as well as the majority of both active and passive transport processes. Goblet cells synthesise and release the multifunctional mucus layer covering the intestinal epithelium. Located on the base of the intestinal crypts, Paneth cells release antimicrobial peptides which renders them a key mediator in host-microbe interactions. Enteroendocrine cells are scattered throughout the intestine yet represent the largest endocrine system in terms of cell number. Long-recognised for their role in the release of hormones and messenger compounds, the cells recently generated interest regarding their impact in gut-brain-axis communication.[59] All of these epithelial cell types originate from the intestinal stem cells. The differentiation takes place while progenitor cells migrate along the crypt-villous axis.

2.4.1 Relevant aspects for the development of intestinal *in vitro* systems

2.4.1.1 The food matrix

It can reasonably be assumed that the majority of ingested particles is transported through the GI-tract in a complex food-derived matrix. Several common food components are known to affect the physico-chemical properties of nanoparticles. Of the three major food constituents, proteins are best studied for their interaction with ENM, forming a part static part dynamic corona around nanoparticles which can impact their hydrodynamic size and biological identity.[49,50] Albeit less investigated, also saccharides and fats are known to interact with nanoparticles. These interactions have been shown to significantly affect various ENM properties, such as their hydrodynamic diameter, colloidal stability and zeta potential[60,61], and to influence ENM-induced cytotoxicity.[62] The presence and concentration of salts may modify the physico-chemical properties of particles depending on the material. In case of silver, salts have been shown to favour the dissolution of particles followed by the complex formation of soluble silver ions and chloride or sulphur groups, and the precipitation of solid Ag species.[63,64] Gold nanoparticles, on the other hand, have been shown to aggregate in the presence of salts.[65] For various ENM, the presence of food-relevant components was shown to significantly affect their sedimentation, uptake and toxicity.[63,66–68]

Several models have been developed to evaluate the interactions of ENM with the food matrix and possibly resulting changes in their toxicokinetic and toxicodynamic behaviour. They range from the inclusion of a single component, e.g. proteins, carbohydrates or fats[66,69,70] to more complex mixtures that include all three main nutrient groups.[71] Zhang *et al.*[72] recently proposed an elegant approach for *in vitro* testing that uses a standardised food model containing fats, proteins, carbohydrates and salts.

2.4.1.2 Gastrointestinal fluids

Throughout the gastrointestinal route, nanoparticles are in contact with complex fluids of changing pH, composition and enzymatic activity. Following contact with saliva in the mouth, which moistens the food bolus and breaks down starch via amylase secretion[73], ingested particles get in contact with the strongly acidic gastric juice, where swallowed microorganisms are inactivated by HCl and the digestion of carbohydrates, fats and proteins continues.[74] Upon exiting the stomach, the gastric fluid is neutralised by alkaline intestinal fluid, a combination of intestinal secrete, pancreatic juice and bile. In addition to neutralising the gastric fluid it contains a multitude of enzymes that are required for the digestion of the ingested food constituents.[75] In addition to the aforementioned impact of salts and proteins, pH conditions have been described to affect both the (agglomerate) size and surface charge of

nanoparticles.[76] Furthermore, changes in pH conditions and macromolecule content accompanied by digestive enzymes might remove, alter or destabilise the corona of ENM.[77,78] Acidic pH conditions can enhance the dissolution of particles which might result in an increased presence of ions.[79–81] In relation to the above discussed precipitation of nanoparticle-derived ions with salts, particulate structures can also be formed *de novo* from ions during intestinal passage. This phenomenon has been described for both silver and aluminium.[35,82] Several approaches of varying complexity were reported to simulate the digestive processes. Gerloff *et al.*[83] presented a simple model that simulates the gastric and intestinal pH conditions following a small meal. Versantvoort *et al.*[84] introduced a more complex approach consisting of artificial saliva, gastric juice and duodenal juice, each with its specific salts, enzyme and protein compositions as well as additional factors like urea, glucuronic acid or bile.[84] Furthermore, the model considered appropriate transit times and volume changes in the different compartments. Other models did not examine the pH conditions but focused on one or more digestive enzymes.[85,86] These digestion models might generate interesting insights into particle characteristics at different stages of the GI passage.

2.4.1.3 Peristalsis and shear stress

The human digestive tract is in constant movement. Contractions in the intestine are divided into two categories: Concentric contractions result in the mixing of the chyme with the digestive juices. Peristalsis represents the co-ordinated contractions of the circular and longitudinal muscles to propel the chyme through the intestinal tract.[87] While the aforementioned digestion strategies used simple shaking or inverting rotation to mimic movement, mechanical peristalsis models are available in other scientific fields. Tharakan *et al.*[88] developed a model of the small intestine mimicking intestinal peristalsis by rhythmically squeezing a flexible tube membrane with inflatable cuffs. Minekus *et al.*[89] describe a commercially available multi-compartmental dynamic model that realistically mimics mixing and transit of chyme, pH values, secretion and composition of digestive fluids and removal of digested compounds and water.

Peristalsis and the movement of the chyme are the major factors for shear stresses acting on the epithelium. In this regard, Jochems *et al.*[90] developed an intestinal 3D model that utilizes the colon-carcinoma cell line Caco-2, which was seeded on hollow membrane tubes. The results presented by Pocock *et al.*[91] suggest that the exposure to a continuous flow induces a rapid differentiation in Caco-2 cells, with microvilli formation after 5 days. Less drastic morphological changes could also be induced by minimal mechanical stimulation using a rocking board.[92] Similar effects were described by Kasendra *et al.*[93] using a complex intestine-on-a-chip model based on biopsy-derived material that combined shear stress and peristalsis. Altogether, the presence of relevant shear stress can induce the formation of villi-like

structures. These morphological changes lead to an increased epithelial surface and modified barrier integrity, bringing the cell models closer to the human *in vivo* situation.

2.4.1.4 The intestinal mucus layer

The human intestine is covered with a viscous mucus layer that is mainly produced and secreted by specialised goblet cells. It consists of mucins, highly glycosylated proteins, which expand upon contact with water. In the context of particle testing, mucus is particularly interesting as it has been described to entrap particles in a surface charge- and size-dependent manner.[94,95] As one of its major tasks consists of protecting the epithelium from xenobiotics, the absence of mucus in *in vitro* systems might lead to a significant overestimation of cell-particle interactions.

Similar to the investigations of the interactions between inhaled ENM and lung surfactant, particle-mucus interactions can be studied in cell-free conditions using animal-derived material, e.g. porcine mucus.[95] Alternatively, cell-based systems can be extended by cell lines that produce mucus autonomously, with HT29-MTX cells being the most widely used goblet-like model. The presence of HT29-MTX cells was found to affect the epithelial permeability for both particles and chemicals.[96,97] However, the thickness of the mucus layer produced by the cell line is far smaller than observed *in vivo* with <10 µm and 200-700 µm, respectively.[98]

2.4.1.5 The microbiome

The bacterial flora is a crucial factor in gut homeostasis and responsible for a variety of functions, including digestion of nutrients, synthesis of vitamins, support of the intestinal barrier and stimulation of the immune system. Research around the intestinal microbiome has increased exponentially over the last 10 years, shedding light on the importance of microbial homeostasis on gastrointestinal and overall health. Intestinal dysbiosis – i.e. a disrupted or imbalanced microbiome – has been described in various physical and mental health conditions[99–101] although the cause-effect relationship remains unclear in most cases.

Several studies on oral ENM exposure have indicated a potential for adverse effects on the gut microbiome, however, the outcomes remain inconclusive. For instance, following oral exposure of rodents to Ag nanoparticles, van den Brule *et al.*[102] reported an increase in *Firmicutes* and *Lactobacillaceae* with concurrent decrease in *Bacteroidetes*, whereas Williams *et al.*[103] observed a decrease in both *Firmicutes* and the *Lactobacillus* genus. In another study, Wilding *et al.*[104] did not observe any alterations in the microbial composition and abundance. Chen *et al.*[68] compared the effects of orally ingested Ag, TiO_2 and SiO_2 ENM in a mouse model and found material-specific effects in both the microbial composition and pro-inflammatory markers. In line with the studies in rodents, microbial changes in response to ENM exposure

have also been observed in zebra fish[105] and the hemolymph *Mytilus galloprovincialis*.[106] The underlying mechanisms of particle-bacteria interactions differ from the mechanisms of ENM-induced toxicity in eukaryotic cells. The endocytosis of nano-objects is thought to be an eukaryote-specific process and has not yet been identified in bacteria.[107] Notwithstanding, the formation of ENM-microbe complexes has been observed[108] and different types of ENM appear to have varying affinities for different types of microbes.[109] Toxic effects and resulting changes in the microbial composition might be a direct consequence of the complexation process or the subsequent release of metal ions in close proximity to the microbes. For more detail on NM-microbe crosstalk and effects we refer the reader to specific reviews on this matter.[109,110] On the other hand, ENM might stimulate or suppress the hosts immune system[111], which could in turn affect the intestinal microbiome that is tightly associated with the mucosal immune system.[112]

Undoubtedly, the incorporation of the intestinal microbiota as a factor in *in vitro* testing presents one of the most challenging tasks. Due to its complexity, it is unlikely that it can be studied in its entirety *in vitro*. Nevertheless, protocols for the culture of faecal sample-derived microbiota are available.[113,114] In regards to cultivating the human microbiome, Liu *et al.*[115] used an advanced, commercially available TWINSHIME system, which consists of five bioreactors to study the composition of microbial communities in the stomach, the small intestine and three regions of the colon. These models can serve as a complementary approach in addition to cell-based *in vitro* testing as the implementation of a bacterial flora into cell cultures has been extremely difficult so far. Instead of co-culturing epithelial cells and bacteria, several studies investigated the effects of bacteria-conditioned supernatant on intestinal cell cultures.[116,117] Richter *et al.*[118] described a co-culture model of Caco-2 and HT29-MTX cells in combination with the commensal strain *Lactobacillus rhamnosus*. An interesting model was presented by Kim *et al.*[119] using Caco-2 cells maintained on a microfluidics device and co-cultured with a commercially available mixture of 8 probiotic strains. The flow prevented the bacterial overgrowth by continuously removing unbound cells. This model was adapted to mimic the intestinal oxygen gradient and co-cultured Caco-2 cells with two obligate anaerobic commensal strains - *Bifidobacterium adolescentis* and *Eubacterium hallii*.[120]

2.4.1.6 Multi-cellular environment and gut architecture

The intestine is comprised of various cell types with specific characteristics and tasks (See **Figure 2.2**). It is, therefore, unlikely that a single cell type can adequately represent the whole organ. Multicellular models combine two or more cell types in 2D or 3D systems with varying degrees of direct contact. The most common set-ups and combinations of multi-cellular models are schematically represented in **Figure 2.3**. Intestinal multi-cell models are usually comprised

of an enterocyte-like cell line with a second epithelial cell types – e.g. mucus-producing goblet cells[121] – or an immunocompetent cell type. The inclusion of immune cells can serve two functions: (1) as a representation of the innate immune system of the gut[122,123] and (2) to induce the formation of Microfold (M) cell formation.[124]

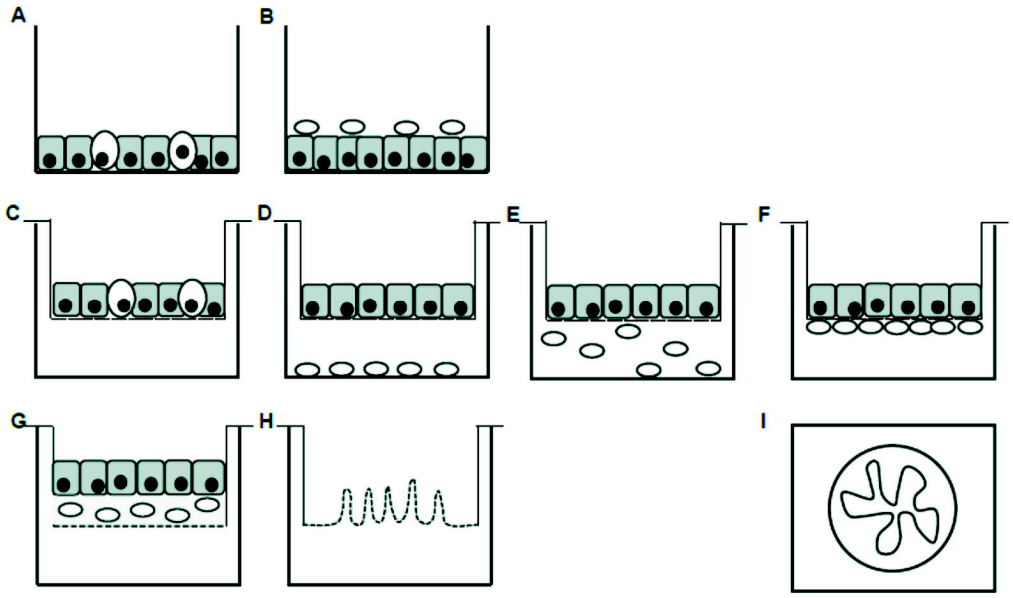

Figure 2.3 Schematic description of the most common multicellular 2D and 3D model set-ups. The early days of *in vitro* research relied on the use of 2-dimensional culture systems (A&B), in which one or more cell types were grown in standard cell culture plates. With the introduction of transwell systems (C-G), co-culture models could be established in more physiological growth conditions (C) and using individual compartments that allowed for more or less physical contact between the cell types: from none to little contact (D&E), to very interactive or even invasive (F&G). A further improvement of these models is aimed for with the use of villi-like scaffolds (H) or a complete imitation of the tube-like structure of the intestine (I) which also allows for the inclusion of fluidics and peristalsis.

The majority of developed models focuses on the inclusion of at least one of the following cell types: M cells, goblet cells (as discussed above) or an immuno-regulatory cell type. M cells are specialized epithelial cells covering the Peyer's Patches, which are part of the gut-associated lymphoid tissue (GALT). Their task is the sampling of luminal antigens by transferring intact macromolecules to the GALT.[125] M cells are known for their role in the uptake and transport of particles[126] and the absence of mature M cells has been demonstrated to result in a significantly reduced accumulation of particulate matter in Peyer's Patches *in vivo*.[127] In this context, their presence is of particular interest when studying the barrier passage – and thereby bioavailability – of ENM *in vitro*. For immune cells both the use of cell lines and primary cells has been described.[123,128,129] A particular type of multicellular system is represented by the so-called "body-on-a-chip" devices, which will not be discussed in detail here. These test

systems incorporate cell types of two or more organs that are interconnected using a flow device.[130,131] Although research in this field has been rather conceptual to date, we believe that especially entero-hepatic systems might be of interest for nanosafety research in the future.
Replication of the 3-dimensional architecture of the intestine is a factor that is often associated with the use of multi-cellular cultures. In this context, the application of transwells marks one of the earliest improvements in intestinal *in vitro* testing.[132,133] Instead of using flat-bottom culture dishes, cells were seeded on filter membranes that allowed for a more realistic growth environment as the cells can be accessed from both apical and basolateral side. Furthermore, it facilitated the conduction of barrier translocation studies, which was of particular interest for the pharmaceutical industry that was strongly involved in the development, improvement and application of these early models.[133–135] More sophisticated systems have turned their backs on transwells and instead use scaffolds to incorporate the villous structure of the intestine.[136]

2.4.1.7 Primary cultures and organoids

The use of primary cell cultures is generally discussed as preferred alternative over cancer-derived cell lines as the latter has been identified with important shortcomings compared to normal intestinal tissue.[137] Early studies focused on the use of human foetal enterocytes[138,139] and were, therefore, confronted with ethical concerns and restricted availability. These cultures were characterised by a very limited life span as their survival critically depends on the presence of the mesenchyme.[140,141] After the use of human primary enterocytes had been largely abandoned in the last decade, new attempts have been reported recently, which include recreated 3-dimensional architecture[142] or shear stress and peristaltic movements.[93]

As also biopsy samples are not widely available, the hottest topic in intestinal *in vitro* models is the development and application of stem cell-derived organoids. The turning point in this regard was the study by Sato *et al.*[143] The authors described a model set-up that allowed the long-term maintenance of unaltered tissue containing all major intestinal epithelial cell types without the requirement for an extracellular matrix. Since then, numerous articles detailing the application and further advancement of organoid cultures have been published.[144–147] As several highly specific reviews have become available on this topic recently[148–150] we refrain from an in-depth discussion of this truly innovative approach.

2.4.2 Application of advanced intestinal *in vitro* models in particle studies

Some, but not all of the discussed *in vitro* model characteristics and testing aspects have already been used in nanosafety research. In this section, an overview on the most relevant and widely applied model adaptions is summarised.

2.4.2.1 Co-culture models

Including the mucus barrier: Caco-2 and HT29-MTX cells

The colon carcinoma cell lines Caco-2 and HT29 are the most commonly used intestinal model specimen. Both can be used for the establishment of a barrier, but the HT29-MTX subtype is preferentially included for its significant mucus secretion.[151] Both cell lines have their limitations and are, as they were derived from diseased material, not a perfect representation of the intestinal epithelium.[152] However, their availability, easy maintenance, adequate reproduction of basic intestinal parameters and, not least, the vastness of available literature still render them the preferred model in basic research.

Co-cultures of Caco-2 and HT29 cells represent the most used intestinal multicell model in ENM hazard assessment. In the majority of studies, Caco-2 and HT29-MTX co-cultures were established on transwells in a 9:1 ratio (**Table 2.1**). The seeding ratio remains a variable factor, and might result in different model characteristics regarding barrier integrity[153,154] and mucus coverage. If and to what extent this might affect the toxicity assessment of ENM is not known.

It has been demonstrated that the presence of HT29 and HT29-MTX cells affects the uptake and translocation of ENM.[96,155,156] This effect is likely material-specific as well as size- and surface charge-dependent.[96,157] Whether the co-culture is more or less sensitive than monocultures remains to be investigated on an ENM-specific case-by-case basis. Georgantzopoulou *et al.*[158] reported the co-culture to be less sensitive to AgNPs and Ag^+ than both respective monocultures regarding cytotoxicity and ROS generation. A similar effect was observed by Ude *et al.*[159,160], who showed a reduced sensitivity of co-cultures to copper oxide (CuO) ENM compared to Caco-2 monocultures. However, the co-cultures might be more sensitive in terms of pro-inflammatory potential especially at lower ENM concentrations. Brun *et al.*[155] demonstrated an increased uptake of TiO_2 in co-cultures compared to Caco-2 monocultures, but no differences in toxicity. In contrast, Strugari *et al.*[154] observed Caco-2/HT29-MTX co-cultures to be more vulnerable towards the treatment with Si-QD and iron oxide ENM than the respective monocultures.

Table 2.1. Characteristics of Caco-2/HT29-MTX co-cultures in nanosafety testing

Seeding density (comb.)	HT29 Type	Seeding ratio (Caco-2:HT29)	Transwell	Reference
NA	MTX	9:1	yes	[161]
$1x10^5$ cm^{-2}	MTX	3:1	yes	[162]
NA	MTX	3:1	yes	[155]
$4x10^4$ cm^{-2}	MTX	3:1	yes	[96]
$1.2x10^5$ mL^{-1}	MTX	9:1	yes	[158]
$2x10^5$ mL^{-1}	parental	7:3	yes	[156]
$2.23x10^5$ cm^{-2}	MTX-E12	8:2	partially	[157]
$1.52x10^5$ cm^{-2}	parental	9:1	yes	[163]
$1x10^5$	MTX	7:3	yes	[154]
$8.3x10^4$ cm^{-2}	MTX	9:1	yes	[164]
$2.4x10^4$ cm^{-2}	MTX	7:3	no	[165]
$3.13x10^5$ cm^{-2}	MTX	9:1	yes	[160]
$4x10^4$ cm^{-2}	MTX	3:1	yes	[166]

Inclusion of M cells: Caco-2 and Raji B cells

Numerous studies have investigated the uptake and transfer of particles *in vitro* using transwell culture models. However, in view of intrinsic limitations of such systems and potential pitfalls in particle detection methods, results have to be interpreted cautiously. This is on the one hand due to the specific physico-chemical properties of ENM including their size, dissolution, aggregation and re-precipitation behavior. On the other hand, the detection of particles often requires an additional label (e.g. fluorescence), or chemical destruction of the particle. In the former case, a detached label can false-positively be identified as particle, whereas in the latter case, an unequivocal identification of the pristine particle is impossible.

As the majority of particle uptake has been recognized to occur via M cells[126], their representation is crucial for investigating the barrier passage of ENM *in vitro*. Whereas particle transfer is usually low to absent in Caco-2 monocultures and Caco-2/HT29-MTX co-cultures, studies on co-cultures with Raji B cells reported an increase in particle uptake and displacement of particles to the basolateral compartment of transwell systems.[153,167,168] The transfer efficiency was demonstrated to be size- and surface charge-depending. Whereas it was increased in a Caco-2/HT29-MTX/M cell model for plain polystyrene nanoparticles (PSNP, 50 and 200 nm)[153], the transport of carboxylated PSNP was only significant for 50 nm but not 200 nm particles.[162]

Large variations in transfer rate have been reported, which might be related to the applied dose and the type of nanomaterial investigated. However, these variations could also result from alterations in the model set up and thereby caused differences in M cell formation rate (**Table 2.2**). The transfer of PSNP (50-200 nm) was between 0.002 – 0.59 % in the Caco-2 M-cell model[153,167], and 0.003 – 0.52 % in the Caco-2/HT29-MTX M cell model.[153,162] Des Rieux *et al.*[168] demonstrated a significantly increased transport of carboxylated polystyrene particles in the inverted compared to the normally oriented model, which might be related to the enhanced transformation of M cells (15-30% and 2.5% in the inverted and normally orientated model, respectively). Bouwmeester *et al.*[169] studied the translocation of Ag nanoparticles and ions at non-toxic concentrations and reported overall low translocation rates <1% regardless of the silver species. For TiO_2 ENM, an increased uptake compared to Caco-2 monocultures and Caco-2/HT29-MTX co-cultures was reported.[155] The occurrence of translocation was not seen.

In contrast to the above, both Walczak *et al.*[96] and Abeer *et al.*[164] observed a reduced particle transfer in an M cell-induced Caco-2/HT29-MTX co-culture compared to a Caco-2 monoculture. For CuO NPs and Cu ions, a concentration and time-dependent permeation between 2.5% (3.17 µg cm^{-2}, 24h) and 14% Cu (12.68 µg cm^{-2}, 48h) was reported.[160] However, the induction of Cu-related cytotoxicity might have had an impact on this study outcome, as the translocation was paralleled by a strong reduction in TEER and was also observed in Caco-2 monocultures.[159]

Altogether, these studies give an interesting and important insight into the interactions between particles and the intestine as biological barrier. Nevertheless, the results need to be carefully interpreted as static systems like these *in vitro* models are can serve on an indicative level at best. In addition to the above briefly addressed difficulties concerning particle stability and detection, transwell systems themselves have their limitations. The transfer to the basolateral compartment of these systems can be affected by factors like the pore size and pore density of the filter. Furthermore, some cells tend to grow into and through these pores, which might present an additional barrier for particle transport. Last but not least, the investigated particles could interact with the material of the transwell inserts and remain attached to it, as strong retention of ENM on plastics has been demonstrated.[170]

Table 2.2. Characteristics of Caco-2/Raji B co-cultures in nanosafety testing

Seeding density (Raji B)	Exposure time (days)	M-cell conversion rate	Orientation	Source
$5x10^5$	4-5	NA	Normal	[167]
$5x10^5$	4-5	NA	Normal	[168]
$5x10^5$	5	15-30 %	Inverted	
$6x10^4$ cm^{-2}	5	NA	Normal	[169]
$1x10^6$	2	2.55 %	Normal	[162]
$1x10^6$	3	NA	Normal	[161]
$5x10^5$	4-5	NA	Normal	[153]
$5x10^5$	4	NA	Inverted	[171]
NA	14	NA	Normal	[155]
$4x10^4$	5	NA	Inverted	[96]
$2x10^6$ mL^{-1}	3	NA	Normal	[156]
$2.5x10^5$	4-6	NA	Inverted	[172]
$1x10^5$	7	NA	Normal	[164]
$7.5x10^5$	5	NA	Normal	[160]

Representation of the immune system: Caco-2 and immune cells

Until now, only a few studies investigating particles made use of co-cultures involving immune cells (**Table 2.3**). Moyes *et al.*[173] co-cultured Caco-2 and phorbol myristate acetate (PMA)-differentiated THP-1 cells to study the translocation of latex microparticles. The authors observed an increased passage in presence of THP-1 cells, which might be related to the reduced barrier integrity. Leonard *et al.*[174] combined Caco-2 cells with PBMC-derived macrophages and dendritic cells and used the model in an inflamed-like state to investigate the therapeutic effect of nano-drug formulations. Susewind *et al.*[175] went on to adapt this model from primary immune cells to cell line-derived macrophages and dendritic cells. The model was used in non-inflamed and IL1β-inflamed state and exposed to TiO_2, Ag, and Au ENM. The triple culture was found to be less sensitive than the Caco-2 monoculture concerning ENM-induced cytotoxicity, independent of the health status. However, both non-inflamed and inflamed triple cultures reacted to Ag exposure with the release of IL8, which was absent in Caco-2 monocultures. In contrast, Kämpfer *et al.*[176] reported an increased sensitivity of a Caco-2/THP-1 co-culture exposed to AgNPs in the inflamed-like but not the non-inflamed model.

Obviously, as these three models used highly individual set-ups and inflammation stimuli, the results are not directly comparable. However, the reported differences underline the impact of model-specific details on the outcome.

Table 2.3. Immune cell models used in ENM hazard assessment

Immune cell type	Seeding density	Disease model	Position in well	Reference
Cell-line derived macophages	~$1x10^5$ cm^{-2} ($1x10^6$)	uncontrolled	BL compartment	[173]
Primary macrophages, dendritic cells	~$9x10^3$ cm^{-2} ($1x10^4$ in total	Yes, IL-1β	On transwell, embedded in collagen	[174]
Cell line-derived Macrophages, dendritic cells	~$9x10^3$ cm^{-2} ($1x10^4$ each)	Yes, IL-1β	On transwell, embedded in collagen	[175]
Cell line-derived macrophages	~$4.7x10^4$ cm^{-2} ($1.8x10^5$)	Yes, LPS and IFN-y	BL compartment	[176]

2.4.2.2 Mono- and co-cultures of the intestinal microbiota

The intestinal microbiome is probably the most complex factor to consider in intestinal *in vitro* testing. Unsurprisingly, not many studies have been published on particle-induced effects in complex models, e.g. multi-strain bacterial communities or epithelial/microbial co-cultures.

Different groups have investigated the effects of ENM, including Ag, ZnO, and TiO_2, in isolated strains and *in vitro* cell-bacterial co-cultures.[63,177,178] Both Das *et al.*[179] and Dudefoi *et al.*[85] used a multi-culture of 33 bacterial strains, known as microbial ecosystem therapeutic-1 (MET1)[113], to study the effects of Ag and TiO_2 ENM, respectively. Das *et al.*[179] observed an overall reduction in bacterial numbers, changes in fatty acid profiles and a significant reduction of *Bacteroides ovatus*.

At least two available studies describe a consecutive incubation between ENM, microbiota and intestinal cells. Garuglieri *et al.*[116] exposed *E. coli* transwell cultures to AgNPs and subsequently collected the basolateral culture medium to expose Caco-2 cells. Cattò *et al.*[117] went on to study AgNPs in an advanced set-up, which substituted the bacterial monoculture with faecal microbiota.

To the best of our knowledge, the only direct epithelial/microbial co-culture used for particle studies so far has been presented by Richter *et al.*[118] The authors established a multi-culture of Caco-2 and HT29-MTX cells with *Lactobacillus rhamnosus* to study the effects of TiO_2 ENM.

Importantly, for several of the aforementioned *in vitro* systems, findings were partly in line with observed *in vivo* effects (discussed in section 2.4.1.5). As van den Brule *et al.*[102] observed in AgNPs-exposed rats, Cattò *et al.*[117] reported a shift in the *Firmicutes/Bacteroidetes* ratio in response to nanosilver. In concordance with the findings by Chen *et al.*[68], Dudefoi *et al.*[85] reported minimal effects of food-grade TiO_2.

2.4.2.3 Simulation of food components and digestion

Simulation of digestive processes and presence of food components are the most-studied non-cellular factors to improve intestinal *in vitro* testing, and are often considered in parallel. They were investigated extensively in both cell-based and cell-free systems. For reasons of conciseness, only selected studies involving particles will be summarised here.

Both Peters *et al.*[180] and Walczak *et al.*[181] used a digestion model in a cell-free context. The authors investigated in which state TiO_2 and Ag ENM can be expected to reach the small intestine. Interestingly, Walczak and colleagues also observed the earlier mentioned *de novo* formation of nano-sized particles from $AgNO_3$. Gerloff *et al.*[83] applied a much simpler approach with focus on the GI pH conditions. Following the digestion, the acellular ROS formation of SiO_2 and ZnO ENM was increased but no difference in toxicity was found in Caco-2 cells. Böhmert *et al.*[182] reported a strong impact of the GI simulation on particle characteristics but no change in Ag ENM-induced cytotoxicity. With a focus on the microbiome, Dudefoi *et al.*[85] investigated the impact of amylase on the effects of TiO_2 in a community of 33 bacterial strains. Interestingly, amylase alone and in combination with TiO_2 significantly affected the composition of the microbial community.

As most cellular *in vitro* models depend on the use of proteins, many studies are available on the impact of different types of proteins on particle characteristics and toxicity. In Caco-2 cells, the protein corona was demonstrated to reduce SiO_2-induced cytotoxicity[67], to affect the cellular responses to AgNPs[183] and to enhance the uptake of magnetite NPs.[184]

Deloid *et al.*[185] pre-incubated iron-oxide nanoparticles in a simple oil-in-water emulsion but did not investigate their biological effects compared to pristine particles. Lichtenstein *et al.*[71] showed that the presence of milk powder, starch and olive oil had a major impact on digestion-induced agglomeration behaviour and subsequent cellular uptake. Using the same model, Kästner *et al.*[186] demonstrated the stabilising and protective effects of proteins compared to

both fat and carbohydrates against digestion-induced dissolution. Cao *et al.*[70] studied synergistic effects of different fatty acids and ZnO nanoparticles on the toxicity in Caco-2 cells. Whereas free fatty acids did not impact ZnO-induced cytotoxicity, the presence of palmitic acid was found to enhance cytotoxicity.

2.5 Summary and concluding remarks: Advancement with advanced models?

For the hazard assessment of ENM an increasing number of intestinal *in vitro* models and testing strategies has become available to replace traditional monoculture models. The different models and approaches are considered to better reflect specific factors of the unique composition, morphology and physiological properties of the intestine, each of which may influence the toxicity of ENM *in vivo*.[43,72,82,185,187] It is tempting to build a model that assembles as many of these factors as possible into one system. This would result in a most realistic *in vitro* testing strategy for ENM that ideally could replace animal exposure studies in nanosafety research. Such advanced, complex *in vitro* models might improve the identification of molecular mechanisms of ENM toxicity by taking into account intestinal barrier architecture, intercellular crosstalk between different cell-types, etc. The inclusion of immune cells to create an inflamed state intestinal model can be useful to address the impact of pre-existing conditions and potential differences in susceptibility on the toxicity of ingested ENM. The incorporation of the microbiome factor may contribute to our understanding of how microbiome changes might affect intestinal ENM toxicity. Observations regarding ENM-induced effects on the microbiome status and composition are of relevance, for instance, in relation to disease risks in association with excessive or long-term exposure. The same applies to observations regarding modulatory ENM effects on inflammatory markers in immune cell models, as both inflammation and microbiome changes have been associated with colon cancer risk.[188,189] The inclusion of food matrix factors in testing may shed light on possible differences in adverse intestinal effects of ENM that can be of relevance for drug prescription regimen in nanomedical applications.

Obviously, the more complex the model, the more insights may be obtained on the role of intestine-specific factors and components, and their possible interactions with ENM. However, for routine hazard assessment and ENM grouping strategies, highly complex *in vitro* models of the intestine are rather disadvantageous. Inter-laboratory comparison assessments have already proven to be a major challenge for ENM testing when simple monoculture models were used.[41] Thus, the incorporation of too numerous and complex factors into a single test system inevitably will reduce its robustness and reproducibility. Indeed, monoculture experiments e.g. with Caco-2 cells, have been helpful in elaborating on potential differences in toxicity of ENM

of different chemical composition or crystal structure for the intestine.[83,190] However, the more advanced models offer a more realistic reflection of the human intestine and, especially when combined in so-called integrative testing strategies (ITS), will benefit risk assessment.[43,191]

Taken together, the investigation of ENM-induced effects on the intestine should be carried out in relation to the specific research needs and questions (see **Figure 2.4**). The selection of the *in vitro* model, or combination of models in a broader testing strategy, should be driven and justified by the intended or actual application of the ENM as well as the specific purpose of the study. Importantly, also possible experimental limitations that may hamper the meaningfulness of the approach should be considered. For instance, when addressing the safety of ENM in intended or already existing food (packaging) applications, the inclusion of the food matrix and appropriate digestion simulation protocols are of obvious relevance. However, the use of a multi-step digestion protocol will lead to a dilution of the initial particle suspension so that the final concentration might be insufficient for adequate testing in a cell-based *in vitro* system. This aspect is directly linked to the most important consideration in *in vitro* toxicity testing – i.e. the choice of exposure dose and application strategy. For the *in vitro* models of the intestine described here, the consideration of an appropriate dosimetry regime is crucial: Whereas single exposures may give clues about intrinsic hazard differences of ENM, long-term and repeated (lower dose) applications are likely of more relevance for human risk assessment. The ongoing developments of (modelling) approaches and SOPs to better define the delivered versus the applied (nominal) dose has led to further improvements in nanosafety research.[192,193] To some extent, these modelling advancements are also applicable to many of the intestinal models. However, for complex organoid-based systems further improvements to the modelling approaches are likely required.

In addition, ENM dispersion protocols using sonication have proven to be useful in nanosafety assessment and appropriate for the lung, as local deposition and uptake depends on particle (agglomeration) size. In contrast, for oral uptake the use of sonication-independent protocols should be considered, especially when digestion simulation protocols are applied.[83]

In conclusion, major advances have been achieved in recent years regarding the establishment of *in vitro* models and testing approaches to address nanosafety aspects of particles, including ENM, in the intestine. As these models span a wide range of complexity, care should be taken when deciding on a testing strategy. The most appropriate model particle (pre-)treatment and exposure should be selected to serve the specific research question to be addressed, e.g. for hazard assessment and grouping, to identify toxicity mechanisms, for the development of therapeutic strategies, or to explore the importance of individual susceptibility.

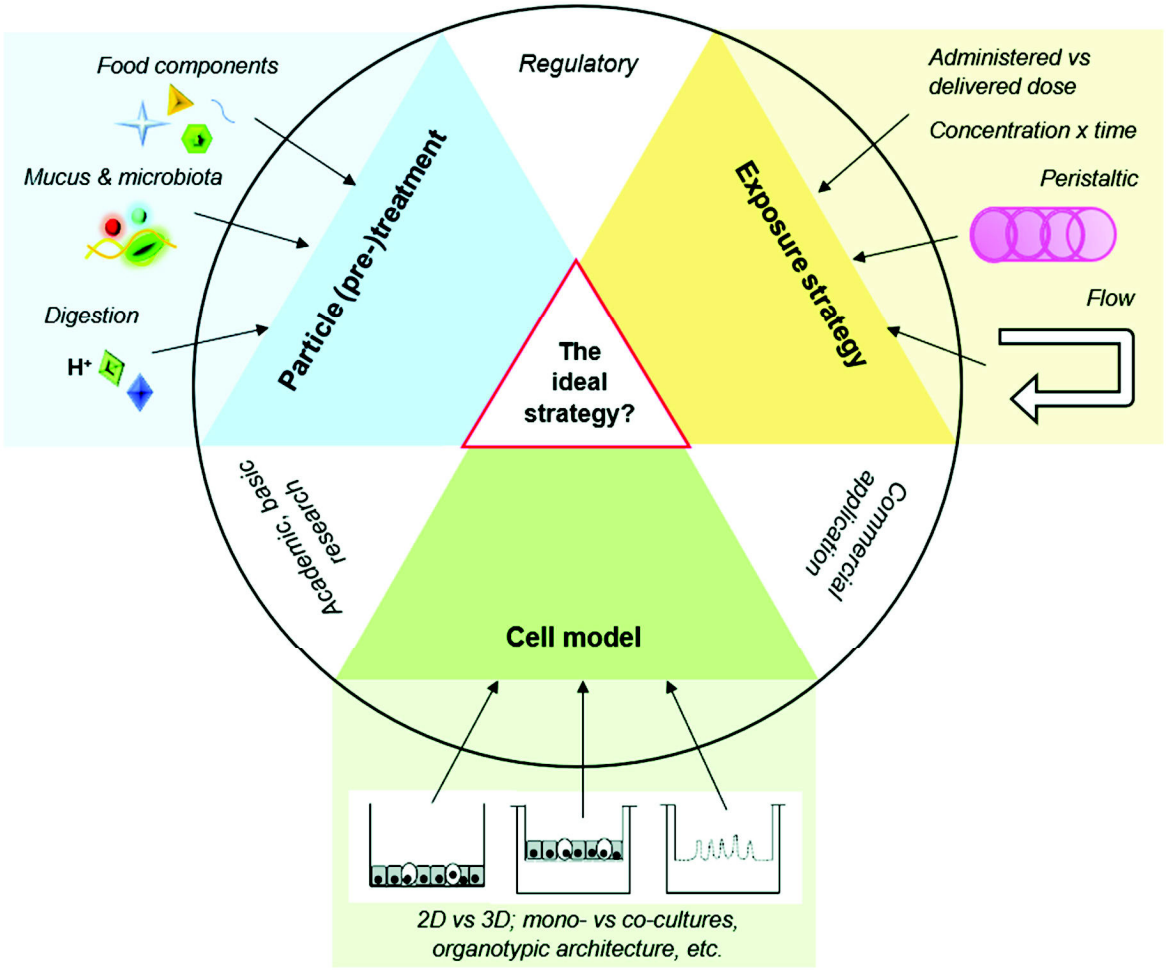

Figure 2.4 *In vitro* testing strategies and models for the evaluation of ENM effects on the intestine. A variety of advanced intestinal *in vitro* models and testing strategies has been developed to include morphological and physiological properties of the intestine that may influence the toxicity of ENM *in vivo*. The more individual factors of particle (pre-)treatment, exposure approach and cell system are incorporated, the more realistic and physiologically relevant the testing strategy becomes. On the downside, this increased complexity will inevitably affect the system's robustness and reproducibility. A testing strategy for nanosafety investigations of the intestine should be based on the research question; studies that specifically address health hazards of ENM may require different approaches than research efforts to unravel the fundamental interactions or toxicity mechanisms of nanomaterials or research that focuses on development of nanomedical applications. Combining various advanced models in integrated testing approach will further strengthen nanosafety research.

Funding

The work has received funding from the European Union's Horizon 2020 research and innovation programme under grant agreement number: 760813 (PATROLS, https://www.patrols-h2020.eu/). Mathias Busch is a grant recipient of the Jürgen Manchot Foundation.

2.6 References

(1) Oberdörster, G., Oberdörster, E. and Oberdörster, J. (2005) Nanotoxicology: An emerging discipline evolving from studies of ultrafine particles. *Environ. Health Perspect. 113*, 823–839.

(2) Donaldson, K., Tran, L., Jimenez, L. A., Duffin, R., Newby, D. E., Mills, N., MacNee, W. and Stone, V. (2005) Combustion-derived nanoparticles: a review of their toxicology following inhalation exposure. *Part. Fibre Toxicol. 2*, DOI: 10.1186/1743-8977-2-10.

(3) Stone, V., Miller, M. R., Clift, M. J. D., Elder, A., Mills, N. L., Møller, P., Schins, R. P. F., Vogel, U., Kreyling, W. G., Alstrup Jensen, K., Kuhlbusch, T. A. J., Schwarze, P. E., Hoet, P., Pietroiusti, A., Vizcaya-Ruiz, A. de, Baeza-Squiban, A., Teixeira, J. P., Tran, C. L. and Cassee, F. R. (2017) Nanomaterials Versus Ambient Ultrafine Particles: An Opportunity to Exchange Toxicology Knowledge. *Environ. Health Perspect. 125*, DOI: 10.1289/EHP424.

(4) Krug, H. and Kraegeloh, A. (2019) Nanosafety: Where Are We Now and Where Must We Go? *Chem. Res. Toxicol. 32*, 535.

(5) Powell, J. J., Ainley, C. C., Harvey, R. S., Mason, I. M., Kendall, M. D., Sankey, E. A., Dhillon, A. P. and Thompson, R. P. (1996) Characterisation of inorganic microparticles in pigment cells of human gut associated lymphoid tissue. *Gut 38*, 390–395.

(6) Powell, J. J., Harvey, R. S., Ashwood, P., Wolstencroft, R., Gershwin, M. E. and Thompson, R. P. (2000) Immune potentiation of ultrafine dietary particles in normal subjects and patients with inflammatory bowel disease. *J. Autoimmun. 14*, 99–105.

(7) Muralidharan, P., Malapit, M., Mallory, E., Hayes, D. and Mansour, H. M. (2015) Inhalable nanoparticulate powders for respiratory delivery. *Nanomedicine 11*, 1189–1199.

(8) Ramos, K., Ramos, L., Cámara, C. and Gómez-Gómez, M. M. (2014) Characterization and quantification of silver nanoparticles in nutraceuticals and beverages by asymmetric flow field flow fractionation coupled with inductively coupled plasma mass spectrometry. *J. Chromatogr. A 5*, 227–236.

(9) Sohal, I. S., O'Fallon, K. S., Gaines, P., Demokritou, P. and Bello, D. (2018) Ingested engineered nanomaterials: State of science in nanotoxicity testing and future research needs. *Part. Fibre Toxicol. 15*, DOI: 10.1186/s12989-018-0265-1.

(10) Carrouel, F., Viennot, S., Ottolenghi, L., Gaillard, C. and Bourgeois, D. (2020) Nanoparticles as Anti-Microbial, Anti-Inflammatory, and Remineralizing Agents in Oral Care Cosmetics: A Review of the Current Situation. *Nanomaterials 10*, DOI: 10.3390/nano10010140.

(11) Echegoyen, Y. and Nerín, C. (2013) Nanoparticle release from nano-silver antimicrobial food containers. *Food. Chem. Toxicol. 62*, 16–22.

(12) Mackevica, A., Olsson, M. E. and Hansen, S. F. (2016) Silver nanoparticle release from commercially available plastic food containers into food simulants. *J. Nanopart. Res. 18*, DOI: 10.1007/s11051-015-3313-x.

(13) Souza, V. G. L. and Fernando, A. L. (2016) Nanoparticles in food packaging: Biodegradability and potential migration to food—A review. *Food Packag. Shelf Life 8*, 63–70.

(14) Lomer, M. C. E., Thompson, R. P. H. and Powell, J. J. (2002) Fine and ultrafine particles of the diet: Influence on the mucosal immune response and association with Crohn's disease. *Proc. Nutr. Soc. 61*, 123–130.

(15) Lomer, M. C. E., Hutchinson, C., Volkert, S., Greenfield, S. M., Catterall, A., Thompson, R. P. H. and Powell, J. J. (2004) Dietary sources of inorganic microparticles and their intake in healthy subjects and patients with Crohn's disease. *Br. J. Nutr. 92*, 947–955.

(16) da Silva, A. B., Miniter, M., Thom, W., Hewitt, R. E., Wills, J., Jugdaohsingh, R. and Powell, J. J. (2020) Gastrointestinal absorption and toxicity of nanoparticles and microparticles: Myth, reality and pitfalls explored through titanium dioxide. *Curr. Opin. Toxicol. 19*, 112–120.

(17) EFSA (2016) Re-evaluation of titanium dioxide (E 171) as a food additive. *EFSA J. 14*, DOI: 10.2903/j.efsa.2016.4545.
(18) Dekkers, S., Krystek, P., Peters, R. J. B., Lankveld, D. P. K., Bokkers, B. G. H., van Hoeven-Arentzen, P. H., Bouwmeester, H. and Oomen, A. G. (2011) Presence and risks of nanosilica in food products. *Nanotoxicol. 5*, 393–405.
(19) Younes, M., Aggett, P., Aguilar, F., Crebelli, R., Dusemund, B., Filipič, M., Frutos, M. J., Galtier, P., Gott, D., Gundert-Remy, U., Kuhnle, G. G., Leblanc, J.-C., Lillegaard, I. T., Moldeus, P., Mortensen, A., Oskarsson, A., Stankovic, I., Waalkens-Berendsen, I., Woutersen, R. A., Wright, M., Boon, P., Chrysafidis, D., Gürtler, R., Mosesso, P., Parent-Massin, D., Tobback, P., Kovalkovicova, N., Rincon, A. M., Tard, A. and Lambré, C. (2018) Re-evaluation of silicon dioxide (E 551) as a food additive. *EFSA J. 16*, DOI: 10.2903/j.efsa.2018.5088.
(20) Moller, W., Felten, K., Sommerer, K., Scheuch, G., Meyer, G., Meyer, P., Haussinger, K. and Kreyling, W. G. (2008) Deposition, retention, and translocation of ultrafine particles from the central airways and lung periphery. *Am. J. Respir. Crit. Care Med. 177*, 426–432.
(21) Kreyling, W. G., Holzwarth, U., Schleh, C., Hirn, S., Wenk, A., Schäffler, M., Haberl, N., Semmler-Behnke, M. and Gibson, N. (2019) Quantitative biokinetics over a 28 day period of freshly generated, pristine, 20 nm titanium dioxide nanoparticle aerosols in healthy adult rats after a single two-hour inhalation exposure. *Part. Fibre Toxicol. 16*, DOI: 10.1186/s12989-019-0303-7.
(22) Bulte, J. W. M., Schmieder, A. H., Keupp, J., Caruthers, S. D., Wickline, S. A. and Lanza, G. M. (2014) MR cholangiography demonstrates unsuspected rapid biliary clearance of nanoparticles in rodents: implications for clinical translation. *Nanomedicine 10*, 1385–1388.
(23) Li, D., Morishita, M., Wagner, J. G., Fatouraie, M., Wooldridge, M., Eagle, W. E., Barres, J., Carlander, U., Emond, C. and Jolliet, O. (2015) *In vivo* biodistribution and physiologically based pharmacokinetic modeling of inhaled fresh and aged cerium oxide nanoparticles in rats. *Part. Fibre Toxicol. 13*, DOI: 10.1186/s12989-016-0156-2.
(24) Yang, L., Kuang, H., Zhang, W., Aguilar, Z. P., Wei, H. and Xu, H. (2017) Comparisons of the biodistribution and toxicological examinations after repeated intravenous administration of silver and gold nanoparticles in mice. *Sci. Rep. 7*, DOI: 10.1038/s41598-017-03015-1.
(25) Unfried, K., Albrecht, C., Klotz, L.-O., Mikecz, A. von, Grether-Beck, S. and Schins, R. P.F. (2009) Cellular responses to nanoparticles: Target structures and mechanisms. *Nanotoxicol. 1*, 52–71.
(26) Fubini, B., Ghiazza, M. and Fenoglio, I. (2010) Physico-chemical features of engineered nanoparticles relevant to their toxicity. *Nanotoxicol. 4*, 347–363.
(27) Oberdörster, G. and Graham, U. (2018) Predicting EMP hazard: Lessons from studies with inhaled fibrous and non-fibrous nano- and micro-particles. *Toxicol. Appl. Pharmacol. 361*, 50–61.
(28) Hewitt, R. E., Chappell, H. F. and Powell, J. J. (2020) Small and dangerous? Potential toxicity mechanisms of common exposure particles and nanoparticles. *Curr. Opin. Toxicol. 19*, 93–98.
(29) Riediker, M., Zink, D., Kreyling, W., Oberdörster, G., Elder, A., Graham, U., Lynch, I., Duschl, A., Ichihara, G., Ichihara, S., Kobayashi, T., Hisanaga, N., Umezawa, M., Cheng, T.-J., Handy, R., Gulumian, M., Tinkle, S. and Cassee, F. (2019) Particle toxicology and health - where are we? *Part. Fibre Toxicol. 16*, DOI: 10.1186/s12989-019-0302-8.
(30) Kendall, M., Ding, P., Mackay, R.-M., Deb, R., McKenzie, Z., Kendall, K., Madsen, J. and Clark, H. (2013) Surfactant protein D (SP-D) alters cellular uptake of particles and nanoparticles. *Nanotoxicol. 7*, 963–973.
(31) Wohlleben, W., Driessen, M. D., Raesch, S., Schaefer, U. F., Schulze, C., Vacano, B. von, Vennemann, A., Wiemann, M., Ruge, C. A., Platsch, H., Mues, S., Ossig, R., Tomm, J. M., Schnekenburger, J., Kuhlbusch, T. A. J., Luch, A., Lehr, C.-M. and Haase, A. (2016)

Influence of agglomeration and specific lung lining lipid/protein interaction on short-term inhalation toxicity. *Nanotoxicol. 10*, 970–980.
(32) Thongkam, W., Gerloff, K., van Berlo, D., Albrecht, C. and Schins, R. P. F. (2017) Oxidant generation, DNA damage and cytotoxicity by a panel of engineered nanomaterials in three different human epithelial cell lines. *Mutagenesis 32*, 105–115.
(33) Kreuter, J. (1991) Peroral administration of nanoparticles. *Adv. Drug. Deliv. Rev. 7*, 71–86.
(34) Munger, M. A., Radwanski, P., Hadlock, G. C., Stoddard, G., Shaaban, A., Falconer, J., Grainger, D. W. and Deering-Rice, C. E. (2014) *In vivo* human time-exposure study of orally dosed commercial silver nanoparticles. *Nanomedicine 10*, 1–9.
(35) van der Zande, M., Vandebriel, R. J., van Doren, E., Kramer, E., Herrera Rivera, Z., Serrano-Rojero, C. S., Gremmer, E. R., Mast, J., Peters, R. J. B. and Hollman, P. C. H. (2012) Distribution, elimination, and toxicity of silver nanoparticles and silver ions in rats after 28-day oral exposure. *ACS Nano 6*, 7427–7442.
(36) Pele, L. C., Thoree, V., Bruggraber, S. F. A., Koller, D., Thompson, R. P. H., Lomer, M. C. and Powell, J. J. (2015) Pharmaceutical/food grade titanium dioxide particles are absorbed into the bloodstream of human volunteers. *Part. Fibre Toxicol. 12*, DOI: 10.1186/s12989-015-0101-9.
(37) Kreyling, W., Holzwarth, U., Schleh, C., Kozempel, J., Wenk, A., Haberl, N., Hirn, S., Schäffler, M., Lipka, J., Semmler-Behnke, M. and Gibson, N. (2017) Quantitative biokinetics of titanium dioxide nanoparticles after oral application in rats: Part 2. *Nanotoxicol. 11*, 443–453.
(38) Eleftheriadou, M., Pyrgiotakis, G. and Demokritou, P. (2017) Nanotechnology to the rescue: using nano-enabled approaches in microbiological food safety and quality. *Curr. Opin. Biotechnol. 44*, 87–93.
(39) Bouwmeester, H., van der Zande, M. and Jepson, M. A. (2018) Effects of food-borne nanomaterials on gastrointestinal tissues and microbiota. *Wiley Interdiscip. Rev. Nanomed. Nanobiotechnol. 10*, DOI: 10.1002/wnan.1481.
(40) Dusinska, M., Boland, S., Saunders, M., Juillerat-Jeanneret, L., Tran, L., Pojana, G., Marcomini, A., Volkovova, K., Tulinska, J., Knudsen, L. E., Gombau, L., Whelan, M., Collins, A. R., Marano, F., Housiadas, C., Bilanicova, D., Halamoda Kenzaoui, B., Correia Carreira, S., Magdolenova, Z., Fjellsbø, L. M., Huk, A., Handy, R., Walker, L., Barancokova, M., Bartonova, A., Burello, E., Castell, J., Cowie, H., Drlickova, M., Guadagnini, R., Harris, G., Harju, M., Heimstad, E. S., Hurbankova, M., Kazimirova, A., Kovacikova, Z., Kuricova, M., Liskova, A., Milcamps, A., Neubauerova, E., Palosaari, T., Papazafiri, P., Pilou, M., Poulsen, M. S., Ross, B., Runden-Pran, E., Sebekova, K., Staruchova, M., Vallotto, D. and Worth, A. (2015) Towards an alternative testing strategy for nanomaterials used in nanomedicine: lessons from NanoTEST. *Nanotoxicol. 9*, 118–132.
(41) Kermanizadeh, A., Gosens, I., MacCalman, L., Johnston, H., Danielsen, P. H., Jacobsen, N. R., Lenz, A.-G., Fernandes, T., Schins, R. P. F., Cassee, F. R., Wallin, H., Kreyling, W., Stoeger, T., Loft, S., Møller, P., Tran, L. and Stone, V. (2016) A Multilaboratory Toxicological Assessment of a Panel of 10 Engineered Nanomaterials to Human Health—ENPRA Project—The Highlights, Limitations, and Current and Future Challenges. *J. Toxicol. Environ. Health Part B Crit. Rev. 19*, 1–28.
(42) Cohen, J. M., Beltran-Huarac, J., Pyrgiotakis, G. and Demokritou, P. (2018) Effective delivery of sonication energy to fast settling and agglomerating nanomaterial suspensions for cellular studies: Implications for stability, particle kinetics, dosimetry and toxicity. *NanoImpact 10*, 81–86.
(43) Oomen, A. G., Bos, P. M. J., Fernandes, T. F., Hund-Rinke, K., Boraschi, D., Byrne, H. J., Aschberger, K., Gottardo, S., Kammer, F. von der, Kühnel, D., Hristozov, D., Marcomini, A., Migliore, L., Scott-Fordsmand, J., Wick, P. and Landsiedel, R. (2014) Concern-driven

integrated approaches to nanomaterial testing and assessment—report of the NanoSafety Cluster Working Group 10. *Nanotoxicol. 8*, 334–348.
(44) Stone, V., Johnston, H. and Schins, R. P. F. (2009) Development of *in vitro* systems for nanotoxicology: Methodological considerations. *Crit. Rev. Toxicol. 39*, 613–626.
(45) Guadagnini, R., Halamoda Kenzaoui, B., Walker, L., Pojana, G., Magdolenova, Z., Bilanicova, D., Saunders, M., Juillerat-Jeanneret, L., Marcomini, A., Huk, A., Dusinska, M., Fjellsbø, L. M., Marano, F. and Boland, S. (2015) Toxicity screenings of nanomaterials: challenges due to interference with assay processes and components of classic *in vitro* tests. *Nanotoxicol. 9*, 13–24.
(46) Puzyn, T., Rasulev, B., Gajewicz, A., Hu, X., Dasari, T. P., Michalkova, A., Hwang, H.-M., Toropov, A., Leszczynska, D. and Leszczynski, J. (2011) Using nano-QSAR to predict the cytotoxicity of metal oxide nanoparticles. *Nat. Nanotechnol. 6*, 175–178.
(47) Landsiedel, R., Sauer, U. G., Ma-Hock, L., Schnekenburger, J. and Wiemann, M. (2014) Pulmonary toxicity of nanomaterials: a critical comparison of published *in vitro* assays and *in vivo* inhalation or instillation studies. *Nanomed. (Lond.) 9*, 2557–2585.
(48) Wiemann, M., Sauer, U. G., Vennemann, A., Bäcker, S., Keller, J.-G., Ma-Hock, L., Wohlleben, W. and Landsiedel, R. (2018) *In Vitro* and *In Vivo* Short-Term Pulmonary Toxicity of Differently Sized Colloidal Amorphous SiO_2. *Nanomaterials 8*, DOI: 10.3390/nano8030160.
(49) Monopoli, M. P., Walczyk, D., Campbell, A., Elia, G., Lynch, I., Baldelli Bombelli, F. and Dawson, K. A. (2011) Physical−Chemical Aspects of Protein Corona: Relevance to *in Vitro* and *in Vivo* Biological Impacts of Nanoparticles. *J. Am. Chem. Soc. 133*, 2525–2534.
(50) Durán, N., Silveira, C. P., Durán, M. and Martinez, D. S. T. (2015) Silver nanoparticle protein corona and toxicity: A mini-review. *J. Nanobiotechnology 13*, DOI: 10.1186/s12951-015-0114-4.
(51) Clift, M. J. D., Gehr, P. and Rothen-Rutishauser, B. (2011) Nanotoxicology: a perspective and discussion of whether or not *in vitro* testing is a valid alternative. *Arch. Toxicol. 85*, 723–731.
(52) Burden, N., Aschberger, K., Chaudhry, Q., Clift, M. J. D., Fowler, P., Johnston, H., Landsiedel, R., Rowland, J., Stone, V. and Doak, S. H. (2017) Aligning nanotoxicology with the 3Rs: What is needed to realise the short, medium and long-term opportunities? *Regul. Toxicol. Pharmacol. 91*, 257–266.
(53) Rothen-Rutishauser, B., Blank, F., Mühlfeld, C. and Gehr, P. (2008) *In vitro* models of the human epithelial airway barrier to study the toxic potential of particulate matter. *Expert Opin. Drug Metab. Toxicol. 4*, 1075–1089.
(54) Fröhlich, E., Bonstingl, G., Höfler, A., Meindl, C., Leitinger, G., Pieber, T. R. and Roblegg, E. (2013) Comparison of two *in vitro* systems to assess cellular effects of nanoparticles-containing aerosols. *Toxicol. In Vitro 27*, 409–417.
(55) Lenz, A.-G., Karg, E., Brendel, E., Hinze-Heyn, H., Maier, K. L., Eickelberg, O., Stoeger, T. and Schmid, O. (2013) Inflammatory and oxidative stress responses of an alveolar epithelial cell line to airborne zinc oxide nanoparticles at the air-liquid interface: a comparison with conventional, submerged cell-culture conditions. *Biomed Res. Int. 2013*, DOI: 10.1155/2013/652632.
(56) Durantie, E., Vanhecke, D., Rodriguez-Lorenzo, L., Delhaes, F., Balog, S., Septiadi, D., Bourquin, J., Petri-Fink, A. and Rothen-Rutishauser, B. (2017) Biodistribution of single and aggregated gold nanoparticles exposed to the human lung epithelial tissue barrier at the air-liquid interface. *Part. Fibre Toxicol. 14*, DOI: 10.1186/s12989-017-0231-3.
(57) Alepee, N., Bahinski, A., Daneshian, M., Wever, B. de, Fritsche, E., Goldberg, A., Hansmann, J., Hartung, T., Haycock, J., Hogberg, H., Hoelting, L., Kelm, J. M., Kadereit, S., McVey, E., Landsiedel, R., Leist, M., Lubberstedt, M., Noor, F., Pellevoisin, C., Petersohn, D., Pfannenbecker, U., Reisinger, K., Ramirez, T., Rothen-Rutishauser, B.,

Schafer-Korting, M., Zeilinger, K. and Zurich, M.-G. (2014) State-of-the-art of 3D cultures (organs-on-a-chip) in safety testing and pathophysiology. *ALTEX 31*, 441–477.
(58) Swidsinski, A., Sydora, B. C., Doerffel, Y., Loening-Baucke, V., Vaneechoutte, M., Lupicki, M., Scholze, J., Lochs, H. and Dieleman, L. A. (2007) Viscosity gradient within the mucus layer determines the mucosal barrier function and the spatial organization of the intestinal microbiota. *Inflamm. Bowel Dis. 13*, 963–970.
(59) Latorre, R., Sternini, C., Giorgio, R. de and Greenwood-Van Meerveld, B. (2016) Enteroendocrine cells: a review of their role in brain-gut communication. *Neurogastroenterol. Motil. 28*, 620–630.
(60) Go, M.-R., Bae, S.-H., Kim, H.-J., Yu, J. and Choi, S.-J. (2017) Interactions between Food Additive Silica Nanoparticles and Food Matrices. *Front. Microbiol. 8*, DOI: 10.3389/fmicb.2017.01013.
(61) Wu, N., Fu, L., Su, M., Aslam, M., Wong, K. C. and Dravid, V. P. (2004) Interaction of Fatty Acid Monolayers with Cobalt Nanoparticles. *Nano Lett. 4*, 383–386.
(62) Lemarchand, C., Gref, R., Passirani, C., Garcion, E., Petri, B., Müller, R., Costantini, D. and Couvreur, P. (2006) Influence of polysaccharide coating on the interactions of nanoparticles with biological systems. *Biomaterials 27*, 108–118.
(63) Levard, C., Mitra, S., Yang, T., Jew, A. D., Badireddy, A. R., Lowry, G. V. and Brown, G. E. (2013) Effect of chloride on the dissolution rate of silver nanoparticles and toxicity to E. coli. *Environ. Sci. Technol. 47*, 5738–5745.
(64) Loza, K., Diendorf, J., Sengstock, C., Ruiz-Gonzalez, L., Gonzalez-Calbet, J. M., Vallet-Regi, M., Köller, M. and Epple, M. (2014) The dissolution and biological effects of silver nanoparticles in biological media. *J. Mater. Chem. B 2*, 1634–1643.
(65) Pamies, R., Cifre, J. G. H., Espín, V. F., Collado-González, M., Baños, F. G. D. and La Torre, J. G. de (2014) Aggregation behaviour of gold nanoparticles in saline aqueous media. *J. Nanopart. Res. 16*, DOI: 10.1007/s11051-014-2376-4.
(66) Tenzer, S., Docter, D., Kuharev, J., Musyanovych, A., Fetz, V., Hecht, R., Schlenk, F., Fischer, D., Kiouptsi, K., Reinhardt, C., Landfester, K., Schild, H., Maskos, M., Knauer, S. K. and Stauber, R. H. (2013) Rapid formation of plasma protein corona critically affects nanoparticle pathophysiology. *Nat. Nanotechnol. 8*, 772–781.
(67) Docter, D., Distler, U., Storck, W., Kuharev, J., Wünsch, D., Hahlbrock, A., Knauer, S. K., Tenzer, S. and Stauber, R. H. (2014) Quantitative profiling of the protein coronas that form around nanoparticles. *Nat. Protoc. 9*, 2030–2044.
(68) Chen, H., Zhao, R., Wang, B., Cai, C., Zheng, L., Wang, H., Wang, M., Ouyang, H., Zhou, X. and Chai, Z. (2017) The effects of orally administered Ag, TiO_2 and SiO_2 nanoparticles on gut microbiota composition and colitis induction in mice. *NanoImpact 8*, 80–88.
(69) Pereira, M. T., Malik, M., Nostro, J. A., Mahler, G. J. and Musselman, L. P. (2018) Effect of dietary additives on intestinal permeability in both Drosophila and a human cell co-culture. *Dis. Model. Mech. 11*, DOI: 10.1242/dmm.034520.
(70) Cao, Y., Roursgaard, M., Kermanizadeh, A., Loft, S. and Møller, P. (2015) Synergistic effects of zinc oxide nanoparticles and Fatty acids on toxicity to caco-2 cells. *Int. J. Toxicol. 34*, 67–76.
(71) Lichtenstein, D., Ebmeyer, J., Knappe, P., Juling, S., Böhmert, L., Selve, S., Niemann, B., Braeuning, A., Thünemann, A. F. and Lampen, A. (2015) Impact of food components during *in vitro* digestion of silver nanoparticles on cellular uptake and cytotoxicity in intestinal cells. *Biol. Chem. 396*, 1255–1264.
(72) Zhang, Z., Zhang, R., Xiao, H., Bhattacharya, K., Bitounis, D., Demokritou, P. and McClements, D. J. (2019) Development of a standardized food model for studying the impact of food matrix effects on the gastrointestinal fate and toxicity of ingested nanomaterials. *NanoImpact 13*, 13–25.
(73) Carpenter, G. H. (2013) The secretion, components, and properties of saliva. *Annu. Rev. Food Sci. Technol. 4*, 267–276.

(74) Kong, F. and Singh, R. P. (2008) Disintegration of solid foods in human stomach. *J. Food Sci. 73*, R67-80.
(75) Knight, J., Williams, N. and Nigam, Y. (2019) Gastrointestinal tract 3: the duodenum, liver and pancreas. *Nurs. Times 115*, 56–60.
(76) Berg, J. M., Romoser, A., Banerjee, N., Zebda, R. and Sayes, C. M. (2009) The relationship between pH and zeta potential of ~ 30 nm metal oxide nanoparticle suspensions relevant to *in vitro* toxicological evaluations. *Nanotoxicol. 3*, 276–283.
(77) Eigenheer, R., Castellanos, E. R., Nakamoto, M. Y., Gerner, K. T., Lampe, A. M. and Wheeler, K. E. (2014) Silver nanoparticle protein corona composition compared across engineered particle properties and environmentally relevant reaction conditions. *Environ. Sci. Nano 1*, 238–247.
(78) Chanana, M., Rivera Gil, P., Correa-Duarte, M. A., Liz-Marzán, L. M. and Parak, W. J. (2013) Physicochemical properties of protein-coated gold nanoparticles in biological fluids and cells before and after proteolytic digestion. *Angew. Chem. Int. Ed. 52*, 4179–4183.
(79) Peretyazhko, T. S., Zhang, Q. and Colvin, V. L. (2014) Size-controlled dissolution of silver nanoparticles at neutral and acidic pH conditions: kinetics and size changes. *Environ. Sci. Technol. 48*, 11954–11961.
(80) Khan, R., Inam, M. A., Zam Zam, S., Akram, M., Shin, S. and Yeom, I. T. (2019) Coagulation and Dissolution of CuO Nanoparticles in the Presence of Dissolved Organic Matter Under Different pH Values. *Sustainability 11*, DOI: 10.3390/su11102825.
(81) Avramescu, M.-L., Rasmussen, P. E., Chénier, M. and Gardner, H. D. (2017) Influence of pH, particle size and crystal form on dissolution behaviour of engineered nanomaterials. *Environ. Sci. Pollut. Res. Int. 24*, 1553–1564.
(82) Sieg, H., Kästner, C., Krause, B., Meyer, T., Burel, A., Böhmert, L., Lichtenstein, D., Jungnickel, H., Tentschert, J., Laux, P., Braeuning, A., Estrela-Lopis, I., Gauffre, F., Fessard, V., Meijer, J., Luch, A., Thünemann, A. F. and Lampen, A. (2017) Impact of an Artificial Digestion Procedure on Aluminum-Containing Nanomaterials. *Langmuir 33*, 10726–10735.
(83) Gerloff, K., Pereira, D. I. A., Faria, N., Boots, A. W., Kolling, J., Förster, I., Albrecht, C., Powell, J. J. and Schins, R. P. F. (2013) Influence of simulated gastrointestinal conditions on particle-induced cytotoxicity and interleukin-8 regulation in differentiated and undifferentiated Caco-2 cells. *Nanotoxicol. 7*, 353–366.
(84) Versantvoort, C. H. M., Oomen, A. G., van de Kamp, E., Rompelberg, C. J. M. and Sips, A. J. A. M. (2005) Applicability of an *in vitro* digestion model in assessing the bioaccessibility of mycotoxins from food. *Food. Chem. Toxicol. 43*, 31–40.
(85) Dudefoi, W., Moniz, K., Allen-Vercoe, E., Ropers, M.-H. and Walker, V. K. (2017) Impact of food grade and nano-TiO_2 particles on a human intestinal community. *Food. Chem. Toxicol. 106*, 242–249.
(86) Markell, L. K., Wezalis, S. M., Roper, J. M., Zimmermann, C. and Delaney, B. (2017) Incorporation of *in vitro* digestive enzymes in an intestinal epithelial cell line model for protein hazard identification. *Toxicol. In Vitro 44*, 85–93.
(87) Guyton, A. C., and Hall, J. E., Eds. (2005) Textbook of Medical Physiology, 11th ed., Saunders: Philadelphia, PA.
(88) Tharakan, A., Norton, I. T., Fryer, P. J. and Bakalis, S. (2010) Mass transfer and nutrient absorption in a simulated model of small intestine. *J. Food Sci. 75*, 339-346.
(89) Minekus, M. (2015) The TNO Gastro-Intestinal Model (TIM), Springer, Cham (CH), http://europepmc.org/books/NBK500162.
(90) Jochems, P. G. M., van Bergenhenegouwen, J., van Genderen, A. M., Eis, S. T., Wilod Versprille, L. J. F., Wichers, H. J., Jeurink, P. V., Garssen, J. and Masereeuw, R. (2019) Development and validation of bioengineered intestinal tubules for translational research aimed at safety and efficacy testing of drugs and nutrients. *Toxicol. In Vitro 60*, 1–11.

(91) Pocock, K., Delon, L., Bala, V., Rao, S., Priest, C., Prestidge, C. and Thierry, B. (2017) Intestine-on-a-Chip Microfluidic Model for Efficient *in Vitro* Screening of Oral Chemotherapeutic Uptake. *ACS Biomater. Sci. Eng. 3*, 951–959.
(92) Navabi, N., McGuckin, M. A. and Lindén, S. K. (2013) Gastrointestinal cell lines form polarized epithelia with an adherent mucus layer when cultured in semi-wet interfaces with mechanical stimulation. *PLoS One 8*, DOI: 10.1371/journal.pone.0068761.
(93) Kasendra, M., Tovaglieri, A., Sontheimer-Phelps, A., Jalili-Firoozinezhad, S., Bein, A., Chalkiadaki, A., Scholl, W., Zhang, C., Rickner, H. and Richmond, C. A. (2018) Development of a primary human Small Intestine-on-a-Chip using biopsy-derived organoids. *Sci. Rep. 8*, DOI: 10.1038/s41598-018-21201-7.
(94) Crater, J. S. and Carrier, R. L. (2010) Barrier properties of gastrointestinal mucus to nanoparticle transport. *Macromol. Biosci. 10*, 1473–1483.
(95) Bhattacharjee, S., Mahon, E., Harrison, S. M., McGetrick, J., Muniyappa, M., Carrington, S. D. and Brayden, D. J. (2017) Nanoparticle passage through porcine jejunal mucus: Microfluidics and rheology. *Nanomedicine 13*, 863–873.
(96) Walczak, A. P., Kramer, E., Hendriksen, P. J. M., Tromp, P., Helsper, J. P. F. G., van der Zande, M., Rietjens, I. M. C. M. and Bouwmeester, H. (2015) Translocation of differently sized and charged polystyrene nanoparticles in *in vitro* intestinal cell models of increasing complexity. *Nanotoxicol. 9*, 453–461.
(97) Lozoya-Agullo, I., Araújo, F., González-Álvarez, I., Merino-Sanjuán, M., González-Álvarez, M., Bermejo, M. and Sarmento, B. (2017) Usefulness of Caco-2/HT29-MTX and Caco-2/HT29-MTX/Raji B Coculture Models To Predict Intestinal and Colonic Permeability Compared to Caco-2 Monoculture. *Mol. Pharm. 14*, 1264–1270.
(98) Lock, J. Y., Carlson, T. L. and Carrier, R. L. (2018) Mucus models to evaluate the diffusion of drugs and particles. *Adv. Drug. Deliv. Rev. 124*, 34–49.
(99) Lloyd-Price, J., Arze, C., Ananthakrishnan, A. N., Schirmer, M., Avila-Pacheco, J., Poon, T. W., Andrews, E., Ajami, N. J., Bonham, K. S. and Brislawn, C. J. (2019) Multi-omics of the gut microbial ecosystem in inflammatory bowel diseases. *Nature 569*, 655–662.
(100) Sampson, T. R., Debelius, J. W., Thron, T., Janssen, S., Shastri, G. G., Ilhan, Z. E., Challis, C., Schretter, C. E., Rocha, S., Gradinaru, V., Chesselet, M.-F., Keshavarzian, A., Shannon, K. M., Krajmalnik-Brown, R., Wittung-Stafshede, P., Knight, R. and Mazmanian, S. K. (2016) Gut Microbiota Regulate Motor Deficits and Neuroinflammation in a Model of Parkinson's Disease. *Cell 167*, 1469-1480.
(101) Naseribafrouei, A., Hestad, K., Avershina, E., Sekelja, M., Linløkken, A., Wilson, R. and Rudi, K. (2014) Correlation between the human fecal microbiota and depression. *Neurogastroenterol. Motil. 26*, 1155–1162.
(102) van den Brûle, S., Ambroise, J., Lecloux, H., Levard, C., Soulas, R., Temmerman, P.-J. de, Palmai-Pallag, M., Marbaix, E. and Lison, D. (2015) Dietary silver nanoparticles can disturb the gut microbiota in mice. *Part. Fibre Toxicol. 13*, DOI: 10.1186/s12989-016-0149-1.
(103) Williams, K., Milner, J., Boudreau, M. D., Gokulan, K., Cerniglia, C. E. and Khare, S. (2015) Effects of subchronic exposure of silver nanoparticles on intestinal microbiota and gut-associated immune responses in the ileum of Sprague-Dawley rats. *Nanotoxicol. 9*, 279–289.
(104) Wilding, L. A., Bassis, C. M., Walacavage, K., Hashway, S., Leroueil, P. R., Morishita, M., Maynard, A. D., Philbert, M. A. and Bergin, I. L. (2016) Repeated dose (28-day) administration of silver nanoparticles of varied size and coating does not significantly alter the indigenous murine gut microbiome. *Nanotoxicol. 10*, 513–520.
(105) Merrifield, D. L., Shaw, B. J., Harper, G. M., Saoud, I. P., Davies, S. J., Handy, R. D. and Henry, T. B. (2013) Ingestion of metal-nanoparticle contaminated food disrupts endogenous microbiota in zebrafish (Danio rerio). *Environ. Pollut. 174*, 157–163.

(106) Auguste, M., Lasa, A., Pallavicini, A., Gualdi, S., Vezzulli, L. and Canesi, L. (2019) Exposure to TiO_2 nanoparticles induces shifts in the microbiota composition of Mytilus galloprovincialis hemolymph. *Sci. Total. Environ. 670*, 129–137.
(107) Clift, M. J. D., Raemy, D. O., Endes, C., Ali, Z., Lehmann, A. D., Brandenberger, C., Petri-Fink, A., Wick, P., Parak, W. J., Gehr, P., Schins, R. P. F. and Rothen-Rutishauser, B. (2013) Can the Ames test provide an insight into nano-object mutagenicity? Investigating the interaction between nano-objects and bacteria. *Nanotoxicol. 7*, 1373–1385.
(108) Westmeier, D., Posselt, G., Hahlbrock, A., Bartfeld, S., Vallet, C., Abfalter, C., Docter, D., Knauer, S. K., Wessler, S. and Stauber, R. H. (2018) Nanoparticle binding attenuates the pathobiology of gastric cancer-associated Helicobacter pylori. *Nanoscale 10*, 1453–1463.
(109) Stauber, R. H., Siemer, S., Becker, S., Ding, G.-B., Strieth, S. and Knauer, S. K. (2018) Small Meets Smaller: Effects of Nanomaterials on Microbial Biology, Pathology, and Ecology. *ACS Nano 12*, 6351–6359.
(110) Westmeier, D., Hahlbrock, A., Reinhardt, C., Fröhlich-Nowoisky, J., Wessler, S., Vallet, C., Pöschl, U., Knauer, S. K. and Stauber R H (2018) Nanomaterial–microbe cross-talk: physicochemical principles and (patho)biological consequences. *Chem. Soc. Rev. 47*, 5312–5337.
(111) Kononenko, V., Narat, M. and Drobne, D. (2015) Nanoparticle interaction with the immune system. *Arh. Hig. Rada. Toksikol. 66*, 97–108.
(112) Shi, N., Li, N., Duan, X. and Niu, H. (2017) Interaction between the gut microbiome and mucosal immune system. *Mil. Med. Res. 4*, DOI: 10.1186/s40779-017-0122-9.
(113) Petrof, E. O., Gloor, G. B., Vanner, S. J., Weese, S. J., Carter, D., Daigneault, M. C., Brown, E. M., Schroeter, K. and Allen-Vercoe, E. (2013) Stool substitute transplant therapy for the eradication of Clostridium difficile infection: 'RePOOPulating' the gut. *Microbiome 1*, DOI: 10.1186/2049-2618-1-3.
(114) Vamanu, E., Ene, M., Biță, B., Ionescu, C., Crăciun, L. and Sârbu, I. (2018) *In Vitro* Human Microbiota Response to Exposure to Silver Nanoparticles Biosynthesized with Mushroom Extract. *Nutrients 10*, DOI: 10.3390/nu10050607.
(115) Liu, L., Firrman, J., Tanes, C., Bittinger, K., Thomas-Gahring, A., Wu, G. D., van den Abbeele, P. and Tomasula, P. M. (2018) Establishing a mucosal gut microbial community *in vitro* using an artificial simulator. *PLoS One 13*, DOI: 10.1371/journal.pone.0197692.
(116) Garuglieri, E., Meroni, E., Cattò, C., Villa, F., Cappitelli, F. and Erba, D. (2017) Effects of Sub-lethal Concentrations of Silver Nanoparticles on a Simulated Intestinal Prokaryotic-Eukaryotic Interface. *Front. Microbiol. 8*, DOI: 10.3389/fmicb.2017.02698.
(117) Cattò, C., Garuglieri, E., Borruso, L., Erba, D., Casiraghi, M. C., Cappitelli, F., Villa, F., Zecchin, S. and Zanchi, R. (2019) Impacts of dietary silver nanoparticles and probiotic administration on the microbiota of an *in vitro* gut model. *Environ. Pollut. 245*, 754–763.
(118) Richter, J. W., Shull, G. M., Fountain, J. H., Guo, Z., Musselman, L. P., Fiumera, A. C. and Mahler, G. J. (2018) Titanium dioxide nanoparticle exposure alters metabolic homeostasis in a cell culture model of the intestinal epithelium and Drosophila melanogaster. *Nanotoxicol. 12*, 390–406.
(119) Kim, H. J., Lee, J., Choi, J.-H., Bahinski, A. and Ingber, D. E. (2016) Co-culture of Living Microbiome with Microengineered Human Intestinal Villi in a Gut-on-a-Chip Microfluidic Device. *J. Vis. Exp.*, DOI: 10.3791/54344.
(120) Shin, W., Wu, A., Massidda, M., Foster, C., Thomas, N., Lee, D.-W., Koh, H. and Kim, H. J. (2019) A robust longitudinal co-culture of obligate anaerobic gut microbiome with human intestinal epithelium in an anoxic-oxic interface-on-a-chip. *Front. Bioeng. Biotechnol. 7*, DOI: 10.3389/fbioe.2019.00013.
(121) Walter, E., Janich, S., Roessler, B. J., Hilfinger, J. M. and Amidon, G. L. (1996) HT29-MTX/Caco-2 cocultures as an *in vitro* model for the intestinal epithelium: *In vitro–in vivo* correlation with permeability data from rats and humans. *J. Pharm. Sci. 85*, 1070–1076.

(122) Nash, S., Parkos, C., Nusrat, A., Delp, C. and Madara, J. L. (1991) *In vitro* model of intestinal crypt abscess. A novel neutrophil-derived secretagogue activity. *J. Clin. Invest. 87*, 1474–1477.
(123) Bisping, G., Lügering, N., Lütke-Brintrup, S., Pauels, H.-G., Schürmann, G., Domschke, W. and Kucharzik, T. (2001) Patients with inflammatory bowel disease (IBD) reveal increased induction capacity of intracellular interferon-gamma (IFN-γ) in peripheral CD8+ lymphocytes co-cultured with intestinal epithelial cells. *Clin. Exp. Immunol. 123*, 15–22.
(124) Kernéis, S., Bogdanova, A., Kraehenbuhl, J.-P. and Pringault, E. (1997) Conversion by Peyer's patch lymphocytes of human enterocytes into M cells that transport bacteria. *Science 277*, 949–952.
(125) Kobayashi, N., Takahashi, D., Takano, S., Kimura, S. and Hase, K. (2019) The Roles of Peyer's Patches and Microfold Cells in the Gut Immune System: Relevance to Autoimmune Diseases. *Front. Immunol. 10*, DOI: 10.3389/fimmu.2019.02345.
(126) Powell, J. J., Faria, N., Thomas-McKay, E. and Pele, L. C. (2010) Origin and fate of dietary nanoparticles and microparticles in the gastrointestinal tract. *J. Autoimmun. 34*, 226-233.
(127) Kanaya, T., Hase, K., Takahashi, D., Fukuda, S., Hoshino, K., Sasaki, I., Hemmi, H., Knoop, K. A., Kumar, N., Sato, M., Katsuno, T., Yokosuka, O., Toyooka, K., Nakai, K., Sakamoto, A., Kitahara, Y., Jinnohara, T., McSorley, S. J., Kaisho, T., Williams, I. R. and Ohno, H. (2012) The Ets transcription factor Spi-B is essential for the differentiation of intestinal microfold cells. *Nat. Immunol. 13*, 729–736.
(128) Watanabe, F., Satsu, H., Mochizuki, T., Nakano, T. and Shimizu, M. (2004) Development of the method for evaluating protective effect of food factors on THP-1-induced damage to human intestinal Caco-2 monolayers. *BioFactors 21*, 145–147.
(129) Trapecar, M., Goropevsek, A., Gorenjak, M., Gradisnik, L. and Slak Rupnik, M. (2014) A co-culture model of the developing small intestine offers new insight in the early immunomodulation of enterocytes and macrophages by Lactobacillus spp. through STAT1 and NF-kB p65 translocation. *PLoS One 9*, DOI: 10.1371/journal.pone.0086297.
(130) Esch, M. B., Mahler, G. J., Stokol, T. and Shuler, M. L. (2014) Body-on-a-chip simulation with gastrointestinal tract and liver tissues suggests that ingested nanoparticles have the potential to cause liver injury. *Lab Chip 14*, 3081–3092.
(131) Maschmeyer, I., Lorenz, A. K., Schimek, K., Hasenberg, T., Ramme, A. P., Hübner, J., Lindner, M., Drewell, C., Bauer, S., Thomas, A., Sambo, N. S., Sonntag, F., Lauster, R. and Marx, U. (2015) A four-organ-chip for interconnected long-term co-culture of human intestine, liver, skin and kidney equivalents. *Lab Chip 15*, 2688–2699.
(132) Phillips, T. E., Huet, C., Bilbo P R, Podolsky D K, Louvard, D. and Neutra, M. R. (1988) Human Intestinal Goblet Cells in Monolayer Culture: Characterization of a Mucus-Secreting Subclone Derived From the HT29 Colon Adenocarcinoma Cell Line. *Gastroenterology 94*, 1390–1403.
(133) Hilgers, A. R., Conradi, R. A. and Burton, P. S. (1990) Caco-2 cell monolayers as a model for drug transport across the intestinal mucosa. *Pharm. Res. 7*, 902–910.
(134) Bailey, C. A., Bryla, P. and Malick, A. W. (1996) The use of the intestinal epithelial cell culture model, Caco-2, in pharmaceutical development. *Adv. Drug. Deliv. Rev. 22*, 85–103.
(135) Yamashita, S., Furubayashi, T., Kataoka, M., Sakane, T., Sezaki, H. and Tokuda, H. (2000) Optimized conditions for prediction of intestinal drug permeability using Caco-2 cells. *Eur. J. Pharm. Sci. 10*, 195–204.
(136) Chen, Y., Lin, Y., Davis, K. M., Wang, Q., Rnjak-Kovacina, J., Li, C., Isberg, R. R., Kumamoto, C. A., Mecsas, J. and Kaplan, D. L. (2015) Robust bioengineered 3D functional human intestinal epithelium. *Sci. Rep. 5*, DOI: 10.1038/srep13708.
(137) Yamaura, Y., Chapron, B. D., Wang, Z., Himmelfarb, J. and Thummel, K. E. (2016) Functional comparison of human colonic carcinoma cell lines and primary small intestinal

epithelial cells for investigations of intestinal drug permeability and first-pass metabolism. *Drug Metab. Dispos. 44*, 329–335.
(138) Sanderson, I. R., Ezzell, R. M., Kedinger, M., Erlanger, M., Xu, Z.-X., Pringault, E., Leon-Robine, S., Louvard, D. and Walker, W. A. (1996) Human fetal enterocytes *in vitro*: modulation of the phenotype by extracellular matrix. *Proc. Natl. Acad. Sci. 93*, 7717–7722.
(139) Perreault, N. and Beaulieu, J.-F. (1998) Primary Cultures of Fully Differentiated and Pure Human Intestinal Epithelial Cells. *Exp. Cell Res. 245*, 34–42.
(140) Kedinger, M., Simon-Assmann, P. M., Lacroix, B., Marxer, A., Hauri, H. P. and Haffen, K. (1986) Fetal gut mesenchyme induces differentiation of cultured intestinal endodermal and crypt cells. *Dev. Biol. 113*, 474–483.
(141) Aldhous, M. C., Shmakov, A. N., Bode, J. and Ghosh, S. (2001) Characterization of conditions for the primary culture of human small intestinal epithelial cells. *Clin. Exp. Immunol. 125*, 32–40.
(142) Madden, L. R., Nguyen, T. V., Garcia-Mojica, S., Shah, V., Le, A. V., Peier, A., Visconti, R., Parker, E. M., Presnell, S. C. and Nguyen, D. G. (2018) Bioprinted 3D primary human intestinal tissues model aspects of native physiology and ADME/Tox functions. *iScience 2*, 156–167.
(143) Sato, T., Vries, R. G., Snippert, H. J., van de Wetering, M., Barker, N., Stange, D. E., van Es, J. H., Abo, A., Kujala, P. and Peters, P. J. (2009) Single Lgr5 stem cells build crypt–villus structures *in vitro* without a mesenchymal niche. *Nature 459*, 262–265.
(144) Spence, J. R., Mayhew, C. N., Rankin, S. A., Kuhar, M. F., Vallance, J. E., Tolle, K., Hoskins, E. E., Kalinichenko, V. V., Wells, S. I. and Zorn, A. M. (2011) Directed differentiation of human pluripotent stem cells into intestinal tissue *in vitro*. *Nature 470*, 105–109.
(145) Sato, T., Stange, D. E., Ferrante, M., Vries, R. G. J., van Es, J. H., van den Brink, S., van Houdt, W. J., Pronk, A., van Gorp, J. and Siersema, P. D. (2011) Long-term expansion of epithelial organoids from human colon, adenoma, adenocarcinoma, and Barrett's epithelium. *Gastroenterology 141*, 1762–1772.
(146) Zhang, Y.-G., Wu, S., Xia, Y. and Sun, J. (2014) Salmonella-infected crypt-derived intestinal organoid culture system for host–bacterial interactions. *Physiol. Rep. 2*, DOI: 10.14814/phy2.12147.
(147) Basak, O., Beumer, J., Wiebrands, K., Seno, H., van Oudenaarden, A. and Clevers, H. (2017) Induced quiescence of Lgr5+ stem cells in intestinal organoids enables differentiation of hormone-producing enteroendocrine cells. *Cell Stem Cell 20*, 177-190.
(148) Fatehullah, A., Tan, S. H. and Barker, N. (2016) Organoids as an *in vitro* model of human development and disease. *Nat. Cell Biol. 18*, 246–254.
(149) Wallach, T. and Bayrer, J. R. (2017) Intestinal organoids: new frontiers in the study of intestinal disease and physiology. *J. Pediatr. Gastroenterol. Nutr. 64*, 180–185.
(150) Bartfeld, S. and Clevers, H. (2017) Stem cell-derived organoids and their application for medical research and patient treatment. *J. Mol. Med. 95*, 729–738.
(151) Lesuffleur, T., Barbat, A., Dussauix, E. and Zweibaum, A. (1990) Growth Adaptation to Methotrexate of HT-19 Human Colon Carcinoma Cells Is Associated with Their Ability to Differentiate into Columnar Absorptive Mucus-secreting Cells. *Cancer Res. 50*, 6334–6343.
(152) Lenaerts, K., Bouwman, F. G., Lamers, W. H., Renes, J. and Mariman, E. C. (2007) Comparative proteomic analysis of cell lines and scrapings of the human intestinal epithelium. *BMC Genomics 8*, DOI: 10.1186/1471-2164-8-91.
(153) Schimpel, C., Teubl, B., Absenger, M., Meindl, C., Fröhlich, E., Leitinger, G., Zimmer, A. and Roblegg, E. (2014) Development of an advanced intestinal *in vitro* triple culture permeability model to study transport of nanoparticles. *Mol. Pharm. 11*, 808–818.

(154) Strugari, A., Stan, M., Gharbia, S., Hermenean, A. and Dinischiotu, A. (2019) Characterization of Nanoparticle Intestinal Transport Using an *In Vitro* Co-Culture Model. *Nanomaterials 9*, DOI: 10.3390/nano9010005.
(155) Brun, E., Barreau, F., Veronesi, G., Fayard, B., Sorieul, S., Chanéac, C., Carapito, C., Rabilloud, T., Mabondzo, A. and Herlin-Boime, N. (2014) Titanium dioxide nanoparticle impact and translocation through *ex vivo, in vivo* and *in vitro* gut epithelia. *Part. Fibre Toxicol. 11*, DOI: 10.1186/1743-8977-11-13.
(156) Banerjee, A., Qi, J., Gogoi, R., Wong, J. and Mitragotri, S. (2016) Role of nanoparticle size, shape and surface chemistry in oral drug delivery. *J. Control. Release 238*, 176–185.
(157) Akbari, A., Lavasanifar, A. and Wu, J. (2017) Interaction of cruciferin-based nanoparticles with Caco-2 cells and Caco-2/HT29-MTX co-cultures. *Acta Biomater. 64*, 249–258.
(158) Georgantzopoulou, A., Serchi, T., Cambier, S., Leclercq, C. C., Renaut, J., Shao, J., Kruszewski, M., Lentzen, E., Grysan, P., Eswara, S., Audinot, J.-N., Contal, S., Ziebel, J., Guignard, C., Hoffmann, L., Murk, A. J. and Gutleb, A. C. (2016) Effects of silver nanoparticles and ions on a co-culture model for the gastrointestinal epithelium. *Part. Fibre Toxicol. 13*, DOI: 10.1186/s12989-016-0117-9.
(159) Ude, V. C., Brown, D. M., Viale, L., Kanase, N., Stone, V. and Johnston, H. J. (2017) Impact of copper oxide nanomaterials on differentiated and undifferentiated Caco-2 intestinal epithelial cells; assessment of cytotoxicity, barrier integrity, cytokine production and nanomaterial penetration. *Part. Fibre Toxicol. 14*, DOI: 10.1186/s12989-017-0211-7.
(160) Ude, V. C., Brown, D. M., Stone, V. and Johnston, H. J. (2019) Using 3D gastrointestinal tract *in vitro* models with microfold cells and mucus secreting ability to assess the hazard of copper oxide nanomaterials. *J. Nanobiotechnology 17*, DOI: 10.1186/s12951-019-0503-1.
(161) Loo, Y., Grigsby, C. L., Yamanaka, Y. J., Chellappan, M. K., Jiang, X., Mao, H.-Q. and Leong, K. W. (2012) Comparative study of nanoparticle-mediated transfection in different GI epithelium co-culture models. *J. Control. Release 160*, 48–56.
(162) Mahler, G. J., Esch, M. B., Tako, E., Southard, T. L., Archer, S. D., Glahn, R. P. and Shuler, M. L. (2012) Oral exposure to polystyrene nanoparticles affects iron absorption. *Nat. Nanotechnol. 7*, 264–271.
(163) García-Rodríguez, A., Vila, L., Cortés, C., Hernández, A. and Marcos, R. (2018) Effects of differently shaped TiO_2NPs (nanospheres, nanorods and nanowires) on the *in vitro* model (Caco-2/HT29) of the intestinal barrier. *Part. Fibre Toxicol. 15*, DOI: 10.1186/s12989-018-0269-x.
(164) Abeer, M. M., Meka, A. K., Pujara, N., Kumeria, T., Strounina, E., Nunes, R., Costa, A., Sarmento, B., Hasnain, S. Z. and Ross, B. P. (2019) Rationally Designed Dendritic Silica Nanoparticles for Oral Delivery of Exenatide. *Pharmaceutics 11*, DOI: 10.3390/pharmaceutics11080418.
(165) Dorier, M., Tisseyre, C., Dussert, F., Béal, D., Arnal, M.-E., Douki, T., Valdiglesias, V., Laffon, B., Fraga, S. and Brandao, F. (2019) Toxicological impact of acute exposure to E171 food additive and TiO_2 nanoparticles on a co-culture of Caco-2 and HT29-MTX intestinal cells. *Mutat. Res. Genet. Toxicol. Environ. Mutagen. 845*, DOI: 10.1016/j.mrgentox.2018.11.004.
(166) Abdelkhaliq, A., van der Zande, M., Undas, A. K., Peters, R. J. B. and Bouwmeester, H. (2019) Impact of *in vitro* digestion on gastrointestinal fate and uptake of silver nanoparticles with different surface modifications. *Nanotoxicol. 14*, 111–126.
(167) Des Rieux, A., Ragnarsson, E. G. E., Gullberg, E., Préat, V., Schneider, Y.-J. and Artursson, P. (2005) Transport of nanoparticles across an *in vitro* model of the human intestinal follicle associated epithelium. *Eur. J. Pharm. Sci. 25*, 455–465.

(168) Des Rieux, A., Fievez, V., Théate, I., Mast, J., Préat, V. and Schneider, Y.-J. (2007) An improved *in vitro* model of human intestinal follicle-associated epithelium to study nanoparticle transport by M cells. *Eur. J. Pharm. Sci. 30*, 380–391.
(169) Bouwmeester, H., Poortman, J., Peters, R. J., Wijma, E., Kramer, E., Makama, S., Puspitaninganindita, K., Marvin, H. J. P., Peijnenburg, A. A. C. M. and Hendriksen, P. J. M. (2011) Characterization of translocation of silver nanoparticles and effects on whole-genome gene expression using an *in vitro* intestinal epithelium coculture model. *ACS Nano 5*, 4091–4103.
(170) Holzwarth, U., Cossío, U., Llop, J. and Kreyling, W. G. (2019) Unpredictable Nanoparticle Retention in Commonly Used Plastic Syringes Introduces Dosage Uncertainties That May Compromise the Accuracy of Nanomedicine and Nanotoxicology Studies. *Front. Pharmacol. 10*, DOI: 10.3389/fphar.2019.01293.
(171) Lasa-Saracibar, B., Guada, M., Sebastian, V. and Blanco-Prieto, M. J. (2014) *In Vitro* Intestinal Co-culture Cell Model to Evaluate Intestinal Absorption of Edelfosine Lipis Nanoparticles. *Curr. Top. Med. Chem. 14*, 1124–1132.
(172) Beloqui, A., Brayden, D. J., Artursson, P., Préat, V. and Des Rieux, A. (2017) A human intestinal M-cell-like model for investigating particle, antigen and microorganism translocation. *Nat. Protoc. 12*, 1387–1399.
(173) Moyes, S. M., Morris, J. F. and Carr, K. E. (2010) Macrophages increase microparticle uptake by enterocyte-like Caco-2 cell monolayers. *J. Anat. 217*, 740–754.
(174) Leonard, F., Ali, H., Collnot, E.-M., Crielaard, B. J., Lammers, T., Storm, G. and Lehr, C.-M. (2012) Screening of budesonide nanoformulations for treatment of inflammatory bowel disease in an inflamed 3D cell-culture model. *ALTEX Altern. Anim. Ex. 29*, 275–285.
(175) Susewind, J., Souza Carvalho-Wodarz, C. de, Repnik, U., Collnot, E.-M., Schneider-Daum, N., Griffiths, G. W. and Lehr, C.-M. (2016) A 3D co-culture of three human cell lines to model the inflamed intestinal mucosa for safety testing of nanomaterials. *Nanotoxicol. 10*, 53–62.
(176) Kämpfer, A. A. M., Urbán, P., La Spina, R., Jiménez, I. O., Kanase, N., Stone, V. and Kinsner-Ovaskainen, A. (2020) Ongoing inflammation enhances the toxicity of engineered nanomaterials: Application of an *in vitro* co-culture model of the healthy and inflamed intestine. *Toxicol. In Vitro 63*, DOI: 10.1016/j.tiv.2019.104738.
(177) Baek, Y.-W. and An, Y.-J. (2011) Microbial toxicity of metal oxide nanoparticles (CuO, NiO, ZnO, and Sb_2O_3) to Escherichia coli, Bacillus subtilis, and Streptococcus aureus. *Sci. Total. Environ. 409*, 1603–1608.
(178) Lin, X., Li, J., Ma, S., Liu, G., Yang, K., Tong, M. and Lin, D. (2014) Toxicity of TiO_2 nanoparticles to Escherichia coli: effects of particle size, crystal phase and water chemistry. *PLoS One 9*, DOI: 10.1371/journal.pone.0110247.
(179) Das, P., McDonald, J. A. K., Petrof, E. O., Allen-Vercoe, E. and Walker, V. K. (2014) Nanosilver-Mediated Change in Human Intestinal Microbiota. *J. Nanomed. Nanotechnol. 5*, DOI: 10.4172/2157-7439.1000235.
(180) Peters, R., Kramer, E., Oomen, A. G., Rivera, Z. E. H., Oegema, G., Tromp, P. C., Fokkink, R., Rietveld, A., Marvin, H. J. P., Weigel, S., Peijnenburg, A. A. C. M. and Bouwmeester, H. (2012) Presence of nano-sized silica during *in vitro* digestion of foods containing silica as a food additive. *ACS Nano 6*, 2441–2451.
(181) Walczak, A. P., Fokkink, R., Peters, R., Tromp, P., Herrera Rivera, Z. E., Rietjens, I. M. C. M., Hendriksen, P. J. M. and Bouwmeester, H. (2013) Behaviour of silver nanoparticles and silver ions in an *in vitro* human gastrointestinal digestion model. *Nanotoxicol. 7*, 1198–1210.
(182) Böhmert, L., Girod, M., Hansen, U., Maul, R., Knappe, P., Niemann, B., Weidner, S. M., Thünemann, A. F. and Lampen, A. (2014) Analytically monitored digestion of silver nanoparticles and their toxicity on human intestinal cells. *Nanotoxicol. 8*, 631–642.

(183) Juling, S., Niedzwiecka, A., Böhmert, L., Lichtenstein, D., Selve, S., Braeuning, A., Thünemann, A. F., Krause, E. and Lampen, A. (2017) Protein Corona Analysis of Silver Nanoparticles Links to Their Cellular Effects. *J. Proteome Res. 16*, 4020–4034.
(184) Di Silvio, D., Rigby, N., Bajka, B., Mackie, A. and Baldelli Bombelli, F. (2016) Effect of protein corona magnetite nanoparticles derived from bread *in vitro* digestion on Caco-2 cells morphology and uptake. *Int. J. Biochem. Cell Biol. 75*, 212–222.
(185) DeLoid, G. M., Wang, Y., Kapronezai, K., Lorente, L. R., Zhang, R., Pyrgiotakis, G., Konduru, N. V., Ericsson, M., White, J. C., La Torre-Roche, R. de, Xiao, H., McClements, D. J. and Demokritou, P. (2017) An integrated methodology for assessing the impact of food matrix and gastrointestinal effects on the biokinetics and cellular toxicity of ingested engineered nanomaterials. *Part. Fibre Toxicol. 14*, DOI: 10.1186/s12989-017-0221-5.
(186) Kästner, C., Lichtenstein, D., Lampen, A. and Thünemann, A. F. (2017) Monitoring the fate of small silver nanoparticles during artificial digestion. *Colloids Surf. A 526*, 76–81.
(187) Farcal, L., Torres Andón, F., Di Cristo, L., Rotoli, B. M., Bussolati, O., Bergamaschi, E., Mech, A., Hartmann, N. B., Rasmussen, K., Riego-Sintes, J., Ponti, J., Kinsner-Ovaskainen, A., Rossi, F., Oomen, A., Bos, P., Chen, R., Bai, R., Chen, C., Rocks, L., Fulton, N., Ross, B., Hutchison, G., Tran, L., Mues, S., Ossig, R., Schnekenburger, J., Campagnolo, L., Vecchione, L., Pietroiusti, A. and Fadeel, B. (2015) Comprehensive *In Vitro* Toxicity Testing of a Panel of Representative Oxide Nanomaterials: First Steps towards an Intelligent Testing Strategy. *PLoS One 10*, DOI: 10.1371/journal.pone.0127174.
(188) Schwabe, R. F. and Jobin, C. (2013) The microbiome and cancer. *Nat. Rev. Cancer 13*, 800–812.
(189) Chen, J., Pitmon, E. and Wang, K. (2017) Microbiome, inflammation and colorectal cancer. *Semin. Immunol. 32*, 43–53.
(190) Gerloff, K., Albrecht, C., Boots, A., Forster, I. and Schins, R. (2009) Cytotoxicity and oxidative DNA damage by nanoparticles in human intestinal Caco-2 cells. *Nanotoxicol. 3*, 355–364.
(191) Gundert-Remy, U., Barth, H., Bürkle, A., Degen, G. H. and Landsiedel, R. (2015) Toxicology: a discipline in need of academic anchoring—the point of view of the German Society of Toxicology. *Arch. Toxicol. 89*, 1881–1893.
(192) Pal, A. K., Bello, D., Cohen, J. and Demokritou, P. (2015) Implications of *in vitro* dosimetry on toxicological ranking of low aspect ratio engineered nanomaterials. *Nanotoxicol. 9*, 871–885.
(193) Thomas, D. G., Smith, J. N., Thrall, B. D., Baer, D. R., Jolley, H., Munusamy, P., Kodali, V., Demokritou, P., Cohen, J. and Teeguarden, J. G. (2018) ISD3: a particokinetic model for predicting the combined effects of particle sedimentation, diffusion and dissolution on cellular dosimetry for *in vitro* systems. *Part. Fibre Toxicol. 15*, DOI: 10.1186/s12989-018-0243-7.

3. Investigations of acute effects of polystyrene and polyvinyl chloride micro- and nanoplastics in an advanced *in vitro* triple culture model of the healthy and inflamed intestine

Mathias Busch[a], Gerrit Bredeck[a], Angela A. M. Kämpfer[a], Roel P. F. Schins[a]

[a] *IUF – Leibniz-Research Institute for Environmental Medicine, Auf'm Hennekamp 50, 40225 Düsseldorf, Germany*

Environmental Research, 2021, 193, 110536

DOI: 10.1016/j.envres.2020.110536

Author contribution: The author of this dissertation planned and performed the *in vitro* experiments and statistical analysis, made the graphs, discussed the results and wrote the manuscript. Relative contribution: 80 %.

3.1 Abstract

The continuous degradation of plastic waste in the environment leads to the generation of micro- and nanoplastic fragments and particles. Due to the ubiquitous presence of plastic particles in natural habitats as well as in food, beverages and tap water, oral exposure of the human population with plastic particles occurs worldwide. We investigated acute toxicological effects of polystyrene (PS) and polyvinyl chloride (PVC) micro- and nanoparticles in an advanced *in vitro* triple culture model (Caco-2/HT29-MTX-E12/THP-1) mimicking the healthy and inflamed human intestine to study the effect of inflammatory processes on plastic particle toxicity. We monitored barrier integrity, cytotoxicity, cell layer integrity, DNA damage, the release of pro-inflammatory cytokines (IL-1β, IL-6, IL-8 and TNF-α) and mucus distribution after 24 h of particle exposure. In addition, we investigated cytotoxicity, DNA damage and IL-1β release in monocultures of the three cell lines. Amine-modified polystyrene nanoparticles (PS-NH_2) served as a positive control for particle-induced toxicity. No acute effects in the investigated endpoints were observed in the model of the healthy intestine after PS or PVC exposure. However, during active inflammatory processes, exposure to PVC particles was found to augment the release of IL-1β and to cause a loss of epithelial cells. Our results suggest that prevalent intestinal inflammation might be an important factor to consider when assessing the hazard of ingested micro- and nanoplastic particles.

3.2 Introduction

Environmental pollution with mismanaged waste is a major problem of our modern society. About 10 % of discarded waste is plastic, which accumulates in the environment due to its highly persistent nature (Barnes *et al.*, 2009). Borrelle *et al.* (2020) estimated that up to 23 million metric tons of plastic waste entered aquatic ecosystems in 2016. Although plastics are generally appreciated for their resistance to degradation, environmental factors like UV radiation and mechanical abrasion can cause the fragmentation of plastic polymers into smaller particles known as micro- and nanoplastics (Andrady, 2012; Julienne *et al.*, 2019). These terms describe a large, heterogenous group of plastic fragments of different chemical composition in size ranges below 5 mm or 1000 nm, respectively (Vianello *et al.*, 2013; Gigault *et al.*, 2016; Lambert and Wagner, 2016). The continuous degradation and accumulation of plastic nanoparticles might increase the health hazard concerning plastic particles, due to the higher biological availability and reactivity of nanoparticles compared to microparticles (Park *et al.*, 2011; Bouwmeester *et al.*, 2015). Through uptake by aquatic and terrestrial organisms, plastic particles are introduced into the food chain. As reviewed by Barboza *et al.* (2018), many studies showed the presence of microplastic particles in various fish and shellfish. Furthermore, contamination with microplastics was demonstrated in other foods and beverages (Kosuth *et al.*, 2018), honey (Liebezeit and Liebezeit, 2015) and salt (Karami *et al.*, 2017). Most importantly, plastic particles were found in drinking water of various sources (Marsden *et al.*, 2019; Mintenig *et al.*, 2019; Shruti *et al.*, 2020; Tong *et al.*, 2020; Zhang *et al.*, 2020) and Schwabl *et al.* (2019) reported the presence of microplastics in human stool samples collected from eight individuals from Europe and Asia. This has led to the reasonable assumption that oral exposure of the human population with plastic particles is present worldwide. Recent animal studies in mice and zebrafish have identified the gastrointestinal tract (GIT) as a possible target organ for plastic particle-induced toxicity, linking the oral uptake of microplastics with intestinal inflammation, microbial dysbiosis and reduced mucus secretion (Lu *et al.*, 2018; Li *et al.*, 2019; Qiao *et al.*, 2019).

Inflammatory bowel diseases (IBD), namely Crohn's disease and ulcerative colitis, are modern western diseases with an estimated prevalence of 0.3 % in Europe and 1.3 % in the US (Burisch *et al.*, 2013; Dahlhamer *et al.*, 2016). IBD is marked by a chronically inflamed GIT and is thought to result from a multi-factorial interaction involving genetics, diet and microbial dysbiosis, yet its precise etiology is still unknown (Cho and Brant, 2011). IBD is characterized by increased levels of pro-inflammatory cytokines (Neurath, 2014), cytotoxicity (Kappeler and Mueller, 2000), oxidative DNA damage (Pereira *et al.*, 2016), impairment of intestinal barrier integrity (Maloy and Powrie, 2011), the decline of goblet cells (Strugala *et al.*, 2008) and an increased risk of colon cancer (Kim and Chang, 2014).

Only limited studies are available regarding toxicological effects of micro- and nanoplastics in the GIT, and a prevalent intestinal inflammation appears to be an overlooked potential risk factor. Major advancements in the development of intestinal *in vitro* models and multifactorial testing strategies provide highly advanced model systems of the human GIT and sophisticated approaches for nanosafety research (Kämpfer *et al.*, 2020a). Still, the majority of *in vitro* studies investigating intestinal plastic particle toxicity is restricted to simple single cell line experiments (Thubagere and Reinhard, 2010; Forte *et al.*, 2016; Riebeling *et al.*, 2018; Wu *et al.*, 2020; Yan *et al.*, 2020). On the other hand, studies using advanced *in vitro* co-culture models of the GIT focused on the transfer across the gastrointestinal barrier (Walczak *et al.*, 2015; Abdelkhaliq *et al.*, 2018) or cellular uptake (Stock *et al.*, 2019) instead of intestinal toxicity. Most of these studies exclusively used polystyrene (PS) as model particles and some were carried out in the context of polymer-based nanoparticle drug delivery instead of nanoplastic hazard assessment.

To address this knowledge gap regarding human health risks, we investigated the acute hazards of micro- and nanoplastics in the context of inflammation. We used an advanced *in vitro* triple culture model of the healthy and inflamed intestine, which we recently developed (Kämpfer *et al.*, 2020b), to investigate possible effects of PS and polyvinyl chloride (PVC) micro- and nanoplastic particles on the healthy or inflamed gut. The model is composed of the human cell lines Caco-2, as a model of enterocytes, HT29-MTX-E12, as a model of mucus-producing goblet cells, and PMA-differentiated THP-1 cells representing macrophages. To mimic an intestinal inflammation, the THP-1 cells were activated with lipopolysaccharide (LPS) and interferon-γ (IFN-γ).

3.3 Materials and Methods

Materials

Dulbecco's Modified Eagle Medium (DMEM), Minimum Essential Medium (MEM), RPMI-1640 Medium, 2-mercaptoethanol (ME), fetal calf serum (FCS) for THP-1 cells, sodium pyruvate, phosphate buffered saline (PBS), Prolong Gold Antifade Reagent, *Zonula Occludens* (ZO)-1 antibody and AlexaFluor594 (goat anti-rabbit) antibody were purchased from Thermo Fisher Scientific. FCS for Caco-2 and HT29-MTX-E12, non-essential amino acids (NEAA), L-glutamine, D-glucose, penicillin/streptomycin (P/S), trypsin, phorbol 12-myristate 13-acetate (PMA), interferon gamma (IFN-γ), lipopolysaccharides (LPS), Accutase, agarose, low melting point agarose, β-nicotinamide adenine dinucleotide sodium salt (NAD), lithium L-lactate, phenazine methosulfate (PMS), iodonitrotetrazolium chloride (INT), alcian blue (AB) (1 % in 3 % acetic acid), periodic acid, Hoechst 33342, ethylenediaminetetraacetic acid (EDTA), dimethyl sulfoxide (DMSO), Triton X-100, sodium hydroxide (NaOH), bovine serum albumin (BSA), Schiff's reagent, sodium meta bisulfite and methyl methanesulfonate (MMS) were

purchased from Sigma-Aldrich/Merck. Tris base, para-formaldehyde (PFA) and sodium chloride (NaCl) were ordered from Carl Roth (Germany).

Model plastic particles

Amine-modified polystyrene (PS-NH_2) nanobeads (50 nm) were ordered from Sigma-Aldrich (L0780). *Polystyrene* (PS) nanobeads (50 nm) were ordered from Polysciences, Inc. (Warrington, USA) (08691-10). Nanobeads were stored at 4 °C in 2.5 % aqueous suspension. *Polyvinyl chloride* (PVC) powder (<50 µm) was purchased from Werth-Metall (Erfurt, Germany). For experiments, particles were brought in or diluted to a 4 mg/ml suspension of sterile, deionized water (dH_2O) and a 10 min sonication was performed using a Branson Sonifier 450 at a duty cycle of 0.2 seconds and an output level of 5.71 (200 watts).

Particle characterization

In preparation of scanning electron microscopy (SEM) analysis, particle suspensions were diluted to 40 µg/ml in treatment medium (MEM containing 1 % FCS) and 50 µl were pipetted on 0.2 µm pore size Whatman filters. After medium removal, the filters were air-dried, coated with a 10 nm gold layer and subsequently analyzed using a field emission SEM (7500F, JEOL (Germany) GmbH, Germany) at magnifications between 50X and 50,000X. For each particle type, ≥300 spheres/agglomerates per filter were analyzed using ImageJ (version 1.51f, http://imagej.nih.gov/ij) to determine the mean and mode diameter of primary particles and particle agglomerates separately.

Dynamic Light Scattering (DLS) analysis was used to determine hydrodynamic diameter and polydispersity index (PDI) of the particles. Particle samples were diluted to 150 µg/ml in treatment medium for optimal measurement conditions. Samples were analyzed in triplicates using a Zetasizer Nano-ZS (Malvern Instruments, Malvern, UK). The criteria for acceptance of DLS data were defined as follows: corresponding correlograms of the three measurements, a correlation coefficient between 0.7 and 1, PDI below 0.5 and less than 10 % deviation in the count rates of the three measurements.

Particle sedimentation modeling with ISDD

The *In vitro* Sedimentation, Diffusion and Dosimetry model (ISDD) (Hinderliter *et al.*, 2010) was used to estimate the delivered dose for particle exposure experiments. By providing a series of parameters describing the particles, treatment medium and experimental setup, the ISDD model simulates the sedimentation of particles in an *in vitro* experiment. Simulations were performed using the ISDD graphic user interface with MATLAB Compiler Runtime v8.3 R2014a. The required input parameters were determined as follows: Primary particle sizes were given by the manufacturer and/or acquired by SEM analysis. Agglomerate diameters

were measured with DLS. Specific material density was given by the manufacturer and the respective packing factor was assigned according to DeLoid *et al.* (2014). The effective densities of particle agglomerates were estimated using the packed cell volume (PCV) centrifugation method as described by (DeLoid *et al.*, 2014). Briefly, defined particle suspensions were centrifuged at 2000 g in PCV tubes that allowed the determination of the volume that is occupied by the particle agglomerates. Refractive index, density and viscosity of the treatment medium were measured with an Abbe refractometer 60/LR, a DMA 5000 density meter and an Ubbelohde viscometer Type 501 13/Ic, respectively. Sedimentation simulations were run for triple culture transwell experiment scenarios (24 h duration, 0.9 cm² filter area, 0.5 ml treatment volume, 50 µg/cm² particle exposure).

Cell culture

Caco-2 (DSMZ, ACC169) cells were cultured in MEM-based cell culture medium substituted with 20 % FCS, 1 % P/S and 1 % L-glutamine. HT29-MTX-E12 (ECACC, 12040401) cells were cultured in DMEM-based cell culture medium substituted with 10 % FCS, 1 % P/S and 1 % NEAA. Caco-2 and HT29-MTX-E12 cells were regularly split at roughly 80 % confluence and used at passages 5 – 25 for experiments. THP-1 (ATCC, TIB-202) cells were cultured in RPMI 1640-based cell culture medium (containing L-glutamine and 25 mM HEPES) substituted with 10 % FCS, 1 % P/S, 1 nM sodium pyruvate, 0.7 % D-glucose and 50 nM ME and maintained at cell concentrations between $2*10^5$ and $8*10^5$ cells/ml. For experiments, THP-1 cells were used at passages 5 – 15.

Prior to triple culture experiments, we investigated cytotoxic effects of the plastic particles in monocultures of all three cell lines via water-soluble tretrazolium salt-1 (WST-1) and lactate dehydrogenase (LDH) assay, the potential to induce DNA damage in both epithelial cell lines (Caco-2 and HT29-MTX-E12) via alkaline comet assay and the ability to induce Interleukin (IL)-1β release in PMA-differentiated THP-1 cells via ELISA as described further below. Cells were seeded as specified in **Table 3.1**. Caco-2 and HT29-MTX-E12 cells were grown for 48 h, and 16 – 20 h prior to experiments, the medium was replaced with treatment medium (MEM or DMEM with 1 % FCS). THP-1 cells were differentiated in 25 cm² flasks with 100 nM PMA for 24 h, re-seeded and were allowed to re-attach for 1.5 h before treatment.

Table 3.1 Plate formats and seeding densities used in monoculture experiments

	Seeding densities (cells/well)			
Assay	**WST-1 assay**	**LDH assay**	**Alkaline comet assay**	**ELISA**
Plate format	96-well	96-well	24-well	24-well
Caco-2	$1.0*10^4$	$1.0*10^4$	$2.4*10^5$	
HT29-MTX-E12	$1.0*10^4$	$1.0*10^4$	$2.4*10^5$	
THP-1	$2.0*10^4$	$2.0*10^4$		$6.0*10^4$

The triple culture in stable/healthy and inflamed state was established as described in detail by Kämpfer *et al.* (2020b). Briefly, Caco-2 and HT29-MTX-E12 cells ($1.8*10^5$/cm², 90:10 ratio) were seeded on 1 µm pore size PET transwell filters (12-well format; Falcon) in Caco-2 medium (MEM) and cultured for 21 days while gradually changing the basolateral medium to THP-1 medium (RPMI 1640) without ME. On day 21, epithelial cells in the inflamed triple culture wells were basolaterally primed with 10 ng/ml IFN-γ for 24 h. In parallel, $3*10^6$ THP-1 cells were differentiated in 25 cm² flasks with 100 nM PMA for 24 h. On day 22, differentiated THP-1 cells were detached with Accutase and seeded in a 12-well plate at a density of $1.8*10^5$ cells per well and allowed to re-attach for 1.5 h. The IFN-γ-primed wells were washed twice with PBS and allowed to rest for 4 h. In parallel, re-attached THP-1 cells for the inflamed triple culture were activated with 10 ng/ml LPS and IFN-γ for 4 h. Stable and inflamed co-cultures were started in parallel by transferring the corresponding transwell inserts to the THP-1-containing wells. Particle treatments were started 24 h after initiation of the triple cultures and continued for 24h.

Treatment procedure

Particle suspensions were diluted in treatment medium (Caco-2 monocultures/Triple cultures: MEM containing 1 % FCS, HT29-MTX-E12 monocultures: DMEM containing 1 % FCS, THP-1 monocultures: RPMI 1640 containing 1 % FCS and no ME) to obtain the desired treatment concentrations. Lower treatment concentrations and particle-free control media were adapted to contain the same volume of dH_2O as the highest treatment concentration.

Cytotoxicity assays

Cell viability in monocultures following 24 h of PS-NH_2, PS or PVC particle exposure was assessed via WST-1 assay. All three cell lines were treated in the same manner with 0, 1, 5, 10 or 50 µg/cm² PS-NH_2, PS or PVC particles in 100 µl of the respective treatment medium. After 24 h exposure, the WST-1 assay was performed as described by Kolling *et al.* (2020), the procedure was based on the SOP “Cellular viability – WST-1 assay” of the nanOxiMet project (https://nanopartikel.info/en/projects/era-net-siinn/nanoximet-en). WST-1 reagent was added undiluted (Caco-2, THP-1) or diluted 1:5 (HT29-MTX-E12) for 1 h (Caco-2, HT29-MTX-E12) or 2 h (THP-1). The LDH assay was used to monitor necrotic cell death following particle exposure in both monocultures and triple cultures. Monoculture experiments were performed as described for the WST-1 assay. After 24 h of particle exposure, 50 µl of supernatant was transferred onto new 96 well plates and 150 µl of reaction mix containing 50 µl Tris buffer (200 mM, pH 8), 50 µl Li-Lactate solution (50 mM), 46 µl NAD^+ solution (5 mM), 2 µl INT solution (65 mM) and 2 µl PMS solution (29 mM) was added per well. After 10 min incubation, the

reaction was stopped with 50 µl 1 M H_2SO_4 and absorbance was measured at 490 nm and 680 nm. For monoculture experiments, $A_{490nm-680nm}$ of the negative control was subtracted from $A_{490nm-680nm}$ of the samples and divided by $A_{490nm-680nm}$ of the Triton X-100 treated wells to obtain "% Cytotoxicity". In triple culture experiments, $A_{490nm-680nm}$ of the treated wells was expressed as fold change compared to the untreated control.

Alkaline comet assay

The alkaline comet assay was used to analyze the induction of DNA single and double strand breaks as well as the occurrence of alkali-labile sites in the epithelial cells following particle exposure. MMS (1.25 mM, 30 min) served as a non-particulate, chemical control. After 4 h (monocultures) or 24 h (triple cultures) incubation, cells were trypsinized and resuspended in 500 µl medium. 40 µl of this cell suspension was mixed with 240 µl low melting point agarose (0.5 % in PBS) and 120 µl mixture was transferred onto slides previously coated with 1.5 % agarose. Slides were prepared in duplicates. After solidification of the agarose, slides were placed in lysis buffer (pH 9.5; 2.5 M NaCl, 100 mM EDTA, 10 mM Tris, 10% DMSO, 1% Triton X-100) overnight at 4 °C. After washing (3x5 min in H_2O), the slides were transferred to an electrophoresis chamber (SL-Comet, Cleaver Scientific, UK) and incubated in electrophoresis buffer (pH 13; 0.3 M NaOH, 1 mM EDTA) for 20 min, followed by 10 min electrophoresis at ~24 V and ~280 mA. Afterwards, the slides were washed twice in neutralization buffer (pH 7.5; 0.4 M Tris), dipped in 100 % ethanol and allowed to air dry. For analysis, 40 µl of 1 % ethidium-bromide in H_2O staining solution was applied to each slide and 50 nuclei per slide were scored using the software Comet Assay IV (Perceptive Instruments, Wiltshire, UK). The results were averaged and expressed as % tail intensity of the comets.

Cytokine quantification by enzyme-linked immuno-sorbent assay (ELISA)

The release of pro-inflammatory cytokines following particle exposure was analyzed using R&D systems DuoSet ELISA kits for human IL-1β, IL-6, IL-8 and tumor necrosis factor (TNF-)α. Antibodies were diluted according to the manufacturer's protocol and high-protein-binding 96-well plates were incubated with capture antibody in coating buffer (0.1 M $NaHCO_3$, pH 8.2) overnight. After blocking with 3 % BSA/PBS, 100 µl of supernatants (basolateral supernatants for the triple culture experiments), diluted if necessary (IL-1β and IL-8: 1:5), were incubated for 2 h. Detection antibody, horse radish peroxidase (1:40 in 1 % BSA/PBS) and BioRad TMB Peroxidase EIA Substrate were consecutively incubated for 2 h, 0.5 h and 5-20 min, respectively, before stopping the reaction with 50 µl 1M H_2SO_4. Absorbance was measured at 450 nm. The standard curve was plotted as a four-parameter logfit.

Measurement of transepithelial electric resistance (TEER)

Barrier integrity during particle exposure in the triple culture model was measured as TEER using a voltohmmeter (EVOM, World Precision Instruments) with a chopstick electrode (STX2). Prior to measurements, the electrode was sterilized in 70 % ethanol and washed with PBS and MEM. TEER measurements were performed at t = 0,4,20,24,44,48 h after start of the triple culture and were corrected for blank value and transwell filter area (0.9 cm²).

Immunocytochemistry

After 24 h of particle exposure in triple cultures, the epithelial cell layers were investigated for effects on the tight junction network and nuclei number. The transwell filters of the triple cultures were fixed (4 % PFA/PBS, 15 min) and permeabilized (0.1 % Triton X-100/PBS, 5 min). After blocking (3 % BSA/PBS, 30 min), filters were incubated with ZO-1 primary antibody (2.5 µg/ml in 1 % BSA/PBS, 1 h). After incubation with secondary antibody (AlexaFluor 594, 6.7 µg/ml) and Hoechst 33342 (0.5 µg/ml) for 30 min at 37 °C, filter membranes were placed on a microscopy glass slide and mounted with Prolong Gold Anti-Fading Mount. Microscopic evaluation was performed using a Zeiss Axio Imager.M2 at 400x magnification. For the semi-quantitative analysis of Hoechst-stained nuclei, 20 images per filter were taken randomly and nuclei (≥4,000 per condition) were counted using an automated ImageJ script. The counted nuclei in each image (given in nuclei per mm² filter area) were expressed as % of untreated control.

Mucus Staining

To investigate effects of particle exposure on the mucus distribution in the epithelial layer of the triple culture, neutral and acidic mucus was visualized with the PAS reaction and AB staining, respectively. Transwell filters were fixed (4 % PFA/PBS, 15 min) and incubated in acetic acid (3 %, 3 min). Subsequently, filters were stained with 1 % AB in 3 % acetic acid for 30 min. Filter membranes were incubated with periodic acid solution (1 %, 10 min) and with Schiff's reagent for 15 min protected from light. After washing with sulphite water (0.556 % sodium disulphite, 45 mM HCl; 3x2 min), filters were washed with dH_2O, placed on a microscopy glass slide and mounted with Prolong Gold Anti-Fading Mount. Microscopic evaluation was done using a Zeiss Axiophot light microscope at 100x magnification.

Statistical Analysis

Statistical analysis and illustration of results was performed using GraphPad Prism 8.3. Unless stated otherwise, experiments were performed in three independent runs with two biological replicates. Data obtained from monoculture experiments were analyzed with ordinary one-way analysis of variance (ANOVA) followed by Dunnett's multiple comparisons test. Statistical

analysis of triple culture experiments in stable or inflamed state was performed with two-way ANOVA and Tukey's test. A p-value of <0.05 was considered statistically significant.

3.4 Results

Particle characterization and sedimentation modeling

The morphology of PS-NH_2, PS and PVC particles was evaluated by SEM (**Figure 3.1**). All three materials are composed of primary spheres with a varying tendency to agglomerate. PS-NH_2 formed larger agglomerates of up to 20 distinguishable individual spheres, while PS mainly occurred as single spheres and small agglomerates consisting of 2-3 particles. PVC was found to form bulky agglomerates almost exclusively. SEM images were subsequently used to determine mean and mode diameters of PS-NH_2, PS and PVC spheres and agglomerates (**Table 3.2*)**.

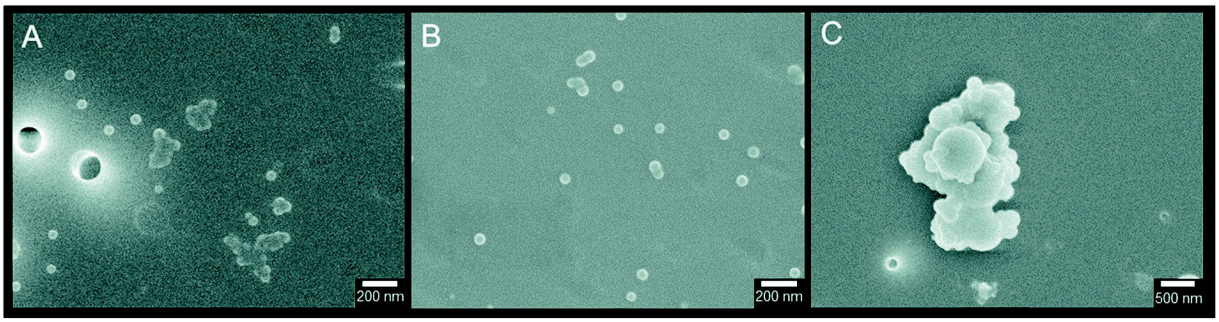

Figure 3.1 SEM images of (A) PS-NH_2 (50 nm nanobeads), (B) PS (50 nm nanobeads) and (C) PVC (<50 µm powder) obtained at 50.000x (A+B) or 20.000x (C) magnification.

Table 3.2 Mean and mode diameter of PS-NH_2, PS and PVC spheres and agglomerates as estimated by SEM image analysis, based on ≥300 measurements.

Polymer type	Appearance	Mean diameter ± SD [nm]	Mode diameter (σ) [nm]
PS-NH_2	Spheres	59 ± 8	58 (1.16)
	Agglomerates	224 ± 286	117 (2.00)
PS	Spheres	59 ± 9	62 (1.10)
	Agglomerates	88 ± 17	77 (1.07)
PVC	Spheres	279 ± 112	235 (1.21)
	Agglomerates	1148 ± 861	480 (1.57)

As indicated by the size distribution histograms (**Figure S 3.1**), PS-NH_2 and PS single spheres show a narrow distribution over 35 – 75 nm, while PS-NH_2 agglomerates cover a broader span of size classes than PS agglomerates (up to 500 nm vs. 100 nm). The majority of PVC single spheres were found to be in size classes of 200 – 350 nm, particles smaller than 100 nm were not observed. PVC particles appear to form agglomerates up to 4 µm in diameter. The hydrodynamic diameters of the particles were determined by DLS analysis, the results are summarized in **Table 3.3**.

Table 3.3 Hydrodynamic diameter and PDI of PS-NH_2, PS and PVC particles in treatment medium as measured by DLS. Mean ± SD of N=3.

Polymer type	Z-Average ± SD [nm]	PDI ± SD
PS-NH_2	308 ± 2	0.213 ± 0.021
PS	80 ± 1	0.105 ± 0.027
PVC	1217 ± 154	0.459 ± 0.078

The *In vitro* Sedimentation, Diffusion and Dosimetry model (ISDD) was used to estimate the delivered dose of PS-NH_2, PS and PVC during triple culture experiments in terms of mass and surface area (**Figure 3.2**). The simulations revealed that, after 24 h, only a fraction of the applied 50 µg/cm² PS-NH_2, PS or PVC has settled (5, 8 or 16 µg, respectively, representing 11, 17 and 35 % of the applied dose). The deposited particle surface area of PS-NH_2, PS or PVC after 24 h was estimated to be roughly 5, 9 or 2.5 cm², respectively.

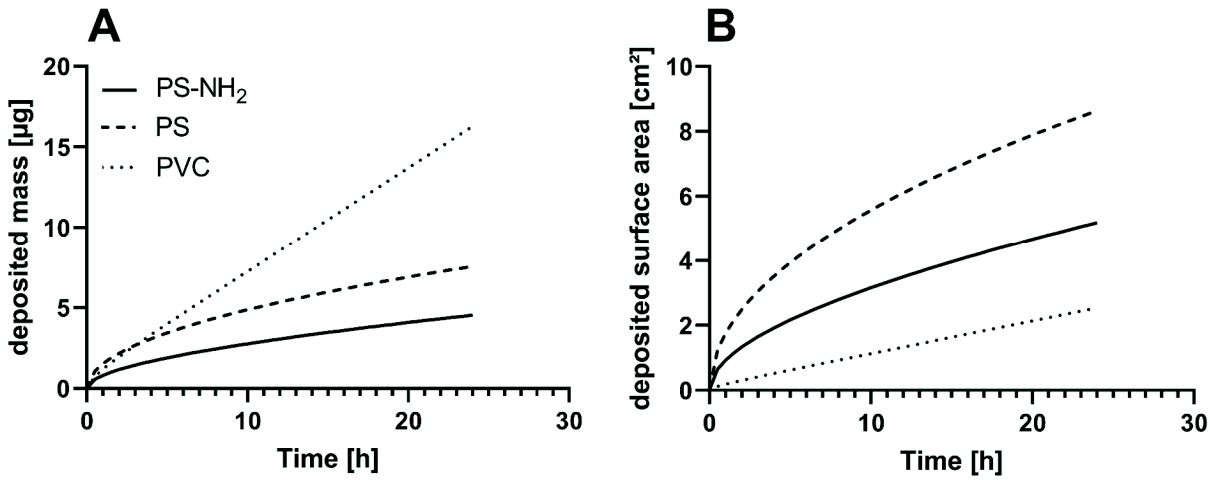

Figure 3.2 Deposited (A) mass and (B) surface area of PS-NH_2, PS and PVC particles during 24 h exposure as simulated by the ISDD model. The exposure scenario resembles the treatment of 0.9 cm² transwell filters with 50 µg/cm² particles in 0.5 ml medium.

Monoculture experiments

Cytotoxicity in monocultures of Caco-2, HT29-MTX-E12 and THP-1 cells

Effects on the cell viability after exposure to PS-NH_2, PS or PVC particles were investigated in monocultures of Caco-2, HT29-MTX-E12 or PMA-diff. THP-1 cells via WST-1 and LDH assay (**Figure 3.3**). A significant, dose-dependent reduction of metabolic activity was found in all three cell lines after 24 h treatment with PS-NH_2 particles at concentrations of 1 µg/cm² (Caco-2), 5 µg/cm² (THP-1) and 10 µg/cm² (HT29-MTX-E12). Treatment with 5 µg/cm² PS-NH_2 caused a complete loss of metabolic activity in Caco-2 and THP-1 cells, while cell viability of HT29-MTX-E12 was not affected. Significant increases in LDH activity were observed at concentrations of 5 µg/cm² (THP-1), 10 µg/cm² (HT29-MTX-E12) and 50 µg/cm² (Caco-2). PS or PVC particles did not affect the metabolic activity or LDH release in all three cell lines at concentrations up to 50 µg/cm².

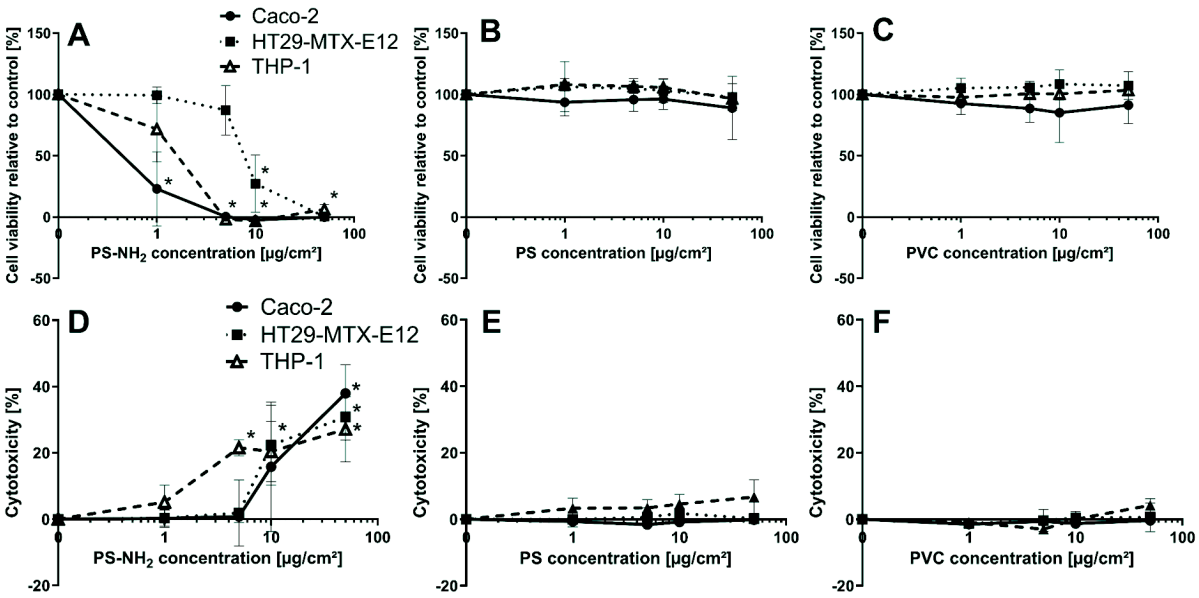

Figure 3.3 Cell viability (A-C) and cytotoxicity (D-F) in Caco-2 (circles), HT29-MTX-E12 (squares) and THP-1 monocultures (triangles) after 24 h exposure to 1 – 50 µg/cm² (A+D) PS-NH_2, (B+E) PS or (C+F) PVC. Cell viability was assessed via WST-1 assay, cytotoxicity was assessed via LDH assay. Mean ± SD of N=3, *p<0.05 compared to the respective control.

DNA damage in epithelial cell monocultures

DNA damage in monocultures of the epithelial cell lines Caco-2 and HT29-MTX-E12 cells was assessed via alkaline comet assay after 4 h of particle exposure (**Figure 3.4**). We observed a reproducible difference in the background DNA damage levels of untreated controls between Caco-2 (~2.5 % DNA in tail) and HT29-MTX-E12 cells (~0.5 % DNA in tail). A small, but statistically significant increase in DNA damage was observed in both cell lines treated with 50 µg/cm² PS-NH_2 particles. For comparison, treatment with the non-particulate, chemical control MMS caused pronounced DNA damage in Caco-2 and HT29-MTX-E12 cells (~70 % and ~40 % DNA in tail, respectively, data not shown). None of the tested PS or PVC concentrations induced significant changes in DNA damage.

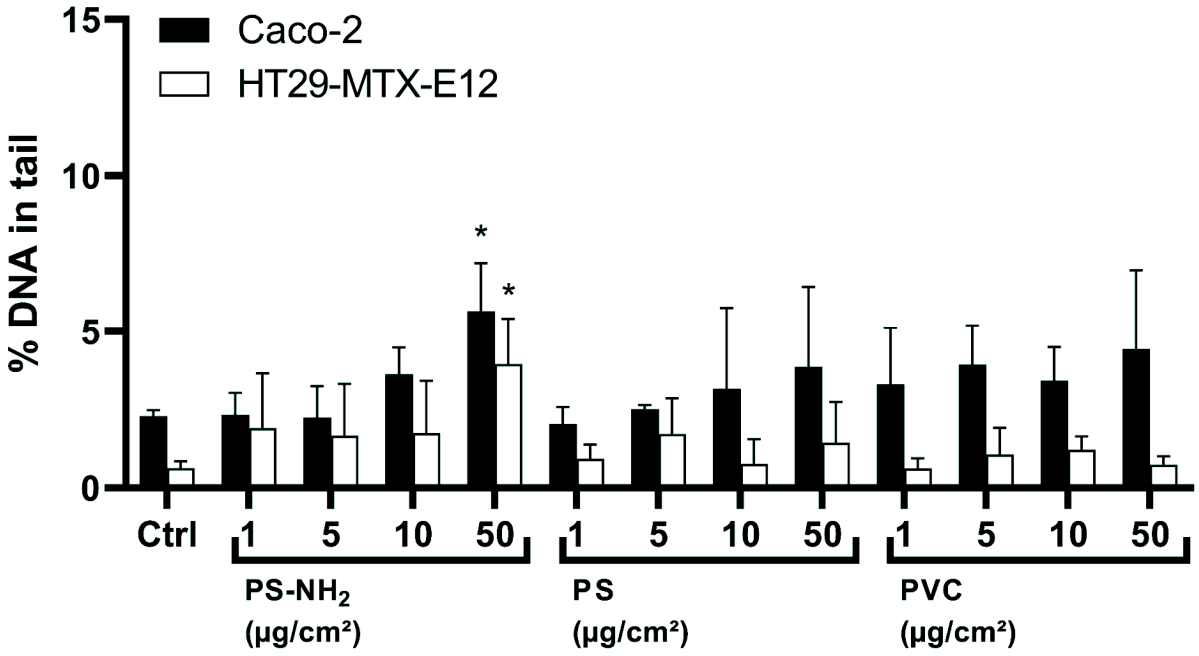

Figure 3.4 DNA damage in monocultures of undifferentiated Caco-2 (solid bars) and HT29-MTX-E12 (open bars) after 4 h of exposure to 1 – 50 µg/cm² PS-NH2, PS or PVC, as assessed by the alkaline comet assay. Mean ± SD of N=3, *p<0.05 compared to the respective control.

IL-1β release in THP-1 monocultures

IL-1β was quantified in supernatants from particle-treated PMA-differentiated THP-1 monocultures (**Figure 3.5**). Untreated THP-1 cells exhibit a basal IL-1β release of ~13±2 pg/ml. 24 h treatment with PS-NH_2 particles induced a significantly increased release of IL-1β (400 - 600 pg/ml) at concentrations of 5 – 10 µg/cm², while exposure to PS and PVC particles induced no effect.

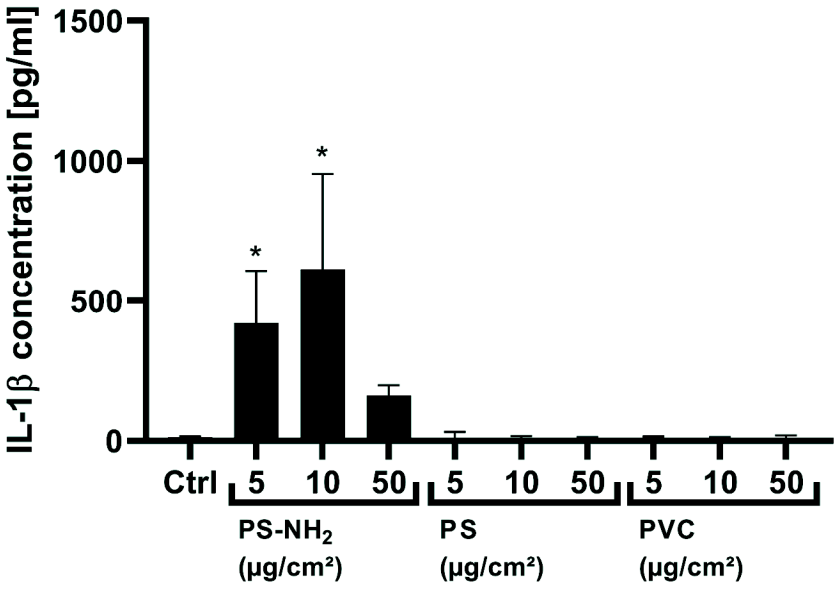

Figure 3.5 IL-1β concentrations in the supernatants of PMA-differentiated THP-1 monocultures after 24 h exposure to 5 – 50 µg/cm² PS-NH_2, PS or PVC. Cytokine content was analyzed via ELISA. Mean ± SD of N=3, *p<0.05 compared to the respective control.

Effects of plastic particles in an *in vitro* triple culture model of the healthy and inflamed intestine

After evaluating the effects of the tested plastic particles in monocultures of the three cell lines Caco-2, HT29-MTX-E12 and THP-1, we applied the particles as apical treatments in the triple culture models of the healthy and inflamed intestine.

Barrier integrity

The triple culture model in inflamed state is characterized by impairment of barrier integrity (**Figure 3.6A**), necrotic processes (**Figure S 3.4**) and the increased release of pro-inflammatory cytokines (**Figure S 3.7**). Treatment with PS-NH_2, PS or PVC particles was initiated 24 h after establishment of the triple culture in stable or inflamed state, when TEER in the inflamed culture was at its minimum. TEER was measured at t=48 after 24 h of particle treatment (**Figure 3.6B**). TEER of the stable cultures at t=48 was found to be generally higher than in the inflamed cultures (~300 Ω*cm² and ~270 Ω*cm², respectively). Treatment with PS-NH_2 particles led to a dose-dependent increase of TEER in both the stable and inflamed triple culture up to 460 and 360 Ω*cm², respectively. PS and PVC particles had no effect on TEER in both stable and inflamed triple culture. To further investigate the effects of plastic particle exposure on the intestinal barrier integrity, ZO-1 proteins in the epithelial layer were immunostained after 24 h of particle exposure in stable or inflamed state (**Figure 3.6C**). The triple culture in stable state is characterized by an organized, evenly structured network of ZO-1 connecting the individual cells. In contrast, inducing the inflamed state in the triple culture caused an irregular, patchy decrease of the ZO-1 fluorescence intensity. Exposure of the stable triple culture to 50 µg/cm² PS-NH_2 for 24 h also resulted in irregularly distributed areas of decreased ZO-1 fluorescence. No effects were observed after treatment of the inflamed triple culture with PS-NH_2. Treatment with PS or PVC did not affect the ZO-1 network fluorescence intensity or structural integrity in both stable or inflamed state when compared to the respective control.

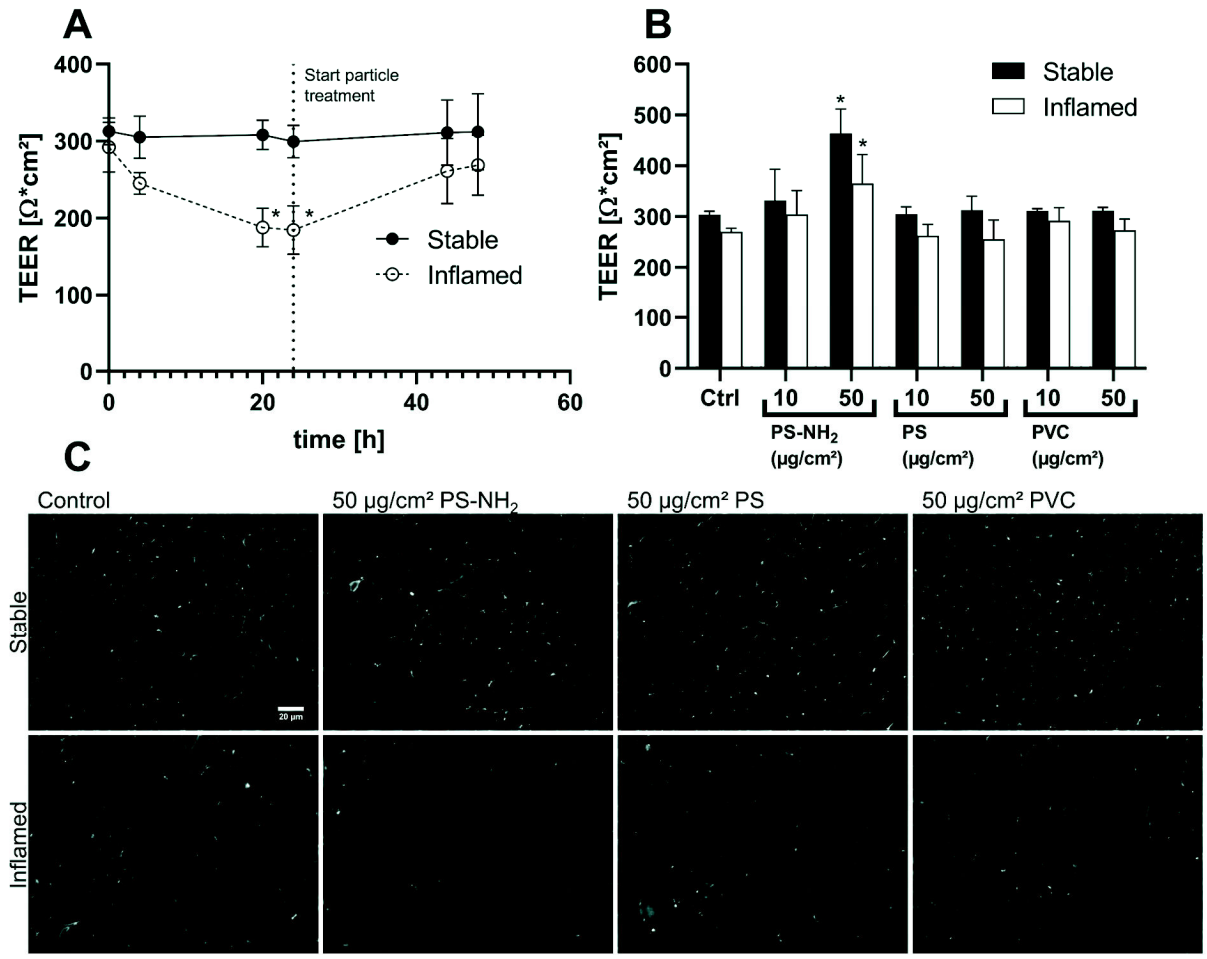

Figure 3.6 (A) Transepithelial electric resistance (TEER) during 48 h of triple culture in stable (solid circles) or inflamed (open circles) state without treatment or (B) at t=48 after 24 h of PS-NH_2, PS or PVC exposure (10 – 50 µg/cm²) in stable (solid bars) or inflamed (open bars) triple cultures. Exposure started at t=24. Mean ± SD of N≥3, *p<0.05 compared to (A) the stable triple culture or (B) the respective control. (C) Representative images of immunostained ZO-1 proteins in the epithelial layer of stable or inflamed triple cultures after 24 h treatment with 50 µg/cm² PS-NH_2, PS or PVC. 400x magnification; scale bar (20 µm) applies to all images.

Cytotoxicity and DNA damage

To investigate cytotoxic processes in the triple cultures, LDH activity was analyzed in the apical supernatant at t=48, after 24 h of particle exposure (**Figure 3.7A**). The LDH activity in the apical supernatant of inflamed cultures was found to be ~200 % compared to the stable cultures (see absolute LDH activity, **Figure S 3.4**). Exposure with 50 µg/cm² PS-NH_2 led to a significant increase in LDH release in the stable triple culture (120 % of the respective control), but did not further increase LDH release in the inflamed culture. Exposure to PS or PVC did not alter LDH release into the apical compartment in stable or inflamed state. Cytotoxicity was further investigated by quantifying the nuclei in the epithelial layer after 24 h exposure to PS-NH_2, PS or PVC (**Figure 3.7B**). In all experiments, we observed a significantly reduced number of nuclei in the inflamed triple cultures, compared to the stable triple cultures (see absolute nuclei numbers, **Figure S 3.5** and representative images, **Figure S 3.6**). Exposure of the

inflamed triple culture to PVC led to a dose-dependent decrease of nuclei in the epithelial layer. After 24 h of treatment with 50 µg/cm² PVC, the number of nuclei was significantly reduced to ~90 % of the respective control. Treatment of the triple cultures with PS-NH_2 or PS in stable or inflamed state had no effect on the number of nuclei. Furthermore, DNA damage in the epithelial cells of the triple culture model was assessed via alkaline comet assay, detecting DNA single and double strand breaks as well as alkali-labile sites (**Figure 3.7C**). No difference in the basal DNA damage of untreated controls was observed between the stable and inflamed triple culture (both ~1.5 % DNA in tail). 24 h exposure with PS-NH_2, PS or PVC did not result in increased DNA damage in the cells of the epithelial layer. Treatment with the non-particulate, chemical control MMS caused similar DNA damage in the stable and inflamed models (~50 % DNA in tail, data not shown).

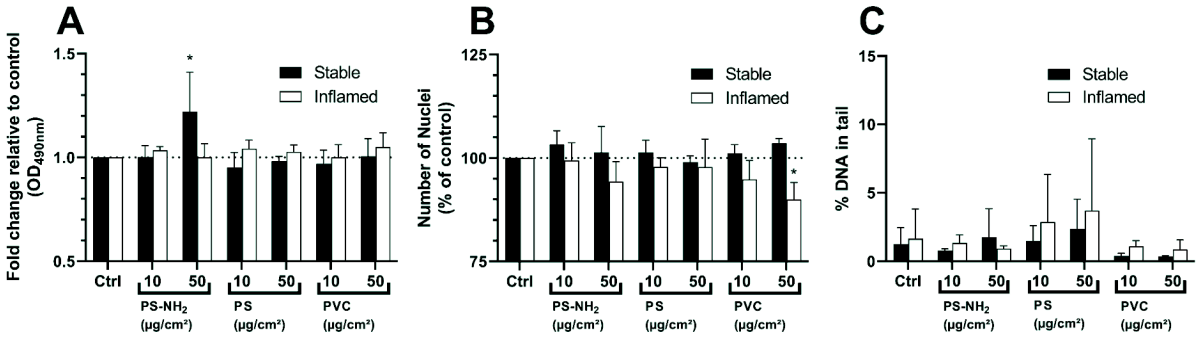

Figure 3.7 (A) LDH-release in the apical compartment after 24 h exposure to 10 or 50 µg/cm² PS-NH_2, PS or PVC in stable (solid bars) or inflamed (open bars) triple cultures as assessed by the LDH assay. (B) Quantification of Hoechst-stained nuclei in the epithelial layer. ≥4000 nuclei were counted per condition and expressed as number of nuclei per mm² filter area, relative to the untreated control. (C) DNA damage in cells of the epithelial layer as assessed by alkaline comet assay. Means ± SD of N=3, *p<0.05 compared to the respective control.

Cytokine release

To detect possible effects of particle exposure on the release of pro-inflammatory cytokines, IL-1β, IL-6, IL-8 and TNF-α concentrations were quantified in the basolateral supernatant of the triple cultures (**Figure 3.8**). IL-1β and IL-8 were present in both stable and inflamed cultures whereas IL-6 and TNF-α could not be detected in supernatants of the stable triple cultures. As expected, all four investigated cytokines were strongly increased in the inflamed compared to the stable triple cultures (for absolute concentrations see **Figure S 3.7**). After 24 h exposure to PS-NH_2 or PS particles, the concentrations of IL-1β, IL-6, IL-8 and TNF-α in the basolateral supernatants of the treated wells did not differ from the concentrations in the wells of the respective controls. Exposure of the inflamed triple culture with 50 µg/cm² PVC particles induced a statistically significant two-fold increase in IL-1β ($p=0.0237$), compared to the untreated control. In addition, a decrease to ~50 % in the release of IL-8 was noted, which was not statistically significant. However, the release of TNF-α and IL-6 was not affected by PVC treatment.

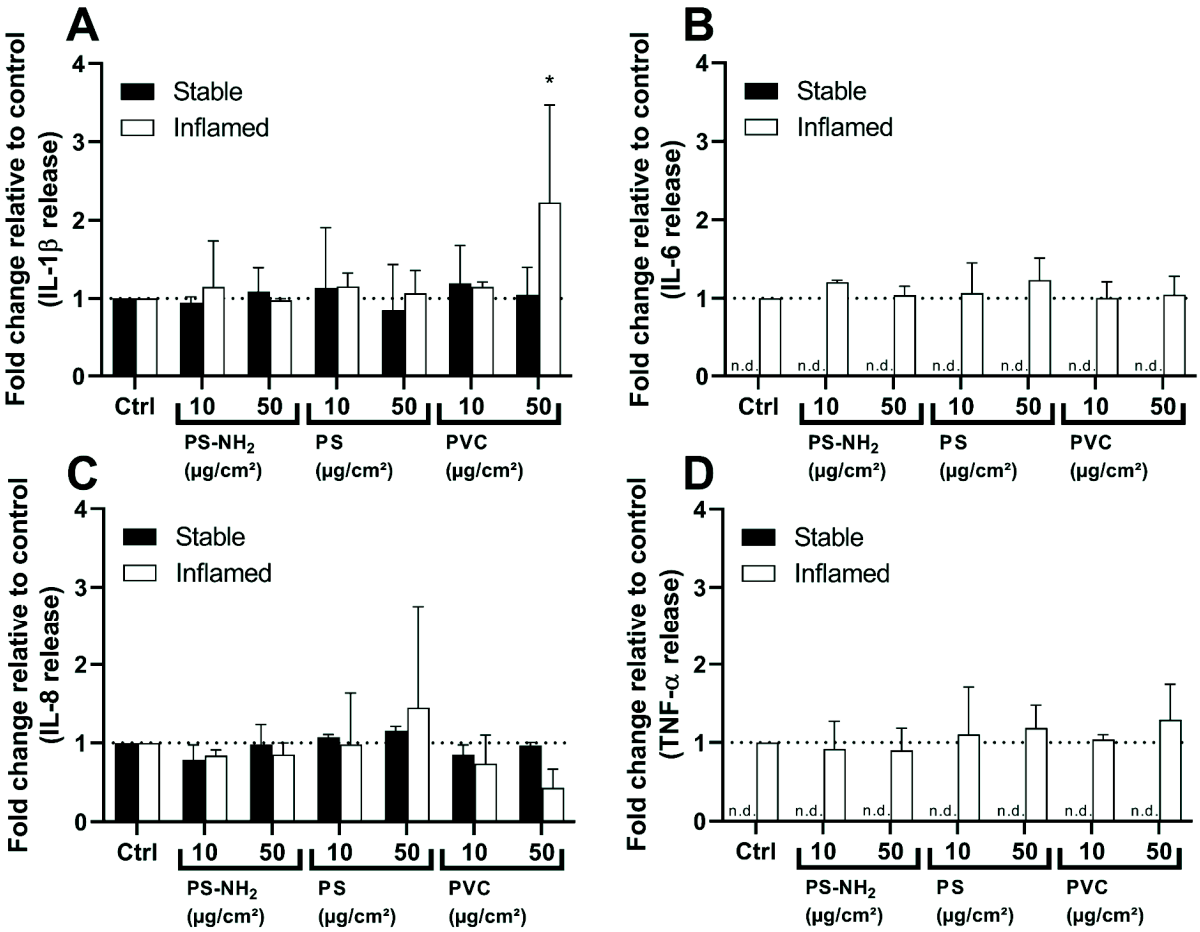

Figure 3.8 (A) IL-1β (B) IL-6 (C) IL-8 or (D) TNF-α release in the basolateral compartment after 24 h exposure to 10 or 50 µg/cm² PS-NH_2, PS or PVC particles in stable (solid bars) or inflamed (open bars) triple cultures (n.d. = not detectable). Means ± SD of N=3, *p<0.05 compared to the respective control.

Mucus presence and distribution

To investigate possible effects of micro- and nanoplastic exposure on the presence and distribution of mucus in the triple culture model, neutral and acidic mucus were stained using the PAS reaction and AB (**Figure 3.9**). The induction of the inflamed state led to a noticeable weaker PAS-associated magenta stain compared to the stable control. In addition, AB-stained areas in the cell layer appeared to be smaller and less frequent in the inflamed triple culture. Exposure of the triple culture in stable state to 50 µg/cm² PS-NH_2 caused an irregular, patchy thinning of the magenta stain. No effect was observed regarding staining intensity, shape or frequency of AB-stained areas after PS-NH_2 treatment in stable state. In comparison to the respective control, no difference in mucus staining was observed after PS-NH_2 exposure in the inflamed triple culture. Exposure to 50 µg/cm² PS or PVC did not induce any changes in staining patterns in both stable or inflamed triple cultures.

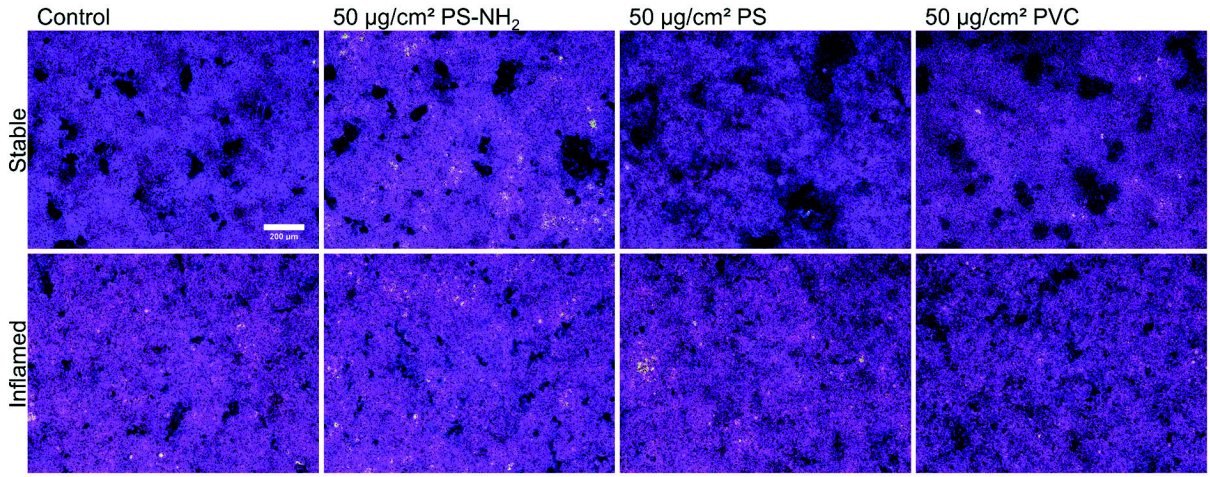

Figure 3.9 Representative images of neutral (magenta color; PAS reaction) and acidic (blue color; AB staining) mucus in stable or inflamed triple cultures after 24 h treatment with 50 µg/cm² PS-NH_2, PS or PVC. 100x magnification; scale bar (200 µm) applies to all images.

3.5 Discussion

The aim of this study was to investigate possible effects of micro- and nanoplastics in a triple culture model of the human intestine under healthy or inflamed conditions. Model particles were chosen based on their relevance: Several studies found polyethylene (PE), polypropylene (PP), PS and PVC to be the most abundant particle polymer types in the environment (Lots *et al.*, 2017; Ter Halle *et al.*, 2017; Lenaker *et al.*, 2019), drinking water (Tong *et al.*, 2020; Zhang *et al.*, 2020), commercial fish (Karbalaei *et al.*, 2019) and human stool (Schwabl *et al.*, 2019). However, PE and PP particles are challenging to study using conventional *in vitro* cell systems due to their buoyant nature in water and cell culture medium. Therefore, PS and PVC were chosen as model particles for the experimental set-up used here. PS-NH_2 nanobeads served as a positive control based on reported cytotoxic properties (Thubagere and Reinhard, 2010; Bhattacharjee *et al.*, 2014), NLRP3 inflammasome activation (Lunov *et al.*, 2011), decrease of transepithelial resistance in a Caco-2/HT29-MTX co-culture model (Walczak *et al.*, 2015) and toxicity towards various aquatic and terrestric microorganisms (Della Torre *et al.*, 2014; Bergami *et al.*, 2017; Marques-Santos *et al.*, 2018). The latter studies used amine-modified polystyrene as a model particle for environmental nanoplastics. Importantly, however, PS-NH_2 particles are synthesized exclusively for R&D purposes and there is no evidence that amine-modifications of plastic polymers occur spontaneously in the environment, in contrast to other chemical modifications such as peroxidation of the carbon backbone structure (Gewert *et al.*, 2015). Therefore, we would not recommend the use of PS-NH_2 as a model particle for the hazard assessment of environmental micro- and nanoplastics but encourage their application as a polymer-based particulate positive control when assessing the toxicity of environmentally relevant polymeric particles.

The particles were characterized via SEM and DLS to confirm the manufacturers' size declarations and acquire the parameters needed for the sedimentation modeling. Visual

analysis and determination of mean diameter by SEM confirmed the primary particle sizes given by the manufacturers for PS-NH_2 and PS particles. The PVC particles used in our studies showed a broad size distribution, mainly in the range between 200 nm and several micrometers. At present, there is no consensus on the definition of “nanoplastics”, as some researchers rely on the definition of a nanomaterial by the European Commission (1 – 100 nm) (EFSA, 2016), while others proposed a size range of 1 – 1000 nm (Browne *et al.*, 2007; da Costa *et al.*, 2016; Gigault *et al.*, 2018). Nonetheless, the observed size distribution makes this type of PVC an appropriate model material representing the highly heterogenous environmental plastic particles in micro- and nanometer range.

The ISDD simulation showed that all three types of plastic particles settle over time and can therefore interact with the cells. Mass-wise, PVC settles the fastest due to the higher density and hydrodynamic diameter, compared to the densities of PS-NH_2 and PS. In studies that have addresses the pulmonary toxicity of nanoparticles, surface area rather than mass dose has been shown to be the crucial parameter (Duffin *et al.*, 2007; Schmid and Stoeger, 2016). The deposited surface area of PS-NH_2 (5 cm²) and PS (9 cm²) exceeds the deposited surface area of PVC (2.5 cm²) due to smaller primary particle size. Altogether, the sedimentation simulation allows an estimation of the delivered dose. Based on an applied dose of 50 µg/cm², the delivered doses in the triple-culture experiments would translate to 5.5 µg/cm², 8.5 µg/cm² and 17.5 µg/cm² for PS-NH_2, PS and PVC, respectively.

Prior to the triple culture experiments, we investigated cytotoxicity, DNA damage and IL-1β release in monocultures of the three cell lines to detect possible cell-line specific effects. Cytotoxic effects in monocultures of Caco-2, HT29-MTX-E12 and THP-1 were assessed via WST-1 and LDH assay as complementary approaches to account for possible particle-specific interferences.

PS-NH_2 particles significantly reduced viability and increased cytotoxicity in all three cell lines in agreement with findings by others (Xia *et al.*, 2008; Thubagere and Reinhard, 2010). The mechanisms behind PS-NH_2 induced cytotoxicity reportedly include membrane destabilization and rupture, generation of reactive oxygen species (ROS) and lysosomal rupture after cellular uptake (Xia *et al.*, 2008; Ivask *et al.*, 2012; Ruenraroengsak *et al.*, 2012). The LDH assay appears to be less sensitive, as cytotoxic effects are observable at higher concentrations than in the WST-1 assay. However, since tetrazolium-based assays are impractical regarding the experimental design of the triple culture studies, we applied the LDH assay in both monoculture and triple culture experiments. Despite the reduced sensitivity, the general outcome of the LDH assay is comparable to the WST-1 assay. We noted a small, statistically significant increase in DNA damage in Caco-2 and HT29-MTX-E12 cells after 4 h treatment with 50 µg/cm² PS-NH_2. This is most likely linked to early cytotoxicity instead of actual genotoxic events, as we

observed drastically reduced metabolic activity and increased release of LDH in Caco-2 and HT29-MTX-E12 cells already after 4 h treatment with 50 µg/cm² PS-NH_2 (**Figure S 3.2**).

As in the monocultures, the exposure to PS-NH_2 caused an increased LDH activity in the supernatant of the stable triple culture model. Furthermore, exposure to PS-NH_2 caused an overall thinning of the neutral mucus layer in the stable triple culture, which is most likely a result of cytotoxicity. It appears that the acidic mucus, which can be attributed to the HT29-MTX-E12 cells, since it is not produced by Caco-2 cells (Antunes *et al.*, 2013; Araújo and Sarmento, 2013), is less affected than the neutral mucus. This matches the observations made with the WST-1 assay, indicating that the Caco-2 cell line is more vulnerable towards PS-NH_2-induced toxicity than the HT29-MTX-E12 cell line. The level of toxicity in the stable triple culture appears to be lower than in the monocultures, with no detectable effect at 10 µg/cm² exposure concentration and no significant increase in DNA damage. This difference in vulnerability could be attributed to the differentiation status of the Caco-2 cells and the reduced particle-to-cell ratio in the confluent triple-cultures, as similar observations were reported by (Gerloff *et al.*, 2013) after exposure of undifferentiated and differentiated, confluent Caco-2 cells to SiO_2 and ZnO nanoparticles. In addition, an increase in cell-cell contacts might have an additional protective function (Wenz *et al.*, 2019). Despite the effects in monocultures and in the stable triple culture, we did not observe any PS-NH_2 induced cytotoxic effects in the inflamed triple culture. We hypothesize that the inflammation-related cytotoxicity and mucus thinning masks the cytotoxic impact of PS-NH_2, which might no longer be detectable via LDH assay or visible via mucus staining.

Furthermore, PS-NH_2-treatment of the triple cultures in stable or inflamed state resulted in a significant, dose-dependent increase of TEER. The TEER-increasing effect of PS-NH_2 is stronger in the stable triple culture compared to the inflamed triple culture (~150% and ~130% of the control, respectively). TEER in an intact cell layer is largely influenced by tight junction proteins (Chen *et al.*, 2015). Therefore, we immunostained the transwell filters for ZO-1, a polypeptide associated with tight junctions (TJ) on cell membranes (Stevenson *et al.*, 1986), to investigate possible changes in the TJ network. We did not observe an increased fluorescence intensity of ZO-1 after PS-NH_2 exposure, but rather a patchy decrease of fluorescent signal in the stable triple culture. The increase of TEER appears not to be connected to an increase in ZO-1 abundance. However, it might be the result of low-level necrotic events caused by PS-NH_2 that could lead to cell swelling, which in turn reduces intercellular space (Olsson *et al.*, 2006), causing the TEER to increase. The observed LDH leakage, the time-dependent increase of TEER over the span of 24 h (**Figure S 3.3**) and the unaltered abundance of nuclei support this hypothesis, as high-level necrosis would cause a loss of cells and therefore a decrease in TEER. Kämpfer *et al.* (2020c) observed a similar phenomenon in Caco-2/THP-1 co-cultures exposed with cytotoxic $AgNO_3$ salts. Although no

additional LDH release was detected in particle-exposed inflamed triple cultures, the increase in TEER suggests the induction of similar mechanisms as in the stable model.

Next, we investigated pro-inflammatory cytokine responses in the triple cultures. Despite the strong increase of IL-1β release in THP-1 monocultures and the activation of the NLRP3 inflammasome as reported by others (Lunov *et al.*, 2011), epithelial exposure to PS-NH_2 did not increase cytokine concentrations in the basolateral supernatant of stable or inflamed triple cultures. This suggests that PS-NH_2 were not able to penetrate the epithelial barrier to interact with the THP-1 cells directly, which is in line with the findings of the translocation studies reported by Walczak *et al.* (2015).

PVC particles did not exhibit any cytotoxic properties in the monocultures or in the stable triple culture. Although no effect on barrier integrity, LDH activity or mucus distribution was noted after treatment with PVC in the inflamed triple culture, we observed a significantly reduced number of nuclei. It appears that exposure to PVC particles during an active inflammation causes an increased loss of epithelial cells that is not connected to any major necrotic processes, as indicated by the absence of increased LDH activity. However, treatment of the inflamed triple culture with PS-NH_2 also had no detectable effect on LDH activity, therefore the occurrence of necrotic processes could be below the detection limit of the LDH assay. The induction of apoptosis might explain this observed effect. A significant two-fold increase of IL-1β concentration was observed after treatment with 50 µg/cm² PVC in the inflamed cultures and IL-1β has been reported to induce apoptosis (Friedlander *et al.*, 1996; Shen *et al.*, 2017). Synergism with other cytokines present in the inflamed triple culture might enhance this effect. Although PVC particles did not directly stimulate an increased IL-1β release in THP-1 monocultures, the THP-1 cells in the triple cultures are most likely the source of the IL-1β in the basolateral supernatant. No IL-1β can be detected in the supernatants of modified triple cultures established with Caspase1- or NLRP3 inflammasome-deficient THP-1 cells (data not shown). The elucidation of the underlying mechanisms leading to an increased IL-1β release should be addressed in further studies. Because of this IL-1β-specific effect, we assume the involvement of an inflammasome complex, activated by mediators released from the PVC-exposed epithelial cells.

These observations indicate an increased vulnerability of the inflamed triple culture towards PVC particles compared to the stable model. Similar observations were reported *in vivo*, where treatment with plastic particles increased several inflammatory parameters in mice with DSS-induced colitis, including serum IL-1β levels (Zheng *et al.*, 2021).

Because no increase in DNA damage was observed after 4 h of exposure with PVC particles in the monocultures of Caco-2 and HT29-MTX-E12, we applied the comet assay after 24 h of particle treatment in the triple cultures to detect possible DNA damage induced by secondary mechanisms, such as inflammation-derived ROS generation (Coussens and Werb, 2002). The

exposure to PVC dust has been linked to pulmonary inflammation (Xu *et al.*, 2004) and an increased risk of lung cancer in PVC workers (Wagoner, 1983; Mastrangelo *et al.*, 2003). Furthermore, an increase of DNA damage in intestinal epithelial cells during prolonged active inflammation has been observed both *in vivo* (Pereira *et al.*, 2016) and *in vitro* (Kämpfer *et al.*, 2020b). However, we did not observe any increased DNA damage in epithelial cells of the inflamed cultures compared to the stable cultures after 48 h and plastic particle exposure had no effect on DNA damage levels.

We did not observe any effects regarding cytotoxicity, DNA damage, barrier integrity or cytokine release after treatment with *PS particles* in any of the experiments. This is in line with the findings of other studies reporting the absence of effects after investigating the toxicity of PS micro- and nanoparticles (Paget *et al.*, 2015; Walczak *et al.*, 2015; Schirinzi *et al.*, 2017), although, in contrast, some studies reported toxicologically relevant effects (Hwang et al, 2020). Furthermore, exposure to PS particles did not change the mucus distribution on the epithelial cell layer of the triple culture model in stable or inflamed state. Aside from observed changes in mucus distribution attributed to acute cytotoxic effects, actual changes in mucin expression and secretion are more likely a result of recurring, chronic exposure to particles instead of an acute reaction to a single dose.

3.6 Conclusions

The *in vitro* triple culture model of the healthy and inflamed intestine used in this study is a promising approach for the assessment of micro- and nanoplastic particle-induced effects while considering IBD-patients as a risk group of the population. We suggest that prevalent intestinal inflammation might be an important factor to consider when assessing the hazardous potential of ingested micro- and nanoplastic particles as exemplified by differences of PVC-induced toxicological effects in regard to the models' health status. The observation of these acute effects spawns the need for further research regarding chronic *in vitro* and *in vivo* testing to elucidate possible risks for human health, since oral micro- and nanoplastic intake can be assumed to be a chronic exposure.

Funding

This work was supported by the Jürgen Manchot foundation, Düsseldorf, Germany through a PhD scholarship for Mathias Busch.

Acknowledgements

The authors are grateful for the contribution by Inci Nur Sahin and Burkhard Stahlmecke of the IUTA e.V. Duisburg, Germany, who conducted the SEM analysis of the plastic particles. Furthermore, we would like to thank Jun. Prof. Dr. Stefan Schmidt and Fabian Schröer of the Heinrich Heine University Düsseldorf, Germany, for providing access to their Zetasizer Nano-

ZS. Moreover, the authors are thankful to Prof. Dr. Stefan Egelhaaf and Manuel Escobedo-Sánchez of the Heinrich Heine University for providing access to the instruments and support needed to characterize the cell culture medium.

3.7 Supplementary material

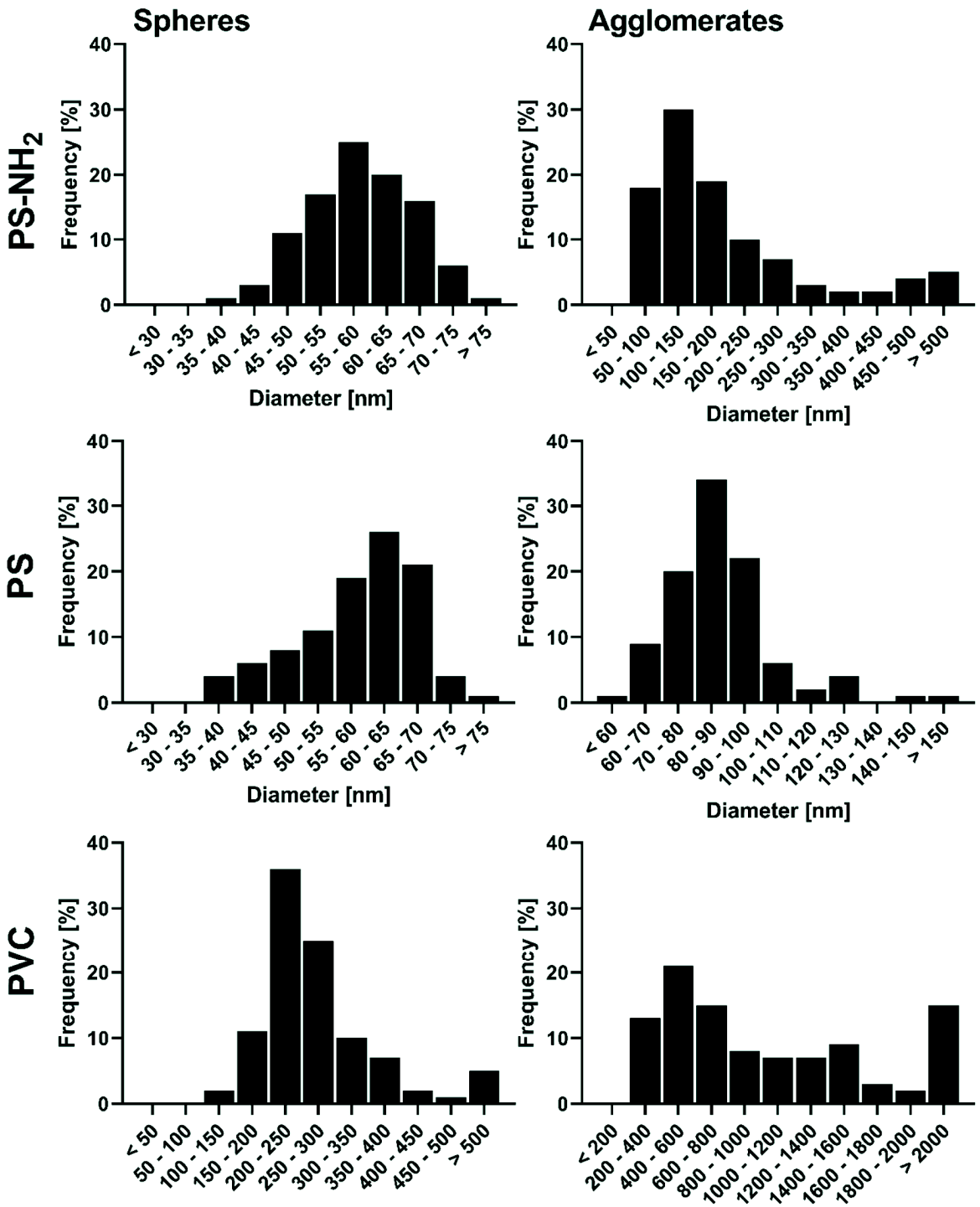

Figure S 3.1 PS-NH_2, PS and PVC sphere and agglomerate size distribution based on SEM analysis. For each type of plastic particle, ≥300 spheres and agglomerates were analyzed.

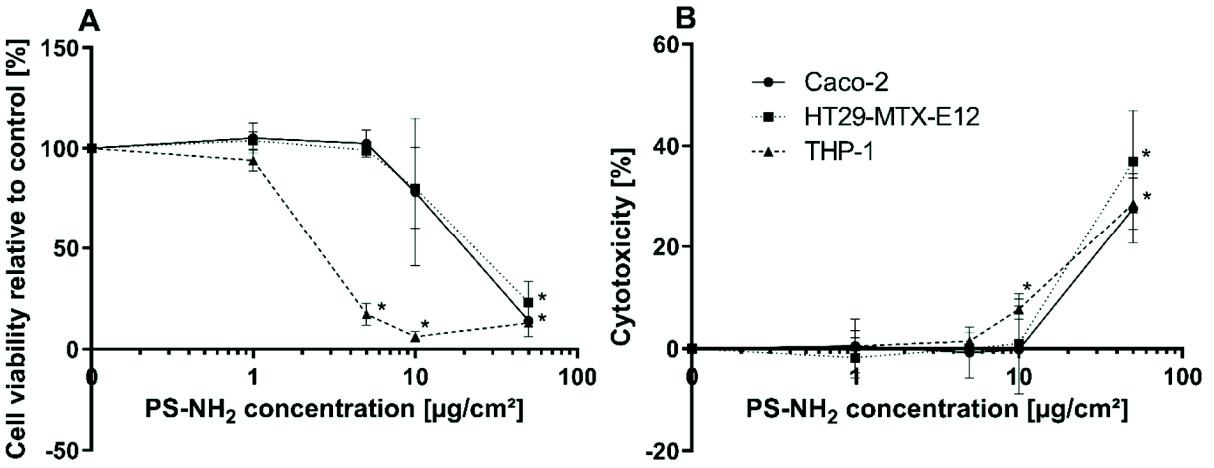

Figure S 3.2 (A) Cell viability or (B) cytotoxicity of undiff. Caco-2 (circles), HT29-MTX-E12 (squares) and THP-1 cells (triangles) after 4 h exposure to 1 – 50 µg/cm² PS-NH_2. Cell viability was assessed via WST-1 assay, cytotoxicity was assessed via LDH assay. Mean ± SD of N=3, *p<0.05 compared to the respective control.

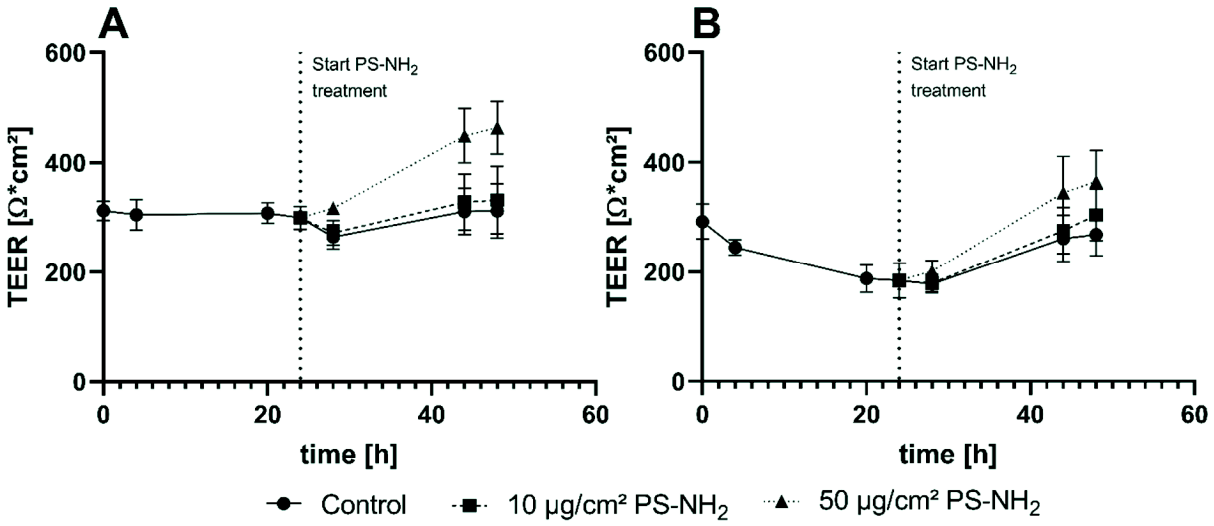

Figure S 3.3 TEER in (A) stable or (B) inflamed triple cultures 24 h before and during exposure to 0 (circles), 10 (squares) or 50 (triangles) µg/cm² PS-NH_2. Mean ± SD of N=4, *p<0.05 compared to the respective control.

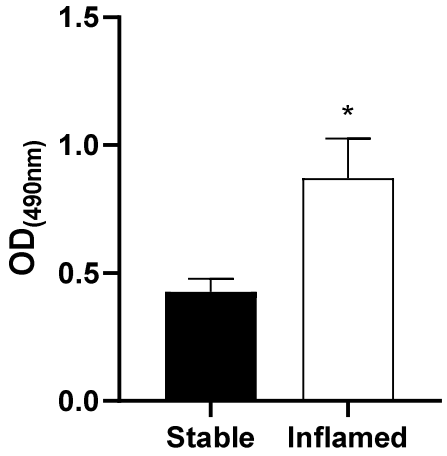

Figure S 3.4 LDH activity in the apical supernatants of stable or inflamed triple cultures. Mean ± SD of N=9, *p<0.05 (unpaired t-test).

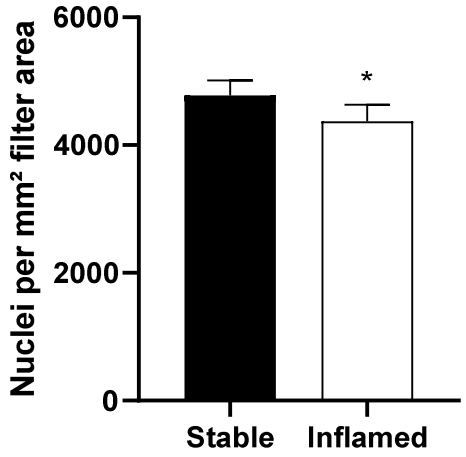

Figure S 3.5 Number of Hoechst-stained nuclei per mm² filter area after 48 h of stable or inflamed state. Mean ± SD of N=9, *p<0.05 (unpaired t-test).

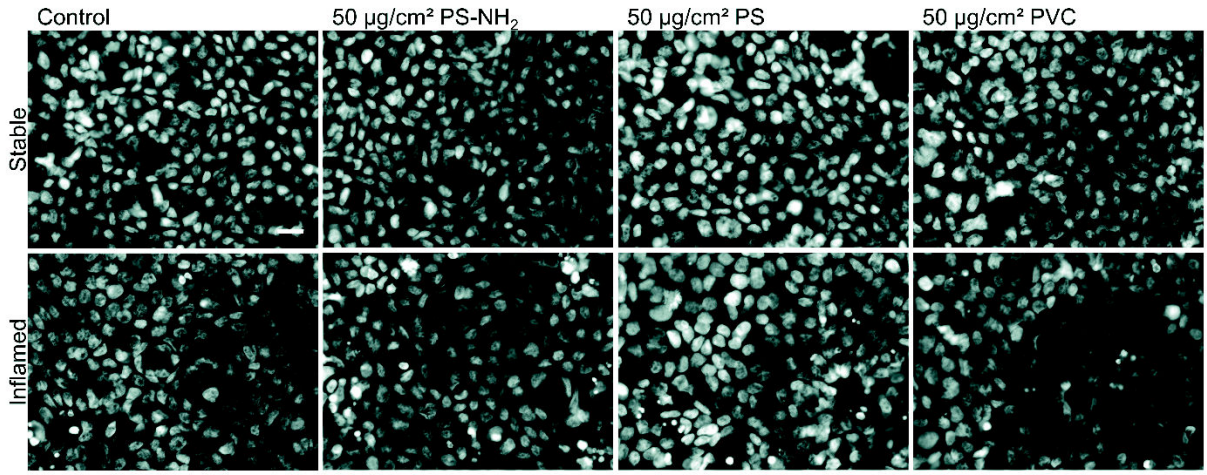

Figure S 3.6 Representative images of Hoechst-stained nuclei in the epithelial layer of stable or inflamed triple cultures after 24 h treatment with 50 µg/cm² PS-NH_2, PS or PVC. 400x magnification; scale bar (20 µm) applies to all images.

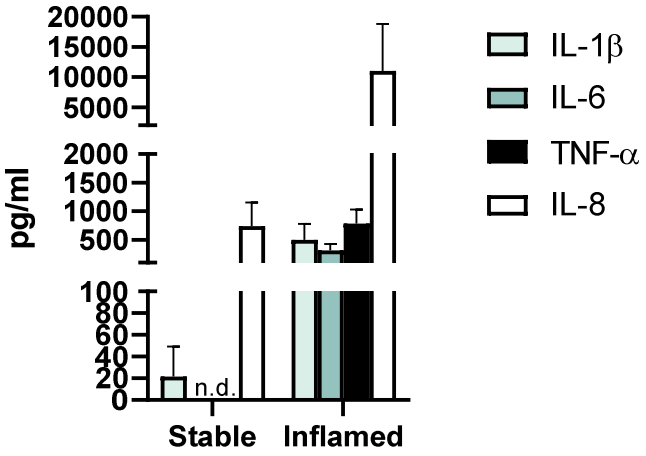

Figure S 3.7 Absolute concentrations of IL-1β, IL-6, IL-8 and TNF-α in the basolateral compartment of the triple culture in stable or inflamed state after 48 h. Mean ± SD of N=9, n.d.=not detectable.

3.8 References

Abdelkhaliq, A., van der Zande, M., Punt, A., Helsdingen, R., Boeren, S., Vervoort, J.J.M., Rietjens, I.M.C.M., Bouwmeester, H., 2018. Impact of nanoparticle surface functionalization on the protein corona and cellular adhesion, uptake and transport. J. Nanobiotechnology 16, 70. https://doi.org/10.1186/s12951-018-0394-6.

Andrady, A.L., 2012. Biodegradation of Plastics: Monitoring what Happens. In: Brewis, D., Briggs, D., Pritchard, G. (Eds.) Plastics Additives. An A-Z reference, vol. 1. Springer Netherlands, Dordrecht, pp. 32–40.

Antunes, F., Andrade, F., Araújo, F., Ferreira, D., Sarmento, B., 2013. Establishment of a triple co-culture in vitro cell models to study intestinal absorption of peptide drugs. Eur. J. Pharm. Biopharm. 83, 427–435. https://doi.org/10.1016/j.ejpb.2012.10.003.

Araújo, F., Sarmento, B., 2013. Towards the characterization of an in vitro triple co-culture intestine cell model for permeability studies. Int. J. Pharm. 458, 128–134. https://doi.org/10.1016/j.ijpharm.2013.10.003.

Barboza, L.G.A., Dick Vethaak, A., Lavorante, B.R.B.O., Lundebye, A.-K., Guilhermino, L., 2018. Marine microplastic debris: An emerging issue for food security, food safety and human health. Mar. Pollut. Bull. 133, 336–348. https://doi.org/10.1016/j.marpolbul.2018.05.047.

Barnes, D.K.A., Galgani, F., Thompson, R.C., Barlaz, M., 2009. Accumulation and fragmentation of plastic debris in global environments. Philos. Trans. R. Soc. Lond. B Biol. Sci. 364, 1985–1998. https://doi.org/10.1098/rstb.2008.0205.

Bergami, E., Pugnalini, S., Vannuccini, M.L., Manfra, L., Faleri, C., Savorelli, F., Dawson, K.A., Corsi, I., 2017. Long-term toxicity of surface-charged polystyrene nanoplastics to marine planktonic species Dunaliella tertiolecta and Artemia franciscana. Aquat. Toxicol. 189, 159–169. https://doi.org/10.1016/j.aquatox.2017.06.008.

Bhattacharjee, S., Ershov, D., Islam, M.A., Kämpfer, A.M., Maslowska, K.A., van der Gucht, J., Alink, G.M., Marcelis, A.T.M., Zuilhof, H., Rietjens, I.M.C.M., 2014. Role of membrane disturbance and oxidative stress in the mode of action underlying the toxicity of differently charged polystyrene nanoparticles. RSC Adv. 4, 19321–19330. https://doi.org/10.1039/C3RA46869K.

Borrelle, S.B., Ringma, J., Law, K.L., Monnahan, C.C., Lebreton, L., McGivern, A., Murphy, E., Jambeck, J., Leonard, G.H., Hilleary, M.A., Eriksen, M., Possingham, H.P., Frond, H. de, Gerber, L.R., Polidoro, B., Tahir, A., Bernard, M., Mallos, N., Barnes, M., Rochman, C.M., 2020. Predicted growth in plastic waste exceeds efforts to mitigate plastic pollution. Science 369, 1515–1518. https://doi.org/10.1126/science.aba3656.

Bouwmeester, H., Hollman, P.C.H., Peters, R.J.B., 2015. Potential Health Impact of Environmentally Released Micro- and Nanoplastics in the Human Food Production Chain: Experiences from Nanotoxicology. Environ. Sci. Technol. 49, 8932–8947. https://doi.org/10.1021/acs.est.5b01090.

Browne, M.A., Galloway, T., Thompson, R., 2007. Microplastic—an emerging contaminant of potential concern? Integr. Environ. Assess. Manag. 3, 559–561. https://doi.org/10.1002/ieam.5630030412.

Burisch, J., Jess, T., Martinato, M., Lakatos, P.L., 2013. The burden of inflammatory bowel disease in Europe. J. Crohns Colitis 7, 322–337. https://doi.org/10.1016/j.crohns.2013.01.010.

Chen, S., Einspanier, R., Schoen, J., 2015. Transepithelial electrical resistance (TEER): A functional parameter to monitor the quality of oviduct epithelial cells cultured on filter supports. Histochem. Cell Biol. 144, 509–515. https://doi.org/10.1007/s00418-015-1351-1.

Cho, J.H., Brant, S.R., 2011. Recent insights into the genetics of inflammatory bowel disease. Gastroenterology 140, 1704–1712. https://doi.org/10.1053/j.gastro.2011.02.046.

Coussens, L.M., Werb, Z., 2002. Inflammation and cancer. Nature 420, 860–867. https://doi.org/10.1038/nature01322.

da Costa, J.P., Santos, P.S.M., Duarte, A.C., Rocha-Santos, T., 2016. (Nano)plastics in the environment - Sources, fates and effects. Sci. Total. Environ. 566-567, 15–26. https://doi.org/10.1016/j.scitotenv.2016.05.041.

Dahlhamer, J.M., Zammitti, E.P., Ward, B.W., Wheaton, A.G., Croft, J.B., 2016. Prevalence of Inflammatory Bowel Disease Among Adults Aged ≥18 Years — United States, 2015. Morb. Mortal. Wkly. Rep. 65, 1166–1169. https://doi.org/10.15585/mmwr.mm6542a3.

Della Torre, C., Bergami, E., Salvati, A., Faleri, C., Cirino, P., Dawson, K.A., Corsi, I., 2014. Accumulation and embryotoxicity of polystyrene nanoparticles at early stage of development of sea urchin embryos Paracentrotus lividus. Environ. Sci. Technol. 48, 12302–12311. https://doi.org/10.1021/es502569w.

DeLoid, G., Cohen, J.M., Darrah, T., Derk, R., Rojanasakul, L., Pyrgiotakis, G., Wohlleben, W., Demokritou, P., 2014. Estimating the effective density of engineered nanomaterials for in vitro dosimetry. Nat. Commun. 5, 3514. https://doi.org/10.1038/ncomms4514.

Duffin, R., Tran, L., Brown, D., Stone, V., Donaldson, K., 2007. Proinflammogenic effects of low-toxicity and metal nanoparticles in vivo and in vitro: highlighting the role of particle surface area and surface reactivity. Inhal. Toxicol. 19, 849–856. https://doi.org/10.1080/08958370701479323.

Forte, M., Iachetta, G., Tussellino, M., Carotenuto, R., Prisco, M., Falco, M. de, Laforgia, V., Valiante, S., 2016. Polystyrene nanoparticles internalization in human gastric adenocarcinoma cells. Toxicol. In Vitro 31, 126–136. https://doi.org/10.1016/j.tiv.2015.11.006.

Friedlander, R.M., Galiardini, V., Rotello, R.J., Yuan, J., 1996. Functional Role of Interleukin 1β (IL-1β) in IL-1β-converting Enzyme-mediated Apoptosis. J. Exp. Med. 184, 717–724. https://doi.org/10.1084/jem.184.2.717.

Gerloff, K., Pereira, D.I.A., Faria, N., Boots, A.W., Kolling, J., Förster, I., Albrecht, C., Powell, J.J., Schins, R.P.F., 2013. Influence of simulated gastrointestinal conditions on particle-induced cytotoxicity and interleukin-8 regulation in differentiated and undifferentiated Caco-2 cells. Nanotoxicol. 7, 353–366. https://doi.org/10.3109/17435390.2012.662249.

Gewert, B., Plassmann, M.M., MacLeod, M., 2015. Pathways for degradation of plastic polymers floating in the marine environment. Environ. Sci. Process. Impacts 17, 1513–1521. https://doi.org/10.1039/c5em00207a.

Gigault, J., Ter Halle, A., Baudrimont, M., Pascal, P.-Y., Gauffre, F., Phi, T.-L., El Hadri, H., Grassl, B., Reynaud, S., 2018. Current opinion: What is a nanoplastic? Environ. Pollut. 235, 1030–1034. https://doi.org/10.1016/j.envpol.2018.01.024.

Gigault, J., Pedrono, B., Maxit, B., Ter Halle, A., 2016. Marine plastic litter: the unanalyzed nano-fraction. Environ. Sci. Nano 3, 346–350. https://doi.org/10.1039/C6EN00008H.

Hinderliter, P.M., Minard, K.R., Orr, G., Chrisler, W.B., Thrall, B.D., Pounds, J.G., Teeguarden, J.G., 2010. ISDD: A computational model of particle sedimentation, diffusion and target cell dosimetry for in vitro toxicity studies. Part. Fibre Toxicol. 7, 36. https://doi.org/10.1186/1743-8977-7-36.

Hwang, J., Choi, D., Han, S., Jung, S.Y., Choi, J., Hong, J., 2020. Potential toxicity of polystyrene microplastic particles. Sci. Rep. 10, 7391. https://doi.org/10.1038/s41598-020-64464-9

Ivask, A., Suarez, E., Patel, T., Boren, D., Ji, Z., Holden, P., Telesca, D., Damoiseaux, R., Bradley, K.A., Godwin, H., 2012. Genome-wide bacterial toxicity screening uncovers the mechanisms of toxicity of a cationic polystyrene nanomaterial. Environ. Sci. Technol. 46, 2398–2405. https://doi.org/10.1021/es203087m.

Julienne, F., Delorme, N., Lagarde, F., 2019. From macroplastics to microplastics: Role of water in the fragmentation of polyethylene. Chemosphere 236, 124409. https://doi.org/10.1016/j.chemosphere.2019.124409.

Kämpfer, A.A.M., Busch, M., Büttner, V., Bredeck, G., Stahlmecke, B., Hellack, B., Masson, I., Sofranko, A., Albrecht, C., Schins, R.P.F., 2020b. Model Complexity as Determining Factor for In Vitro Nanosafety Studies: Effects of Silver and Titanium Dioxide Nanomaterials in Intestinal Models. Small. https://doi.org/10.1002/smll.202004223.

Kämpfer, A.A.M., Busch, M., Schins, R.P.F., 2020a. Advanced In Vitro Testing Strategies and Models of the Intestine for Nanosafety Research. Chem. Res. Toxicol. 33, 1163–1178. https://doi.org/10.1021/acs.chemrestox.0c00079.

Kämpfer, A.A.M., Urbán, P., La Spina, R., Jiménez, I.O., Kanase, N., Stone, V., Kinsner-Ovaskainen, A., 2020c. Ongoing inflammation enhances the toxicity of engineered nanomaterials: Application of an *in vitro* co-culture model of the healthy and inflamed intestine. Toxicol. In Vitro 63, 104738. https://doi.org/10.1016/j.tiv.2019.104738.

Kappeler, A., Mueller, C., 2000. The role of activated cytotoxic T cells in inflammatory bowel disease. Histol. Histopathol. 15, 167–172. https://doi.org/10.14670/HH-15.167.

Karami, A., Golieskardi, A., Keong Choo, C., Larat, V., Galloway, T.S., Salamatinia, B., 2017. The presence of microplastics in commercial salts from different countries. Sci. Rep. 7, 46173. https://doi.org/10.1038/srep46173.

Karbalaei, S., Golieskardi, A., Watt, D.U., Boiret, M., Hanachi, P., Walker, T.R., Karami, A., 2019. Analysis and inorganic composition of microplastics in commercial Malaysian fish meals. Mar. Pollut. Bull. 150, 110687. https://doi.org/10.1016/j.marpolbul.2019.110687.

Kim, E.R., Chang, D.K., 2014. Colorectal cancer in inflammatory bowel disease: the risk, pathogenesis, prevention and diagnosis. World J. Gastroenterol. 20, 9872–9881. https://doi.org/10.3748/wjg.v20.i29.9872.

Kolling, J., Tigges, J., Hellack, B., Albrecht, C., Schins, R., 2020. Evaluation of the NLRP3 Inflammasome Activating Effects of a Large Panel of TiO_2 Nanomaterials in Macrophages. Nanomaterials 10, 1876. https://doi.org/10.3390/nano10091876

Kosuth, M., Mason, S.A., Wattenberg, E.V., 2018. Anthropogenic contamination of tap water, beer, and sea salt. PLoS One 13, e0194970. https://doi.org/10.1371/journal.pone.0194970.

Lambert, S., Wagner, M., 2016. Characterisation of nanoplastics during the degradation of polystyrene. Chemosphere 145, 265–268. https://doi.org/10.1016/j.chemosphere.2015.11.078.

Lenaker, P.L., Baldwin, A.K., Corsi, S.R., Mason, S.A., Reneau, P.C., Scott, J.W., 2019. Vertical Distribution of Microplastics in the Water Column and Surficial Sediment from the Milwaukee River Basin to Lake Michigan. Environ. Sci. Technol. 53, 12227–12237. https://doi.org/10.1021/acs.est.9b03850.

Li, B., Ding, Y., Cheng, X., Sheng, D., Xu, Z., Rong, Q., Wu, Y., Zhao, H., Ji, X., Zhang, Y., 2019. Polyethylene microplastics affect the distribution of gut microbiota and inflammation development in mice. Chemosphere 244, 125492. https://doi.org/10.1016/j.chemosphere.2019.125492.

Liebezeit, G., Liebezeit, E., 2015. Origin of Synthetic Particles in Honeys. Pol. J. Food Nutr. Sci. 65, 143–147. https://doi.org/10.1515/pjfns-2015-0025.

Lots, F.A.E., Behrens, P., Vijver, M.G., Horton, A.A., Bosker, T., 2017. A large-scale investigation of microplastic contamination: Abundance and characteristics of microplastics in European beach sediment. Mar. Pollut. Bull. 123, 219–226. https://doi.org/10.1016/j.marpolbul.2017.08.057.

Lu, L., Wan, Z., Luo, T., Fu, Z., Jin, Y., 2018. Polystyrene microplastics induce gut microbiota dysbiosis and hepatic lipid metabolism disorder in mice. Sci. Total. Environ. 631-632, 449–458. https://doi.org/10.1016/j.scitotenv.2018.03.051.

Lunov, O., Syrovets, T., Loos, C., Nienhaus, G.U., Mailänder, V., Landfester, K., Rouis, M., Simmet, T., 2011. Amino-functionalized polystyrene nanoparticles activate the NLRP3 inflammasome in human macrophages. ACS Nano 5, 9648–9657. https://doi.org/10.1021/nn203596e.

Maloy, K.J., Powrie, F., 2011. Intestinal homeostasis and its breakdown in inflammatory bowel disease. Nature 474, 298–306. https://doi.org/10.1038/nature10208.

Marques-Santos, L.F., Grassi, G., Bergami, E., Faleri, C., Balbi, T., Salis, A., Damonte, G., Canesi, L., Corsi, I., 2018. Cationic polystyrene nanoparticle and the sea urchin immune system: biocorona formation, cell toxicity, and multixenobiotic resistance phenotype. Nanotoxicol. 12, 847–867. https://doi.org/10.1080/17435390.2018.1482378.

Marsden, P., Koelmans, A.A., Bourdon-Lacombe, J., Gouin, T., Anglada, L.D.', Cunliffe, D., Jarvis, P., Fawell, J., France, J.D., 2019. Microplastics in drinking water 9789241516198. World Health Organization, Geneva. https://edepot.wur.nl/498693.

Mastrangelo, G., Fedeli, U., Fadda, E., Milan, G., Turato, A., Pavanello, S., 2003. Lung cancer risk in workers exposed to poly(vinyl chloride) dust: a nested case-referent study. Occup. Environ. Med. 60, 423–428. https://doi.org/10.1136/oem.60.6.423.

Mintenig, S.M., Löder, M.G.J., Primpke, S., Gerdts, G., 2019. Low numbers of microplastics detected in drinking water from ground water sources. Sci. Total. Environ. 648, 631–635. https://doi.org/10.1016/j.scitotenv.2018.08.178.

Neurath, M.F., 2014. Cytokines in inflammatory bowel disease. Nat. Rev. Immunol. 14, 329–342. https://doi.org/10.1038/nri3661.

Olsson, T., Broberg, M., Pope, K.J., Wallace, A., Mackenzie, L., Blomstrand, F., Nilsson, M., Willoughby, J.O., 2006. Cell swelling, seizures and spreading depression: an impedance study. Neuroscience 140, 505–515. https://doi.org/10.1016/j.neuroscience.2006.02.034.

Paget, V., Dekali, S., Kortulewski, T., Grall, R., Gamez, C., Blazy, K., Aguerre-Chariol, O., Chevillard, S., Braun, A., Rat, P., Lacroix, G., 2015. Specific uptake and genotoxicity induced by polystyrene nanobeads with distinct surface chemistry on human lung epithelial cells and macrophages. PLoS One 10, e0123297. https://doi.org/10.1371/journal.pone.0123297.

Park, M.V.D.Z., Neigh, A.M., Vermeulen, J.P., La Fonteyne, L.J.J. de, Verharen, H.W., Briedé, J.J., van Loveren, H., Jong, W.H. de, 2011. The effect of particle size on the cytotoxicity, inflammation, developmental toxicity and genotoxicity of silver nanoparticles. Biomaterials 32, 9810–9817. https://doi.org/10.1016/j.biomaterials.2011.08.085.

Pereira, C., Coelho, R., Grácio, D., Dias, C., Silva, M., Peixoto, A., Lopes, P., Costa, C., Teixeira, J.P., Macedo, G., Magro, F., 2016. DNA Damage and Oxidative DNA Damage in Inflammatory Bowel Disease. J. Crohns Colitis 10, 1316–1323. https://doi.org/10.1093/ecco-jcc/jjw088.

Qiao, R., Sheng, C., Lu, Y., Zhang, Y., Ren, H., Lemos, B., 2019. Microplastics induce intestinal inflammation, oxidative stress, and disorders of metabolome and microbiome in zebrafish. Sci. Total. Environ. 662, 246–253. https://doi.org/10.1016/j.scitotenv.2019.01.245.

Riebeling, C., Piret, J.-P., Trouiller, B., Nelissen, I., Saout, C., Toussaint, O., Haase, A., 2018. A guide to nanosafety testing: Considerations on cytotoxicity testing in different cell models. NanoImpact 10, 1–10. https://doi.org/10.1016/j.impact.2017.11.004.

Ruenraroengsak, P., Novak, P., Berhanu, D., Thorley, A.J., Valsami-Jones, E., Gorelik, J., Korchev, Y.E., Tetley, T.D., 2012. Respiratory epithelial cytotoxicity and membrane damage (holes) caused by amine-modified nanoparticles. Nanotoxicol. 6, 94–108. https://doi.org/10.3109/17435390.2011.558643.

Schirinzi, G.F., Pérez-Pomeda, I., Sanchís, J., Rossini, C., Farré, M., Barceló, D., 2017. Cytotoxic effects of commonly used nanomaterials and microplastics on cerebral and epithelial human cells. Environ. Res. 159, 579–587. https://doi.org/10.1016/j.envres.2017.08.043.

Schmid, O., Stoeger, T., 2016. Surface area is the biologically most effective dose metric for acute nanoparticle toxicity in the lung. J. Aerosol Sci. 99, 133–143. https://doi.org/10.1016/j.jaerosci.2015.12.006.

Schwabl, P., Köppel, S., Königshofer, P., Bucsics, T., Trauner, M., Reiberger, T., Liebmann, B., 2019. Detection of Various Microplastics in Human Stool: A Prospective Case Series. Ann. Intern. Med. 171, 453–457. https://doi.org/10.7326/M19-0618.

Shen, J., Xu, S., Zhou, H., Liu, H., Jiang, W., Hao, J., Hu, Z., 2017. IL-1β induces apoptosis and autophagy via mitochondria pathway in human degenerative nucleus pulposus cells. Sci. Rep. 7, 41067. https://doi.org/10.1038/srep41067.

Shruti, V.C., Pérez-Guevara, F., Kutralam-Muniasamy, G., 2020. Metro station free drinking water fountain- A potential “microplastics hotspot” for human consumption. Environ. Pollut. 261, 114227. https://doi.org/10.1016/j.envpol.2020.114227.

Stevenson, B., Siliciano, J., Mooseker, M., Goodenough, D., 1986. Identification of ZO-1: A High Molecular Weight Polypeptide Associated with the Tight Junction (Zonula Occludens) in a Varierty of Epithelia. J. Cell Biol. 103, 755–766. https://doi.org/10.1083/jcb.103.3.755.

Stock, V., Böhmert, L., Lisicki, E., Block, R., Cara-Carmona, J., Pack, L.K., Selb, R., Lichtenstein, D., Voss, L., Henderson, C.J., Zabinsky, E., Sieg, H., Braeuning, A., Lampen, A., 2019. Uptake and effects of orally ingested polystyrene microplastic particles in vitro and in vivo. Arch. Toxicol. 93, 1817–1833. https://doi.org/10.1007/s00204-019-02478-7.

Strugala, V., Dettmar, P.W., Pearson, J.P., 2008. Thickness and continuity of the adherent colonic mucus barrier in active and quiescent ulcerative colitis and Crohn's disease. Int. J. Clin. Pract. 62, 762–769. https://doi.org/10.1111/j.1742-1241.2007.01665.x.

Ter Halle, A., Jeanneau, L., Martignac, M., Jardé, E., Pedrono, B., Brach, L., Gigault, J., 2017. Nanoplastic in the North Atlantic Subtropical Gyre. Environ. Sci. Technol. 51, 13689–13697. https://doi.org/10.1021/acs.est.7b03667.

Thubagere, A., Reinhard, B.M., 2010. Nanoparticle-induced apoptosis propagates through hydrogen-peroxide-mediated bystander killing: Insights from a human intestinal epithelium in vitro model. ACS Nano 4, 3611–3622. https://doi.org/10.1021/nn100389a.

Tong, H., Jiang, Q., Hu, X., Zhong, X., 2020. Occurrence and identification of microplastics in tap water from China. Chemosphere 252, 126493. https://doi.org/10.1016/j.chemosphere.2020.126493.

Vianello, A., Boldrin, A., Guerriero, P., Moschino, V., Rella, R., Sturaro, A., Da Ros, L., 2013. Microplastic particles in sediments of Lagoon of Venice, Italy: First observations on occurrence, spatial patterns and identification. Estuar. Coast Shelf Sci. 130, 54–61. https://doi.org/10.1016/j.ecss.2013.03.022.

Wagoner, J.K., 1983. Toxicity of vinyl chloride and poly(vinyl chloride): a critical review. Environ. Health Perspect. 52, 61–66. https://doi.org/10.1289/ehp.835261.

Walczak, A.P., Kramer, E., Hendriksen, P.J.M., Helsdingen, R., van der Zande, M., Rietjens, I.M.C.M., Bouwmeester, H., 2015. *In vitro* gastrointestinal digestion increases the translocation of polystyrene nanoparticles in an *in vitro* intestinal co-culture model. Nanotoxicol. 9, 886–894. https://doi.org/10.3109/17435390.2014.988664.

Wenz, C., Faust, D., Linz, B., Turmann, C., Nikolova, T., Dietrich, C., 2019. Cell-cell contacts protect against t-BuOOH-induced cellular damage and ferroptosis in vitro. Arch. Toxicol. 93, 1265–1279. https://doi.org/10.1007/s00204-019-02413-w.

Wu, S., Wu, M., Tian, D., Qiu, L., Li, T., 2020. Effects of polystyrene microbeads on cytotoxicity and transcriptomic profiles in human Caco-2 cells. Environ. Toxicol. 35, 495–506. https://doi.org/10.1002/tox.22885.

Xia, T., Kovochich, M., Liong, M., Zink, J.I., Nel, A.E., 2008. Cationic polystyrene nanosphere toxicity depends on cell-specific endocytic and mitochondrial injury pathways. ACS Nano 2, 85–96. https://doi.org/10.1021/nn700256c.

Xu, H., Verbeken, E., Vanhooren, H.M., Nemery, B., Hoet, P.H.M., 2004. Pulmonary toxicity of polyvinyl chloride particles after a single intratracheal instillation in rats. Time course and comparison with silica. Toxicol. Appl. Pharmacol. 194, 111–121. https://doi.org/10.1016/j.taap.2003.09.018.

Yan, X., Zhang, Y., Lu, Y., He, L., Qu, J., Zhou, C., Hong, P., Sun, S., Zhao, H., Liang, Y., Ren, L., Zhang, Y., Chen, J., Li, C., 2020. The Complex Toxicity of Tetracycline with Polystyrene Spheres on Gastric Cancer Cells. Int. J. Environ. Res. Public Health 17, E2808. https://doi.org/10.3390/ijerph17082808.

Zhang, Q., Xu, E.G., Li, J., Chen, Q., Ma, L., Zeng, E.Y., Shi, H., 2020. A Review of Microplastics in Table salt, Drinking Water, and Air: Direct Human Exposure. Environ. Sci. Technol. 54, 3740-3751. https://doi.org/10.1021/acs.est.9b04535.

Zheng, H., Wang, J., Wei, X., Chang, L., Liu, S., 2021. Proinflammatory properties and lipid disturbance of polystyrene microplastics in the livers of mice with acute colitis. Sci. Total. Environ. 750, 143085. https://doi.org/10.1016/j.scitotenv.2020.143085.

4. An inverted *in vitro* triple culture model of the healthy and inflamed intestine: adverse effects of polyethylene particles

Mathias Busch[a], Angela A. M. Kämpfer[a], Roel P. F. Schins[a]

[a] *IUF – Leibniz-Research Institute for Environmental Medicine, Auf'm Hennekamp 50, 40225 Düsseldorf, Germany*

Chemosphere, 2021, 284, 131345

DOI: 10.1016/j.chemosphere.2021.131345

Author contribution: The author of this dissertation performed the inverted triple culture experiments, as well as parts of the non-inverted diclofenac control. Furthermore, the author performed the statistical analysis, made the graphs, discussed the results and wrote the manuscript. Relative contribution: 70 %.

4.1 Abstract

As environmental pollution with plastic waste is increasing, numerous reports show the contamination of natural habitats, food and drinking water with plastic particles in the micro- and nanometer range. Since oral exposure to these particles is virtually unavoidable, health concerns towards the general population have been expressed and risk assessment regarding ingested plastic particles is of great interest. To study the intestinal effects of polymeric particles with a density of <1 g/cm³ *in vitro*, we spatially inverted a triple culture transwell model of the healthy and inflamed intestine (Caco-2/HT29-MTX-E12/THP-1), which allows contact between buoyant particles and cells. We validated the inverted model against the original model using the enterotoxic, non-steroidal anti-inflammatory drug diclofenac and subsequently assessed the cytotoxic and pro-inflammatory effects of polyethylene (PE) microparticles. The results show that the inverted model exhibits the same distinct features as the original model in terms of barrier development and inflammatory parameters. Treatment with 2 mM diclofenac causes severe cytotoxicity, DNA damage and complete barrier disruption in both models. PE particles induced cytotoxicity and pro-inflammatory effects in the inverted model, which would have remained undetected in conventional *in vitro* approaches, as no effect was observed in non-inverted control cultures.

4.2 Introduction

Environmental pollution with plastic waste is a global problem with increasing public concern. An estimated 11% of globally generated plastic waste enters aquatic ecosystems (Borrelle *et al.*, 2020) and slowly degrades to particles in micro- and nanometer range as a consequence of embrittlement through UV radiation and mechanical abrasion (Andrady, 2012; Julienne *et al.*, 2019). These particles can be found in food and drinking water of various sources (Marsden *et al.*, 2019; Mintenig *et al.*, 2019; Shruti *et al.*, 2020), leading to oral exposure of the general human population. The weekly oral uptake of microplastics in humans has been estimated to be 0.1–5 g (Senathirajah *et al.*, 2021), but the consequences of such exposure remain unknown. Thus, the importance of a toxicological risk assessment regarding oral uptake of micro- and nanoplastics is evident. Validated *in vitro* systems representing human organs are needed in order to replace, reduce and refine the use of animal experiments.

The polymers polyethylene (PE) and polypropylene (PP) are amongst the most produced plastics in Europe (PlasticsEurope, 2019) and the most abundant polymer types of micro- and nanoplastic particles in the majority of environmental samples (Klein *et al.*, 2015; Kor and Mehdinia, 2019; Ramírez-Álvarez *et al.*, 2019), drinking water (Mintenig *et al.*, 2019) and fish (James *et al.*, 2020). However, their density of less than 1 g/cm³ makes particles consisting of these polymers buoyant in cell culture media. Thus, specific approaches are necessary to conduct *in vitro* testing, as conventional methods of *in vitro* particle toxicology cannot be applied.

The gastrointestinal tract represents the first point of contact for any ingested contaminants and has been identified as a possible target organ for plastic particle induced toxicity in animal studies (Li *et al.*, 2019; Lu *et al.*, 2018; Qiao *et al.*, 2019). Despite major developments in the realm of *in vitro* nanosafety research regarding intestinal toxicity (Kämpfer *et al.*, 2020a), strategies for testing buoyant particles in the intestine have received little attention. Inspired by the works of Watson *et al.* (2016) and Stock *et al.* (2019, 2020), we have adapted our previously described intestinal triple culture model (Busch *et al.*, 2021; Kämpfer *et al.*, 2021) to an inverted orientation to facilitate the testing of buoyant particles. The original version of this triple culture model of the healthy and inflamed intestine has been used in our laboratory to study the effects of sedimenting micro- and nanoplastics (Busch *et al.*, 2021) or metallic engineered nanomaterials (Kämpfer *et al.*, 2021) in a healthy or inflammatory setting.

In this study, we inverted our triple-culture model of the intestine, composed of the human cell lines Caco-2, HT29-MTX-E12 and THP-1, in order to develop a suitable, complex *in vitro* system to investigate toxicological effects of buoyant particles. We validated the inverted model against the original model using the enterotoxic non-steroidal anti-inflammatory drug

(NSAID) diclofenac [2-(2,6-dichloroanilino)-phenylacetic acid] and subsequently evaluated toxicological effects of PE particles.

4.3 Materials and Methods

Materials

Polyethylene (PE) microspheres with diameters of 200–9900 nm were ordered as dry powder from Cospheric LLC (Santa Barbara, USA). Diclofenac sodium salt was purchased from Sigma Aldrich/Merck. The cell culture media DMEM (4.5 g/L d-glucose, l-glutamine), MEM (Earle's salts, non-essential amino acids), RPMI 1640 (l-glutamine, 25 mM HEPES), 2-mercaptoethanol (ME), fetal calf serum (FCS) for THP-1 cells, sodium pyruvate and phosphate buffered saline (PBS) were purchased from Thermo Fisher Scientific. FCS for Caco-2 and HT29-MTX-E12, non-essential amino acids (NEAA), l-glutamine, d-glucose, penicillin/streptomycin (P/S), trypsin, phorbol 12-myristate 13-acetate (PMA), interferon gamma (IFN-γ), lipopolysaccharides from E. coli O111:B4 (LPS), Accutase, agarose, low melting point agarose, β-nicotinamide adenine dinucleotide sodium salt (NAD), lithium l-lactate, phenazine methosulfate (PMS), iodonitrotetrazolium chloride (INT), ethylenediaminetetraacetic acid (EDTA), dimethyl sulfoxide (DMSO), Triton X-100, sodium hydroxide (NaOH) and bovine serum albumin (BSA) were purchased from Sigma-Aldrich/Merck. Tris base and sodium chloride (NaCl) were ordered from Carl Roth (Germany).

Cell culture

Caco-2 (DSMZ, ACC169) cells were cultured in MEM-based cell culture medium substituted with 20% FCS, 1% P/S and 1% l-glutamine. HT29-MTX-E12 (ECACC, 12040401) cells were cultured in DMEM-based cell culture medium substituted with 10% FCS, 1% P/S and 1% NEAA. Caco-2 and HT29-MTX-E12 cells were regularly split at ~80% confluence and used at passages 5–25 after thawing for experiments (Caco-2 cells were stored in N2 at P23 after purchase, HT29-MTX-E12 at P7). THP-1 (ATCC, TIB-202) cells were cultured in RPMI 1640-based cell culture medium (containing l-glutamine and 25 mM HEPES) substituted with 10% FCS, 1% P/S, 1 nM sodium pyruvate, 0.7% d-glucose and 50 nM ME and maintained at cell concentrations between $2*10^5$ and $8*10^5$ cells/mL. For experiments, THP-1 cells were used at passages 5–15 after thawing (stored at P9).

The stable and inflamed triple cultures in original orientation were established as described in detail by Kämpfer *et al.* (2021) and treated with 2 mM diclofenac for 24 h for the comparison with the inverted triple cultures. The diclofenac concentration is based on the work of Arisan *et al.* (2018) and Bhatt *et al.* (2018) and was chosen to induce an effect strong enough for valuable comparison between both models. To avoid confusion between the original and

inverted model in terms of epithelial cell orientation, we will refer to the apical and basolateral transwell compartments as “upper” and “lower” compartment.

The inverted triple cultures were set up as depicted in **Figure 4.1**. In detail, a PVC tube (12 mm diameter, bought from a hardware store) was cut into pieces of ~10 mm length. These pieces were sterilized in 70% ethanol before being slipped over 1 µm pore size PET transwell inserts (12-well format; Falcon) from the basolateral side of the filter (**Figure S 4.1**). The transwell-tube construct was then placed upside-down in 6-well plates. Caco-2 and HT29-MTX-E12 cells ($1.62*10^5$, 9:1 ratio) were seeded on the bottom side of the insert in 250 µL MEM-based culture medium. After 4 h incubation at 37 °C, 5% CO2, the PVC tubes were carefully removed, the inserts transferred onto 12-well plates in regular orientation, and 0.5 mL and 1.5 mL MEM-based culture medium was added to the upper and lower compartment, respectively. During the growth and differentiation period of 21 days, medium was changed every 2–3 days, while the medium in the upper compartment was gradually adapted to RPMI-based THP-1 medium. On day 21, epithelial cells in the inflamed triple culture wells were primed with 10 ng/mL IFN-γ in the upper compartment for 24 h. In parallel, $3*10^6$ THP-1 cells were differentiated in 25 cm^2 flasks with 100 nM PMA for 24 h. On day 22, differentiated THP-1 cells were detached with Accutase and cell suspensions containing $3.6*10^5$ cells/mL were transferred into two separate 50 mL conical tubes. For the inflamed triple cultures, THP-1 cells in one tube were activated with 10 ng/mL LPS and IFN-γ. To avoid attachment of the THP-1 cells during the activation phase, both tubes were horizontally rotated at 6.5 rpm for 4 h at 37 °C in a Biometra OV5 incubator. During this 4 h activation period, the THP-1 cells formed small clumps, but did not adhere to the walls of the conical tubes, allowing the subsequent transfer to the transwell inserts. The IFN-γ-primed wells were washed twice with PBS and allowed to rest for 4 h. Stable and inflamed co-cultures were started in parallel by transferring 500 µL of the THP-1 cell suspensions to the upper compartment of the corresponding transwells. Treatments with diclofenac (2 mM) or PE particles (0–50 µg/cm^2) were started 24 h after initiation of the triple cultures and continued for 24h.

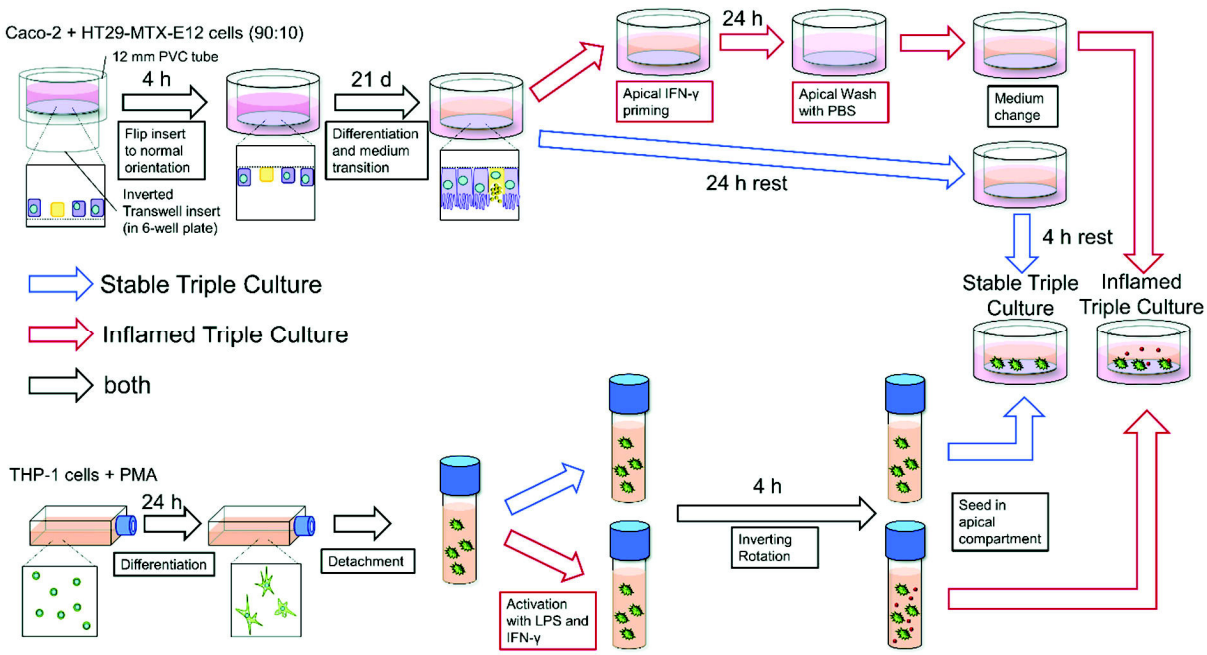

Figure 4.1 Inverted triple culture setup. Caco-2 and HT29-MTX-E12 cells were seeded on the bottom side of transwells and incubated for 4 h. The transwells were put back in regular orientation in 12-well plates and grown for 21 days while gradually changing the medium in the upper compartment from MEM to RPMI. For the inflamed triple cultures, epithelial cells were primed with IFN-γ for 24 h. THP-1 cells were PMA-differentiated for 24 h, detached with accutase and transferred into 50 mL conical tubes. For the inflamed triple cultures, THP-1 cells were activated with LPS and IFN-γ for 4 h while rotating to prevent reattachment. After washing the IFN-γ-primed transwells, they were allowed to rest for 4 h. To start the triple cultures, the THP-1 cells were transferred into the upper compartment of the respective transwells.

Pilot studies showed no effect of PE particles in transwell cultures of regular orientation. To avoid the usage of expensive inserts, we completed the experiments with co-cultures in regular well plates as a non-inverted control for the lactate dehydrogenase (LDH) assay. Caco-2 and HT29-MTX-E12 cells ($1.62*10^5$, 9:1 ratio) were seeded in regular 24-well plates and maintained for 21 days before exposure. During the growth phase, the medium (MEM-based) was changed every 2–3 days.

Cell count during epithelial growth phase

During the epithelial growth phase of the inverted model, we observed the presence of proliferating cells on the well bottom of the companion plate and the presence of detached, dead cells in the lower supernatant in a recurring pattern after each medium change. To quantify this cellular turnover, proliferating and dead cells were counted on the well bottom and in the lower supernatant, respectively. Right before changing the medium during the growth and differentiation phase, the lower compartment supernatant containing dead cells was transferred into 1.5 mL Eppendorf tubes and the well bottom was washed with PBS, 200 µL trypsin was added for 5 min and the detached cells were resuspended in 500 µL MEM. Both

cell suspensions were counted microscopically using a Neubauer hemocytometer. The counted cell number was multiplied by the total cell suspension volume and divided by the number of days since the last medium change.

Measurement of transepithelial electric resistance (TEER)

Barrier integrity during growth and particle/diclofenac exposure in the triple culture model was measured as TEER using a voltohmmeter (EVOM, World Precision Instruments) with a chopstick electrode (STX2). Prior to measurements, the electrode was sterilized in 70% ethanol and washed with PBS and MEM. TEER measurements were performed during the growth phase right before the medium change and at t = 0, 4, 20, 24, 44 and 48 h of the triple cultures. The measurements were corrected for blank value and transwell filter area (0.9 cm^2), and expressed in Ohm * centimeter squared ($\Omega \bullet cm^2$).

LDH assay and cytokine quantification by enzyme-linked immuno-sorbent assay (ELISA)

After 24 h of particle/diclofenac exposure, 50 µL of upper (original triple culture) or lower (inverted triple culture) supernatant was transferred onto 96 well plates and the LDH assay was performed as described previously (Busch *et al.*, 2021). No interference of the LDH assay with PE particles was observed at concentrations up to 160 µg/mL (**Figure S 4.2**), which translates to ~63 µg/cm^2.

The secretion of proinflammatory cytokines into the supernatant of the upper compartment following particle exposure was analyzed as described previously (Busch *et al.*, 2021), using R&D systems DuoSet Antibody kits for human IL-1β, IL-6, IL-8 and TNF-α. Supernatants were diluted if necessary (IL-1β: 1:5 and IL-8: 1:10).

Alkaline comet assay

The alkaline comet assay was used to analyze the induction of DNA single and double strand breaks as well as the occurrence of alkali-labile sites in the epithelial cells following particle/diclofenac exposure. After 24 h incubation with particles/diclofenac, cells were trypsinized and resuspended in 500 µL medium. In the case of inverted triple cultures treated with 2 mM diclofenac, the epithelial cells spontaneously detached from the filter after 20–24 h and were collected from the lower supernatant without trypsinization. Forty µL of this cell suspension was mixed with 240 µL low melting point agarose (0.5% in PBS) and 120 µL mixture was transferred onto slides previously coated with 1.5% agarose. Slides were prepared in duplicates. Lysis, electrophoresis and analysis was performed as described previously (Busch *et al.*, 2021).

Polyethylene particle characterization and treatment procedure

PE particles were suspended at 25 mg/mL in dH_2O supplemented with 0.01% Tween 80 and stored at 4 °C. This procedure was adapted from the manufacturer (https://www.cospheric.com/tween_solutions_density_marker_beads.htm) and modified regarding Tween 80 concentration. The concentration of <0.0001% Tween 80 (resulting from dilution to treatment concentrations) in cell culture experiments was found to be not toxic towards Caco-2/HT29-MTX-E12 co-cultures (**Figure S 4.3**). For experiments, PE particles were diluted to a 4 mg/mL suspension of sterile dH_2O and a 10 min sonication was performed using a Branson Sonifier 450 at a duty cycle of 0.2 s and an output level of 5.71 (200 W).

In preparation of scanning electron microscopy (SEM) analysis, particle suspensions were diluted to 40 µg/mL in treatment medium (MEM containing 1% FCS, culture conditions) and 50 µL was pipetted on 0.2 µm pore size Whatman filters. After medium removal, the filters were air-dried, coated with a 10 nm gold layer and subsequently analyzed using a field emission SEM 7500F (JEOL (Germany) GmbH, Germany) at magnifications between 50X and 6,500X. ≥300 spheres/agglomerates were analyzed using ImageJ (version 1.51f, http://imagej.nih.gov/ij) to determine the size distributions of primary particles and particle agglomerates separately.

For cell culture experiments, the particle suspension (4 mg/mL) and freshly prepared diclofenac stock solution (100 mM in dH_2O at 37 °C) were diluted in treatment medium (MEM-based culture medium containing 1% FCS) to obtain the desired treatment concentrations (0–50 µg/cm^2 PE or 2 mM diclofenac). Lower treatment concentrations and control media were adapted to contain the same final volume of dH_2O as the highest treatment concentration. In the original triple culture model, diclofenac treatment was applied in the upper compartment, while in the inverted model, diclofenac and particle treatment was applied in the lower compartment.

Statistical analysis

Statistical analysis and illustration of results was performed using GraphPad Prism 8.3. Unless stated otherwise, experiments were performed in three independent runs with two biological replicates. Data sets were tested for normal distribution via Shapiro-Wilk test. Statistical analysis of triple culture experiments in stable and inflamed state was performed with two-way ANOVA and Tukey's test using the mean value of each independent run. A p-value of <0.05 was considered statistically significant.

4.4 Results

We characterized the inverted model during the growth phase of the epithelial layer and during the triple culture in stable and inflamed state. Furthermore, we validated the inverted model against the original model using the enterotoxic NSAID Diclofenac and ultimately used the inverted model to assess the effects of PE microplastics in the intestine.

Characterization of the inverted model during the growth phase and during triple culture in stable and inflamed state

The development of the epithelial cell layer and intestinal barrier during the growth phase was monitored by measuring TEER and by counting proliferating and dead cells that detached from the epithelial layer on the filter (**Figure 4.2a–b**). After addition of the THP-1 cells, the inverted model was further characterized during 48 h of triple culture in stable or inflamed state. The TEER, the release of LDH and secretion of pro-inflammatory cytokines at t_{48} were monitored (**Figure 4.2c–e**).

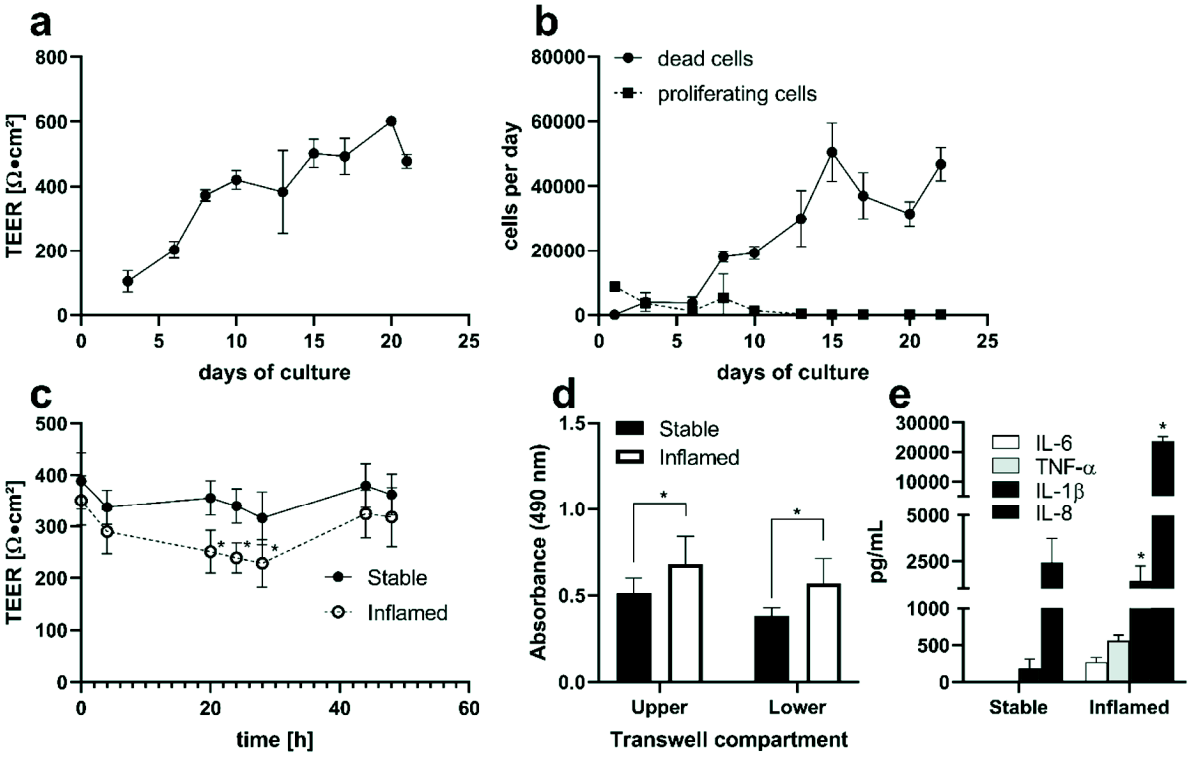

Figure 4.2 (a) TEER of the epithelial layer and (b) detached cells per day in the lower supernatant ("dead cells") or reattached to the well bottom ("proliferating cells") during 21 days of growth. Mean ± SD of N ≥ 2. (c) TEER during 48 h of triple-culture and (d) LDH release in stable (full bars) or inflamed (open bars) triple-cultures at t_{48}. (e) Pro-inflammatory cytokine secretion in the upper compartment of stable or inflamed inverted triple cultures at t_{48}. Mean ± SD of N ≥ 4, *p < 0.05 compared to the stable triple culture.

The TEER during the epithelial growth phase of the inverted model showed a continuous increase until reaching a plateau of ~500 Ω●cm^2 at day 15. Regarding the epithelial cells

detaching from the filter, only small numbers of cells continued to grow on the well bottom after detachment (max. ~10,000 per day) during the first two weeks. No more proliferating cells were observed on the well bottom during the third week, while the number of dead cells in the lower supernatant continuously increased until day 15. In the third week, approximately 25,000–50,000 dead cells per day detached from the epithelial layer.

During the triple culture, the TEER of the stable model remained at ~350 Ω●cm^2 with only small variation, while the TEER of the inflamed model showed a significant decrease and reached a minimum of ~240 Ω●cm^2 at t_{20} – t_{28} (**Figure 4.2c**). At t_{44} and t_{48}, the TEER of the inflamed model increased again to ~320 Ω●cm^2, reaching similar TEER levels as the stable model. The release of LDH in the inflamed triple cultures was significantly increased after 48 h compared to the stable triple cultures, in both the upper and lower compartment of the transwell system (**Figure 4.2 d**). At t_{48}, the pro-inflammatory cytokines IL-1β and IL-8 were detected in stable state at concentrations of ~200 pg/mL and ~2500 pg/mL, respectively (**Figure 4.2e**). In the inflamed state, the secretion of IL-1β and IL-8 was significantly increased to concentrations of ~1400 pg/mL and ~23000 pg/mL, respectively. While IL-6 and TNF-α were below the detection limit in the stable state, quantification via ELISA revealed concentrations of ~270 pg/mL (IL-6) and ~560 pg/mL (TNF-α) in the inflamed state of the model.

Effects of diclofenac treatment in the original and inverted triple culture models

To assess the comparability of both models, a 24 h exposure to 2 mM diclofenac in the lower compartment (inverted model) or upper compartment (original model) of stable and inflamed triple cultures was investigated. The effects on barrier integrity, cytotoxicity and DNA damage were compared via TEER measurement, LDH assay and alkaline comet assay (**Figure 4.3**).

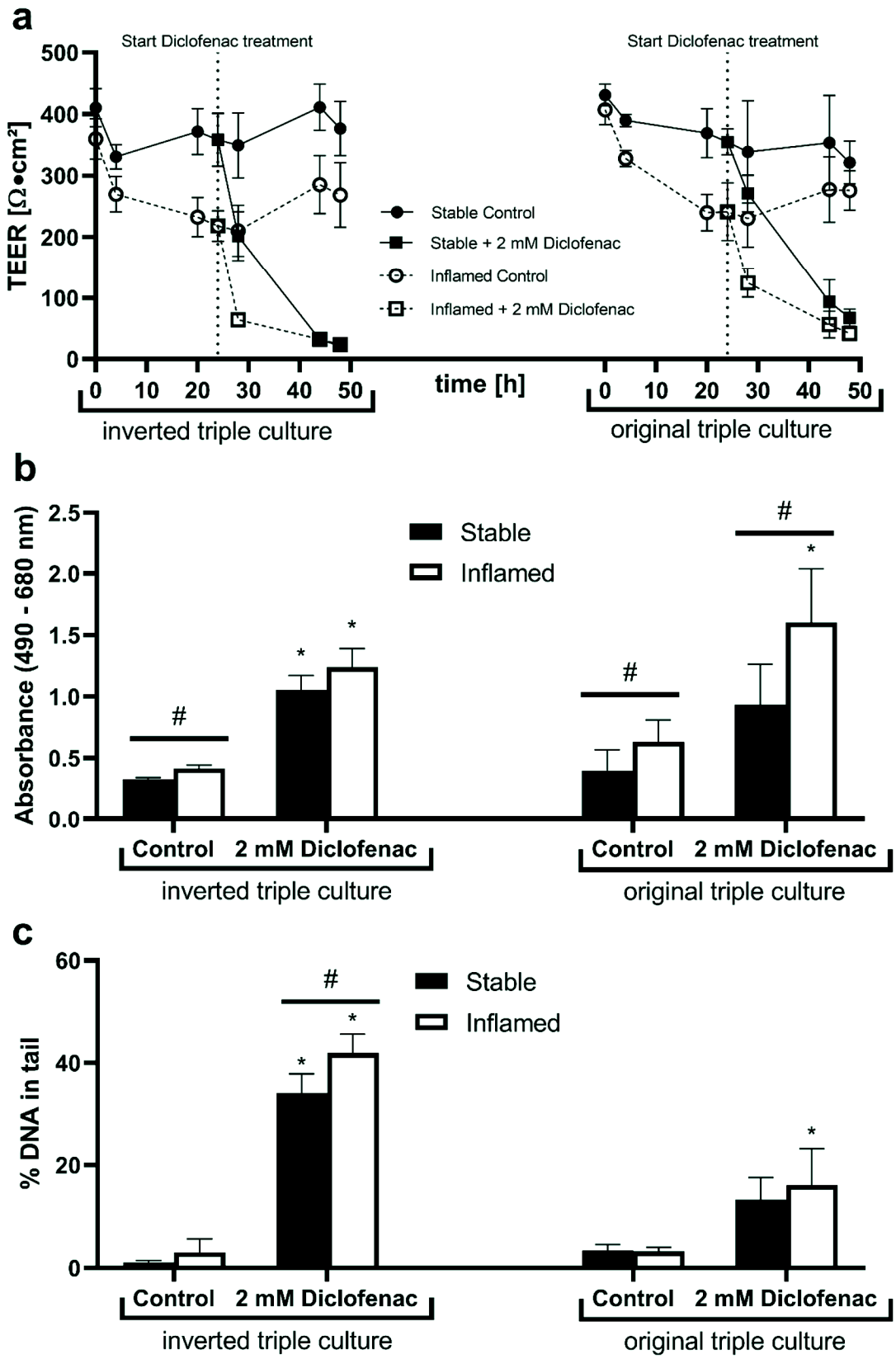

Figure 4.3 Effects of 24 h treatment with 2 mM Diclofenac in inverted (left) and original (right) triple cultures. (a) TEER during 48 h in stable (solid circle/square) or inflamed (open circle/square) triple cultures (b) LDH release into the lower (inverted model) or upper (original model) supernatants of stable (solid bars) and inflamed (open bars) triple cultures (c) DNA damage, assessed via alkaline comet assay. Mean ± SD of N ≥ 3. *p < 0.05 compared to the respective control, #p < 0.05 compared to the stable triple culture of the same treatment group.

In both models, treatment with 2 mM diclofenac caused a time-dependent decrease of TEER (**Figure 4.3a**). After 4 h of exposure (t_{28}), the TEER of the stable cultures was found to be at 200–250 Ω●cm^2, while the TEER of the inflamed cultures was at 60–100 Ω●cm^2. In all conditions, a complete disruption of the barrier was observed after 20 h of treatment (t_{44}), regardless of the inflammation status and model orientation. In the inverted model, the diclofenac treatment caused a complete detachment of the epithelial cell layer from the transwell filter after 20–24 h of exposure (t_{44} – t_{48}).

The analysis of cytotoxic effects revealed that diclofenac induced a significantly increased release of LDH (2.5–3.5-fold compared to the respective control) (**Figure 4.3b**) in the inverted triple culture model (stable and inflamed) and in the original model (inflamed only). In stable state of the original model, the release of LDH was also elevated (~2.4-fold compared to control) but failed to reach statistical significance.

Similar to the increased release of LDH, DNA damage levels were significantly elevated in the inverted triple culture model (stable and inflamed) and in the original model (inflamed only) after diclofenac treatment (**Figure 4.3c**). DNA damage was also substantially increased in the original model in stable state, but did not reach statistical significance. Notably, the DNA damage levels in the inverted model treated with diclofenac were overall higher than in the original model (~35% compared to ~15%), while the levels of background DNA damage were comparable in the controls (1–3%).

In general, all observed effects were more severe in the inflamed cultures, regardless of model orientation.

Polyethylene microplastics particle characterization and effects in an inverted *in vitro* triple culture model of the healthy and inflamed intestine

The PE microplastic particles used in this study were characterized regarding size distribution and morphology (**Figure 4.4a-c**) and the inverted triple culture models in stable and inflamed state were treated with PE particles for 24 h. TEER, the release of LDH, the secretion of the pro-inflammatory cytokines IL-1β, IL-6, IL-8 and TNF-α, and DNA damage was analyzed (**Figure 4.4d–g**). As control for the LDH assay, non-inverted Caco-2/HT29-MTX-E12 epithelial co-cultures were treated with the same concentrations of PE.

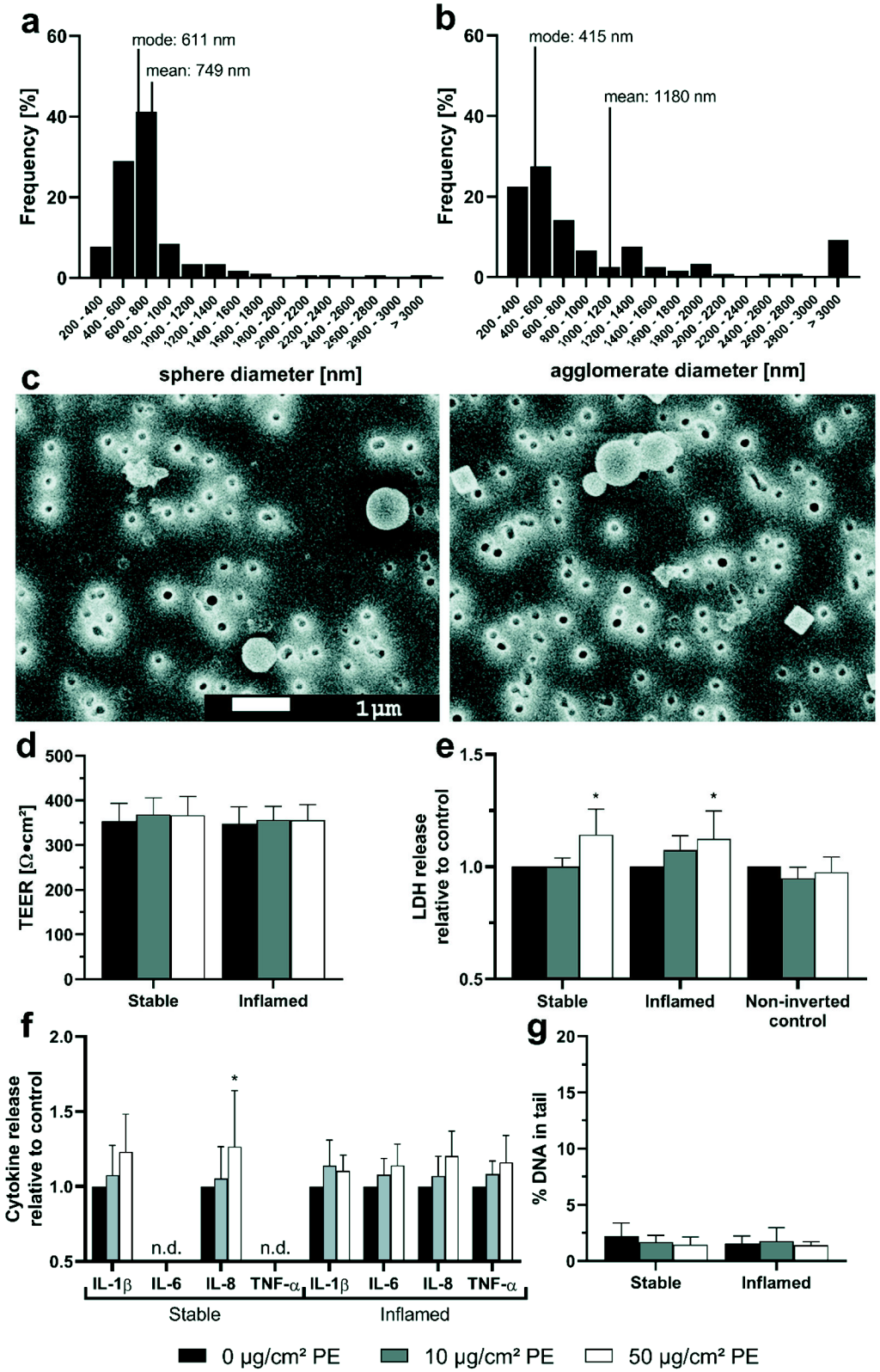

Figure 4.4 Size distribution, mode and mean diameter of PE (a) spheres and (b) agglomerates. (c) Representative SEM images of individual or agglomerated PE spheres at 6,000X magnification. Scale bar (1 µm, white bar) applies to all images. Filter pores (200 µm) and salt crystals (squares) were excluded from size analysis. (d) TEER, (e) LDH release, (f) secretion of pro-inflammatory cytokines in the upper compartment and (g) DNA damage in the epithelial cells of inverted stable or inflamed triple-cultures after treatment with 0–50 µg/cm^2 PE for 24 h "n.d." = "not detectable". Mean ± SD of N ≥ 3, *p < 0.05 compared to the respective untreated control.

The size distribution histograms revealed that the majority of PE spheres and agglomerates is found in a size range below 1000 nm. The smallest individual sphere was found to be 200.9 nm, while the largest had a diameter of 3.3 µm. The agglomerates formed by the PE spheres appear to be loosely bound and still allow clear distinction between individual spheres. Agglomerates of up to 13 µm in diameter were observed.

A significantly increased release of LDH (~15%) into the lower supernatant of inverted triple cultures was observed after 24 h treatment (t_{48}) with 50 µg/cm^2 PE particles (**Figure 4.4e**). For absolute absorbance values, see **Table S 4.1**. No difference was measured between the stable and inflamed triple cultures. An inverted culture without any THP-1 cells showed similar levels of LDH release after PE treatment (data not shown). As anticipated, the LDH release in the non-inverted control culture was not increased by PE particle treatment. In addition to LDH, we quantified the secretion of the pro-inflammatory cytokines IL-1β, IL-6, IL-8 and TNF-α in the upper supernatant of stable and inflamed triple-cultures (**Figure 4.4f**). While the concentrations of IL-6 and TNF-α were below the detection limit in the stable triple cultures, the secretion of IL-1β and IL-8 was increased in a dose-dependent manner after PE treatment. However, only the increase of IL-8 by ~25% after treatment with 50 µg/cm^2 PE was statistically significant. In the inflamed triple cultures, a trend describing a dose-dependent increase of IL-6, IL-8 and TNF-α secretion after PE treatment was evident, but did not prove statistically significant. For absolute cytokine concentrations, see **Table S 4.2**. Furthermore, no PE-induced effects in inverted triple cultures were observed regarding changes in TEER or DNA damage (**Figure 4.4d+g**).

4.5 Discussion

Our results show that PE particles can induce adverse effects in intestinal *in vitro* models when their physical properties are considered in the experimental setup. Low density polymers, e.g. PE or polypropylene, are major contributors to the plastic particles found in the environment, food products (James *et al.*, 2020; Klein *et al.*, 2015) and, unsurprisingly, in human colon tissue (Ibrahim *et al.*, 2021) and stool samples (Schwabl *et al.*, 2019). Particles from these materials present a unique challenge for *in vitro* research, as the majority of models largely rely on gravity-driven sedimentation in cell culture media, which is absent when the material density is below 1 g/cm³. Several *in vivo* studies are available, where the buoyant nature of the particles is not the principle limiting factor. Exposing zebrafish or nematodes to PE particles, adverse effects including intestinal damage, behavioral changes, and increased gene expression of intestinal glutathione S-transferase were observed (Lei *et al.*, 2018; Mak *et al.*, 2019). Furthermore, ingested PE microplastics have been found to induce intestinal inflammation in mice (Li *et al.*, 2019), which raises questions concerning their pro-inflammatory

or inflammation-enhancing potential. The outcomes suggest potentially harmful effects of PE particles in biological systems, which had not yet been discovered *in vitro* due to the particles' challenging physical properties. Recently, we have demonstrated that the prevalence of inflammatory processes may influence the toxicity of plastic nanoparticles (Busch *et al.*, 2021), which have otherwise been regarded to be of low hazard (Paul *et al.*, 2020). As also the accumulation behavior of particles has been demonstrated to differ between healthy tissue and inflamed lesions in human subjects (Schmidt *et al.*, 2013), inflammatory conditions should be considered in the hazard assessment.

To be able to address these questions *in vitro*, we adapted our previously described triple culture model of the intestine (Kämpfer *et al.*, 2021) by inverting the orientation of the three cell lines similar to the recent publication by Stock *et al.* (2020). To ascertain that the reactions of the inverted model are comparable to the original setup, the model was thoroughly characterized throughout the development stage, the stable and inflamed state as well as in response to a chemical control of known effects – diclofenac.

The barrier development of inverted Caco-2/HT29-MTX-E12 co-cultures followed a highly comparable TEER range as in the original model. However, we observed a consistent presence of shed cells in the basolateral compartment. Since the TEER values did not indicate a disruption of the barrier, we hypothesized that the epithelial layer continuously replaces these cells at an estimated daily turnover of 5–10% (based on the total number of approx. 5×10^5 epithelial cells on a 0.9 cm^2 transwell filter, data not shown). Whereas the HT29-MTX-E12 cells are regarded as a mature model for goblet cells (Behrens *et al.*, 2001), Caco-2 cells undergo a differentiation process towards an enterocyte-like phenotype when reaching confluence (Pinto *et al.*, 1983). The confluence of Caco-2 cells is generally associated with the downregulation of proliferation-associated genes (Buhrke *et al.*, 2011) and resulting cell cycle arrest in the G0/G1 phase (Ding *et al.*, 1998; Mariadson *et al.*, 2000). In contrast, the rapid enterocyte turnover – estimated to be 3.5 days in humans (Darwich *et al.*, 2014) – is an important characteristic of the intestinal physiology and may present a bottleneck of differentiated Caco-2 cultures. Our observation suggests that the *in vitro* model is more dynamic than previously assumed, albeit to lesser extent than intestinal tissue *in vivo*. We believe that this finding is not exclusive to the inverted model, but rather has not been reported in regular Caco-2 transwell cultures, since shed cells will typically be removed in medium changes.

For the establishment of the stable and inflamed state triple cultures in the inverted model, the protocol was kept as similar as possible to the original model. To prepare for the inflamed state, the epithelial cells were primed with IFN-γ to induce the expression of TNF receptor 2, which is crucial for the subsequent induction of barrier disruption (Wang *et al.*, 2006), triggered

by the TNF-α secretion from the activated THP-1 cells. As reported by Kämpfer *et al.* (2017), the THP-1 cells were pre-activated to avoid down-regulation of the inflammatory response by the epithelial cells. In the original model, this is achieved by simply transferring the transwell inserts onto the pre-activated THP-1 cells in well plates. Due to their location on the apical side of the transwell filter in the inverted model, the THP-1 cells needed to be pre-activated using a dynamic setup to prevent premature cell attachment. The THP-1 cell number was not changed, as the ratio of THP-1 to epithelial cells was found to be a crucial parameter for the successful establishment of co-cultures involving Caco-2 cells (Kämpfer *et al.*, 2017). However, the now closer proximity of the THP-1 cells to the epithelial barrier marks a major difference. As both the stable and inflamed state of the inverted model were highly comparable to the original model, this did not appear to negatively affect the system's integrity or any of the investigated endpoints. Furthermore, the inflamed state was in compliance with the previously defined criteria by Kämpfer *et al.* (2017): a significant reduction of TEER after 24 h, a significant increase in LDH activity, and a significant increase of the pro-inflammatory cytokines compared to the stable control. The higher cytokine concentrations quantified in the inverted compared to the original model (see Busch *et al.* (2021), supplementary material) is most likely due to their accumulation in a smaller volume of culture medium (i.e. 0.5 mL vs. 1.5 m, respectively). A direct comparison of the THP-1 activation protocols of both models revealed a ~3-fold higher cytokine secretion in the inverted model, while gene expression levels remained comparable (**Figure S 4.4**).

Following the model adaptation and characterization, we used diclofenac as a benchmark compound to assess the model-specific susceptibility of different endpoints. We observed a strong decrease in TEER, increased LDH release, and DNA damage after 24 h treatment in both models, all of which were substantially enhanced in the inflamed state. Whereas the results on TEER and LDH release were comparable between inverted and original model, DNA damage was clearly more elevated in the former. Diclofenac is a non-selective inhibitor of cyclooxygenases and reportedly induces intestinal damage and inflammation in patients (Bjarnason *et al.*, 1993; Gentric and Pennec, 1992) and in animal models (Colucci *et al.*, 2018; Singh *et al.*, 2017). Effects on TEER and cytotoxicity have been previously reported in primary human intestinal epithelial cell transwell cultures with similar treatment conditions (Bhatt *et al.*, 2018). The overall enhanced exposure effect in the inflamed condition may be related to an increased susceptibility of the model, as previously shown in the response to silver nanoparticles (Kämpfer *et al.*, 2020b). In addition, diclofenac was found to synergize with TNF-α and IFN-y, which significantly enhanced its toxicity in human hepatocytes (Maiuri *et al.*, 2016).

The higher percentage of DNA damage in the inverted model might be related to the observed complete detachment of the epithelial cell layer from the filter, presumably a result of strong cytotoxicity affecting the barrier's integrity in combination with gravity. For the analysis, the cells were collected with the supernatant of the lower compartment, thus including heavily damaged cells that would have been removed in the original model when transferring the supernatant and washing the epithelial cells. In the original model, the analysis was limited to trypsinized cells, while the comet assay performed in the inverted model includes detached, necrotic, and apoptotic cells. Diclofenac is classified as a “Non-DNA-reactive chemical (including non-genotoxic carcinogens) that should give negative results in *in vitro* mammalian cell genotoxicity tests” (Kirkland *et al.*, 2016). We therefore think that the here observed DNA damage is a secondary effect caused by preceding cytotoxicity rather than genotoxic potential. Diclofenac has been shown to produce reactive oxygen species (ROS) in Caco-2 cells (Boonyong *et al.*, 2020), which could lead to oxidative stress and substantial genomic DNA fragmentation, which has been previously observed *in vivo* (Amin and Hamza, 2005; Hickey *et al.*, 2001) and *in vitro* (Inoue *et al.*, 2004). This model-specific difference should be considered when cells are treated with a strong cytotoxic agent as it might result in exaggerated outcomes.

Suitable application for buoyant particles

Having characterized and validated the inverted model, we applied it for the analysis of PE particle effects in the intestine under healthy and inflamed-like conditions. The size of the batch of PE spheres used in this study was found to be mainly below 1000 nm in diameter, despite the given size range of 200–9900 nm, as indicated by the manufacturer. It appears that the agglomeration behavior is size dependent, as the modal size of agglomerates is below the modal size of single spheres (415 nm vs. 611 nm). The increased tendency of smaller particles to form agglomerates has also been described for TiO_2 nanoparticles (Murugadoss *et al.*, 2020). However, based on the size distribution, we consider this type of PE particles an appropriate model for the substantially heterogeneous size distribution of particles found in the environment, food and drinking water.

The highest tested exposure concentration induced a significant increase in LDH release in both stable and inflamed conditions, which was absent in non-inverted epithelial co-cultures serving as control. *In vitro* studies investigating the toxicity of PE particles are scarce, likely due to their earlier mentioned challenging nature. Stock *et al.* (2020) reported an absence of cytotoxic effects in an inverted Caco-2 monoculture system treated with larger PE particles (1-4 µm, 10-20 µm or ~90 µm) at concentrations of up to 100 mg/mL. This striking contrast to our own results, which show cytotoxicity when using a ~3000 fold lower dose, could be a consequence of the contrasting size distributions and/or the presence of the mucus-producing

goblet-like cells. On the other hand, Choi *et al.* (2021) also demonstrated cytotoxic and pro-inflammatory effects of PE microdebris (25-75 µm and 75-200 µm) in different cell lines and primary cells using conventional, non-inverted cellular models. The authors attributed the observed effects to the initial, short-term contact between particles and cells right after the application of the particle suspension, which renders an estimation of the delivered dose as well as time-dependency of the observed effects impossible. However, these different studies are difficult to compare as particles above a certain size (~20 µm) are larger than the exposed cells themselves and effects are expected to differ from particles small enough for cellular uptake.

In addition to an increased LDH release, the highest exposure concentration of PE induced a significant increase in IL-8 in the stable state. This pro-inflammatory effect might be more prominent in the stable state, because the inflammation, as present in the triple culture model in inflamed state, is already quite strong regarding secreted cytokines. Effects induced by small pro-inflammatory stimuli might be masked. The pro-inflammatory properties of PE particles have previously been investigated in the context of wear debris from prosthetics. Green *et al.* (1998) reported elevated IL-1β, IL-6 and TNF-α levels after treating murine peritoneal macrophages with PE particles ranging from 0.49 to 7.2 µm. The authors embedded the particles in the surface layer of agarose and seeded the macrophages on top to circumvent the buoyancy problem. In theory, PE particles below 1 µm in diameter could translocate through the pores of the transwell membrane into the upper compartment and interact with the THP-1 cells. However, since the intestinal barrier seems to remain unimpaired by PE treatment (indicated by no changes in TEER levels), the translocation of particles across the membrane in unlikely. The close proximity of the THP-1 cells and the epithelial layer allows direct cellular communication, which could result in a pro-inflammatory effect mediated by the PE-exposed epithelial cells, increasing the secretion of cytokines by THP-1 cells, which are the main source of the pro-inflammatory cytokines in this cell system (Kämpfer *et al.*, 2017). We previously reported a similar phenomenon in the original model in inflamed state exposed to PVC microparticles (Busch *et al.*, 2021).

4.6 Conclusion

Our results underline the importance of making available and using applicable *in vitro* models and exposure strategies to be able to adequately address a research question and draw robust conclusions based on the outcomes. Using the inverted triple culture model of the healthy and inflamed intestine, we were able to detect effects caused by particles of the most ubiquitous type of plastic, PE, which were absent in non-inverted cultures. Soluble benchmark substances, like the NSAID diclofenac in the case of assessing intestinal effects, could be considered as control during the characterization and validation of *in vitro* models.

Funding

This work was supported by the Jürgen Manchot foundation, Düsseldorf, Germany through a PhD scholarship for Mathias Busch.

Acknowledgements

The authors are grateful for the contribution by Inci Nur Sahin and Burkhard Stahlmecke of the IUTA e.V. Duisburg, Germany, who conducted the SEM analysis of the PE particles.

4.7 Supplementary material

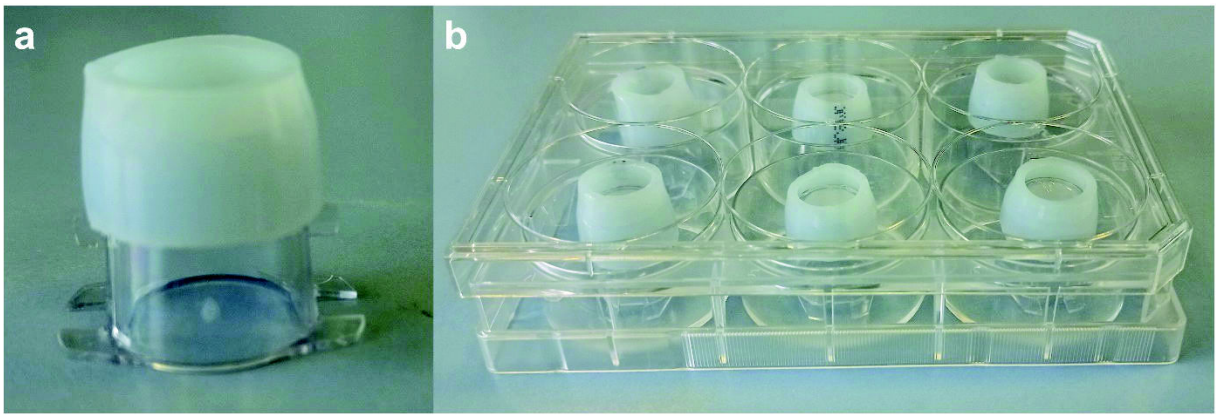

Figure S 4.1 (A) Sterilized 12 mm PVC tube slipped over inverted transwell inserts and (B) placed in 6-well plates for incubation.

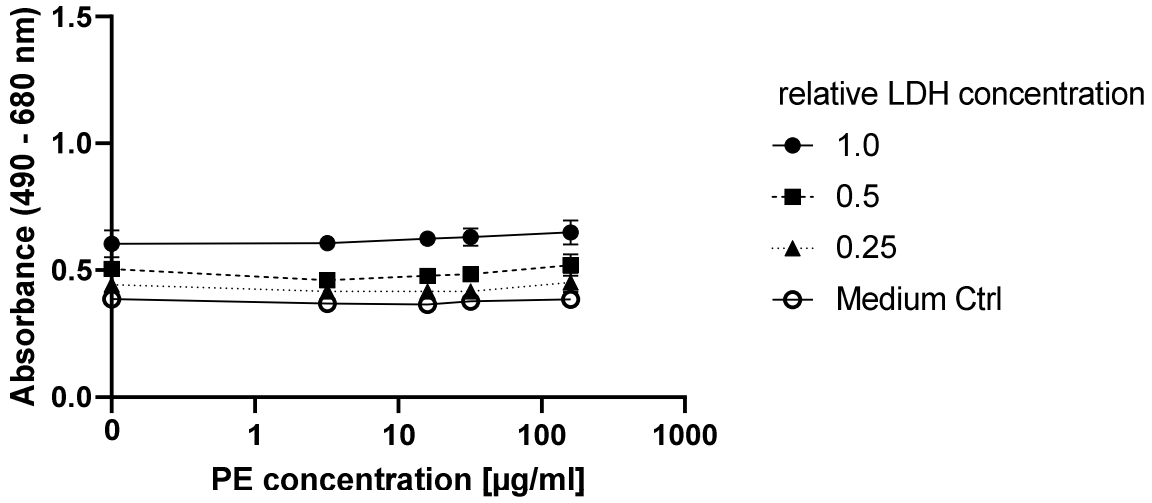

Figure S 4.2 Interference of PE particle with the LDH assay. 50 µl Caco-2 cell lysate at relative concentrations of 0.25 – 1.0 was incubated with 50 µl of PE particle suspension (0 – 160 µg/ml) in a 96-well plate for 24 h at 37 °C. LDH assay was performed as described and absorbance was measured at 490 and 680 nm.

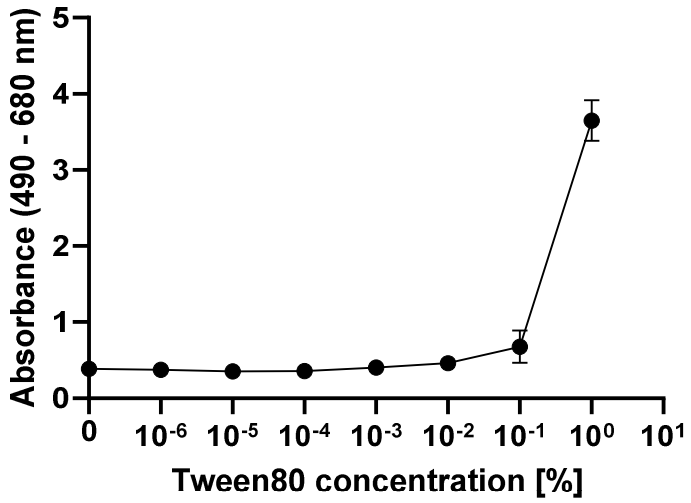

Figure S 4.3 LDH release in differentiated Caco-2/HT29-MTX-E12 co-cultures after 24 h treatment with 1 – 0.000001 % Tween 80. Mean ± SD of N = 2.

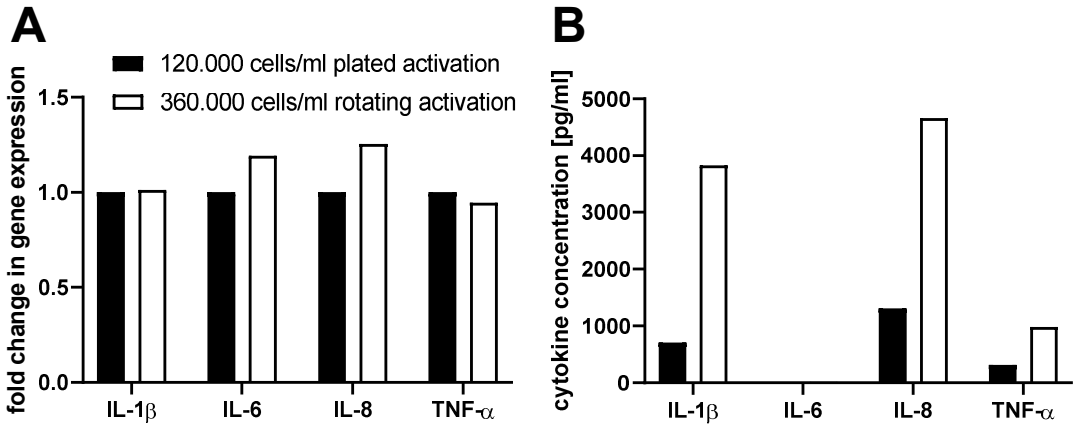

Figure S 4.4 Gene expression (A) and cytokine secretion (B) of IL-1β, IL-6, IL-8 and TNF-α after 4 h of activation phase (10 ng/ml LPS and IFN-γ) in THP-1 cells either plated at 120.000 cells/ml (as in the original triple culture) or rotating at 360.000 cells/ml (as in the inverted triple culture). IL-6 was below detection limit at this early timepoint. N=1.

Table S 4.1 Absolute absorbance values ($_{A490\text{-}680\ nm}$) of the LDH assay after treatment of the stable and inflamed inverted triple cultures and non-inverted control with 0 – 50 µg/cm² PE (Figure 4.4e).

	Stable triple culture		**Inflamed triple culture**		**Non-inverted control**	
PE [µg/cm²]	Mean [$A_{490\text{-}680\ nm}$]	SD	Mean [$A_{490\text{-}680\ nm}$]	SD	Mean [$A_{490\text{-}680\ nm}$]	SD
0	0.412	0.020	0.666	0.091	0.420	0.069
10	0.410	0.029	0.729	0.091	0.398	0.057
50	0.477	0.030	0.764	0.063	0.410	0.074

Table S 4.2 Absolute cytokine concentrations in the stable and inflamed inverted triple cultures after treatment with 0 – 50 µg/cm² PE (Figure 4.4f).

		Stable triple culture		Inflamed triple culture	
Cytokine	**PE [µg/cm²]**	Mean [pg/ml]	SD	Mean [pg/ml]	SD
IL-1β	0	185.9	109.7	1405.2	721.7
	10	234.2	140.3	1644.5	1007.8
	50	250.0	123.9	1533.7	761.1
IL-6	0	below detection limit		272.3	53.9
	10			291.9	50.0
	50			310.7	67.1
IL-8	0	2421.3	1129.8	23772.5	1334.4
	10	3020.0	1354.8	25437.5	3015.2
	50	3246.0	966.1	28557.5	3457.0
TNF-α	0	below detection limit		560.1	65.2
	10			610.3	103.5
	50			656.0	140.5

4.8 References

Amin, A., Hamza, A.A., 2005. Oxidative stress mediates drug-induced hepatotoxicity in rats: a possible role of DNA fragmentation. Toxicology 208 (3), 367–375. doi:10.1016/j.tox.2004.11.039.

Andrady, A.L., 2012. Biodegradation of plastics: monitoring what happens. In: Brewis, D., Briggs, D., Pritchard, G. (Eds.), Plastics Additives. An A-Z Reference, vol. 1. Springer Netherlands, Dordrecht, pp. 32–40.

Arisan, E.D., Ergül, Z., Bozdağ, G., Rencüzoğulları, Ö., Çoker-Gürkan, A., Obakan-Yerlikaya, P., Coşkun, D., Palavan-Ünsal, N., 2018. Diclofenac induced apoptosis via altering PI3K/Akt/MAPK signaling axis in HCT 116 more efficiently compared to SW480 colon cancer cells. Mol. Biol. Rep. 45 (6), 2175–2184. doi:10.1007/s11033-018-4378-2.

Behrens, I., Stenberg, P., Artursson, P., Kissel, T., 2001. Transport of lipophilic drug molecules in a new mucus-secreting cell culture model based on HT29-MTX cells. Pharm. Res. 18 (8), 1138–1145. doi:10.1023/A:1010974909998.

Bhatt, A.P., Gunasekara, D.B., Speer, J., Reed, M.I., Peña, A.N., Midkiff, B.R., Magness, S.T., Bultman, S.J., Allbritton, N.L., Redinbo, M.R., 2018. Nonsteroidal anti-inflammatory drug-induced leaky gut modeled using polarized monolayers of primary human intestinal epithelial cells. ACS Infect. Dis. 4 (1), 46–52. doi:10.1021/acsinfecdis.7b00139.

Bjarnason, I., Hayllar, J., Macpherson, A.J., Russell, A.S., 1993. Side effects of nonsteroidal anti-inflammatory drugs on the small and large intestine in humans. Gastroenterology 104 (6), 1832–1847. doi:10.5555/uri:pii:0016508593906672.

Boonyong, C., Vardhanabhuti, N., Jianmongkol, S., 2020. Natural polyphenols prevent indomethacin-induced and diclofenac-induced Caco-2 cell death by reducing endoplasmic reticulum stress regardless of their direct reactive oxygen species scavenging capacity. J. Pharm. Pharmacol. 72 (4), 583–591. doi:10.1111/jphp.13227.

Borrelle, S.B., Ringma, J., Law, K.L., Monnahan, C.C., Lebreton, L., McGivern, A., Murphy, E., Jambeck, J., Leonard, G.H., Hilleary, M.A., Eriksen, M., Possingham, H.P., Frond, H. de, Gerber, L.R., Polidoro, B., Tahir, A., Bernard, M., Mallos, N., Barnes, M., Rochman, C.M., 2020. Predicted growth in plastic waste exceeds efforts to mitigate plastic pollution. Science 369, 1515–1518. doi:10.1126/science.aba3656.

Buhrke, T., Lengler, I., Lampen, A., 2011. Analysis of proteomic changes induced upon cellular differentiation of the human intestinal cell line Caco-2. Dev. Growth Differ. 53 (3), 411–426. doi:10.1111/j.1440-169X.2011.01258.x.

Busch, M., Bredeck, G., Kämpfer, A.A.M., Schins, R.P.F., 2021. Investigations of acute effects of polystyrene and polyvinyl chloride micro- and nanoplastics in an advanced in vitro triple culture model of the healthy and inflamed intestine. Environ. Res. 193, 110536. doi:10.1016/j.envres.2020.110536.

Choi, D., Hwang, J., Bang, J., Han, S., Kim, T., Oh, Y., Hwang, Y., Choi, J., Hong, J., 2021. In vitro toxicity from a physical perspective of polyethylene microplastics based on statistical curvature change analysis. Sci. Total Environ. 752, 142242. doi:10.1016/j.scitotenv.2020.142242.

Colucci, R., Pellegrini, C., Fornai, M., Tirotta, E., Antonioli, L., Renzulli, C., Ghelardi, E., Piccoli, E., Gentile, D., Benvenuti, L., Natale, G., Fulceri, F., Palazón-Riquelme, P., López-Castejón, G., Blandizzi, C., Scarpignato, C., 2018. Pathophysiology of NSAID-associated intestinal lesions in the rat: luminal bacteria and mucosal inflammation as targets for prevention. Front. Pharmacol. 9, 1340. doi:10.3389/fphar.2018.01340.

Darwich, A.S., Aslam, U., Ashcroft, D.M., Rostami-Hodjegan, A., 2014. Meta-analysis of the turnover of intestinal epithelia in preclinical animal species and humans. Drug Metab. Dispos. 42 (12), 2016–2022. doi:10.1124/dmd.114.058404.

Ding, Q.M., Ko, T.C., Evers, B.M., 1998. Caco-2 intestinal cell differentiation is associated with G1 arrest and suppression of CDK2 and CDK4. Am. J. Phys. 275 (5), 1193–1200. doi:10.1152/ajpcell.1998.275.5.C1193.

Gentric, A., Pennec, Y.L., 1992. Diclofenac-induced pseudomembranous colitis. Lancet 340, 126–127. doi:10.1016/0140-6736(92)90459-G.

Green, T.R., Fisher, J., Stone, M., Wroblewski, B.M., Ingham, E., 1998. Polyethylene particles of a 'critical size' are necessary for the induction of cytokines by macrophages in vitro. Biomaterials 19 (24), 2297–2302. doi:10.1016/S0142-9612(98)00140-9.

Hickey, E.J., Raje, R.R., Reid, V.E., Gross, S.M., Ray, S.D., 2001. Diclofenac induced in vivo nephrotoxicity may involve oxidative stress-mediated massive genomic DNA fragmentation and apoptotic cell death. Free Radic. Biol. Med. 31 (2), 139–152. doi:10.1016/S0891-5849(01)00560-3.

Ibrahim, Y.S., Tuan Anuar, S., Azmi, A.A., Wan Mohd Khalik, W.M.A., Lehata, S., Hamzah, S.R., Ismail, D., Ma, Z.F., Dzulkarnaen, A., Zakaria, Z., Mustaffa, N., Tuan Sharif, S.E., Lee, Y.Y., 2021. Detection of microplastics in human colectomy specimens. JGH Open 5 (1), 116–121. doi:10.1002/jgh3.12457.

Inoue, A., Muranaka, S., Fujita, H., Kanno, T., Tamai, H., Utsumi, K., 2004. Molecular mechanism of diclofenac-induced apoptosis of promyelocytic leukemia: dependency on reactive oxygen species, Akt, Bid, cytochrome and caspase pathway. Free Radic. Biol. Med. 37 (8), 1290–1299. doi:10.1016/j.freeradbiomed.2004.07.003.

James, K., Vasant, K., Padua, S., Gopinath, V., K S, A., R, J., Babu, A., John, S., 2020. An assessment of microplastics in the ecosystem and selected commercially important fishes off Kochi, south eastern Arabian Sea, India. Mar. Pollut. Bull. 154, 111027. doi:10.1016/j.marpolbul.2020.111027.

Julienne, F., Delorme, N., Lagarde, F., 2019. From macroplastics to microplastics: role of water in the fragmentation of polyethylene. Chemosphere 236, 124409. doi:10.1016/j.chemosphere.2019.124409.

Kämpfer, A.A.M., Busch, M., Büttner, V., Bredeck, G., Stahlmecke, B., Hellack, B., Masson, I., Sofranko, A., Albrecht, C., Schins, R.P.F., 2021. Model complexity as determining factor for in vitro nanosafety studies: effects of silver and titanium dioxide nanomaterials in intestinal models. Small 2004223. doi:10.1002/smll.202004223.

Kämpfer, A.A.M., Busch, M., Schins, R.P.F., 2020a. Advanced in vitro testing strategies and models of the intestine for nanosafety research. Chem. Res. Toxicol. 33 (5), 1163–1178. doi:10.1021/acs.chemrestox.0c00079.

Kämpfer, A.A.M., Urbán, P., Gioria, S., Kanase, N., Stone, V., Kinsner-Ovaskainen, A., 2017. Development of an in vitro co-culture model to mimic the human intestine in healthy and diseased state. Toxicol. In Vitro 45, 31–43. doi:10.1016/j.tiv.2017.08.011.

Kämpfer, A.A.M., Urbán, P., La Spina, R., Jiménez, I.O., Kanase, N., Stone, V., Kinsner-Ovaskainen, A., 2020b. Ongoing inflammation enhances the toxicity of engineered nanomaterials: application of an in vitro co-culture model of the healthy and inflamed intestine. Toxicol. In Vitro 63, 104738. doi:10.1016/j.tiv.2019.104738.

Kirkland, D., Kasper, P., Martus, H.-J., Müller, L., van Benthem, J., Madia, F., Corvi, R., 2016. Updated recommended lists of genotoxic and non-genotoxic chemicals for assessment of the performance of new or improved genotoxicity tests. Mutat. Res. Genet. Toxicol. Environ. Mutagen 795, 7–30. doi:10.1016/j.mrgentox.2015.10.006.

Klein, S., Worch, E., Knepper, T.P., 2015. Occurrence and spatial distribution of microplastics in river shore sediments of the rhine-main area in Germany. Environ. Sci. Technol. 49 (10), 6070–6076. doi:10.1021/acs.est.5b00492.

Kor, K., Mehdinia, A., 2019. Neustonic microplastic pollution in the Persian Gulf. Mar. Pollut. Bull. 150, 110665. doi:10.1016/j.marpolbul.2019.110665.

Lei, L., Wu, S., Lu, S., Liu, M., Song, Y., Fu, Z., Shi, H., Raley-Susman, K.M., He, D., 2018. Microplastic particles cause intestinal damage and other adverse effects in zebrafish Danio rerio and nematode Caenorhabditis elegans. Sci. Total Environ. 619–620, 1–8. doi:10.1016/j.scitotenv.2017.11.103.

Li, B., Ding, Y., Cheng, X., Sheng, D., Xu, Z., Rong, Q., Wu, Y., Zhao, H., Ji, X., Zhang, Y., 2019. Polyethylene microplastics affect the distribution of gut microbiota and inflammation development in mice. Chemosphere 244, 125492. doi:10.1016/j.chemosphere.2019.125492.

Lu, L., Wan, Z., Luo, T., Fu, Z., Jin, Y., 2018. Polystyrene microplastics induce gut microbiota dysbiosis and hepatic lipid metabolism disorder in mice. Sci. Total Environ. 631–632, 449–458. doi:10.1016/j.scitotenv.2018.03.051.

Maiuri, A.R., Breier, A.B., Turkus, J.D., Ganey, P.E., Roth, R.A., 2016. Calcium contributes to the cytotoxic interaction between diclofenac and cytokines. Toxicol. Sci. 149 (2), 372–384. doi:10.1093/toxsci/kfv249.

Mak, C.W., Ching-Fong Yeung, K., Chan, K.M., 2019. Acute toxic effects of polyethylene microplastic on adult zebrafish. Ecotoxicol. Environ. Saf. 182, 109442. doi:10.1016/j.ecoenv.2019.109442.

Mariadson, J.M., Rickard, K.L., Barkla, D.H., Augenlicht, L.H., Gibson, P.R., 2000. Divergent phenotypic patterns and commitment to apoptosis of Caco-2 cells during spontaneous and butyrate-induced differentiation. J. Cell. Physiol. 183 (3), 347–354. doi:10.1002/(SICI)1097-4652(200006)183:3<347:AID-JCP7>3.0.CO;2-W.

Marsden, P., Koelmans, A.A., Bourdon-Lacombe, J., Gouin, T., Anglada, L.D., Cunliffe, D., Jarvis, P., Fawell, J., France, J.D., 2019. Microplastics in Drinking Water. World Health Organization, Geneva. https://edepot.wur.nl/498693.

Mintenig, S.M., Löder, M.G.J., Primpke, S., Gerdts, G., 2019. Low numbers of microplastics detected in drinking water from ground water sources. Sci. Total Environ. 648, 631–635. doi:10.1016/j.scitotenv.2018.08.178.

Murugadoss, S., Brassinne, F., Sebaihi, N., Petry, J., Cokic, S.M., van Landuyt, K.L., Godderis, L., Mast, J., Lison, D., Hoet, P.H., van den Brule, S., 2020. Agglomeration of titanium dioxide nanoparticles increases toxicological responses in vitro and in vivo. Part. Fibre Toxicol 17 (1), 10. doi:10.1186/s12989-020-00341-7.

Paul, M.B., Stock, V., Cara-Carmona, J., Lisicki, E., Shopova, S., Fessard, V., Braeuning, A., Sieg, H., Böhmert, L., 2020. Micro- and nanoplastics – current state of knowledge with the

focus on oral uptake and toxicity. Nanoscale Adv 2 (10), 4350–4367. doi:10.1039/D0NA00539H.

Pinto, M., Robine-Leon, S., Appay, M.-D., Kedinger, M., Triadou, N., 1983. Enterocyte-like differentation and polarization of the human-colon carcinoma cell-line Caco-2 in culture. Biol. Cell. 47, 323–330.

PlasticsEurope. Plastics - the Facts 2019: an analysis of European plastics production, demand and waste data. retrieved 09.10.20 https://www.plasticseurope.org/application/files/9715/7129/9584/FINAL_web_version_Plastics_the_facts2019_14102019.pdf, 2019.

Qiao, R., Sheng, C., Lu, Y., Zhang, Y., Ren, H., Lemos, B., 2019. Microplastics induce intestinal inflammation, oxidative stress, and disorders of metabolome and microbiome in zebrafish. Sci. Total Environ. 662, 246–253. doi:10.1016/j.scitotenv.2019.01.245.

Ramírez-Álvarez, N., Rios Mendoza, L.M., Macías-Zamora, J.V., Oregel-Vázquez, L., Alvarez-Aguilar, A., Hernández-Guzmán, F.A., Sánchez-Osorio, J.L., Moore, C.J., Silva-Jiménez, H., Navarro-Olache, L.F., 2019. Microplastics: sources and distribution in surface waters and sediments of todos santos bay, Mexico. Sci. Total Environ. 703, 134838. doi:10.1016/j.scitotenv.2019.134838.

Schmidt, C., Lautenschlaeger, C., Collnot, E.-M., Schumann, M., Bojarski, C., Schulzke, J.-D., Lehr, C.-M., Stallmach, A., 2013. Nano- and microscaled particles for drug targeting to inflamed intestinal mucosa: a first in vivo study in human patients. J. Contr. Release 165 (2), 139–145. doi:10.1016/j.jconrel.2012.10.019.

Schwabl, P., Köppel, S., Königshofer, P., Bucsics, T., Trauner, M., Reiberger, T., Liebmann, B., 2019. Detection of various microplastics in human stool: a prospective case series. Ann. Intern. Med. 171 (7), 453–457. doi:10.7326/M19-0618.

Senathirajah, K., Attwood, S., Bhagwat, G., Carbery, M., Wilson, S., Palanisami, T., 2021. Estimation of the mass of microplastics ingested – a pivotal first step towards human health risk assessment. J. Hazard Mater. 404, 124004. doi:10.1016/j.jhazmat.2020.124004.

Shruti, V.C., Pérez-Guevara, F., Kutralam-Muniasamy, G., 2020. Metro station free drinking water fountain- A potential “microplastics hotspot” for human consumption. Environ. Pollut. 261, 114227. doi:10.1016/j.envpol.2020.114227.

Singh, D.P., Borse, S.P., Rana, R., Nivsarkar, M., 2017. Curcumin, a component of turmeric, efficiently prevents diclofenac sodium-induced gastroenteropathic damage in rats: a step towards translational medicine. Food Chem. Toxicol. 108, 43–52. doi:10.1016/j.fct.2017.07.034.

Stock, V., Böhmert, L., Dönmez, M.H., Lampen, A., Sieg, H., 2019. An inverse cell culture model for floating plastic particles. Anal. Biochem. 591, 113545. doi:10.1016/j.ab.2019.113545.

Stock, V., Laurisch, C., Franke, J., Dönmez, M.H., Voss, L., Böhmert, L., Braeuning, A., Sieg, H., 2020. Uptake and cellular effects of PE, PP, PET and PVC microplastic particles. Toxicol. In Vitro 70, 105021. doi:10.1016/j.tiv.2020.105021.

Wang, F., Schwarz, B.T., Graham, W.V., Wang, Y., Su, L., Clayburgh, D.R., Abraham, C., Turner, J.R., 2006. IFN-gamma-induced TNFR2 upregulation is required for TNF-dependent intestinal epithelial barrier dysfunction. Gastroenterology 131 (4), 1153–1163.

Watson, C.Y., DeLoid, G.M., Pal, A., Demokritou, P., 2016. Buoyant nanoparticles: implications for nano-biointeractions in cellular studies. Small 12 (23), 3172–3180. doi:10.1002/smll.201600314.

5. NLRP3-proficient and -deficient THP-1 cells as an *in vitro* screening tool for inflammasome activation by micro- and nanoplastics

Mathias Busch[a], Gerrit Bredeck[a], Friedrich Waag[b], Khosrow Rahimi[c], Haribaskar Ramachandran[a], Tobias Bessel[b], Stephan Barcikowski[b], Andreas Herrmann[c], Andrea Rossi[a], Roel P.F. Schins[a]*

[a] *IUF – Leibniz-Research Institute for Environmental Medicine, 40225 Duesseldorf, Germany*

[b] *Technical Chemistry I, Center for Nanointegration Duisburg-Essen (CENIDE), University of Duisburg-Essen, 45141 Essen, Germany*

[c] *DWI – Leibniz Institute for Interactive Materials and Institute of Technical and Macromolecular Chemistry RWTH Aachen University, 52074 Aachen, Germany*

Submitted manuscript

Author contribution: The author of this dissertation performed parts of the *in vitro* experiments, performed the statistical analysis, made the graphs, discussed the results and wrote the manuscript. Relative contribution: 55 %.

5.1 Abstract

Due to the ubiquity of environmental micro- and nanoplastics (MNP), inhalation and ingestion by humans is very likely, but human health effects remain largely unknown. The NLRP3 inflammasome is a key player of the innate immune system and is involved in responses towards foreign particulate matter and the development of chronic intestinal and respiratory inflammatory diseases.

We established NLRP3-proficient and -deficient THP-1 cells as an alternative *in vitro* screening tool to assess the potential of MNP to activate the NLRP3 inflammasome. By investigating cytokine release (IL-1β and IL-8) and cytotoxicity after treatment with engineered nanomaterials, this *in vitro* approach was validated against earlier published *ex vivo* murine bone marrow-derived macrophages and *in vivo* data. This approach showed a strong correlation with previously published data, verifying that THP-1 cells are a suitable model to investigate NLRP3 inflammasome activation.

We then investigated the proinflammatory potential of eight MNP of different size, shape, and chemical composition. Only amine-modified polystyrene (PS-NH_2) acted as a direct NLRP3 activator. However, polyethylene terephthalate (PET) induced a significant increase in IL-8 release. Our results suggest that most MNP are not direct activators of the NLRP3 inflammasome, but specific MNP types might still possess pro-inflammatory potential via other pathways.

5.2 Introduction

The increasing production and use of plastic products since the 1950s in combination with waste mismanagement, has led to global environmental pollution. Physical forces, UV radiation, and heat cause the embrittlement and abrasion of plastic products and waste, ultimately leading to fragments in the micro- and nanometer range (Andrady, 2012; Julienne *et al.*, 2019). Further sources include plastic beads in cosmetics (Guerranti *et al.*, 2019) as well as synthetic microfibers originating from clothes (Falco *et al.*, 2019). These highly persistent particles, fragments, beads, and fibers can be found in any place on the planet, including water (Andrady, 2011), soil (Nizzetto *et al.*, 2016), air (Amato-Lourenço *et al.*, 2020), plants (Kalčíková, 2020), animals (Barboza *et al.*, 2019) and humans (Ibrahim *et al.*, 2021). The presence of these micro- and nanoplastics (MNP) implies human exposure via oral, inhalation, and dermal route. Accordingly, the “One Health Concept” calls for designing research on the effects of such pollutants, to achieve better public health outcomes (Destoumieux-Garzón *et al.*, 2018). Recent *in vivo* studies suggested a pro-inflammatory potential of plastic particles after ingestion (Li *et al.*, 2019) or inhalation (Lim *et al.*, 2021).

As an important player of the innate immune system, the NOD-, LRR- and pyrin domain-containing protein 3 (NLRP3) inflammasome is involved in a variety of inflammatory responses towards external stimuli, as well as in the development of chronic inflammatory diseases (He *et al.*, 2016; Ozaki *et al.*, 2015). These external stimuli include viral infections, the presence of bacterial components, and foreign particulate matter. For example, lung inflammation and fibrosis induced by crystalline silica or asbestos fibers have been shown to be NLRP3-dependent (Cassel *et al.*, 2008; Dostert *et al.*, 2008; Palomäki *et al.*, 2011) and several studies suggested a connection between intestinal inflammation and the oral uptake of particulate matter (Busch *et al.*, 2021a; Lomer *et al.*, 2002; Zheng *et al.*, 2021). Due to their ability to actively phagocytize foreign particles, macrophages play a major role in the innate immune defense in the lung and the gastrointestinal tract following inhalation or ingestion of particles (LeFevre *et al.*, 1985; Lehnert, 1992). Depending on the particle type and their specific physicochemical properties (e.g. size, shape), contact or uptake might lead to an activation of the NLRP3 inflammasome. Upon activation, the NLRP3 inflammasome recruits procaspase-1, which leads to the formation of active caspase-1. Caspase-1 cleaves the inactive pro-interleukin (IL)-1β, resulting in the formation and secretion of mature IL-1β (Zhao and Zhao, 2020). As an early pro-inflammatory cytokine, IL-1β is able to induce subsequent pro-inflammatory cascades (Siegmund, 2002), including the activation of transcription factor Nuclear factor-kappa B (NF-κB) (Parikh *et al.*, 1997). NF-κB is capable of regulating secondary inflammatory mediators like IL-8, an important chemoattractant during inflammation (Kunsch and Rosen, 1993; Vlahopoulos *et al.*, 1999).

The release of IL-1β after particle treatment of bone marrow-derived macrophages (BMDMs), isolated from wildtype (WT) or *Nlrp3* knockout mice, has previously been assessed in our lab as an *ex vivo* approach to investigate the ability of a large panel of different titanium dioxide (TiO_2) nanomaterials to activate the NLRP3 inflammasome (Kolling *et al.*, 2020). In light of the 3Rs, especially to replace the use of animals with alternative *in vitro* methods (Russell and Burch, 1992), we used CRISPR/Cas technology in our present study to generate THP-1 *NLRP3*$^{-/-}$ cells and validated the THP-1 cell line as a suitable alternative to BMDMs isolated from mice. We applied the same TiO_2 samples to validate the THP-1 cell model against BMDM data. Furthermore, we compared the pro-inflammatory potential of two multi-walled carbon nanotubes (MWCNTs) of different aspect ratios, in THP-1 cells to their outcomes in a previous *in vivo* study in mice (van Berlo *et al.*, 2014). Ultimately, we investigated the secretion of the NLRP3-specific cytokine IL-1β, secretion of the NLRP3-independent cytokine IL-8, and release of the cytotoxicity indicator lactate dehydrogenase (LDH) in THP-1 WT and *NLRP3*$^{-/-}$ cells after treatment with a large panel of MNP. This principle of comparing the reaction of NLRP3-proficient and -deficient THP-1 cells as an indicator of specific NLRP3 activation has been used in infectious disease research (Eisfeld *et al.*, 2021; Gram *et al.*, 2021) and has already been described for silica particles (Sharma *et al.*, 2018). A critical aspect of state-of-the-art *in vitro* testing of nanomaterials is to avoid misclassification due to assay artefacts resulting from their large specific surface areas and reactivities (Stone *et al.*, 2009). Therefore, prior to *in vitro* experiments, we tested all investigated materials (TiO_2, MWCNTs and MNP) for interference with the used assays. Investigated MNP included commercially available MNP such as polystyrene (PS), polyvinyl chloride (PVC), polyethylene (PE); as well as MNP generated by novel methods, such as polyethylene terephthalate (PET), polyester (PES), polyacrylonitrile (PAN) and polyamide 6 (PA6, also known as nylon). Generated MNP were thoroughly characterized prior to *in vitro* application

5.3 Materials and Methods

Chemicals and test materials

RPMI 1640 cell culture medium, 2-mercaptoethanol (ME), sodium pyruvate, and phosphate-buffered saline (PBS) were purchased from Thermo Fisher Scientific. Fetal calf serum (FCS), D-glucose, penicillin/streptomycin (P/S), phorbol 12-myristate 13-acetate (PMA), lipopolysaccharides (LPS) from *E. coli O111:B4*, Accutase, agarose, β-nicotinamide adenine dinucleotide sodium salt (NAD), lithium L-lactate, phenazine methosulfate (PMS), iodonitrotetrazolium chloride (INT) and bovine serum albumin (BSA) were purchased from Sigma-Aldrich/Merck. Tris base was ordered from Carl Roth (Germany). The TiO_2 nanoparticles, carbon nanotubes, and MNP samples used in the following experiments are listed in **Table 5.1**.

Table 5.1 TiO_2 samples, carbon nanotubes, and MNP used for experiments.

	Material	Abbreviation	Size	Source	Characterization/ previous use
Titanium dioxides	TiO_2 (P25)	NT1	12-18 nm	Evonik, Germany	Kolling *et al.* (2020)
	TiO_2 (PC105)	NT2	10 nm	Cristal, Saudi Arabia	Kolling *et al.* (2020)
	TiO_2 (SX001)	NT3	12-15 nm	Solaronix, Switzerland	Kolling *et al.* (2020)
	TiO_2 (UT001)	NT4	16-17 nm	UNITO, Italy	Kolling *et al.* (2020)
Carbon Nanotubes	Multi-walled carbon nanotubes 1 “Mitsui”	Mitsui 7	40-100 nm (diameter); 13 µm (length)	Mitsui & Co., Japan	van Berlo *et al.* (2014)
	Multi-walled carbon nanotubes 2	NM400	30 nm (diameter); 5 µm (length)	JRC repository, Italy	van Berlo *et al.* (2014)
Micro/nanoplastics	amine-modified polystyrene spheres	$PS\text{-}NH_2$	50 nm	Sigma Aldrich, Germany (L0780)	Busch *et al.* (2021a)
	polystyrene spheres	PS	50 nm	Polysciences Inc., USA (08691–10)	Busch *et al.* (2021a)
	polyvinyl chloride powder	PVC	235 nm (mode)	Werth-Metall, Germany	Busch *et al.* (2021a)
	polyethylene spheres	PE	611 nm (mode)	Cospheric LLC, USA	Busch *et al.* (2021b)
	polyethylene terephthalate fragments	PET	16 nm (nanofraction); 5.7 µm (microfraction)	Produced via laser ablation	
	polyester fibers	PES	17.5 µm (diameter); 10 µm (length)	Produced via cryotome	
	polyacrylonitrile fibers	PAN	18.5 µm (diameter); 10 µm (length)	Produced via cryotome	
	polyamide 6 (nylon) fibers	PA6	27.5 µm (diameter); 10 µm (length)	Produced via cryotome	

Generation and characterization of PET particles

The PET particles were produced by ablating a piece of PET immersed in ultrapure water (Merck Milli-Q, 18,2 MΩ/cm) with a 1.064 nm nanosecond-pulsed laser (Rofin Powerline E20). This laser synthesis method has been proven to give access to highly pure nanoparticle colloids (Zhang *et al.*, 2017), providing ideal reference materials for nanotoxicological assays (Rehbock *et al.*, 2014), scalable to tens of liters per hour (Waag *et al.*, 2021), but has rarely been studied for plastic particles yet (Elaboudi *et al.*, 2008; Magrì *et al.*, 2018). The piece of PET, which had dimensions of 17 mm x 17 mm x 5 mm was fabricated by cutting a commercial, disposable drink bottle into pieces followed by heat-induced fusion of these pieces. For this, some pieces were filled into a quadratic mold made of steel, which was placed onto a heating plate at 300 °C. The transparent PET pieces fused to a shiny white block. This block was placed into a custom-made sealable chamber made of PTFE, which had a stirrer and which was filled with water. More details on the chamber can be found elsewhere (Nachev *et al.*, 2012). All components of the setup were washed with ethanol (analytical grade), fully assembled, and autoclaved for 20 min at 121 °C and 110 kPa (CertoClav Vac Pro). Afterwards, the setup was placed onto an xyz-stage in front of a galvanometer xy-scanner with an f-theta lens with 100 mm focal length. The distance between the focus lens and the ablation chamber was adjusted to achieve a maximum ablation rate, which was indicated by a bright plasma and a loud sound. The applied laser parameters were a laser pulse duration of 5 ns, a laser repetition rate of 10 kHz, and a laser power of 3 W leading to a laser pulse energy of 0.3 mJ. The scan speed was 2 m/s. One ablation run was 30 min and yielded 20 mg of ablated material. Five runs were applied. After each run, the produced colloid was extracted from the chamber in a clean bench (W.H. Mahl MSC-II-48) under UV-C radiation and was then collected in a flask. The setup was prepared for the next run as described above. The collected colloid was shock-frozen with liquid nitrogen and then freeze-dried (Christ Alpha 1-4) at 30 Pa.

For size analysis, 4 ml of the PET colloid were separated into the nanoparticle and microparticle fraction by sedimentation at 1 g for 10 min. 10 µl of the supernatant, i.e. the nanoparticle fraction, were drop casted on a carbon-coated copper grid. Analysis of the nanometer size fraction was done by TEM (JEOL JEM 1400 Plus). The sediment, i.e. the microparticle fraction, was redispersed in 4 ml of ultrapure water. 1 ml of the suspension was drop casted on a glass slide. Analysis of the micrometer size fraction was done by light microscopy (Olympus CX40).

The chemical structure of the laser-generated micro- and nanoparticles was investigated by FT-IR (Shimadzu IRTracer-100). 10 µg of each fraction were dried and measured in an ATR setup. The PET target was also analyzed.

Production and characterization PES, PAN, and PA6 microfibers

Model fibrous microplastics were prepared using the method initially developed by M. Cole (Cole, 2016). Briefly, three types of textile-relevant fibers, including PES and PAN (Reinhard Strauss GmbH & Co. KG) and PA6 (Heimbach Group GmbH), were aligned, embedded in a water-soluble freezing agent (Tissue-Tek® O.C.T. Compound), and sectioned into microfibers with a length of 10 µm. The sectioning was performed using a cryotome (Leica CM1950). The freezing agent was washed off and powders of microfibers were obtained using lyophilization. The resulting particles were imaged via a Hitachi S3000 scanning electron microscope (SEM) and their size distribution was analyzed using ImageJ.

Cell culture

THP-1 (ATCC, TIB-202) cells were cultured in RPMI 1640-based cell culture medium (containing L-glutamine and 25 mM HEPES) substituted with 10 % FCS, 1 % P/S, 1 nM sodium pyruvate, 0.7 % D-glucose and 50 nM ME at 37 °C and 5 % CO_2 atmosphere. Cells were maintained at concentrations between $2*10^5$ and $8*10^5$ cells/ml.

Generation of an NLRP3-deficient THP-1 cell line using the CRISPR/Cas9 system

NLRP3 THP-1 mutant cells were generated as previously described (Ramachandran *et al.*, 2021). Briefly, gRNAs were designed using the CRISPR design tool CHOPCHOP (http://chopchop.cbu.uib.no/) and cloned into a modified PX458 plasmid (Addgene #48138). The resulting bicistronic vector encoded the respective gRNA, Cas9 nuclease, and a GFP selection marker. gRNAs efficiency was assessed using High-Resolution Melt Analysis (HRMA). An efficient gRNA targeting *NLRP3* exon 2 (5'-GCTAATGATCGACTTCAATG-3') was chosen for further experiments (HRMA primers Fwd 5'-CAGACCATGTGGATCTAGCC-3 5'-TGTTGATCGCAGCGAAGAT-3'). THP-1 cells were electroporated using a Neon transfection system (Thermofisher) according to the manufacturer's instructions. After 48 h, cells were FACS sorted and plated as single cells into 96-well plates. Cells were duplicated into maintenance and lysis plates after a week. Clones were then lysed with proteinase K and genotyped by PCR followed by deep sequencing using a miSeq Illumina sequencer and a V2 Nano cassette.

Experimental procedure

For experiments, $3*10^6$ THP-1 cells at passages 5 – 10 were differentiated to a macrophage-like cell type in 25 cm² flasks using 100 nM PMA. After 24 h, differentiated THP-1 cells were washed with PBS, detached with Accutase, and seeded in 24-well plates ($1.2*10^5$ cells/well in 1 ml medium) and allowed to re-attach for 1 h. MNP, TiO_2 nanoparticles, and carbon nanotubes were brought into suspension with treatment medium (RPMI-based cell culture medium

containing 1% FCS; 4 mg/ml) and a 10 min sonication was performed using a Branson Sonifier 450 at a duty cycle of 0.2 seconds and an output level of 5.71 (240 watts). Sonicated suspensions were diluted to obtain 50 µg/cm² exposure concentration in 1 ml volume. Exposure with 10 ng/ml LPS was used as a positive control. The volume of sonicated medium was the same in all control and exposure groups. In the case of PE (density < 1 g/cm³), particles were embedded in the superficial layer of agarose to enable contact between buoyant particles and cells. The PE stock suspension was prepared as described previously (Busch *et al.*, 2021b) and diluted to 50 µg/cm² in 1 % agarose, then transferred into 24-well plates. The plates were centrifuged at 2000 g for 1 h at 40 °C, causing the PE particles to accumulate at the surface of the liquid agarose and centrifuged again at 4 °C, causing the agarose to become solid. After solidification of the agarose, $1.2*10^5$ differentiated THP-1 cells per well were seeded on top of the particle layer. Agarose without particles was used as an additional negative control. After 24 h of treatment, supernatants were collected, the LDH assay was performed immediately and residues were stored at -20 °C (ELISA).

Cytokine quantification by enzyme-linked immuno-sorbent assay (ELISA)

The release of IL-1β and IL-8 into the supernatant following treatment was analyzed using R&D systems DuoSet ELISA kits. Antibodies were diluted according to the manufacturer's protocol and high-protein-binding 96-well plates were incubated with capture antibody in coating buffer (0.1 M $NaHCO_3$, pH 8.2) overnight. After blocking with 3 % BSA/PBS, 100 µl of supernatants, diluted if necessary (IL-1β: 5 to 20-fold and IL-8: 10 to 20-fold), were incubated for 2 h. Detection antibody, horseradish peroxidase (1:40 in 1 % BSA/PBS), and BioRad TMB Peroxidase EIA Substrate was consecutively incubated for 2 h, 0.5 h, and 5-20 min, respectively, before stopping the reaction with 50 µl 1M H_2SO_4. Absorbance was measured at 450 and 540 nm. The standard curve was plotted as a four-parameter log fit. Interference of all materials with the ELISA was assessed by spiking cell-free particle samples (50 µg/cm²) with 500 pg/ml of each cytokine. After 24 h incubation, cytokine concentrations were quantified via ELISA and compared to the particle-free control.

Assessment of cytotoxicity via LDH assay

Following 24 h of exposure, 50 µl of supernatant was transferred onto 96-well plates (in duplicates) and 150 µl of reaction mix containing 50 µl Tris buffer (200 mM, pH 8), 50 µl Li-Lactate solution (50 mM), 46 µl NAD^+ solution (5 mM), 2 µl INT solution (65 mM) and 2 µl PMS solution (29 mM) was added per well. After 10 min incubation, the reaction was stopped with 50 µl 1 M H_2SO_4, and absorbance was measured at 490 and 680 nm. Interference of all materials with the LDH assay was assessed by spiking particle samples (50 µg/cm²) with diluted cell lysate. After 24 h incubation, LDH activity was quantified and compared to the particle-free control.

Statistical Analysis

Statistical analysis and illustration of results were performed using GraphPad Prism 9.1. *In vitro* experiments were performed in at least four independent runs with two biological replicates. Data for negative (untreated) and positive control (LPS) are shown as absolute values. Particle data are depicted as fold change compared to the WT control (ELISA) or compared to the respective control (LDH). Statistical analysis was performed with two-way ANOVA and Dunnett's multiple comparison test. A p-value of <0.05 was considered statistically significant.

5.4 Results

PET particles generated by laser ablation

The products of PET laser ablation in water were a mixture of microparticles and nanoparticles. The nanoparticle fraction accounted for 60% of the total mass of the ablated material, as determined in a sedimentation experiment. **Figure 5.1A** shows the size distribution of the nanoparticle fraction with a mean value of 16.4 nm derived from TEM analysis. Individual particles with dimensions up to 120 nm were found. The particles exhibited different shapes ranging from nearly circular to irregular structures, which were not clearly dependent on particle size (**Figure S 5.1**). The microparticle fraction mainly contained particles with diameters below 10 µm (**Figure 5.1B**). Similar morphologies compared to the nanoparticle fraction were observed (**Figure S 5.2**). Larger microparticles with diameters greater than 200 µm usually had a branched or network-like morphology.

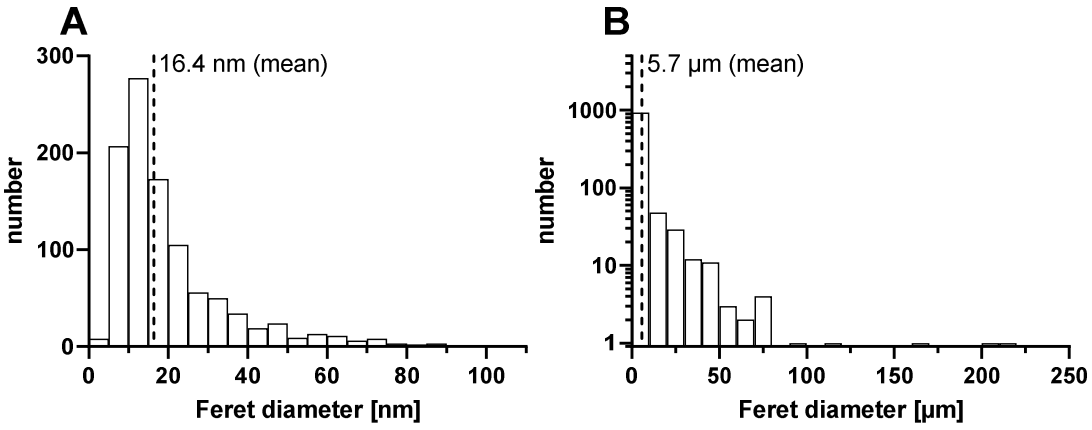

Figure 5.1 (A) Particle size distribution of laser-generated colloidal PET nanoparticles determined by TEM analysis. 1011 particles were analyzed. (B) Particle size distribution of PET microparticles determined by light microscopy at a magnification of 5x. 1050 particles were analyzed.

The chemical structure of both size fractions was investigated by FT-IR spectroscopy. Both fractions showed strong chemical similarity to the PET target (**Figure S 5.3**). Consequently, the chemical structure of PET was largely preserved during laser ablation. However, the ablation products exhibited lower amounts of phenyl-related bonds compared to the PET target, likely due to laser-induced photodegradation of PET. The ratio of C=O to C-O ester bonds was also lower for the ablation products. In addition, a higher intensity of C-H stretching (2915 1/cm) and H-C=O groups (280 1/cm) was observed for the nanoparticles than for the microparticles. Moreover, the spectrum of the dried nanoparticle fraction shows features of OH groups and possibly even water, indicating hydroxylation of the plastic during laser ablation in the presence of water. Note that hydroxylation also happens during the plastics' degradation in environmental water, in accordance with what has been observed in UV-exposed plastic materials in the environment. Overall, laser ablation of PET in water yields highly pure (that is, surfactant-free) colloidal MNP, with preserved chemical structure and higher hydroxylation for the nanoparticles compared to the microparticles.

Characterization of PES, PAN, and PA6 microparticles produced via cryotome

SEM analysis revealed the majority of produced microfibers to be of ~10 µm length, while small quantities of longer or shorter fibers were also present in all three samples (**Figure 5.2**). Due to the low ratio of length/diameter, the majority of produced plastic particles describe a cylindric shape rather than a true fiber shape (**Figures S 5.4-6**). However, due to limitations of the methodology, singular longer particles, exhibiting a true "fiber" shape, were also observed. Image analysis further revealed PAN fibers to possess a fissured surface on the outside as well as on the sectional areas, while the surfaces of PES and PA6 fibers appeared smooth within the resolution of the electron microscope.

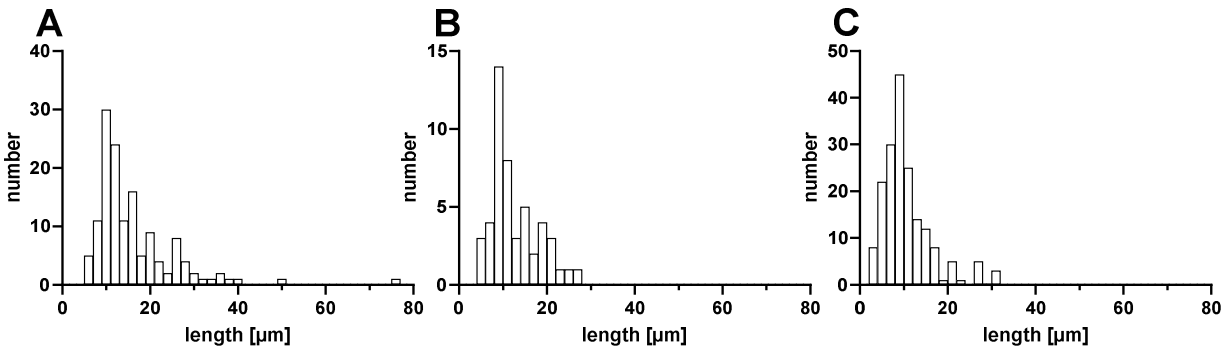

Figure 5.2 Fiber length distribution of (A) PES, (B) PAN, and (C) PA6 microfibers as determined by SEM analysis.

Interference of materials with the ELISA and LDH assay

Prior to in vitro experiments, all investigated materials were tested for interference with the ELISA and LDH assay. None of the samples interfered with the IL-1β ELISA (**Figure S 5.7A**). Incubation with the TiO_2 materials NT2 and NT3 caused a decrease of recovered IL-8 to approximately 50 % (**Figure S 5.7B**). Furthermore, incubation with PS-NH_2 caused a two-fold increase in detected IL-8 compared to the control. No interference with the LDH assay was observed for any of the materials (**Figure S 5.8**).

Validation of THP-1 cells as a screening tool for NLRP3 activation

First, THP-1 WT and *NLRP3*$^{-/-}$ cells were treated with the positive control LPS in order to confirm the successful knockout and to evaluate the differences between both cell lines regarding cytokine secretion. To interpret the cytokine data in the light of possible cytotoxic effects, the LDH assay was performed in addition to ELISA. After 24 h of treatment, the release of IL-1β and IL-8 into the supernatant was quantified, and LDH activity in the supernatant was assessed (**Figure 5.3**).

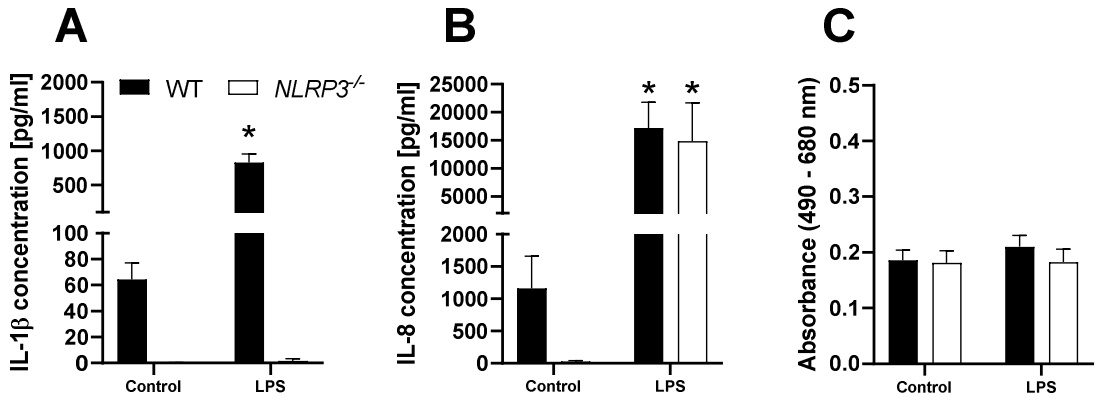

Figure 5.3 Release of IL-1β (A) and IL-8 (B), as well as LDH activity (C) in the supernatant of PMA-differentiated THP-1 WT (full bars) or NLRP3$^{-/-}$ (open bars) cells after 24 h treatment with 10 ng/ml LPS. Mean±SD of N=5, *p<0.05 compared to the respective control.

Treatment of WT cells with LPS induced a significantly increased release of IL-1β, compared to the untreated control (~800 pg/ml vs. ~60 pg/ml). IL-1β secretion by *NLRP3*$^{-/-}$ cells was either below or barely above the detection level of the ELISA, independent of LPS exposure. Furthermore, untreated WT cells exhibited an IL-8 concentration of ~1100 pg/ml in the supernatant, while the concentration released from *NLRP3*$^{-/-}$ cells was significantly lower at ~25 pg/ml. However, treatment with LPS caused a significant increase of IL-8 to ~15000 pg/ml

in both cell lines. Background LDH activity in the supernatant of both cell lines showed no difference and treatment with LPS did not induce an increase.

To compare the reaction of THP-1 cells with the reaction of BMDMs reported by Kolling *et al.* (2020), WT and *NLRP3*$^{-/-}$ cells were treated with four different samples of TiO_2 nanoparticles (**Figure 5.4**).

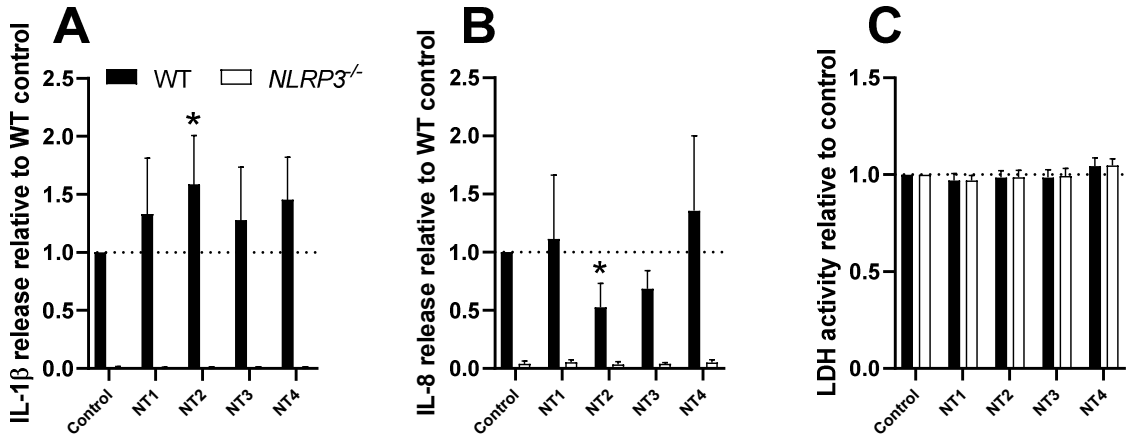

Figure 5.4 Release of IL-1β (A) and IL-8 (B), as well as LDH activity (C) in the supernatant of PMA-differentiated THP-1 WT (full bars) or NLRP3$^{-/-}$ (open bars) cells after 24 h treatment with 50 µg/cm² of four different TiO_2 samples. Cytokine data is depicted as relative values compared to the WT control, LDH data is depicted as relative values compared to the respective control. Mean±SD of N=4, *p<0.05 compared to the respective control.

Of the four tested TiO_2 samples, only NT2 induced a significant increase in IL-1β secretion (~1.5 fold compared to the untreated control) in THP-1 WT cells. Treatment with NT4 caused similarly elevated IL-1β levels but failed to reach statistical significance (p=0.08). After treatment with NT2 and NT3, IL-8 concentrations in the supernatant of WT cells were lower than the untreated control. As described above, IL-8 release in response to NT2 and NT3 may be underestimated due to interference with the ELISA. Furthermore, no effects regarding cytokine secretion were observed in *NLRP3*$^{-/-}$ cells and none of the TiO_2 treatments induced an increase in LDH activity in the supernatants of both cell lines.

To further compare the applied model to published *in vivo* data, THP-1 WT and *NLRP3*$^{-/-}$ cells were treated with the two different MWCNTs Mitsui 7 and NM400 (**Figure 5.5**). These MWCNTs were used in an *in vivo* study conducted by van Berlo *et al.* (2014).

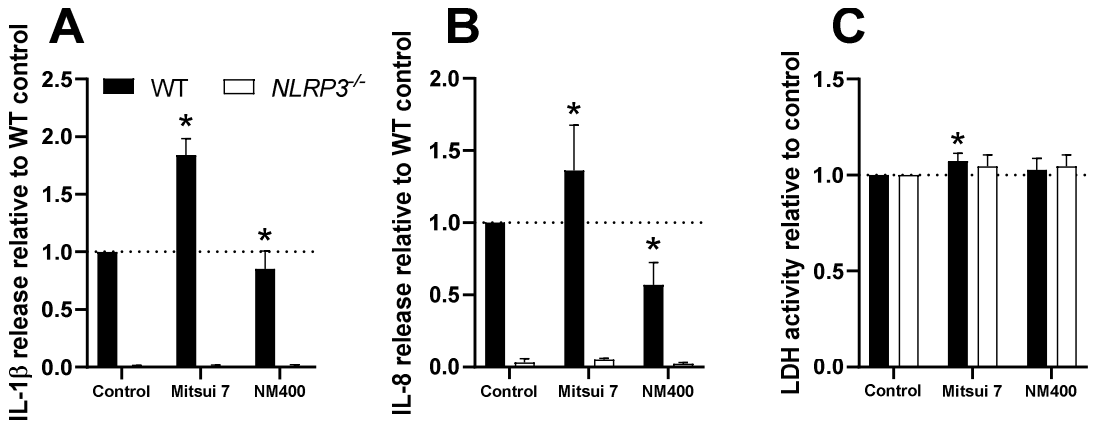

Figure 5.5 Release of IL-1β (A) and IL-8 (B), as well as LDH activity (C) in the supernatant of PMA-differentiated THP-1 WT (full bars) or NLRP3$^{-/-}$ (open bars) cells after 24 h treatment with 50 µg/cm² of two different MWCNTs. Cytokine data is depicted as relative values compared to the WT control, LDH data is depicted as relative values compared to the respective control. Mean±SD of N=4, *p<0.05 compared to the respective control.

Treatment with Mitsui 7 induced a significant increase of IL-1β and IL-8 secretion, as well as an increased activity of LDH in the supernatant, all exclusively in the WT cells. Treatment of WT cells with the shorter NM400 tubes caused a slight decrease in cytokine release. No effects were noted in *NLRP3*$^{-/-}$ cells.

Screening of eight different MNP for NLRP3 activation in THP-1 cells

To finally assess the ability of MNP to activate the inflammasome and induce a pro-inflammatory reaction, THP-1 WT and *NLRP3*$^{-/-}$ cells were treated with a large panel of different samples (**Figure 5.6**).

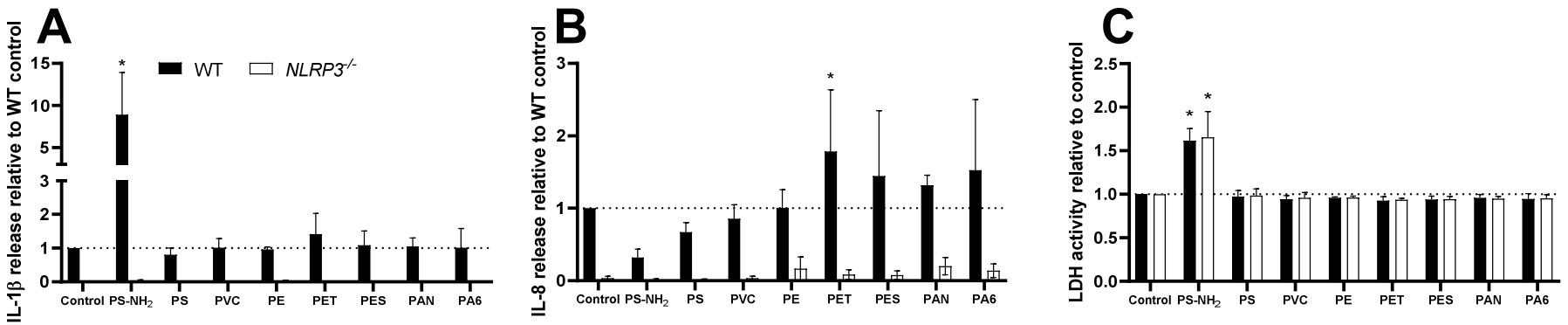

Figure 5.6 Release of IL-1β (A) and IL-8 (B), as well as LDH activity (C) in the supernatant of PMA-differentiated THP-1 WT (full bars) or NLRP3$^{-/-}$ (open bars) cells after 24 h treatment with 50 µg/cm² of different plastic particles. Cytokine data is depicted as relative values compared to the WT control, LDH data is depicted as relative values compared to the respective control. Mean±SD of N=4, *p<0.05 compared to the respective control.

Within this group of plastic samples, only PS-NH_2 induced a significant increase in IL-1β secretion in WT cells, accompanied by a strong cytotoxic effect as indicated by an increased release of LDH into the supernatant. The cytotoxic effect was also present in the *NLRP3*$^{-/-}$ cells, while no effect on IL-1β release was observed. Furthermore, PET particles stimulated a significant increase of IL-8 secretion (~1.8 fold) in the WT, but not in *NLRP3*$^{-/-}$ cells. The other types of plastic particles did not show any effects in the investigated endpoints.

5.5 Discussion

The present study aimed to validate an animal-free *in vitro* tool for investigating NLRP3 inflammasome activation in a macrophage-like cell type and to subsequently apply a large panel of different MNP. To prove the involvement of the inflammasome in particle effects, we generated an NLRP3-deficient THP-1 cell line. PMA-differentiated THP-1 cells are broadly used as a model for macrophages in monoculture (Genin *et al.*, 2015; Kim *et al.*, 2011) or co-culture models of the intestine (Kämpfer *et al.*, 2017; Susewind *et al.*, 2016) and respiratory tract (Cappellini *et al.*, 2020; Diabaté *et al.*, 2008). First, we confirmed the knockout using the NLRP3 activator LPS. Next, we validated this THP-1 tool against *in vitro* BMDM data using TiO_2 nanoparticles and against murine *in vivo* data using MWCNTs. Finally, we applied different samples of MNP to investigate NLRP3 activation. In addition to analyzing IL-1β, an NLRP3-specific cytokine, we investigated IL-8 secretion and cytotoxic effects as unspecific, pro-inflammatory reactions to particle exposure. We did not observe any suppression of cytokine release due to cytotoxicity in any of the investigated groups.

After the successful knockout of the *NLRP3* gene, THP-1 cells exhibited virtually no IL-1β release, even after treatment with strong inflammasome activators like LPS (Kelley *et al.*, 2019) or PS-NH_2 (Lunov *et al.*, 2011). *NLRP3*$^{-/-}$ cells also showed a drastically reduced background release of IL-8, which is most likely the consequence of absent IL-1β. Even without particle exposure, THP-1 cells produce IL-1β, which acts as an activator of the NF-κB pathway (Parikh *et al.*, 1997). In turn, NF-κB regulates IL-8 expression (Kunsch and Rosen, 1993; Vlahopoulos *et al.*, 1999). But despite the far lower background levels of IL-8, *NLRP3*$^{-/-}$ cells show the same IL-8 levels as the WT after LPS treatment, implying that they still possess the full potential of releasing cytokines not directly depending on NLRP3 activation.

To validate the use of THP-1 WT and *NLRP3*$^{-/-}$ cells as a particle screening tool for NLRP3 activation, we compared their reaction to previously published data generated with BMDMs isolated from WT and *Nlrp3* knockout mice. In the study by Kolling *et al.* (2020), BMDMs were treated with the four different TiO_2 samples NT1-4, and IL-1β release was assessed. TiO_2 in its nanoform affects the extent of intestinal inflammation in an NLRP3-dependent manner and triggers the activation of NLRP3 in human macrophages (Ruiz *et al.*, 2017). Although the magnitude of the effects is much higher in BMDMs, presumably due to species differences,

the ranking of the different TiO_2 materials presented by Kolling *et al.* is in agreement with our data obtained from THP-1 cells: treatment with NT2 caused the highest increase in IL-1β release, followed by NT4. Furthermore, our results confirm that the IL-1β release induced by TiO_2 nanoparticles is NLRP3-dependent.

Next, we compared the reaction of THP-1 cells to MWCNT treatment to an *in vivo* study (van Berlo *et al.*, 2014). Long, rigid, needle-like carbon nanotubes are potent activators of the NLRP3 inflammasome, very similar to asbestos fibers (Palomäki *et al.*, 2011). Van Berlo *et al.* reported a much more profound pro-inflammatory and associated fibrogenic potential of the longer, rigid "Mitsui 7" MWCNTs, compared to the shorter, more entangled NM400. This is in strong agreement with our study, as "Mitsui 7" induced an increase of IL-1β and IL-8 secretion as well as low, NLRP3-dependent cytotoxic effects, which are not present with NM400. Cytotoxic properties of "Mitsui 7" were also observed by van Berlo *et al.* in the murine lung.

Based on the strong correlation with previously published data in other models, our THP-1-based NLRP3 activation testing assay presents a valid, early *in vitro* screening approach for implementation in a hierarchical testing strategy during the hazard assessment of nanoparticles, fibers, and MNP. Our present approach could complement the "Tier 1" in an integrated approach to testing and assessment (IATA), as recently proposed for nanomaterials regarding oral exposure (Di Cristo *et al.*, 2021). However, assessment of possible interference with the used assays prior to *in vitro* testing is necessary to correctly interpret the obtained results (Stone *et al.*, 2009). For example, interference of TiO_2 particles has been described for photometric biological assays by absorption of light or adsorption of proteins on the particle surface (Guadagnini *et al.*, 2015; Kroll *et al.*, 2012), as also observed for IL-8 in the present study.

Finally, we evaluated the NLRP3 inflammasome activating potential of a large panel of different MNP. Except for PS-NH_2 particles, which have been previously investigated in detail by Lunov *et al.* (2011), none of the MNP samples activated the NLRP3 inflammasome in THP-1 cells, at the tested concentration. There have been multiple reports of pro-inflammatory effects of MNP in simple (Brown *et al.*, 2001; Forte *et al.*, 2016) and complex *in vitro* models (Busch *et al.*, 2021a; Busch *et al.*, 2021b), as well as in *in vivo* studies (Li *et al.*, 2019; Qiao *et al.*, 2019), but our presented data suggest that the mechanisms behind these effects are, with the exception of PS-NH_2, NLRP3-independent. In contrast, some *in vivo* studies reported the activation of the NLRP3 inflammasome in heart tissue (Wei *et al.*, 2021) or ovaries (Hou *et al.*, 2021) of rats after 90 days of oral uptake of PS microplastics. The authors suggest an activation of NLRP3 in these tissues as a consequence of systemic inflammation and oxidative stress, instead of direct interaction of microplastics with cardiac or ovarian immune cells. Furthermore, these studies did not investigate the presence of microplastics in target tissue. Therefore, the

possibly indirect activation of NLRP3 in secondary tissue after subchronic exposure is hardly comparable to the direct activation of NLRP3 in macrophages after direct single-exposure as observed in the present study.

Interestingly, PET particles induced a significant increase in IL-8 secretion in the WT cells, without any effect on IL-1β release. Although this increase in IL-8 is not present in *NLRP3*$^{-/-}$ cells, this observation points towards an NLRP3-independent pro-inflammatory effect. A certain level of IL-1β, caused by a constitutively active inflammasome in PMA-differentiated THP-1 cells (Netea *et al.*, 2009), might be required to induce detectable reactions via other pathways after treatment with a weak stressor like PET particles. Since PET particles are not commercially available and the laser-based generation procedure in our study is quite novel, literature data on PET particle toxicity is scarce. Magrì *et al.* (2018) produced PET particles in a similar manner and assessed their toxicity in a Caco-2 intestinal transwell model. In contrast to the present study employing infrared laser pulses, the authors used a UV laser resulting in nanoplastics of ~100 nm diameter. No toxic effects were reported, but PET particles were internalized by the epithelial cells and showed a high propensity to cross the gut barrier. Taken together with our findings, ingested PET particles might exhibit toxicologically relevant, pro-inflammatory effects by crossing the epithelial barrier of the intestine and interacting with intestinal macrophages of the *lamina propria*. The PET particles used in this study are a mixture of micro- and nanoparticles. Thus, size dependency and the underlying mechanisms of the observed effect will be investigated in future studies.

In conclusion, MNP do not appear to act as potent NLRP3 inflammasome activators, but can nevertheless provoke pro-inflammatory effects which remain to be mechanistically investigated. The here presented use of THP-1 WT and *NLRP3*$^{-/-}$ cells as a screening tool for inflammasome activation represents a valid non-animal alternative for the use of BMDMs isolated from WT or *Nlrp3*$^{-/-}$ mice. In view of the recognized importance of the NLRP3 pathway in particle-induced diseases, such as MWCNT-induced lung fibrosis, we propose to use our approach as an early *in vitro* screening tool when assessing the hazard of particles, fibers, and MNP in a hierarchical testing strategy.

Acknowledgments

Mathias Busch is thankful to the Jürgen Manchot Foundation, Duesseldorf, Germany, for supporting this project through a PhD scholarship. Tobias Bessel and Friedrich Waag thank the European Union and the Ministry of Economic Affairs, Innovation, Digitalization and Energy of the German State of North Rhine-Westphalia for funding through the European Regional Development Fund in the START-UP transfer.NRW program (AutoProNANO, EFRE-0400339). This work was also partially performed at the Center for Chemical Polymer

Technology CPT, which was supported by the EU and the federal state of North Rhine-Westphalia (grant EFRE-300088302). The authors thank Julian Koslowski for his contribution in preparing fibrous microplastics.

5.6 Supplementary Material

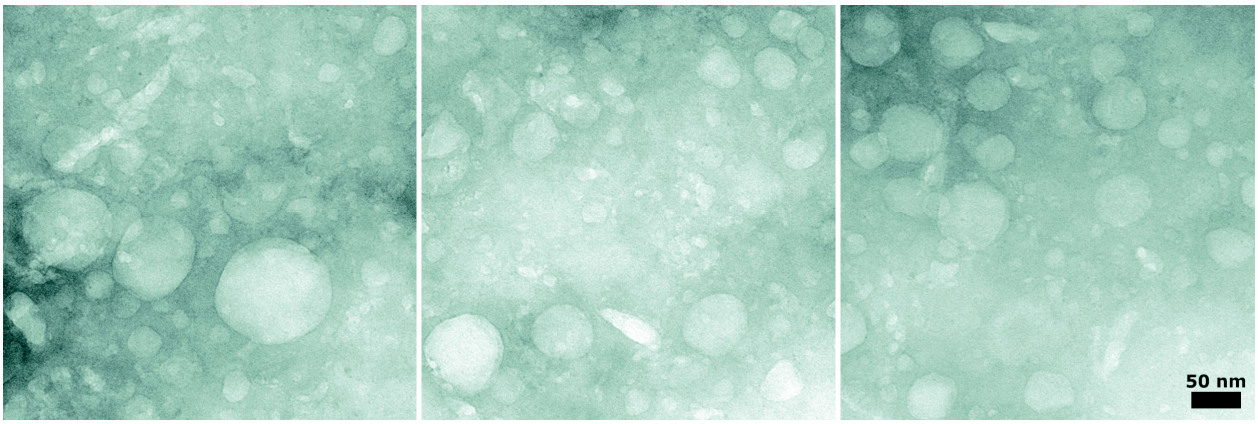

Figure S 5.1 Exemplary TEM micrographs of the laser-generated PET nanoparticles. All micrographs have the same scale.

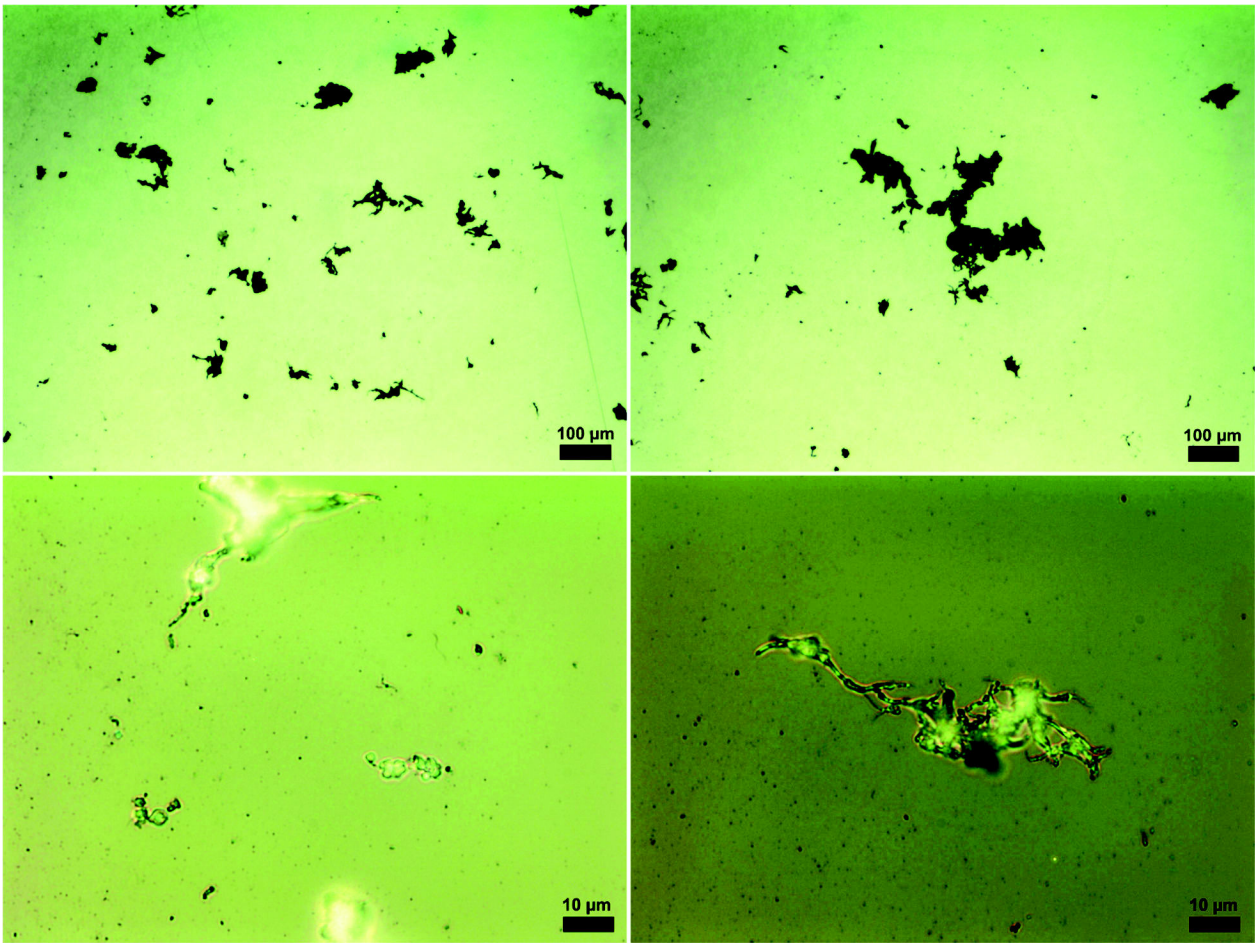

Figure S 5.2 Exemplary light microscope images of the laser-generated PET microparticle fraction at 5x (top) and 50x (bottom) magnification.

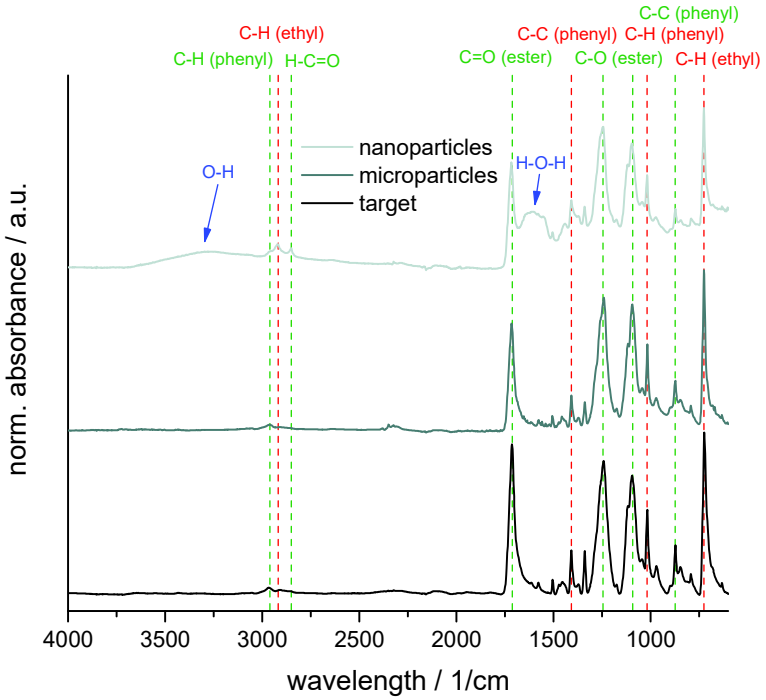

Figure S 5.3 Normalized FT-IR absorbance spectra of the PET laser ablation target, the microparticle fraction, and the nanoparticle fraction. All spectra were normalized to the height of the peak of the C-H ethyl bond at 722 1/cm.

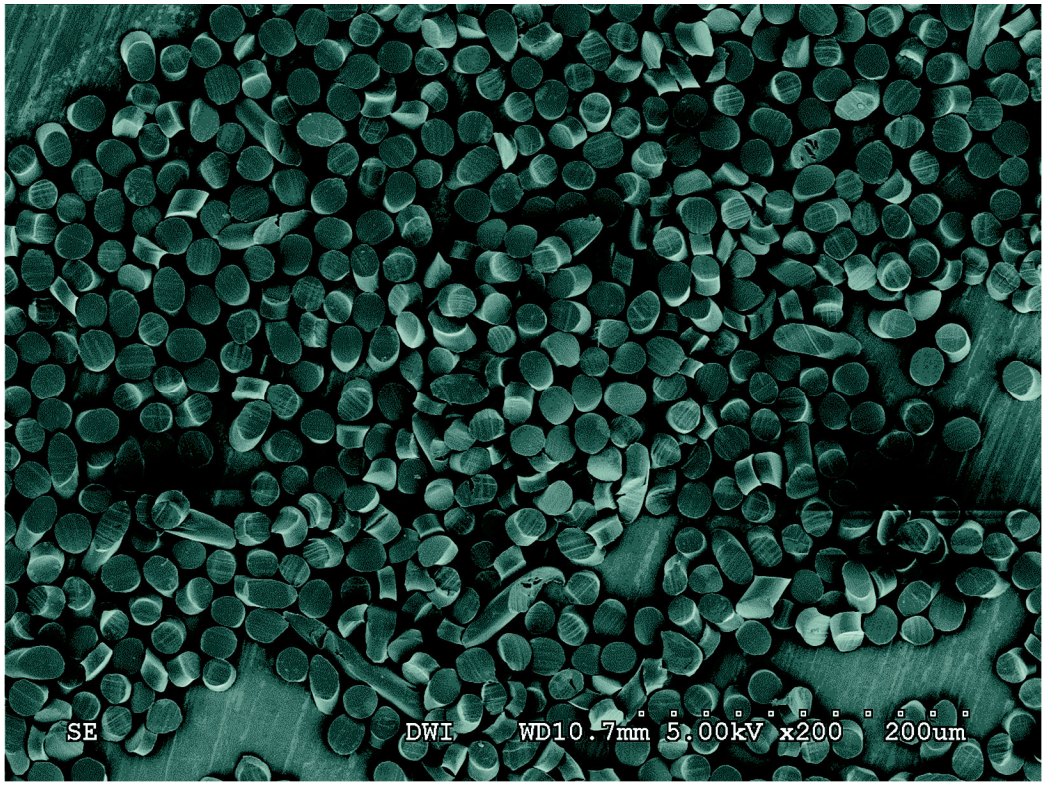

Figure S 5.4 Exemplary SEM images of PES microfibers at 200x magnification.

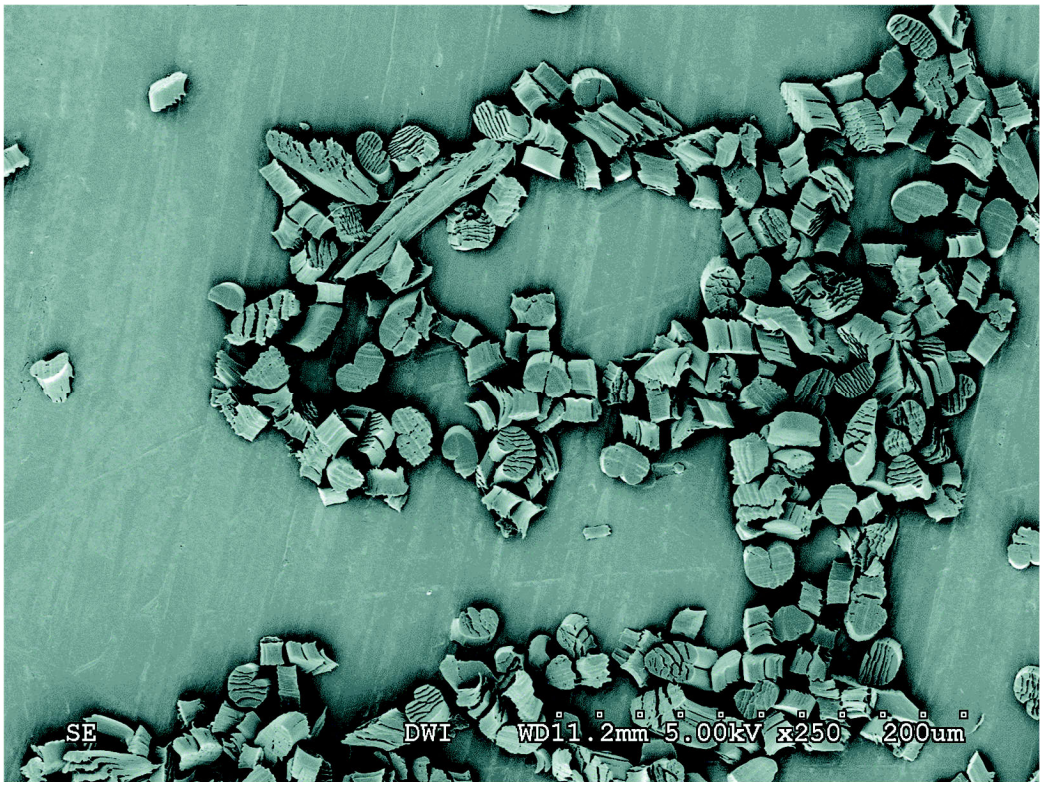

Figure S 5.5 Exemplary SEM images of PAN microfibers at 250x magnification.

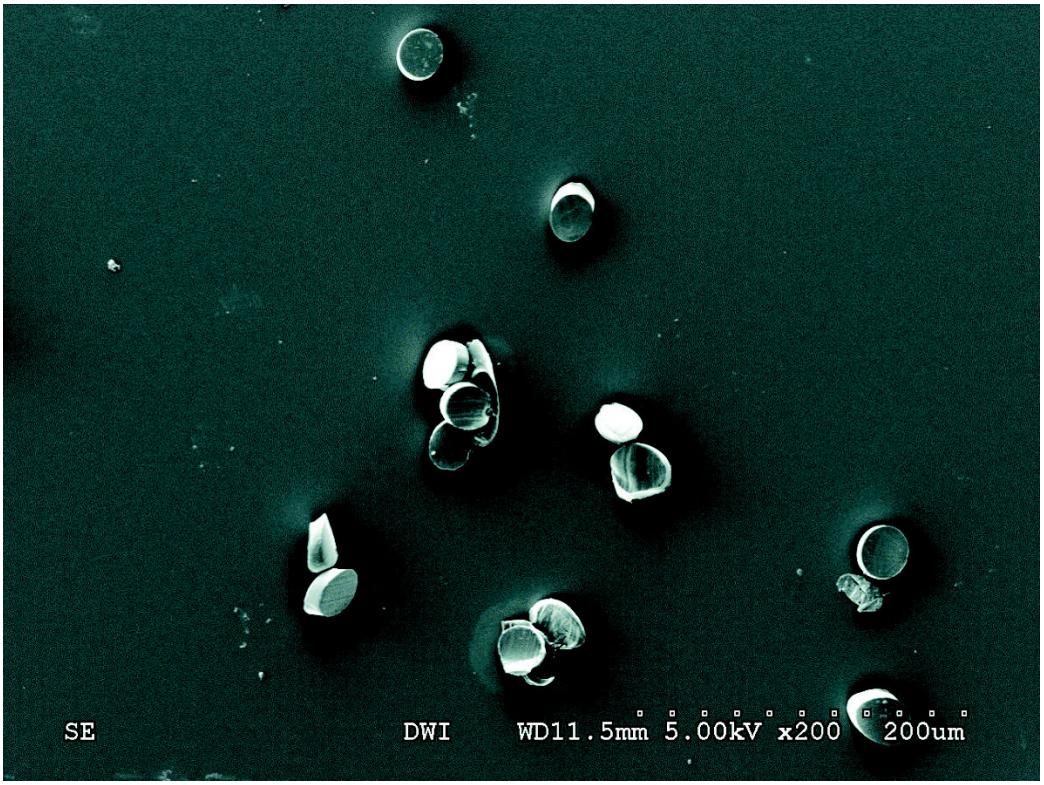

Figure S 5.6 Exemplary SEM images of PA6 microfibers at 250x magnification.

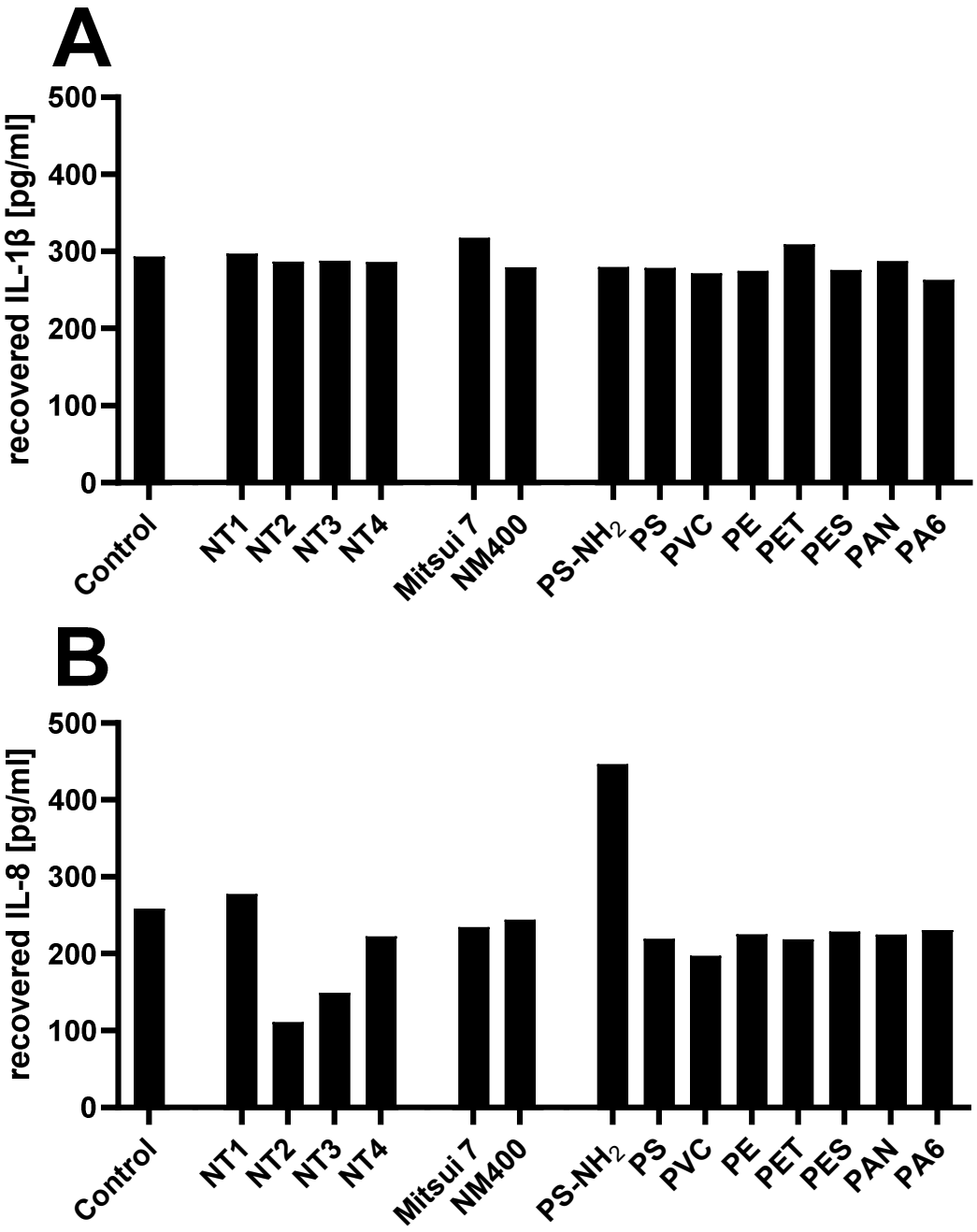

Figure S 5.7 Recovered IL-1β (A) or IL-8 (B) after 24 h incubation of 500 pg/ml cytokine standard with 50 µg/cm² particle sample under experimental conditions, as assessed by ELISA. N=1.

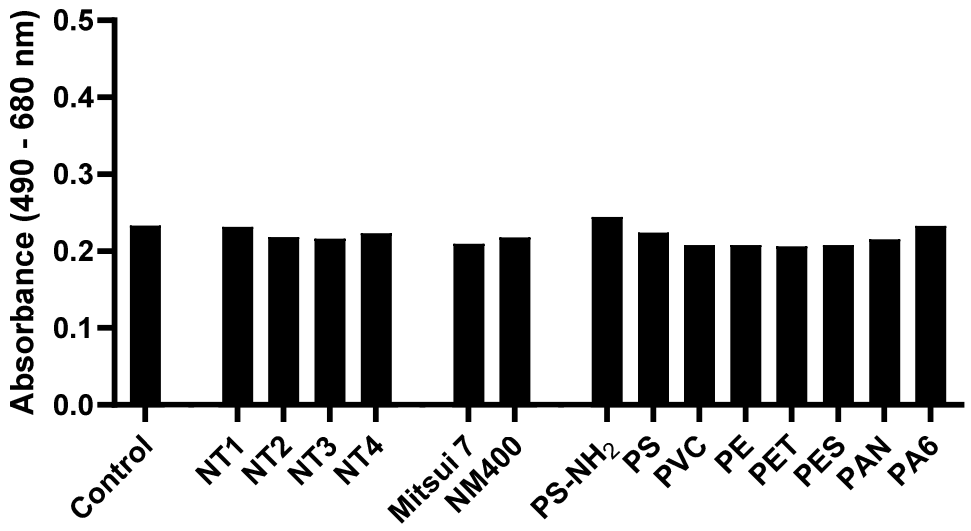

Figure S 5.8 LDH activity in the supernatant after 24 h incubation of diluted cell lysate with 50 µg/cm² particle sample, as assessed by the LDH assay. N=1.

5.7 References

Amato-Lourenço, L.F., Dos Santos Galvão, L., Weger, L.A. de, Hiemstra, P.S., Vijver, M.G., Mauad, T., 2020. An emerging class of air pollutants: Potential effects of microplastics to respiratory human health? Sci. Total Environ. 749, 141676. https://doi.org/10.1016/j.scitotenv.2020.141676.

Andrady, A.L., 2011. Microplastics in the marine environment. Mar. Pollut. Bull. 62, 1596–1605. https://doi.org/10.1016/j.marpolbul.2011.05.030.

Andrady, A.L., 2012. Biodegradation of Plastics: Monitoring what Happens, in: Brewis, D., Briggs, D., Pritchard, G. (Eds.), Plastics Additives: An A-Z reference, vol. 1. Springer Netherlands, Dordrecht, pp. 32–40.

Barboza, L.G.A., Lopes, C., Oliveira, P., Bessa, F., Otero, V., Henriques, B., Raimundo, J., Caetano, M., Vale, C., Guilhermino, L., 2019. Microplastics in wild fish from North East Atlantic Ocean and its potential for causing neurotoxic effects, lipid oxidative damage, and human health risks associated with ingestion exposure. Sci. Total Environ., 134625. https://doi.org/10.1016/j.scitotenv.2019.134625.

Brown, D.M., Wilson, M.R., MacNee, W., Stone, V., Donaldson, K., 2001. Size-dependent proinflammatory effects of ultrafine polystyrene particles: a role for surface area and oxidative stress in the enhanced activity of ultrafines. Toxicol. Appl. Pharmacol. 175, 191–199. https://doi.org/10.1006/taap.2001.9240.

Busch, M., Bredeck, G., Kämpfer, A.A., Schins, R.P., 2021a. Investigations of acute effects of polystyrene and polyvinyl chloride micro- and nanoplastics in an advanced in vitro triple culture model of the healthy and inflamed intestine. Environ. Res. 193, 110536. https://doi.org/10.1016/j.envres.2020.110536.

Busch, M., Kämpfer, A.A., Schins, R.P., 2021b. An inverted in vitro triple culture model of the healthy and inflamed intestine: Adverse effects of polyethylene particles. Chemosphere 284, 131345. https://doi.org/10.1016/j.chemosphere.2021.131345.

Cappellini, F., Di Bucchianico, S., Karri, V., Latvala, S., Malmlöf, M., Kippler, M., Elihn, K., Hedberg, J., Odnevall Wallinder, I., Gerde, P., Karlsson, H.L., 2020. Dry Generation of CeO2 Nanoparticles and Deposition onto a Co-Culture of A549 and THP-1 Cells in Air-

Liquid Interface-Dosimetry Considerations and Comparison to Submerged Exposure. Nanomaterials 10. https://doi.org/10.3390/nano10040618.
Cassel, S., Eisenbarth, S., Iyer, S., Sadler, J., Colegio, O., Tephly, L., Carter, A., Rothman, P., Flavell, R., Sutterwala, F., 2008. The Nalp3 inflammasome is essential for the development of silicosis. Proc. Natl. Acad. Sci. 26, 26, 9035–9040. https://doi.org/10.1073/pnas.0803933105.
Cole, M., 2016. A novel method for preparing microplastic fibers. Sci. Rep. 6, 34519. https://doi.org/10.1038/srep34519.
Destoumieux-Garzón, D., Mavingui, P., Boetsch, G., Boissier, J., Darriet, F., Duboz, P., Fritsch, C., Giraudoux, P., Le Roux, F., Morand, S., Paillard, C., Pontier, D., Sueur, C., Voituron, Y., 2018. The One Health Concept: 10 Years Old and a Long Road Ahead. Front. Vet. Sci. 5, 14. https://doi.org/10.3389/fvets.2018.00014.
Di Cristo, L., Oomen, A.G., Dekkers, S., Moore, C., Rocchia, W., Murphy, F., Johnston, H.J., Janer, G., Haase, A., Stone, V., Sabella, S., 2021. Grouping Hypotheses and an Integrated Approach to Testing and Assessment of Nanomaterials Following Oral Ingestion. Nanomaterials 11. https://doi.org/10.3390/nano11102623.
Diabaté, S., Mülhopt, S., Paur, H.-R., Krug, H.F., 2008. The response of a co-culture lung model to fine and ultrafine particles of incinerator fly ash at the air-liquid interface. Altern. Lab. Anim. 36, 285–298. https://doi.org/10.1177/026119290803600306.
Dostert, C., Pétrilli, V., van Bruggen, R., Steele, C., Mossman, B.T., Tschopp, J., 2008. Innate immune activation through Nalp3 inflammasome sensing of asbestos and silica. Science 320, 674–677. https://doi.org/10.1126/science.1156995.
Eisfeld, H.S., Simonis, A., Winter, S., Chhen, J., Ströh, L.J., Krey, T., Koch, M., Theobald, S.J., Rybniker, J., 2021. Viral Glycoproteins Induce NLRP3 Inflammasome Activation and Pyroptosis in Macrophages. Viruses 13. https://doi.org/10.3390/v13102076.
Elaboudi, I., Lazare, S., Belin, C., Talaga, D., Labrugère, C., 2008. Underwater excimer laser ablation of polymers. Appl. Phys. A 92, 743–748. https://doi.org/10.1007/s00339-008-4567-2.
Falco, F. de, Di Pace, E., Cocca, M., Avella, M., 2019. The contribution of washing processes of synthetic clothes to microplastic pollution. Sci. Rep. 9, 6633. https://doi.org/10.1038/s41598-019-43023-x.
Forte, M., Iachetta, G., Tussellino, M., Carotenuto, R., Prisco, M., Falco, M. de, Laforgia, V., Valiante, S., 2016. Polystyrene nanoparticles internalization in human gastric adenocarcinoma cells. Toxicol. In Vitro 31, 126–136. https://doi.org/10.1016/j.tiv.2015.11.006.
Genin, M., Clement, F., Fattaccioli, A., Raes, M., Michiels, C., 2015. M1 and M2 macrophages derived from THP-1 cells differentially modulate the response of cancer cells to etoposide. BMC Cancer 15, 577. https://doi.org/10.1186/s12885-015-1546-9.
Gram, A.M., Wright, J.A., Pickering, R.J., Lam, N.L., Booty, L.M., Webster, S.J., Bryant, C.E., 2021. Salmonella Flagellin Activates NAIP/NLRC4 and Canonical NLRP3 Inflammasomes in Human Macrophages. J. Immunol. 206, 631–640. https://doi.org/10.4049/jimmunol.2000382.
Guadagnini, R., Halamoda Kenzaoui, B., Walker, L., Pojana, G., Magdolenova, Z., Bilanicova, D., Saunders, M., Juillerat-Jeanneret, L., Marcomini, A., Huk, A., Dusinska, M., Fjellsbø, L.M., Marano, F., Boland, S., 2015. Toxicity screenings of nanomaterials: challenges due to interference with assay processes and components of classic in vitro tests. Nanotoxicology 9, 13–24. https://doi.org/10.3109/17435390.2013.829590.
Guerranti, C., Martellini, T., Perra, G., Scopetani, C., Cincinelli, A., 2019. Microplastics in cosmetics: Environmental issues and needs for global bans. Environ. Toxicol. Pharmacol. 68, 75–79. https://doi.org/10.1016/j.etap.2019.03.007.

He, Y., Hara, H., Núñez, G., 2016. Mechanism and Regulation of NLRP3 Inflammasome Activation. Trends Biochem. Sci. 41, 1012–1021. https://doi.org/10.1016/j.tibs.2016.09.002.

Hou, J., Lei, Z., Cui, L., Hou, Y., Yang, L., An, R., Wang, Q., Li, S., Zhang, H., Zhang, L., 2021. Polystyrene microplastics lead to pyroptosis and apoptosis of ovarian granulosa cells via NLRP3/Caspase-1 signaling pathway in rats. Ecotoxicol. Environ. Saf. 212, 112012. https://doi.org/10.1016/j.ecoenv.2021.112012.

Ibrahim, Y.S., Tuan Anuar, S., Azmi, A.A., Wan Mohd Khalik, W.M.A., Lehata, S., Hamzah, S.R., Ismail, D., Ma, Z.F., Dzulkarnaen, A., Zakaria, Z., Mustaffa, N., Tuan Sharif, S.E., Lee, Y.Y., 2021. Detection of microplastics in human colectomy specimens. JGH Open 5, 116–121. https://doi.org/10.1002/jgh3.12457.

Julienne, F., Delorme, N., Lagarde, F., 2019. From macroplastics to microplastics: Role of water in the fragmentation of polyethylene. Chemosphere 236, 124409. https://doi.org/10.1016/j.chemosphere.2019.124409.

Kalčíková, G., 2020. Aquatic vascular plants – A forgotten piece of nature in microplastic research. Environ. Pollut. 262, 114354. https://doi.org/10.1016/j.envpol.2020.114354.

Kämpfer, A.A.M., Urbán, P., Gioria, S., Kanase, N., Stone, V., Kinsner-Ovaskainen, A., 2017. Development of an in vitro co-culture model to mimic the human intestine in healthy and diseased state. Toxicol. In Vitro 45, 31–43. https://doi.org/10.1016/j.tiv.2017.08.011.

Kelley, N., Jeltema, D., Duan, Y., He, Y., 2019. The NLRP3 Inflammasome: An Overview of Mechanisms of Activation and Regulation. Int. J. Mol. Sci. 20, 3328. https://doi.org/10.3390/ijms20133328.

Kim, J.-A., Ahn, B.-N., Kong, C.-S., Kim, S.-K., 2011. Anti-inflammatory action of sulfated glucosamine on cytokine regulation in LPS-activated PMA-differentiated THP-1 macrophages. Inflamm. Res. 60, 1131–1138. https://doi.org/10.1007/s00011-011-0377-7.

Kolling, J., Tigges, J., Hellack, B., Albrecht, C., Schins, R.P.F., 2020. Evaluation of the NLRP3 Inflammasome Activating Effects of a Large Panel of TiO2 Nanomaterials in Macrophages. Nanomaterials 10, 1876. https://doi.org/10.3390/nano10091876.

Kroll, A., Pillukat, M.H., Hahn, D., Schnekenburger, J., 2012. Interference of engineered nanoparticles with in vitro toxicity assays. Arch. Toxicol. 86, 1123–1136. https://doi.org/10.1007/s00204-012-0837-z.

Kunsch, C., Rosen, C.A., 1993. NF-kappa B subunit-specific regulation of the interleukin-8 promoter. Mol. Cell Biol. 13, 6137–6146. https://doi.org/10.1128/mcb.13.10.6137-6146.1993.

LeFevre, M.E., Warren, J.B., Joel, D.D., 1985. Particles and macrophages in murine Peyer's patches. Exp. Cell Biol. 53, 121–129. https://doi.org/10.1159/000163304.

Lehnert, B.E., 1992. Pulmonary and thoracic macrophage subpopulations and clearance of particles from the lung. Environ. Health Perspect. 97, 17–46. https://doi.org/10.1289/ehp.929717.

Li, B., Ding, Y., Cheng, X., Sheng, D., Xu, Z., Rong, Q., Wu, Y., Zhao, H., Ji, X., Zhang, Y., 2019. Polyethylene microplastics affect the distribution of gut microbiota and inflammation development in mice. Chemosphere 244, 125492. https://doi.org/10.1016/j.chemosphere.2019.125492.

Lim, D., Jeong, J., Song, K.S., Sung, J.H., Oh, S.M., Choi, J., 2021. Inhalation toxicity of polystyrene micro(nano)plastics using modified OECD TG 412. Chemosphere 262, 128330. https://doi.org/10.1016/j.chemosphere.2020.128330.

Lomer, M.C.E., Thompson, R.P.H., Powell, J.J., 2002. Fine and ultrafine particles of the diet: Influence on the mucosal immune response and association with Crohn's disease. Proc. Nutr. Soc. 61, 123–130. https://doi.org/10.1079/PNS2001134.

Lunov, O., Syrovets, T., Loos, C., Nienhaus, G.U., Mailänder, V., Landfester, K., Rouis, M., Simmet, T., 2011. Amino-functionalized polystyrene nanoparticles activate the NLRP3

inflammasome in human macrophages. ACS Nano 5, 9648–9657. https://doi.org/10.1021/nn203596e.

Magrì, D., Sánchez-Moreno, P., Caputo, G., Gatto, F., Veronesi, M., Bardi, G., Catelani, T., Guarnieri, D., Athanassiou, A., Pompa, P.P., Fragouli, D., 2018. Laser Ablation as a Versatile Tool To Mimic Polyethylene Terephthalate Nanoplastic Pollutants: Characterization and Toxicology Assessment. ACS Nano 12, 7690–7700. https://doi.org/10.1021/acsnano.8b01331.

Nachev, P., van 'T Zand, D.D., Coger, V., Wagener, P., Reimers, K., Vogt, P.M., Barcikowski, S., Pich, A., 2012. Synthesis of hybrid microgels by coupling of laser ablation and polymerization in aqueous medium. J. Laser Appl. 24, 42012. https://doi.org/10.2351/1.4730803.

Netea, M.G., Nold-Petry, C.A., Nold, M.F., Joosten, L.A.B., Opitz, B., van der Meer, J.H.M., van de Veerdonk, F.L., Ferwerda, G., Heinhuis, B., Devesa, I., Funk, C.J., Mason, R.J., Kullberg, B.J., Rubartelli, A., van der Meer, J.W.M., Dinarello, C.A., 2009. Differential requirement for the activation of the inflammasome for processing and release of IL-1β in monocytes and macrophages. Blood 113, 2324–2335. https://doi.org/10.1182/blood-2008-03-146720.

Nizzetto, L., Futter, M., Langaas, S., 2016. Are Agricultural Soils Dumps for Microplastics of Urban Origin? Environ. Sci. Technol. 50, 10777–10779. https://doi.org/10.1021/acs.est.6b04140.

Ozaki, E., Campbell, M., Doyle, S.L., 2015. Targeting the NLRP3 inflammasome in chronic inflammatory diseases: current perspectives. J. Inflamm. Res. 8, 15–27. https://doi.org/10.2147/JIR.S51250.

Palomäki, J., Välimäki, E., Sund, J., Vippola, M., Clausen, P.A., Jensen, K.A., Savolainen, K., Matikainen, S., Alenius, H., 2011. Long, needle-like carbon nanotubes and asbestos activate the NLRP3 inflammasome through a similar mechanism. ACS Nano 5, 6861–6870. https://doi.org/10.1021/nn200595c.

Parikh, A.A., Salzman, A.L., Kane, C.D., Fischer, J.E., Hasselgren, P., 1997. IL-6 Production in Human Intestinal Epithelial Cells Following Stimulation with IL-1β Is Associated with Activation of the Transcription Factor NF-kB. J. Surg. Res. 69, 139–144. https://doi.org/10.1006/jsre.1997.5061.

Qiao, R., Sheng, C., Lu, Y., Zhang, Y., Ren, H., Lemos, B., 2019. Microplastics induce intestinal inflammation, oxidative stress, and disorders of metabolome and microbiome in zebrafish. Sci. Total Environ. 662, 246–253. https://doi.org/10.1016/j.scitotenv.2019.01.245.

Ramachandran, H., Martins, S., Kontarakis, Z., Krutmann, J., Rossi, A., 2021. Fast but not furious: a streamlined selection method for genome-edited cells. Life Sci. Alliance 4, e202101051. https://doi.org/10.26508/lsa.202101051.

Rehbock, C., Jakobi, J., Gamrad, L., van der Meer, S., Tiedemann, D., Taylor, U., Kues, W., Rath, D., Barcikowski, S., 2014. Current state of laser synthesis of metal and alloy nanoparticles as ligand-free reference materials for nano-toxicological assays. Beilstein J. Nanotechnol. 5, 1523–1541. https://doi.org/10.3762/bjnano.5.165.

Ruiz, P.A., Morón, B., Becker, H.M., Lang, S., Atrott, K., Spalinger, M.R., Scharl, M., Wojtal, K.A., Fischbeck-Terhalle, A., Frey-Wagner, I., Hausmann, M., Kraemer, T., Rogler, G., 2017. Titanium dioxide nanoparticles exacerbate DSS-induced colitis: role of the NLRP3 inflammasome. Gut 66, 1216–1224. https://doi.org/10.1136/gutjnl-2015-310297.

Russell, W.M.S., Burch, R.L., 1992. The principles of humane experimental technique. UFAW, Potters Bar, 238 pp.

Sharma, B., McLeland, C.B., Potter, T.M., Stern, S.T., Adiseshaiah, P.P., 2018. Assessing NLRP3 Inflammasome Activation by Nanoparticles, in: McNeil, S.E. (Ed.), Characterization of Nanoparticles Intended for Drug Delivery, 2nd ed. Humana Press, New York, NY, pp. 135–147.

Siegmund, B., 2002. Interleukin-1β converting enzyme (caspase-1) in intestinal inflammation. Biochem. Pharmacol. 64, 1–8. https://doi.org/10.1016/S0006-2952(02)01064-X.

Stone, V., Johnston, H., Schins, R.P.F., 2009. Development of *in vitro* systems for nanotoxicology: Methodological considerations. Crit. Rev. Toxicol. 39, 613–626. https://doi.org/10.1080/10408440903120975.

Susewind, J., Souza Carvalho-Wodarz, C. de, Repnik, U., Collnot, E.-M., Schneider-Daum, N., Griffiths, G.W., Lehr, C.-M., 2016. A 3D co-culture of three human cell lines to model the inflamed intestinal mucosa for safety testing of nanomaterials. Nanotoxicol. 10, 53–62. https://doi.org/10.3109/17435390.2015.1008065.

van Berlo, D., Wilhelmi, V., Boots, A.W., Hullmann, M., Kuhlbusch, T.A.J., Bast, A., Schins, R.P.F., Albrecht, C., 2014. Apoptotic, inflammatory, and fibrogenic effects of two different types of multi-walled carbon nanotubes in mouse lung. Arch. Toxicol. 88, 1725–1737. https://doi.org/10.1007/s00204-014-1220-z.

Vlahopoulos, S., Boldogh, I., Casola, A., Brasier, A.R., 1999. Nuclear Factor-κB–Dependent Induction of Interleukin-8 Gene Expression by Tumor Necrosis Factor α: Evidence for an Antioxidant Sensitive Activating Pathway Distinct From Nuclear Translocation. Blood 94, 1878–1889. https://doi.org/10.1182/blood.V94.6.1878.

Waag, F., Streubel, R., Gökce, B., Barcikowski, S., 2021. Synthesis of gold, platinum, and gold-platinum alloy nanoparticle colloids with high-power megahertz-repetition-rate lasers: the importance of the beam guidance method. Appl. Nanosci. 11, 1303–1312. https://doi.org/10.1007/s13204-021-01693-y.

Wei, J., Wang, X., Liu, Q., Zhou, N., Zhu, S., Li, Z., Li, X., Yao, J., Zhang, L., 2021. The impact of polystyrene microplastics on cardiomyocytes pyroptosis through NLRP3/Caspase-1 signaling pathway and oxidative stress in Wistar rats. Environ. Toxicol., 1–10. https://doi.org/10.1002/tox.23095.

Zhang, D., Gökce, B., Barcikowski, S., 2017. Laser Synthesis and Processing of Colloids: Fundamentals and Applications. Chem. Rev. 117, 3990–4103. https://doi.org/10.1021/acs.chemrev.6b00468.

Zhao, C., Zhao, W., 2020. NLRP3 Inflammasome-A Key Player in Antiviral Responses. Front. Immunol. 11, 211. https://doi.org/10.3389/fimmu.2020.00211.

Zheng, H., Wang, J., Wei, X., Le Chang, Liu, S., 2021. Proinflammatory properties and lipid disturbance of polystyrene microplastics in the livers of mice with acute colitis. Sci. Total Environ. 750, 143085. https://doi.org/10.1016/j.scitotenv.2020.143085.

6. Investigating the role of the NLRP3 inflammasome pathway in acute intestinal inflammation: use of THP-1 knockout cell lines in an advanced triple culture model

Mathias Busch[a], Haribaskar Ramachandran[a], Tina Wahle[a], Andrea Rossi[a], Roel P.F. Schins[a]

[a] *IUF – Leibniz-Research Institute for Environmental Medicine, Duesseldorf, Germany*

submitted manuscript

Author contribution: The author of this dissertation performed the *in vitro* and *ex vivo* experiments, performed the statistical analysis, made the graphs, discussed the results and wrote the manuscript. Relative contribution: 90 %.

6.1 Abstract

The NLRP3 inflammasome plays an important role in intestinal homeostasis as well as inflammation. However, *in vivo* studies investigating the role of the NLRP3 inflammasome in inflammatory bowel disease (IBD) report contrasting results, leaving it unclear if the NLRP3 inflammasome augments or attenuates intestinal inflammation. To investigate the role of the NLRP3/caspase-1 pathway in a model of acute intestinal inflammation, we modified a previously established *in vitro* triple culture model of the healthy and inflamed intestine (Caco-2/HT29-MTX-E12/THP-1). Using THP-1 knockout cell lines, we analyzed how the NLRP3 inflammasome and its downstream enzyme caspase-1 (CASP1) affect inflammatory parameters including barrier integrity and cytotoxicity, as well as gene expression and secretion of pro-inflammatory cytokines and mucus. Furthermore, we investigated differences in inflammation-mediated cytotoxicity towards enterocyte-like (Caco-2) or goblet-like (HT29-MTX-E12) epithelial cells. As a complementary approach, inflammation-related cytotoxicity was analyzed in intestinal tissue explants from wildtype (WT) and *Nlrp3*$^{-/-}$ mice. Induction of intestinal inflammation impaired the barrier, caused cytotoxicity, and altered gene expression of pro-inflammatory cytokines and mucins *in vitro*, while the knockout of *NLRP3* and *CASP1* in THP 1 cells led to attenuation of these inflammatory parameters. The knockout of *CASP1* tended to show a slightly stronger attenuating effect compared to the *NLRP3* knockout model. We also found that the inflammation-mediated death of goblet-like cells is NLRP3/caspase-1 dependent. Furthermore, inflammation-related cytotoxicity was present in ileal tissue explants from WT, but not *Nlrp3*$^{-/-}$ mice. The here presented observations indicate a pro-inflammatory and adverse role of the NLRP3 inflammasome in macrophages during acute intestinal inflammation.

6.2 Introduction

Inflammatory bowel disease (IBD), namely Crohn's disease (CD) or ulcerative colitis (UC) are characterized by chronic, relapsing inflammation of the gastrointestinal tract (Ponder and Long, 2013). IBD is thought to originate from an exaggerated immune response towards constituents of the mucosal microbiome, but the precise etiology is still not known (Bouma and Strober, 2003; Cho and Brant, 2011). As a central activator of the innate immune system, the NOD-, LRR- and pyrin domain-containing protein 3 (NLRP3) inflammasome is a crucial regulator of intestinal homeostasis and has been implicated in the pathogenesis of IBD (Sutterwala *et al.*, 2006; Zhen and Zhang, 2019). After activation via pathogen-associated molecular patterns (PAMPs) or damage-associated molecular patterns (DAMPs), the NLRP3 inflammasome oligomerizes and recruits procaspase-1, which leads to the formation of the active caspase-1 (CASP1) (McKee and Coll, 2020). CASP1 cleaves the inactive pro-IL-1β, which results in the secretion of mature IL-1β (Lopez-Castejon and Brough, 2011). As an early pro-inflammatory cytokine, IL-1β induces subsequent inflammatory cascades (Siegmund, 2002), including the activation of the transcription factor NF-κB (Parikh *et al.*, 1997). In turn, NF-κB regulates secondary inflammatory cytokines like IL-6 and IL-8 (Brasier, 2010; Kunsch and Rosen, 1993).

However, the exact role of the NLRP3 inflammasome in IBD is not clear (Perera *et al.*, 2018), as different studies report conflicting results: genetic polymorphisms decreasing *NLRP3* expression in patients were linked to higher susceptibility towards CD (Villani *et al.*, 2009), while *Nlrp3* knockout mice developed less severe DSS-induced colitis compared to the wild type (WT) (Bauer *et al.*, 2010). The latter effect could be reversed by cohousing *Nlrp3*$^{-/-}$ mice with WT mice (Bauer *et al.*, 2012), which implies a crucial role of the microbiome in IBD susceptibility. Other studies reported increased colitis symptoms in *Nlrp3*$^{-/-}$ mice when compared to WT mice (Allen *et al.*, 2010; Hirota *et al.*, 2011).

The gastrointestinal epithelium is covered in mucus, which plays an important protective role in intestinal homeostasis. Mucus primarily consists of different mucins, highly glycosylated proteins mainly produced and secreted by goblet cells, but also in parts by enterocytes. Mucins can be divided into two classes: secreted mucins and membrane-associated mucins. Secreted mucins, such as MUC2 and MUC5AC, and also transmembrane mucins, such as MUC1, MUC13, and MUC20, have been shown to be altered or aberrantly expressed in patients suffering from IBD (Forgue-Lafitte *et al.*, 2007; Furr *et al.*, 2010; Larsson *et al.*, 2011; Sheng *et al.*, 2011; Sheng *et al.*, 2012; Yamamoto-Furusho *et al.*, 2015). This indicates a major role of mucus not only during homeostasis, but also during intestinal inflammation.

We have previously developed an *in vitro* triple culture model of the healthy and inflamed intestine, comprised of the human cell lines Caco-2, HT29-MTX-E12, and THP-1. This system is capable of replicating several hallmarks of intestinal inflammation, including impairment of

barrier integrity, cytotoxicity, an increase of pro-inflammatory cytokine secretion, reduction of acidic mucus secretion, and DNA damage in epithelial cells after prolonged inflammation (Busch *et al.*, 2021; Kämpfer *et al.*, 2021). In these previous studies, this model was applied in toxicological research investigating particle effects in the context of inflammation.

The aim of the present study was to investigate the role of the NLRP3 inflammasome and its downstream enzyme CASP1 in macrophages during initial acute intestinal inflammation by using the *in vitro* triple culture model with different THP-1 cell lines (WT, *CASP1*$^{-/-}$ and *NLRP3*$^{-/-}$). As a complementary approach, we studied short-term inflammation-related cytotoxicity in intestinal tissue explants from WT and *Nlrp3*$^{-/-}$ mice.

6.3 Materials and Methods

Materials

The cell culture media (DMEM, MEM, RPMI 1640), 2-mercaptoethanol (ME), horse serum, sodium pyruvate, and phosphate-buffered saline (PBS) were purchased from Thermo Fisher Scientific. Fetal calf serum (FCS) for Caco-2 and HT29-MTX-E12, non-essential amino acids (NEAA), L-glutamine, D-glucose, penicillin/streptomycin (P/S), trypsin, phorbol 12-myristate 13-acetate (PMA), interferon-gamma (IFN-γ), lipopolysaccharides (LPS), Accutase, β-nicotinamide adenine dinucleotide sodium salt (NAD), lithium L-lactate, phenazine methosulfate (PMS), iodonitrotetrazolium chloride (INT), Triton X-100, bovine serum albumin (BSA), and 50 nm amine-modified polystyrene nanobeads (PS-NH_2) were purchased from Sigma-Aldrich/Merck. Paraformaldehyde (PFA) was ordered from Carl Roth (Germany). The DQ12 quartz sample used in this study was kindly provided by the Institute of Occupational Medicine (IOM, Edinburgh, UK).

Cell culture

Caco-2 (DSMZ, ACC169) cells were cultured in MEM-based cell culture medium substituted with 20 % FCS, 1 % P/S and 1 % L-glutamine. HT29-MTX-E12 (ECACC, 12040401) cells were cultured in DMEM-based cell culture medium substituted with 10 % FCS, 1 % P/S, and 1 % NEAA. Caco-2 and HT29-MTX-E12 cells were regularly split at roughly 80 % confluence and used at passages 5 – 25 for experiments. THP-1 (ATCC, TIB-202) cells were cultured in RPMI 1640-based cell culture medium (containing L-glutamine and 25 mM HEPES) substituted with 10 % FCS, 1 % P/S, 1 nM sodium pyruvate, 0.7 % D-glucose and 50 nM ME and maintained between $2*10^5$ and $8*10^5$ cells/ml. For experiments, THP-1 cells were used at passages 5 – 15.

Generation of CASP1-deficient and NLRP3-deficient THP-1 cell lines

CASP1 and *NLRP3* THP-1 mutant cells were generated as previously described (Ramachandran *et al.*, 2021) Briefly, gRNAs were designed using the CRISPR design tool CHOPCHOP (http://chopchop.cbu.uib.no/) and cloned into a modified PX458 plasmid (Addgene #48138). The resulting bicistronic vector encoded the respective gRNA, Cas9 nuclease, and a GFP selection marker. gRNAs efficiency was assessed using High-Resolution Melt Analysis (HRMA). A gRNA targeting *CASP1* exon 5 (5'-TAATGAGAGCAAGACGTGTG-3') and *NLRP3* exon 2 (5'-GCTAATGATCGACTTCAATG-3') were chosen for further experiments (HRMA primers, *CASP1*: Fwd 5'-CACCGTAATGAGAGCAAGACGTGTG-3' Rev 5'-AAACCACACGTCTTGCTCTCATTAC-3'; *NLRP3*: Fwd 5'-CAGACCATGTGGATCTAGCC-3 Rev 5'-TGTTGATCGCAGCGAAGAT-3'). THP-1 cells were electroporated using a Neon transfection system (Thermofisher) according to the manufacturer's instructions. After 48 h, cells were FACS sorted and plated as single cells into 96-well plates. Cells were duplicated into maintenance and lysis plates after a week. Clones were then lysed with proteinase K and genotyped by PCR followed by deep sequencing using a miSeq Illumina sequencer and a V2 Nano cassette.

Investigation of the cytokine profile of THP-1 ko cell lines

THP-1 cells (WT, *CASP1*$^{-/-}$ and *NLRP3*$^{-/-}$, at the same passage number) were seeded into T25 flasks at 6*10^5 cells/ml, differentiated with 100 nM PMA for 24 h, detached with accutase, and seeded in 24-well plates at 120.000 cells/well. Cells were allowed to re-attach for 1.5 h and were treated with different NLRP3 inflammasome activators in RPMI-based medium containing 1% FCS: 10 µg/cm² amino-modified polystyrene nanospheres (PS-NH_2), 200 µg/cm² crystalline silica (DQ12), 10 ng/ml LPS or a combination of 10 ng/ml LPS and 10 ng/mL IFN-γ. After 24 h, supernatants were collected and stored at -20 °C until analysis via ELISA.

Stable and inflamed triple cultures

The set-up of the stable and inflamed triple cultures was established as described previously (Busch *et al.*, 2021). Briefly, Caco-2 and HT29-MTX-E12 cells were seeded in transwell inserts (12-well format) and grown for 21 days to allow differentiation of Caco-2 and mucus production by HT29-MTX-E12 cells. For the stable triple culture, the inserts were transferred onto PMA-differentiated THP-1 cells seeded in 12-well plates (WT, *CASP1*$^{-/-}$ and *NLRP3*$^{-/-}$, at the same passage number). For the inflamed triple culture, epithelial cells were primed with 10 ng/ml IFN-γ for 24 h and then transferred onto PMA-differentiated THP-1 cells, which were pre-activated with 10 ng/ml LPS/IFN-γ for 4 h. Stable and inflamed triple cultures were started in parallel and maintained for 48 h.

Cytokine quantification by enzyme-linked immuno-sorbent assay (ELISA)

The release of IL-1β, IL-8, and TNF-α into the supernatant of THP-1 monocultures (t=24 h) or the basolateral supernatant of triple cultures (t=48 h) was analyzed using R&D systems DuoSet ELISA kits for these proinflammatory cytokines. Antibodies were diluted according to the manufacturer's protocol and high-protein-binding 96-well plates were incubated with capture antibody in coating buffer (0.1 M $NaHCO_3$, pH 8.2) overnight. After blocking with 3 % BSA/PBS, 100 µl of supernatants, diluted if necessary (IL-1β: 1:5 and IL-8: 1:10), were incubated for 2 h. Detection antibody, horseradish peroxidase (1:40 in 1 % BSA/PBS), and BioRad TMB Peroxidase EIA Substrate was consecutively incubated for 2 h, 0.5 h, and 5-20 min, respectively, before stopping the reaction with 50 µl 1 M H_2SO_4. Absorbance was measured at 450 nm and 540 nm. The standard curve was plotted as a four-parameter log fit.

Measurement of transepithelial electric resistance (TEER)

Barrier integrity during triple cultures was measured as TEER using a voltohmmeter (EVOM, World Precision Instruments) with a chopstick electrode (STX2). Before measurements, the electrode was sterilized in 70 % ethanol and washed with PBS and MEM. TEER measurements were performed at t = 0,4,20,24,44,48 after the start of the triple cultures and were corrected for blank value and transwell filter area (0.9 cm^2).

LDH assay

To investigate cytotoxicity in the epithelial cells after 48 h of triple culture, 50 µl of apical supernatant was transferred onto 96-well plates and 150 µl of reaction mix containing 50 µl Tris buffer (200 mM, pH 8), 50 µl Li-Lactate solution (50 mM), 46 µl NAD^+ solution (5 mM), 2 µl INT solution (65 mM) and 2 µl PMS solution (29 mM) was added per well. After 5 min incubation, the reaction was stopped with 50 µl 1 M H_2SO_4, and absorbance was measured at 490 nm and 680 nm.

Analysis of cell-specific cytotoxicity during inflammation

To analyze differences in cytotoxicity between Caco-2 and HT29-MTX-E12 cells during inflammation, 10^4 Caco-2 or HT29-MTX-E12 cells per well were seeded in 96-well plates. After 48 h of growth, cells were treated with basolateral supernatants (t=48h; relative concentrations of 0.25, 0.5 and 1; diluted with RPMI-based medium). Treatment with 0.5 % Triton-X 100 for 15 min served as positive control, supernatant at the relative concentrations without cells served as blanks. After 48 h incubation, the LDH assay was performed as described above. Cytotoxicity was calculated as follows: $\% \, Cytotoxicity = \frac{sample - blank}{pos.\ control - blank}$.

Immunofluorescent MUC5AC staining

To further investigate the cell-specificity of inflammation-derived cytotoxicity, the epithelial cell layer was stained for MUC5AC, a mucin produced by the goblet-like HT29-MTX-E12 cell line, but not Caco-2 (Elzinga *et al.*, 2021). After 48 h of triple culture, the filters were fixed in 4 % paraformaldehyde, permeabilized in 0.1 % Triton-X 100/PBS, and blocked with 3 % BSA/PBS. Filters were incubated with MUC5AC primary antibody (mouse; 2 µg/ml) in 1 % BSA/PBS for 1 h at RT and with Alexa 488 goat-anti-mouse antibody (1:300) and Hoechst 33342 (0.5 µg/ml) for 30 min at 37 °C. Filters were placed on microscopy slides, mounted with Prolong Gold Antifade, and sealed with a cover slip. Microscopic evaluation was performed using a Zeiss Axio Imager.M2 at 100x magnification. For each condition, 20 images were taken and MUC5AC coverage was quantified as fluorescent area [%], using a macro in ImageJ version 1.53c (see supplementary material).

Gene expression analysis

Following 48 h of triple culture, gene expression was investigated in the epithelial cell layer and THP-1 cells separately. RNA was isolated using the Roche High Pure RNA Isolation kit. Filters containing epithelial cells were cut out of the inserts using a scalpel and placed in 200 µl ice-cold PBS. THP-1 cells were collected from the well bottom using a cell scraper in 200 µl PBS. 400 µl lysis buffer was added to each sample and vortexed for 15 s. Subsequently, the RNA isolation kit was used according to the manufacturer's instructions. RNA quantification, DNase I digestion with the Amplification Grade DNase I Kit (Sigma-Aldrich), reverse transcription with the iScript cDNA Synthesis Kit (Bio-Rad), and qRT-PCR were performed as described previously (Kämpfer *et al.*, 2021). The expression of *IL-1β*, *IL-8,* and *TNF-α* was investigated in both epithelial and THP-1 cells and the expression of *MUC1*, *MUC2*, *MUC5AC*, *MUC13,* and *MUC20* was analyzed in epithelial cells only. *β-actin* was used as reference gene. Primers are listed in **Table S 6.1**. Changes in gene expression dependent on inflammation status, or dependent on THP-1 cell line were calculated using the $\Delta\Delta C_T$ method (Livak and Schmittgen, 2001).

Cultivation and treatment of ileal tissue explants

Ileal tissue was collected from healthy mice (C57BL6/J) under the study approval by the Landesamt für Natur, Umwelt und Verbraucherschutz (LANUV, Northrhine Westphalia, Germany, reference number 81-02.05.50.17.018). WT and *Nlrp3*$^{-/-}$ mice, pairs of female siblings from heterozygous parents, were sacrificed by cervical dislocation, transferred to a semi-sterile lab bench, and dissected. The ileum was isolated, rinsed with HBSS$^{+/+}$ supplemented with 1 % P/S, cut open length-wise and cut into 12 equally sized pieces (~2 mm²). Tissues were separately placed in the wells of a 24-well plate containing 1 ml HBSS$^{+/+}$

supplemented with 1 % P/S and the 24-well plate was transferred to a sterile lab bench. Using sterile forceps, the explants were transferred to a new 24-well plate containing 1 ml explant medium (DMEM, high glucose, supplemented with 10 % horse serum, 1 % P/S, 1 µM hydrocortisone, 14.3 nM glucagon, 1 nM 3,3',5-triiodo-L-thyronine, 200 µM ascorbate-2-phosphate, 20 µM linoleic acid and 10 nM β-estradiol). This procedure and medium composition were adapted from Bareiss *et al.* (2008). 6 of the 12 explants were immediately treated with 1 µg/ml LPS and murine IFN-γ and incubated at 37 °C and 5 % CO_2 for 6 h. Pilot studies indicated that the viability of these tissue explants decreased significantly when cultivated for longer than 6 h. After 1, 3, and 6 h, 100 µl of supernatant was collected, stored at -20 °C, and replaced with 100 µl of fresh medium. The LDH assay was performed with 50 µl of supernatants as described above. 50 µl of medium without tissue served as negative control.

Statistical Analysis

Statistical analysis and illustration of results were performed using GraphPad Prism 8.3. Unless stated otherwise, experiments were performed in three independent runs with two biological replicates. Statistical analysis of triple culture experiments in stable and inflamed state was performed with two-way ANOVA and Tukey's test. A p-value of <0.05 was considered statistically significant.

6.4 Results

First, we confirmed the successful knockout of *CASP1* and *NLRP3* in THP-1 cells by quantifying the release of pro-inflammatory cytokines after treatment with different NLRP3 activators. Next, the role of CASP1 and the NLRP3 inflammasome during intestinal inflammation was investigated in an advanced *in vitro* triple culture model by analyzing inflammation parameters including barrier integrity, cytotoxicity, gene expression, and secretion of cytokines and mucins. Furthermore, we investigated differences in susceptibility of enterocyte- and goblet-like cell types towards inflammation-derived cytotoxicity and investigated inflammation-related cytotoxicity in intestinal tissue explants from WT and *Nlrp3*$^{-/-}$ mice.

Reaction of THP-1 knockout cell lines to inflammatory stimuli

To investigate the reaction of the *CASP1*$^{-/-}$ and *NLRP3*$^{-/-}$ cells towards pro-inflammatory stimuli, monocultures were treated with the different NLRP3 activators PS-NH_2 (Lunov *et al.*, 2011), DQ12 quartz (Peeters *et al.*, 2014), LPS (Schumann *et al.*, 1998) and the combination of LPS and IFN-γ, the activators used to induce the inflamed state in the triple cultures (Kämpfer *et*

al., 2017). The pro-inflammatory cytokines IL-1β, IL-8, and TNF-α were analyzed after 24 h via ELISA (**Figure 6.1**).

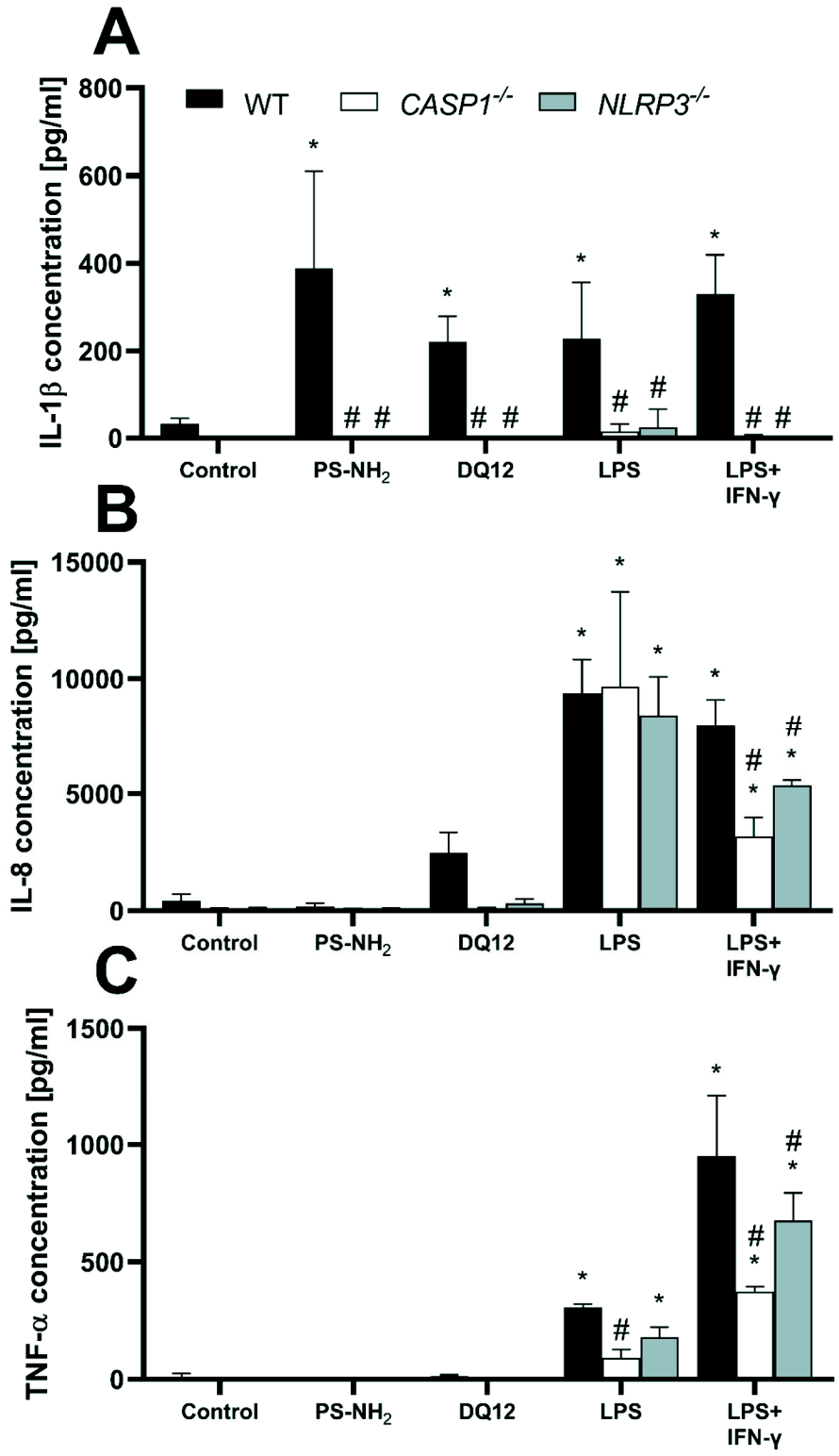

Figure 6.1 Secretion of (A) IL-1β, (B) IL-8 and (C) TNF-α into the supernatant by differentiated THP-1 cells (wild type, CASP1$^{-/-}$ or NLRP3$^{-/-}$) after 24 h incubation with 10 µg/cm² amine-modified polystyrene nanobeads (PS-NH_2), 200 µg/cm² crystalline silica (DQ12), LPS (10 ng/ml) or LSP/IFN-γ (both 10 ng/ml). Mean ± SD of N=3; * $p<0.05$, compared to the untreated control; # $p<0.05$, compared to the WT of the same treatment group.

Treatment with all NLRP3 activators induced a significantly increased secretion of IL-1β by the WT cells, which was absent in both knockout cell lines (**Figure 6.1 A**). Treatment with LPS alone induced a similarly strong increase in IL-8 secretion in all three cell lines, while increase in TNF-α secretion was statistically significant only in WT and *NLRP3*$^{-/-}$ THP-1 cells. Treatment with LPS in combination with IFN-γ resulted in a significantly increased secretion of IL-8 and TNF-α in all three cell lines compared to the respective control, but was significantly decreased in both knockout cell lines compared to the WT. The decrease was more prominent in the *CASP1*$^{-/-}$ THP-1 cells.

Transepithelial electrical resistance (TEER) during triple culture

Next, intestinal triple cultures were established with either WT, *CASP1*$^{-/-}$ or *NLRP3*$^{-/-}$ THP-1 cells, in both stable or inflamed state. As a primary indicator of barrier integrity, TEER was measured after 24 and 48 h (**Figure 6.2**).

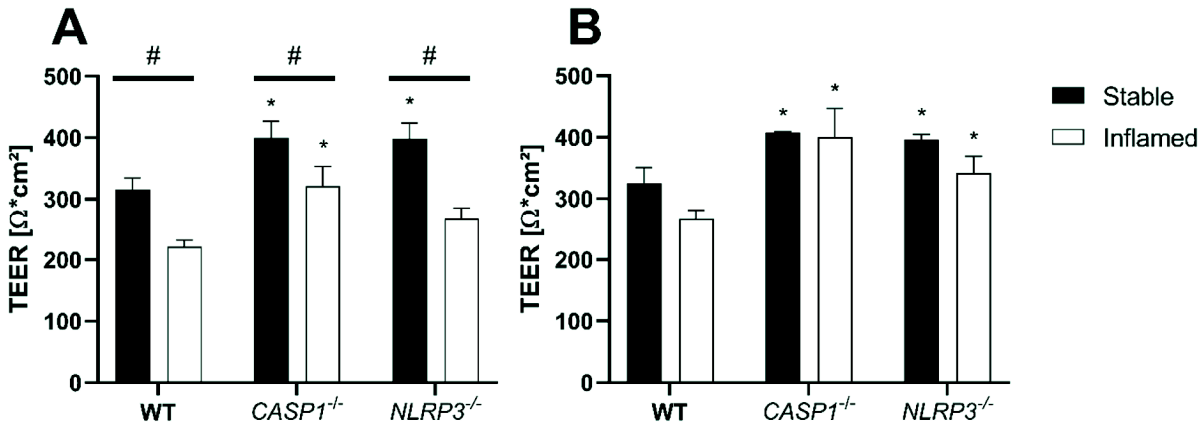

Figure 6.2 TEER at (A) t=24 h and (B) t=48 h of stable (full bars) and inflamed (open bars) triple-cultures with WT, *CASP1*$^{-/-}$ or *NLRP3*$^{-/-}$ THP-1 cells. Mean ± SD of N=3; * $p<0.05$, compared to the respective WT control; # $p<0.05$ compared to the respective stable culture.

After 24 h, TEER in inflamed triple cultures was significantly decreased in all three models, compared to the respective stable cultures (**Figure 6.2 A**). Compared to the WT cultures, TEER of *CASP1*$^{-/-}$ cultures was significantly increased in both states, while TEER of *NLRP3*$^{-/-}$ cultures was significantly increased only in stable state. After 48 h, the differences in TEER between stable and inflamed cultures of the same model were no longer statistically significant, but TEER of stable and inflamed *CASP1*$^{-/-}$ and *NLRP3*$^{-/-}$ cultures was significantly increased compared to the respective WT cultures (**Figure 6.2 B**). A more detailed depiction of TEER development over 48 h is given in **Figure S 6.1**.

Cytotoxicity after 48 h of triple culture

To assess inflammation-derived cytotoxicity in the epithelial layer, the LDH assay was applied after 48 h of triple culture (**Figure 6.3**).

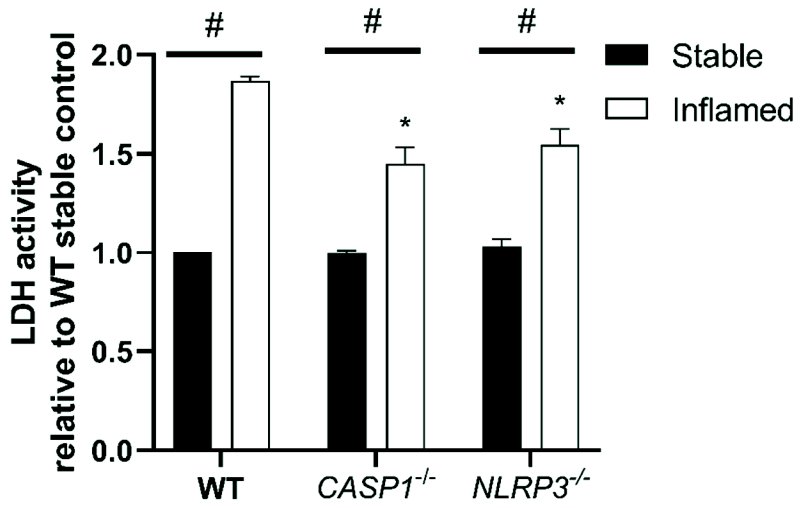

Figure 6.3 LDH activity in the apical compartment after 48 h of triple culture with WT, *CASP1*$^{-/-}$ or *NLRP3*$^{-/-}$ THP-1 cells. Mean + SD of N=3. *p<0.05 compared to the respective WT triple culture, #p<0.05 compared to the respective stable culture.

In all three models, the LDH release into the apical supernatant in inflamed triple cultures was increased compared to the stable cultures. In both inflamed knockout triple cultures, LDH activity was significantly lower compared to the respective WT culture. No difference was observed between the stable cultures of the three models.

Cytokine release

The cytokine concentrations in the basolateral supernatant of the three different triple cultures in stable or inflamed state were analyzed at t=48h (**Figure 6.4**).

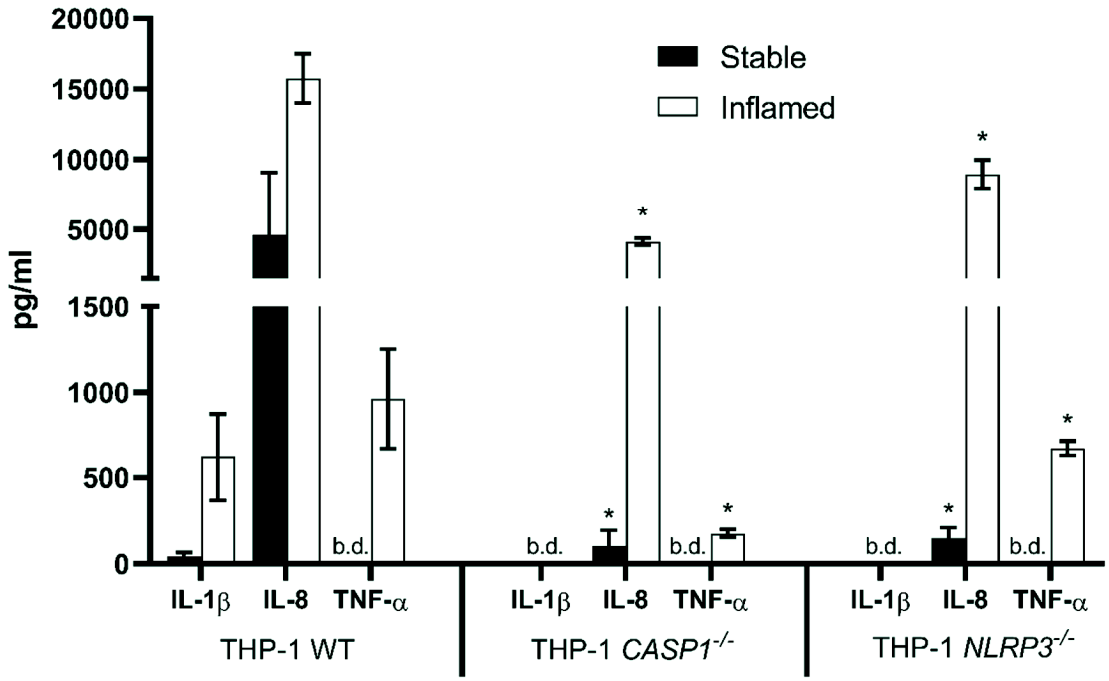

Figure 6.4 Cytokine release into the basolateral compartment after 48 h of stable (full bars) and inflamed (open bars) triple culture with WT, *CASP1*$^{-/-}$ or *NLRP3*$^{-/-}$ THP-1 cells, as assessed by ELISA. Mean ± SD of N=3. *p<0.05, compared to the respective WT triple culture. "b.d." = below detection limit.

As expected, no IL-1β was detected in the *CASP1*$^{-/-}$ and *NLRP3*$^{-/-}$ triple cultures, while its release was present in the stable WT culture and strongly increased in the inflamed WT culture. In all three triple cultures, the pro-inflammatory cytokines IL-8 and TNF-α were either strongly increased or only present in the inflamed state. IL-8 concentrations in stable or inflamed state were significantly lower in both knockout cultures when compared to the respective WT culture. TNF-α concentrations were below the detection limit in all three stable cultures. In inflamed state, TNF-α levels were significantly lower in the *CASP1*$^{-/-}$ and *NLRP3*$^{-/-}$ triple cultures compared to the WT.

Gene expression analysis

After 48 h of triple culture, gene expression of pro-inflammatory cytokines and mucins was analyzed in the epithelium and THP-1 cells (**Figure 6.5**).

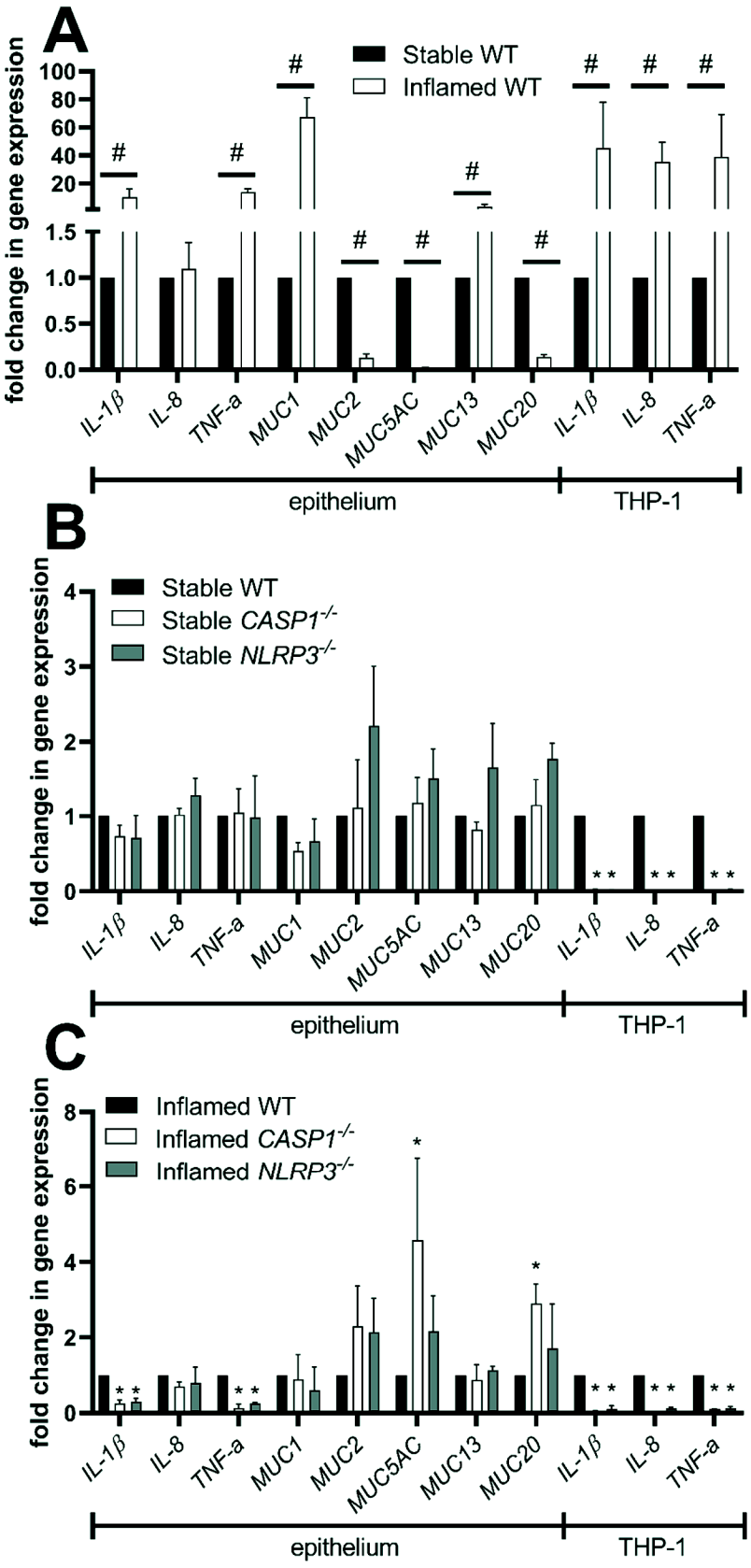

Figure 6.5 Gene expression in the epithelium or THP-1 cells after 48 h of triple culture. (A) Gene expression in the inflamed WT culture compared to the stable WT culture. (B) Gene expression in the stable knockout cultures compared to the stable WT culture. (C) Gene expression in the inflamed knockout cultures compared to the inflamed WT culture. Mean ± SD of N=3. #p<0.05, compared to the stable control; *p<0.05, compared to the WT control.

Induction of the inflamed state in WT triple cultures resulted in a significant upregulation of *IL-1β*, *TNF-α*, *MUC1,* and *MUC13* in the epithelium (**Figure 6.5 A**). Furthermore, *MUC2*, *MUC5AC,* and *MUC20* were significantly downregulated. In THP-1 cells, the gene expression of *IL-1β*, *IL-8,* and *TNF-α* was significantly increased in the inflamed state. When comparing the stable triple cultures, no differences in gene expression were observed in the epithelium (**Figure 6.5 B**). At the same time, the expression of *IL-1β*, *IL-8,* and *TNF-α* was significantly lower in *CASP1*$^{-/-}$ and *NLRP3*$^{-/-}$ THP-1 cells in stable triple cultures. Comparing the inflamed triple cultures, the epithelial expression of *IL-1β* and *TNF-α* was significantly lower in both knockout cultures, while *MUC5AC* and *MUC20* were upregulated only in inflamed *CASP1*$^{-/-}$ triple cultures (**Figure 6.5 C**). In both inflamed knockout cultures, the expression of *IL-1β*, *IL-8,* and *TNF-α* was significantly downregulated in THP-1 cells.

MUC5AC staining and quantification

To specifically investigate the presence and distribution pattern of mucus after 48 h of triple culture, the epithelial cell layer was stained for MUC5AC, a mucin produced and secreted by HT29-MTX-E12 cells (**Figure 6.6**).

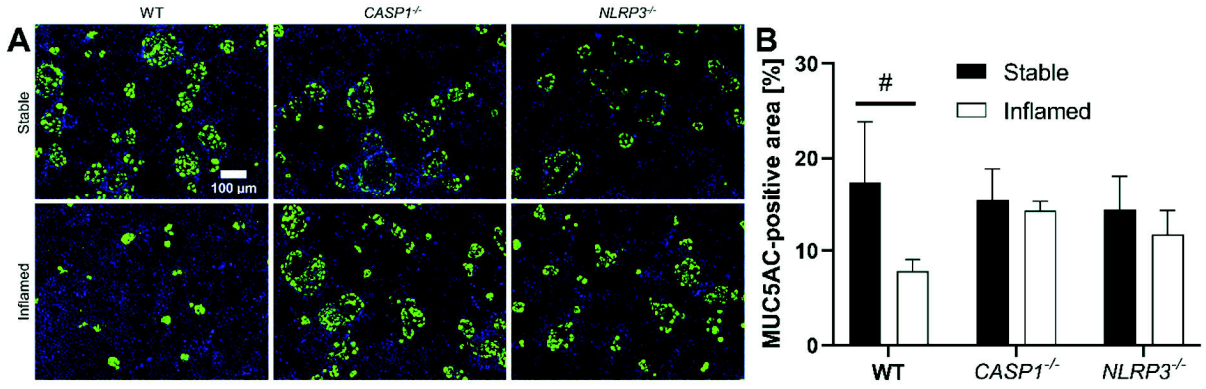

Figure 6.6 (A) Representative images of MUC5AC-stained epithelial layers of stable (top row) and inflamed (bottom row) triple cultures with WT, *CASP1*$^{-/-}$ or *NLRP3*$^{-/-}$ THP-1 cells. Blue: nuclei (Hoechst 33342), green: MUC5AC (Alexa Fluor 488). Images were acquired at 100x magnification. Scale bar (100 µm) applies to all images. (B) Quantitative analysis of MUC5AC-stained area in stable (full bars) or inflamed (open bars) triple cultures. Mean±SD of N=3, #p<0.05 compared to the respective stable culture.

All stable cultures showed large areas of up to several dozen cells, positive for MUC5AC staining distributed across the epithelial layer (**Figure 6.6 A**), which accounts for ~15 % of the total area. No statistically significant difference was observed between stable WT, *CASP1*$^{-/-}$ and *NLRP3*$^{-/-}$ cultures (**Figure 6.6 B**). In the inflamed WT cultures, however, these areas are drastically reduced in size, and the area covered in MUC5AC is significantly reduced (~8 %) compared to the stable WT cultures. Such difference between the stable and inflamed state was not present in the *CASP1*$^{-/-}$ or *NLRP3*$^{-/-}$ triple cultures.

Cytotoxic effects of triple culture supernatants on epithelial cell monocultures

To investigate cell-specific cytotoxicity in triple cultures, monocultures of Caco-2 or HT29-MTX-E12 cells were treated with the basolateral supernatants of the triple cultures and the LDH assay was performed (**Figure 6.7**).

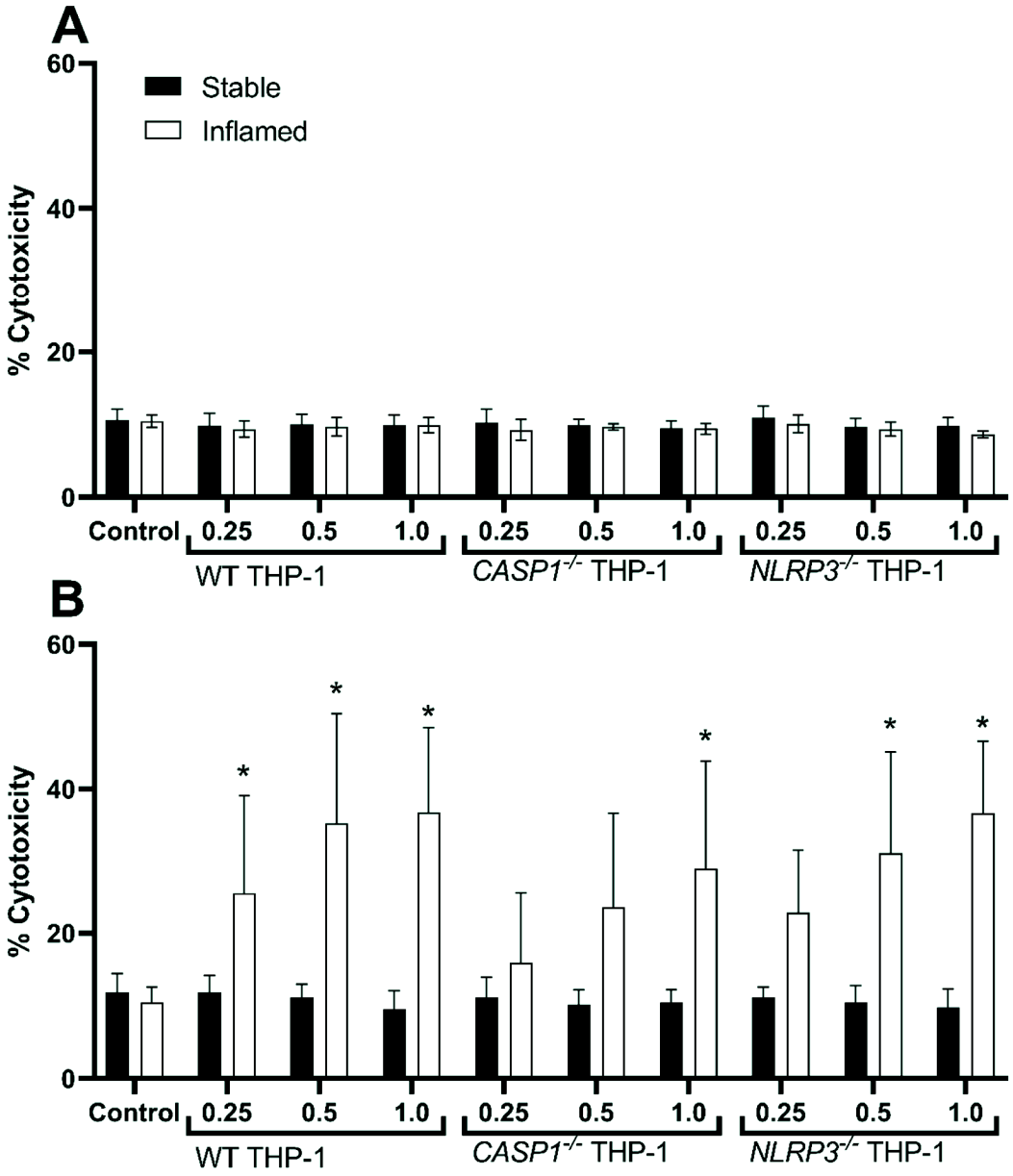

Figure 6.7 Cytotoxicity in Caco-2 (A) or HT29-MTX-E12 (B) monocultures after treatment with basolateral supernatants (t=48h; relative concentration 0.25, 0.5 or 1) from stable (full bars) or inflamed (open bars) triple cultures (WT, *CASP1*$^{-/-}$ or *NLRP3*$^{-/-}$ THP-1 cells) for 48 h. Cytotoxicity was assessed via LDH assay. Mean ± SD of N=5, *p<0.05 compared to the untreated control.

Treatment with triple culture supernatants did not cause any increased release of LDH in Caco-2 cells. In HT29-MTX-E12 monocultures, however, the supernatants of all inflamed triple cultures resulted in cytotoxicity in a dose-dependent manner (**Figure 6.7 B**). Treatment with

WT supernatants caused a significant increase in cytotoxicity at a concentration as low as 0.25, treatment with *NLRP3*$^{-/-}$ supernatant at a concentration as low as 0.5, and treatment with *CASP1*$^{-/-}$ at a concentration of 1. No effects were observed in HT29-MTX-E12 monocultures when treated with the supernatants of stable triple cultures.

Inflammation-related cytotoxicity in intestinal tissue explants from WT and Nlrp3-/- mice

To further investigate the role of NLRP3 in intestinal inflammation and compare the *in vitro* results to *ex vivo* data, we analyzed the role of the NLRP3 inflammasome on inflammation-related cytotoxicity in murine intestinal tissue explants. Ileal tissue from WT and *Nlrp3*$^{-/-}$ mice was incubated with the same pro-inflammatory stimuli as the triple cultures (LPS and IFN-γ) and cytotoxicity was assessed after 1, 3, and 6 h (**Figure 6.8**).

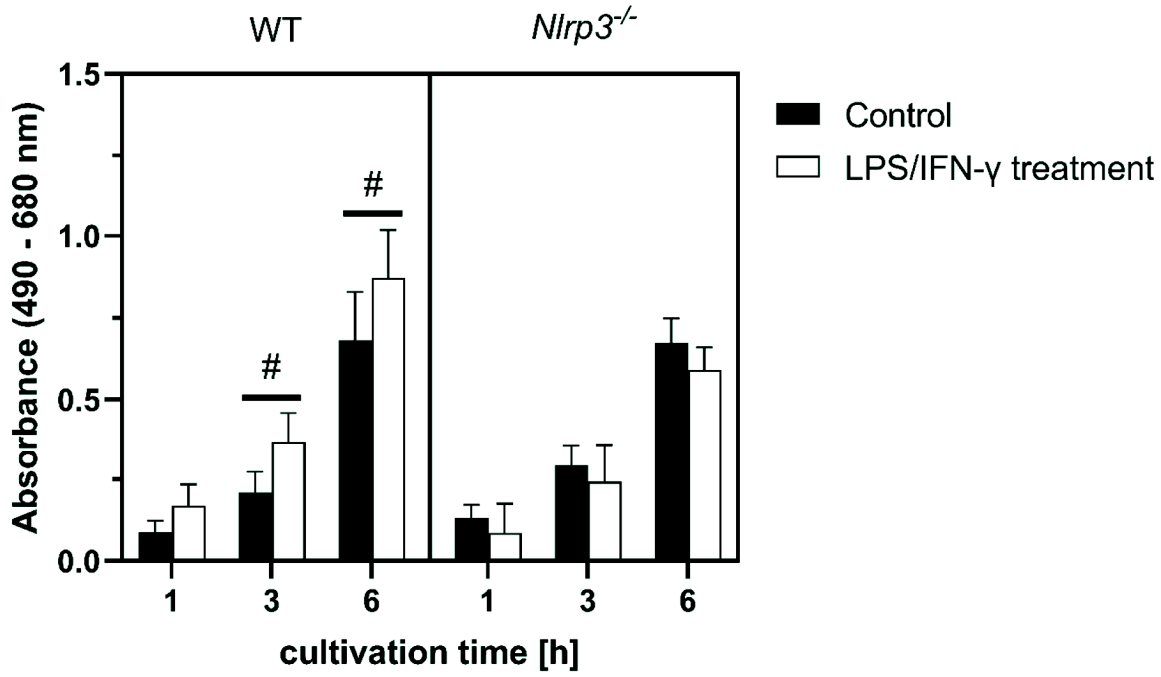

Figure 6.8 LDH activity in the supernatants of LPS/IFN-γ-treated ileal tissue explants from WT or *Nlrp3*$^{-/-}$ mice after 1, 3, or 6 h. Mean ± SEM of N=4, #p<0.05 compared to the untreated control of the corresponding time point.

During cultivation, LDH activity in the supernatant of all explant cultures increased over time. No difference was observed between control tissue of WT or *Nlrp3*$^{-/-}$ mice. However, treatment with LPS and IFN-γ induced a significant increase of LDH activity after 3 and 6 h in the WT explants compared to the untreated control. This effect was not observed in the *Nlrp3*$^{-/-}$ explants.

6.5 Discussion

The precise role of the NLRP3 inflammasome in intestinal inflammation is not understood yet. Although there is consensus about the crucial involvement of NLRP3 in intestinal homeostasis and inflammation, it is not clear if NLRP3 itself is a harmful or protective player (Zhen and Zhang, 2019). *In vivo* studies investigating DSS-induced colitis in *Nlrp3*$^{-/-}$ mice reported contrasting results on the severity of inflammation-related parameters compared to WT mice (Perera *et al.*, 2018).

To investigate the role of NLRP3 in a different model of intestinal inflammation that does not involve animal experiments, we used an advanced *in vitro* human triple cell line culture of the healthy and inflamed intestine. Regarding inflammatory parameters, the inflamed version of the triple culture offers similar hallmarks as IBD, including an impaired barrier (Maloy and Powrie, 2011), inflammation-derived cytotoxicity (Kappeler and Mueller, 2000), and increased concentrations of pro-inflammatory cytokines (Neurath, 2014). IBD-associated loss of goblet cells has also been reported in rectal biopsies (Strugala *et al.*, 2008). We were able to replicate and detect all these effects when comparing the inflamed model with the stable, healthy model with WT THP-1 cells. Furthermore, we observed very specific changes in the mucin gene expression profile of the inflamed triple culture. *MUC1* and *MUC13*, both transmembrane mucins, were strongly upregulated during inflammation *in vitro*. Both mucins have been shown to be upregulated in IBD patients (Furr *et al.*, 2010; Sheng *et al.*, 2011). The membrane-associated *MUC20* was significantly downregulated during inflammation, which is in line with observations in IBD patients (Yamamoto-Furusho *et al.*, 2015). *MUC2* and *MUC5AC*, secreted mucins, were downregulated during inflammation *in vitro*. A reduced expression of *muc2* has also been reported in colitis mice (Itani *et al.*, 2016), while in contrast, an increased expression of *muc5ac* was observed in murine colitis (Olli *et al.*, 2020). Apart from this discrepancy, the mucin expression profile of the inflamed triple culture model correlates very well with data from IBD patients and *in vivo* studies.

Investigating the effects of knocking out *CASP1* or *NLRP3* in the THP-1 cells, we found that both deficiencies significantly attenuated the aforementioned inflammatory parameters. Regarding barrier impairment, cytokine concentrations, and cytotoxicity towards goblet cells, the *CASP1* knockout tended to show some slightly stronger attenuating effect than *NLRP3*. When comparing the mucin gene expression profiles of inflamed triple cultures, the knockout of *CASP1* in THP-1 caused a significant upregulation of *MUC5AC* and *MUC20*. MUC5AC is predominantly secreted by HT29-MTX-E12 cells (Elzinga *et al.*, 2021), which appear to be highly sensitive towards the contents of the basolateral supernatant, based on the cytotoxicity assessment in monocultures. This is in line with the MUC5AC staining of the epithelium, where MUC5AC-positive area is strongly reduced in the inflamed WT cultures. Taking these results

together, it appears that HT29-MTX-E12 cells are proportionally more vulnerable during the inflamed state, compared to Caco-2 cells, which might explain the strong downregulation of *MUC5AC*. This downregulation is attenuated especially in *CASP1*$^{-/-}$ triple cultures, where the supernatant is less toxic towards HT29-MTX-E12 cells and more MUC5AC-positive cells remain on the filter after 48 h.

The expression and secretion of IL-1β, IL-8, and TNF-α, all crucial cytokines in inflammatory responses, is significantly reduced in LPS/IFN-γ treated *CASP1*$^{-/-}$ and *NLRP3*$^{-/-}$ THP-1 monocultures, as well as in inflamed *CASP1*$^{-/-}$ and *NLRP3*$^{-/-}$ triple cultures. This indicates that their release in THP-1 cells is directly dependent on (IL-1β) or influenced (IL-8 and TNF-α) by the NLRP3/CASP1 pathway. Furthermore, the gene expression of IL-1β and TNF-α is significantly lower in the epithelium of inflamed knockout cultures as well, meaning that the NLRP3/CASP1 pathway of the macrophage-like THP-1 cells affects the gene expression of the same cytokines in epithelial cells. While IL-1β is no longer detectable in knockout cultures, the concentrations of the cytokines IL-8 and TNF-α follow a gradient showing the highest concentrations in the WT cultures, followed by the *NLRP3*$^{-/-}$ and *CASP1*$^{-/-}$ cultures. Pro-apoptotic properties have been demonstrated for both IL-1β and TNF-α (Friedlander *et al.*, 1996; Shen *et al.*, 2017; van Antwerp *et al.*, 1998), while for IL-8, anti-apoptotic properties have been reported (Guo *et al.*, 2017; Kettritz *et al.*, 1998; Osawa *et al.*, 2002). Since IL-1β is completely absent in the knockout cultures, TNF-α might be the main cytokine responsible for apoptotic processes in the epithelium, which are still present, although to a lesser degree than in the WT cultures.

Our results show an enhanced susceptibility of goblet-like HT29-MTX-E12 cells towards inflammation-mediated cytotoxicity, compared to enterocyte-like Caco-2 cells. Strong synergistic cytotoxicity of TNF-α and IFN-γ towards HT29 cells has been described previously (Deem *et al.*, 1991; Woznicki *et al.*, 2021). For our investigations, a high dose of IFN-γ is used to initially activate the THP-1 cells, so it is unlikely that the concentration of this cytokine differs significantly between the three inflamed cultures. However, analysis via ELISA revealed significant differences in TNF-α concentrations, which correlates to the cytotoxicity levels in inflamed triple cultures discussed above and HT29-MTX-E12 monocultures. Furthermore, TNF-α reportedly affects epithelial tight junctions and permeability (Mullin and Snock, 1990). This might explain the lesser reduction of TEER in inflamed knockout cultures compared to the WT cultures. The relevance of TNF-α in intestinal inflammatory processes is well known, as anti-TNF-therapy is approved for the treatment of Crohn's disease since 1998 (Adegbola *et al.*, 2018). However, the interplay between the different cytokines, as well as other factors, is likely responsible for the differences in cytotoxicity and barrier impairment. Thus, further studies are necessary to investigate the exact role of TNF-α in this specific approach.

Summarizing the results of the triple culture experiments, the NLRP3/CASP1 pathway seems to play an adverse role in acute intestinal inflammation, as several inflammatory parameters are less severe in knockout cultures. The concentration of TNF-α, a secondary pro-inflammatory cytokine, is NLRP3-dependent and could be responsible for the alteration of specific cytotoxic processes during inflammation. The findings of the intestinal explant experiments support the harmful role of NLRP3: In contrast to tissues from WT mice, ileal tissues from *Nlrp3*$^{-/-}$ mice showed no signs of increased cytotoxicity after treatment with the same pro-inflammatory stimuli as the *in vitro* cultures. Interestingly, different studies investigating the role of the NLRP3/CASP1 pathway in mice with DSS-induced colitis are either in line with our findings or report the complete opposite. Bauer *et al.* (2010) and Elinav *et al.* (2011) also describe a harmful role of NLRP3 based on data from *Nlrp3*$^{-/-}$ mice, while Allen *et al.* (2010) and Hirota *et al.* (2011) report a protective role. Siegmund *et al.* (2001) observed complete protection against DSS-induced colitis in *CASP1*$^{-/-}$ mice, while Dupaul-Chicoine *et al.* (2010) reported that *CASP1*$^{-/-}$ mice died rapidly after DSS administration. Factors responsible for these contradicting findings are currently discussed and could include differences in microbiome and genetic background of the mice, as well as different protocols to induce experimental colitis (Zhen and Zhang, 2019). The triple culture, however, exhibits several differences compared to mouse models, including a drastically reduced number of different cell types and the lack of a microbiome. The method of induction of the inflammation and the duration of it differ as well. One major difference is the knockout of *NLRP3* only in macrophage-representing THP-1 cells, while in mouse models, all cell types are deficient of *Nlrp3*$^{-/-}$. This means the mentioned *in vivo* studies investigated the role of NLRP3 during intestinal inflammation in general, while the presented triple culture experiments investigated the precise role of NLRP3 in macrophages. Zaki *et al.* (2010) generated chimeric mice with *Nlrp3*-deficient hematopoietic cells (including macrophages) by transplanting bone marrow from *Nlrp3*$^{-/-}$ into WT mice, which represent a better *in vivo* analogue to our triple cultures with THP-1 knockouts. These mice were less susceptible to DSS-induced colitis than non-chimeric *Nlrp3*$^{-/-}$ mice, comparable to WT mice. The authors concluded that NLRP3 in non-hematopoietic cells (i.e. the epithelium) is more important for protection against intestinal inflammation than in hematopoietic cells. This is supported by the findings of Song-Zhao *et al.* (2014); the authors showed that epithelial Nlrp3 offers early protection against bacterial-driven intestinal inflammation. Therefore, the NLRP3 inflammasome could have different, or even opposite roles during intestinal inflammation, depending on the cell type.

One limitation of the present study is the limited comparability to the *in vivo* studies. Inflammation itself is an *in vivo* phenomenon and only parts of it can be recreated *in vitro*. Furthermore, IBD is a chronic disease, while this *in vitro* model only allows investigations of initial, acute inflammatory responses. Nevertheless, our model exhibits several important

hallmarks of the disease and compares well to data from intestinal tissue explants. Most importantly, it allows easy investigation and/or manipulation of separate cell types, which would be much more complex in an *in vivo* setup.

In conclusion, the use of THP-1 knockout cell lines in a triple culture model of the inflamed intestine presents a valid approach to investigate the role of the NLRP3/CASP1 pathway during acute intestinal inflammation. Our *in vitro* experiments suggest an adverse and pro-inflammatory role of NLRP3 in macrophages. The adverse role of NLRP3 was supported by data obtained from murine intestinal explants. The death of goblet cells and the subsequent changes in mucin expression and secretion appear to play an important role in acute intestinal inflammation, which seems to be indirectly linked to the activation of NLRP3.

Funding

This project was funded by the Juergen Manchot Foundation, Duesseldorf, Germany through a Ph.D. scholarship for Mathias Busch.

Acknowledgments

The authors are thankful to Gerrit Bredeck of the IUF – Leibniz-Research Institute for Environmental Medicine, Duesseldorf, for critically reviewing the manuscript.

6.6 Supplementary Material

Table S 6.1 Human primer sequences and concentrations used for qPCR

Gene		5’ -> 3’ sequence	Concentration [nM]
β-actin	Forward primer	CCTGGCACCCAGCACAAT	60
	Reverse primer	GCCGATCCACACGGAGTACT	60
IL-1β	Forward primer	GCCAGTGAAATGATGGCTTATT	50
	Reverse primer	AGGAGCACTTCATCTGTTTAGG	50
IL-8	Forward primer	ACTCCAAACCTTTCCACCC	60
	Reverse primer	CCCTCTTCAAAAACTTCTCCAC	60
TNF-α	Forward primer	ACTTTGGAGTGATCGGCC	200
	Reverse primer	GCTTGAGGGTTTGCTACAAC	200
MUC1	Forward primer	AGACGTCAGCGTGAGTGATG	37.5
	Reverse primer	GACAGCCAAGGCAATGAGAT	37.5
MUC2	Forward primer	GTCCGTCTCCAACATCACCT	60
	Reverse primer	GCTGGCTGGTTTTCTCCTCT	60
MUC5AC	Forward primer	CAGCACAACCCCTGTTTCAAA	60
	Reverse primer	GCGCACAGAGGATGACAGT	37.5
MUC13	Forward primer	CAGAGACAGCCAGATGCAAA	60
	Reverse primer	CGGAGGCCAGATCTTTACTG	37.5
MUC20	Forward primer	GTGCAGGTGAAAATGGAGGT	60
	Reverse primer	ACGCAGTAAGGAGACCTGGA	37.5

ImageJ macro used for the automated analysis of fluorescent MUC5AC images

```
dir = getDirectory("…\MUC5AC_quantitative_analysis")
list = getFileList(dir);
dir2 = getDirectory("…\MUC5AC_quantitative_analysis_results")
//setBatchMode(true);
for (f=0; f<list.length; f++) {
     path = dir+list[f];
     if (!endsWith(path,"/")) open(path);
     if (nImages>=1) {
          setAutoThreshold("Default dark");
          run("Analyze Particles...", "size=100-Infinity show=Masks
clear include in_situ");
          run("Maximum...", "radius=80");
          run("Minimum...", "radius=70");
          run("Measure");
          t=getTitle();
          s=lastIndexOf(t, '.');
          t=substring(t, 0,s);
          t=replace(t," ","_");
          t2= t +' bin';
          rename(t2);
          saveAs("Tiff", dir2 + t2 + ".tif");
          selectWindow("t");
          run("Close");
     }
}
```

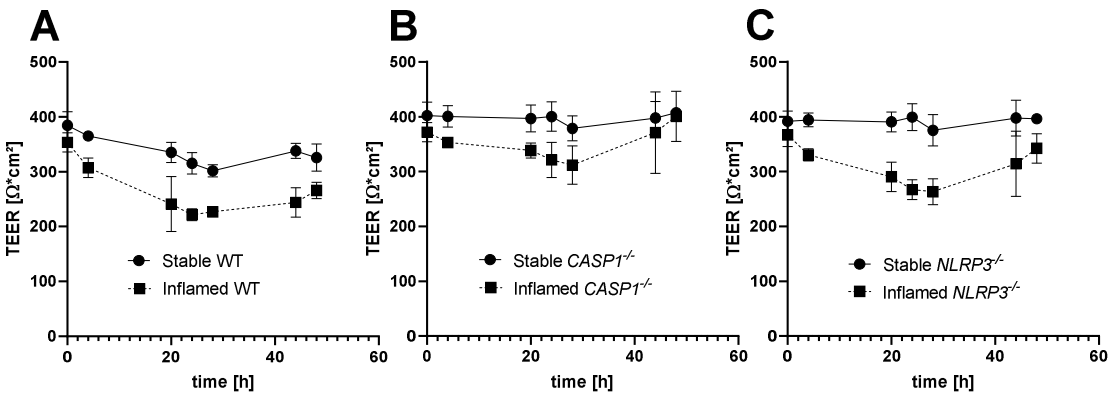

Figure S 6.1. TEER during 48 h of stable (circles) or inflamed (squares) triple cultures with WT (A), *CASP1*$^{-/-}$ (B), or *NLRP3*$^{-/-}$ (C) THP-1 cells.

6.7 References

Adegbola, S. O., Sahnan, K., Warusavitarne, J., Hart, A., and Tozer, P. (2018). Anti-TNF Therapy in Crohn's Disease. Int. J. Mol. Sci. 19. doi: 10.3390/ijms19082244.

Allen, I. C., TeKippe, E. M., Woodford, R.-M. T., Uronis, J. M., Holl, E. K., Rogers, A. B. *et al.* (2010). The NLRP3 inflammasome functions as a negative regulator of tumorigenesis during colitis-associated cancer. J. Exp. Med. 207, 1045–1056. doi: 10.1084/jem.20100050.

Bareiss, P. M., Metzger, M., Sohn, K., Rupp, S., Frick, J. S., Autenrieth, I. B. *et al.* (2008). Organotypical tissue cultures from adult murine colon as an in vitro model of intestinal mucosa. Histochem. Cell Biol. 129, 795–804. doi: 10.1007/s00418-008-0405-z.

Bauer, C., Duewell, P., Lehr, H.-A., Endres, S., and Schnurr, M. (2012). Protective and aggravating effects of Nlrp3 inflammasome activation in IBD models: influence of genetic and environmental factors. Dig. Dis. 30(suppl 1), 82–90. doi: 10.1159/000341681.

Bauer, C., Duewell, P., Mayer, C., Lehr, H. A., Fitzgerald, K. A., Dauer, M. *et al.* (2010). Colitis induced in mice with dextran sulfate sodium (DSS) is mediated by the NLRP3 inflammasome. Gut 59, 1192–1199. doi: 10.1136/gut.2009.197822.

Bouma, G., and Strober, W. (2003). The immunological and genetic basis of inflammatory bowel disease. Nat. Rev. Immunol. 3, 521–533. doi: 10.1038/nri1132.

Brasier, A. R. (2010). The nuclear factor-kappaB-interleukin-6 signalling pathway mediating vascular inflammation. Cardiovasc. Res. 86, 211–218. doi: 10.1093/cvr/cvq076.

Busch, M., Bredeck, G., Kämpfer, A. A., and Schins, R. P. (2021). Investigations of acute effects of polystyrene and polyvinyl chloride micro- and nanoplastics in an advanced in vitro triple culture model of the healthy and inflamed intestine. Environ. Res. 193, 110536. doi: 10.1016/j.envres.2020.110536.

Cho, J. H., and Brant, S. R. (2011). Recent insights into the genetics of inflammatory bowel disease. Gastroenterology 140, 1704–1712. doi: 10.1053/j.gastro.2011.02.046.

Deem, R., Shanahan, F., and Targan, S. (1991). Triggered human mucosal T cells release tumour necrosis factor-alpha and interferon-gamma which kill human colonic epithelial cells. Clin. Exp. Immunol. 83, 79–84. doi: 10.1111/j.1365-2249.1991.tb05592.x.

Dupaul-Chicoine, J., Yeretssian, G., Doiron, K., Bergstrom, K. S. B., McIntire, C. R., LeBlanc, P. M. *et al.* (2010). Control of intestinal homeostasis, colitis, and colitis-associated colorectal cancer by the inflammatory caspases. Immunity 32, 367–378. doi: 10.1016/j.immuni.2010.02.012.

Elinav, E., Strowig, T., Kau, A. L., Henao-Mejia, J., Thaiss, C. A., Booth, C. J. *et al.* (2011). NLRP6 inflammasome regulates colonic microbial ecology and risk for colitis. Cell 145, 745–757. doi: 10.1016/j.cell.2011.04.022.

Elzinga, J., van der Lugt, B., Belzer, C., and Steegenga, W. T. (2021). Characterization of increased mucus production of HT29-MTX-E12 cells grown under Semi-Wet interface with Mechanical Stimulation. PloS one 16, e0261191. doi: 10.1371/journal.pone.0261191.

Forgue-Lafitte, M.-E., Fabiani, B., Levy, P. P., Maurin, N., Fléjou, J.-F., and Bara, J. (2007). Abnormal expression of M1/MUC5AC mucin in distal colon of patients with diverticulitis, ulcerative colitis and cancer. Int. J. Cancer. 121, 1543–1549. doi: 10.1002/ijc.22865.

Friedlander, R. M., Galiardini, V., Rotello, R. J., and Yuan, J. (1996). Functional Role of Interleukin 1β (IL-1β) in IL-1β-converting Enzyme-mediated Apoptosis. J. Exp. Med. 184, 717–724. doi: 10.1084/jem.184.2.717.

Furr, A. E., Ranganathan, S., and Finn, O. J. (2010). Aberrant expression of MUC1 mucin in pediatric inflammatory bowel disease. Pediatr. Dev. Pathol. 13, 24–31. doi: 10.2350/08-06-0479.1.

Guo, Y., Zang, Y., Lv, L., Cai, F., Qian, T., Zhang, G. *et al.* (2017). IL-8 promotes proliferation and inhibition of apoptosis via STAT3/AKT/NF-κB pathway in prostate cancer. Mol. Med. Rep. 16, 9035–9042. doi: 10.3892/mmr.2017.7747.

Hirota, S. A., Ng, J., Lueng, A., Khajah, M., Parhar, K., Li, Y. *et al.* (2011). NLRP3 inflammasome plays a key role in the regulation of intestinal homeostasis. Inflamm. Bowel Dis. 17, 1359–1372. doi: 10.1002/ibd.21478.

Itani, S., Watanabe, T., Nadatani, Y., Sugimura, N., Shimada, S., Takeda, S. *et al.* (2016). NLRP3 inflammasome has a protective effect against oxazolone-induced colitis: a possible role in ulcerative colitis. Sci. Rep. 6, 39075. doi: 10.1038/srep39075.

Kämpfer, A. A. M., Busch, M., Büttner, V., Bredeck, G., Stahlmecke, B., Hellack, B. *et al.* (2021). Model Complexity as Determining Factor for In Vitro Nanosafety Studies: Effects of Silver and Titanium Dioxide Nanomaterials in Intestinal Models. Small, 2004223. doi: 10.1002/smll.202004223.

Kämpfer, A. A. M., Urbán, P., Gioria, S., Kanase, N., Stone, V., and Kinsner-Ovaskainen, A. (2017). Development of an in vitro co-culture model to mimic the human intestine in healthy and diseased state. Toxicol. In Vitro 45, 31–43. doi: 10.1016/j.tiv.2017.08.011.

Kappeler, A., and Mueller, C. (2000). The role of activated cytotoxic T cells in inflammatory bowel disease. Histol. Histopathol. 15, 167–172. doi: 10.14670/HH-15.167.

Kettritz, R., Gaido, M. L., Haller, H., Luft, F. C., Jennette, C. J., and Falk, R. J. (1998). Interleukin-8 delays spontaneous and tumor necrosis factor-alpha-mediated apoptosis of human neutrophils. Kidney Int. 53, 84–91. doi: 10.1046/j.1523-1755.1998.00741.x.

Kunsch, C., and Rosen, C. A. (1993). NF-kappa B subunit-specific regulation of the interleukin-8 promoter. Mol. Cell Biol. 13, 6137–6146. doi: 10.1128/mcb.13.10.6137-6146.1993.

Larsson, J. M. H., Karlsson, H., Crespo, J. G., Johansson, M. E. V., Eklund, L., Sjövall, H. *et al.* (2011). Altered O-glycosylation profile of MUC2 mucin occurs in active ulcerative colitis and is associated with increased inflammation. Inflamm. Bowel Dis. 17, 2299–2307. doi: 10.1002/ibd.21625.

Livak, K. J., and Schmittgen, T. D. (2001). Analysis of Relative Gene Expression Data Using Real-Time Quantitative PCR and the DDCT Method. Methods 25, 402–408. doi: 10.1006/meth.2001.1262.

Lopez-Castejon, G., and Brough, D. (2011). Understanding the mechanism of IL-1β secretion. Cytokine Growth Factor Rev. 22, 189–195. doi: 10.1016/j.cytogfr.2011.10.001.

Lunov, O., Syrovets, T., Loos, C., Nienhaus, G. U., Mailänder, V., Landfester, K. *et al.* (2011). Amino-functionalized polystyrene nanoparticles activate the NLRP3 inflammasome in human macrophages. ACS Nano 5, 9648–9657. doi: 10.1021/nn203596e.

Maloy, K. J., and Powrie, F. (2011). Intestinal homeostasis and its breakdown in inflammatory bowel disease. Nature 474, 298–306. doi: 10.1038/nature10208.

McKee, C. M., and Coll, R. C. (2020). NLRP3 inflammasome priming: A riddle wrapped in a mystery inside an enigma. J. Leukoc. Biol. 108, 937–952. doi: 10.1002/JLB.3MR0720-513R.

Mullin, J. M., and Snock, K. V. (1990). Effect of Tumor Necrosis Factor on Epithelial Tight Junctions and Transepithelial Permeability. Cancer Res. 50, 2172–2176.

Neurath, M. F. (2014). Cytokines in inflammatory bowel disease. Nat. Rev. Immunol. 14, 329–342. doi: 10.1038/nri3661.

Olli, K. E., Rapp, C., O'Connell, L., Collins, C. B., McNamee, E. N., Jensen, O. *et al.* (2020). Muc5ac Expression Protects the Colonic Barrier in Experimental Colitis. Inflamm. Bowel Dis. 26, 1353–1367. doi: 10.1093/ibd/izaa064.

Osawa, Y., Nagaki, M., Banno, Y., Brenner, D. A., Asano, T., Nozawa, Y. *et al.* (2002). Tumor necrosis factor alpha-induced interleukin-8 production via NF-kappaB and phosphatidylinositol 3-kinase/Akt pathways inhibits cell apoptosis in human hepatocytes. Infect. Immun. 70, 6294–6301. doi: 10.1128/IAI.70.11.6294-6301.2002.

Parikh, A. A., Salzman, A. L., Kane, C. D., Fischer, J. E., and Hasselgren, P. (1997). IL-6 Production in Human Intestinal Epithelial Cells Following Stimulation with IL-1β Is Associated with Activation of the Transcription Factor NF-kB. J. Surg. Res. 69, 139–144. doi: 10.1006/jsre.1997.5061.

Peeters, P. M., Eurlings, I. M. J., Perkins, T. N., Wouters, E. F., Schins, R. P. F., Borm, P. J. A. *et al.* (2014). Silica-induced NLRP3 inflammasome activation in vitro and in rat lungs. Part Fibre Toxicol 11, 58. doi: 10.1186/s12989-014-0058-0.

Perera, A. P., Sajnani, K., Dickinson, J., Eri, R., and Körner, H. (2018). NLRP3 inflammasome in colitis and colitis-associated colorectal cancer. Mamm. Genome 29, 817–830. doi: 10.1007/s00335-018-9783-2.

Ponder, A., and Long, M. D. (2013). A clinical review of recent findings in the epidemiology of inflammatory bowel disease. Clin. Epidemiol. 5, 237–247. doi: 10.2147/CLEP.S33961.

Ramachandran, H., Martins, S., Kontarakis, Z., Krutmann, J., and Rossi, A. (2021). Fast but not furious: a streamlined selection method for genome-edited cells. Life Sci. Alliance 4, e202101051. doi: 10.26508/lsa.202101051.

Schumann, R. R., Belka, C., Reuter, D., Lamping, N., Kirschning, C. J., Weber, J. R. *et al.* (1998). Lipopolysaccharide Activates Caspase-1 (Interleukin-1–Converting Enzyme) in Cultured Monocytic and Endothelial Cells. Blood 91, 577–584. doi: 10.1182/blood.V91.2.577.

Shen, J., Xu, S., Zhou, H., Liu, H., Jiang, W., Hao, J. *et al.* (2017). IL-1β induces apoptosis and autophagy via mitochondria pathway in human degenerative nucleus pulposus cells. Sci. Rep. 7, 41067. doi: 10.1038/srep41067.

Sheng, Y. H., Hasnain, S. Z., Florin, T. H. J., and McGuckin, M. A. (2012). Mucins in inflammatory bowel diseases and colorectal cancer. JGH Open 27, 28–38. doi: 10.1111/j.1440-1746.2011.06909.x.

Sheng, Y. H., Lourie, R., Lindén, S. K., Jeffery, P. L., Roche, D., Tran, T. V. *et al.* (2011). The MUC13 cell-surface mucin protects against intestinal inflammation by inhibiting epithelial cell apoptosis. Gut 60, 1661–1670. doi: 10.1136/gut.2011.239194.

Siegmund, B. (2002). Interleukin-1β converting enzyme (caspase-1) in intestinal inflammation. Biochem. Pharmacol. 64, 1–8. doi: 10.1016/S0006-2952(02)01064-X.

Siegmund, B., Lehr, H. A., Fantuzzi, G., and Dinarello, C. A. (2001). IL-1b-converting enzyme (caspase-1) in intestinal inflammation. Proc. Natl. Acad. Sci. 98, 13249–13254. doi: 10.1073/pnas.23147399.

Song-Zhao, G. X., Srinivasan, N., Pott, J., Baban, D., Frankel, G., and Maloy, K. J. (2014). Nlrp3 activation in the intestinal epithelium protects against a mucosal pathogen. Mucosal Immunol. 7, 763–774. doi: 10.1038/mi.2013.94.

Strugala, V., Dettmar, P. W., and Pearson, J. P. (2008). Thickness and continuity of the adherent colonic mucus barrier in active and quiescent ulcerative colitis and Crohn's disease. Int. J. Clin. Pract. 62, 762–769. doi: 10.1111/j.1742-1241.2007.01665.x.

Sutterwala, F. S., Ogura, Y., Szczepanik, M., Lara-Tejero, M., Lichtenberger, G. S., Grant, E. P. *et al.* (2006). Critical role for NALP3/CIAS1/Cryopyrin in innate and adaptive immunity through its regulation of caspase-1. Immunity 24, 317–327. doi: 10.1016/j.immuni.2006.02.004.

van Antwerp, D. J., Martin, S. J., Verma, I. M., and Green, D. R. (1998). Inhibition of TNF-induced apoptosis by NF-κB. Trends Cell Biol. 8, 107–111. doi: 10.1016/S0962-8924(97)01215-4.

Villani, A.-C., Lemire, M., Fortin, G., Louis, E., Silverberg, M. S., Collette, C. *et al.* (2009). Common variants in the NLRP3 region contribute to Crohn's disease susceptibility. Nat. Genet. 41, 71–76. doi: 10.1038/ng.285.

Woznicki, J. A., Saini, N., Flood, P., Rajaram, S., Lee, C. M., Stamou, P. *et al.* (2021). TNF-α synergises with IFN-γ to induce caspase-8-JAK1/2-STAT1-dependent death of intestinal epithelial cells. Cell Death Dis. 12, 864. doi: 10.1038/s41419-021-04151-3.

Yamamoto-Furusho, J. K., Ascaño-Gutiérrez, I., Furuzawa-Carballeda, J., and Fonseca-Camarillo, G. (2015). Differential Expression of MUC12, MUC16, and MUC20 in Patients with Active and Remission Ulcerative Colitis. Mediators. Inflamm. 2015, 659018. doi: 10.1155/2015/659018.

Zaki, M. H., Boyd, K. L., Vogel, P., Kastan, M. B., Lamkanfi, M., and Kanneganti, T.-D. (2010). The NLRP3 inflammasome protects against loss of epithelial integrity and mortality during experimental colitis. Immunity 32, 379–391. doi: 10.1016/j.immuni.2010.03.003.

Zhen, Y., and Zhang, H. (2019). NLRP3 Inflammasome and Inflammatory Bowel Disease. Front. Immunol. 10, 276. doi: 10.3389/fimmu.2019.00276.

7. General Discussion

Due to the presence of micro- and nanoplastic particles in the environment, food and water, humans are constantly exposed via the oral route. Based on toxicological data of engineered nanomaterials, uptake of plastic particles could pose a threat towards human health (Yee *et al.*, 2021). Recent animal studies have linked intestinal inflammation to microplastic uptake (Lei *et al.*, 2018; Li *et al.*, 2019); and the pathogenesis of IBD, as well as pro-inflammatory effects of particles, have been linked to the NLRP3 inflammasome (Baron *et al.*, 2015; Bauer *et al.*, 2012: Lunov *et al.*, 2011).

The aim of the studies described in this thesis was the development and application of advanced *in vitro* models to investigate (I) the link between intestinal inflammation and plastic particle toxicity, (II) the ability of plastic particles to activate the NLRP3 inflammasome in macrophages and (III) to determine the role of NLRP3 during intestinal inflammation.

In **chapter 2**, the current literature was reviewed regarding the availability and applicability of intestinal *in vitro* models. Only a very limited number of intestinal *in vitro* models representing inflammatory diseases are used in research, each with its own advantages. Based on the aims defined in this thesis, the Caco-2/THP-1 transwell disease model developed by Kämpfer *et al.* (2017), later extended by the cell line HT29-MTX-E12 (Kämpfer *et al.*, 2021), was used for the subsequent experimental work. It enables a controlled, inflammation-like state while allowing specific investigations of mucus and macrophage-like cells.

In **chapter 3**, the effects of two standard polymers, PS and PVC, were assessed in the previously established triple culture model of the healthy and inflamed intestine (Caco-2/HT29-MTX-E12/THP-1) (Kämpfer *et al.*, 2021). Toxicologically relevant endpoints were assessed after treatment in either healthy or inflamed state. It was found that PVC particles induce an increase in IL-1β release, as well as a decrease in epithelial cell number. Both effects were only observed during active inflammation. These findings suggest a crucial role of the inflammation status in plastic particle toxicity. This hypothesis was further supported by the findings of Zheng *et al.* (2021). The authors observed increased pro-inflammatory parameters in colitis mice fed with microplastics, compared to mice without colitis.

In **chapter 4**, the *in vitro* model applied in chapter 3 was modified to allow the investigation of buoyant plastic particles. PE and PP, two of the most produced polymers, have a density of less than 1 g/cm³ and do therefore not sediment in traditional cell culture approaches. The entire triple culture model was spatially inverted to allow contact between epithelial cells and floating plastic particles. To ensure comparability to the original model, the enterotoxic drug diclofenac was used as a soluble benchmark compound in both models. Subsequently, PE particles were investigated in this inverted triple culture model of the healthy and inflamed intestine. PE particles induced cytotoxic effects in the epithelium, as well as increased pro-inflammatory cytokine concentrations. Pro-inflammatory effects in the intestine after PE uptake

have also been demonstrated in mice (Li *et al.*, 2019); and the amount of microplastics in feces correlates to the clinical score of IBD-patients (Yan *et al.*, 2021). Wang *et al.* (2022) reported the ability of PE nanoplastics to form pores and damage the lipid bilayer of biological membranes, leading to cytotoxic effects in exposed cells.

In **chapter 5**, a large panel of different micro- and nanoplastics was investigated regarding their ability to directly activate the NLRP3 inflammasome in a macrophage-like cell type. THP-1 WT and *NLRP3*$^{-/-}$ cells as a screening tool for NLRP3 activation were validated against data obtained from bone marrow-derived macrophages and an *in vivo* study using a set of well-studied engineered nanomaterials. It was found that the tested plastic particles were not able to directly activate the NLRP3 inflammasome, but PET particles showed pro-inflammatory properties via other pathways, which only in part depended on the NLRP3 inflammasome. Therefore, it can be concluded that the pro-inflammatory properties of PVC and PE, observed in chapters 3 and 4, are not linked to the direct activation of NLRP3 in the macrophage-like THP-1 cells after passing the epithelial barrier. In contrast, several *in vivo* studies reported activation of the NLRP3 inflammasome after oral uptake of microplastics in the liver (Mu *et al.*, 2021), ovaries (Hou *et al.*, 2021), and heart (Wei *et al.*, 2021). However, the effects described in these studies are likely the consequence of systemic inflammation instead of direct NLRP3 activation in tissue macrophages. In these studies, no attempt was made to investigate the presence of microplastics in these target organs.

In **chapter 6**, the role of the NLRP3 inflammasome during intestinal inflammation was investigated. In modified triple cultures (Caco-2/HT29-MTX-E12/THP-1$^{CASP1-/-}$ or THP-1$^{NLRP3-/-}$) of stable and inflamed state, inflammatory parameters were assessed after knockout of NLRP3 or its downstream enzyme CASP1 in THP-1 cells. It was found that the NLRP3/CASP1 pathway in macrophages has a direct influence on epithelial barrier integrity, cytotoxicity, and pro-inflammatory cytokines. Furthermore, the death of goblet cells and the connected changes in expression and secretion of mucins appears to be NLRP3/CASP1-dependent. Based on these data, the role of the NLRP3 inflammasome in acute intestinal inflammation can be described as adverse, as supported by analog intestinal explant experiments using WT and *Nlrp3*$^{-/-}$ mice. There is controversy about the exact role of the NLRP3 inflammasome, but there is consensus that it is an important key player in intestinal inflammation and the pathogenesis of IBD (Zhen and Zhang, 2019).

Taking all these findings together, it can be concluded that, depending on particle type, microplastic toxicity could be influenced by the inflammation status of the intestine. This was observed for PVC particles (chapter 3). Furthermore, PE particles were able to enhance intestinal inflammation (chapter 4). In turn, the inflammation status of the intestine depends on the NLRP3 inflammasome (chapter 6). Therefore, plastic particle toxicity could be indirectly

connected to the NLRP3 inflammasome, although the particles are not able to activate it directly in macrophages (chapter 5). However, as suggested by animal studies, systemic inflammation induced by oral uptake of plastic particles can subsequently activate the NLRP3 inflammasome in other organs (Hou *et al.*, 2021; Mu *et al.*, 2021; Wei *et al.*, 2021). In addition, background activity of the NLRP3 inflammasome appears to be necessary for low-level pro-inflammatory reactions in macrophages, as it was observed for PET particles (chapter 5). **Figure 7.1** schematically depicts the relationships between intestinal inflammation, plastic particle toxicity, and the NLRP3 inflammasome, based on the main findings of this thesis.

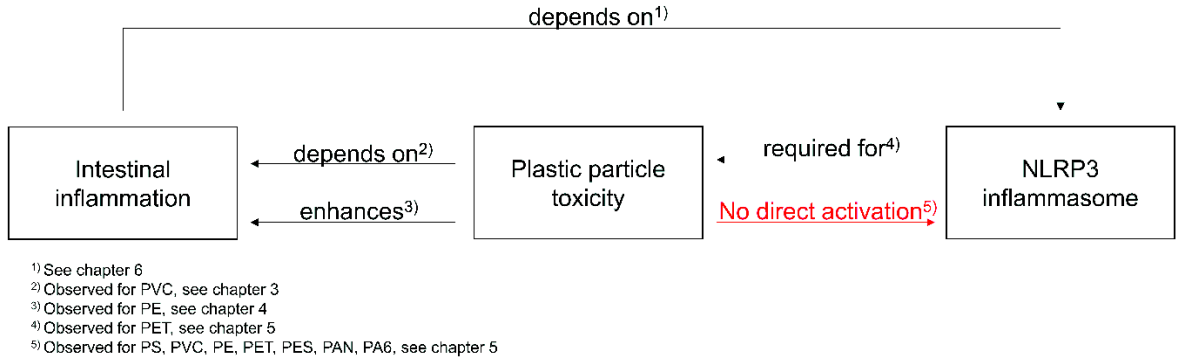

Figure 7.1 The interplay between plastic particle toxicity, intestinal inflammation, and the NLRP3 inflammasome. The results of this dissertation demonstrated that the toxicity of polyvinyl chloride (PVC) particles depends on the inflammation status. Meanwhile, the extent of intestinal inflammation is directly dependent on the NLRP3 inflammasome. Polyethylene (PE) particles have been observed to enhance intestinal inflammation. In the case of polyethylene terephthalate (PET) particles, background activity of the NLRP3 inflammasome is required for low levels of toxicity. Direct activation of NLRP3 was not observed for polystyrene (PS), PVC, PE, PET, polyester (PES), polyacrylonitrile (PAN), or polyamide 6 (PA6). Only the positive control PS-NH_2 acted as a direct activator of NLRP3.

The findings reported in this thesis contribute to the general understanding of the complex interactions between plastic particle toxicity, intestinal inflammation, and the involvement of the NLRP3 inflammasome. This, in turn, could contribute to a future risk assessment carried out on orally taken up plastic particles, with specific regard to susceptible groups of the population, such as IBD-patients. A possible connection between chronic intestinal inflammation, unintentional food contaminants like microplastics, and the NLRP3 inflammasome has also been proposed and discussed in a very recent review (Sandys and te Velde, 2022). However, it has to be kept in mind that exposure to plastic particles, as assumed for the general population, means exposure to an immense variety of different polymers, shapes, and sizes. The different polymers types could induce synergistic effects, for example, PVC, PE, and PET particles could induce pro-inflammatory reactions via different pathways. Synergistic toxicity for plastic particles of different sizes has already been observed *in vivo* (Liang *et al.*, 2021). The toxicity testing of homogenous, single polymer particles only presents the very first step in the process of evaluating possible health risks that arise from oral

exposure to micro- and nanoplastics. Future research might identify the most hazardous polymer, size range, or shape of plastics. Ultimately, the results of these hazard rankings will have to be put in relation to their actual occurrence in the environment, food, and water, to establish reasonable risk assessment. Unfortunately, there is already a strong disproportion between available data and environmental occurrence in the current scientific literature: for example, the vast majority of toxicological studies on micro- and nanoplastics has been carried out using PS spheres, while PS makes up only 6.1 % of globally produced polymers (www.plasticseurope.org) and shapes of microplastics have been described to be primarily fibers, fragments, and sheets (Hongprasith *et al.*, 2020). These discrepancies might distort the perception of possible health risks and have to be considered carefully. Further, environmental plastic particles are likely different from model plastics in terms of aging-related properties (Liu *et al.*, 2019) and adsorption of contaminants, e.g. polycyclic aromatic hydrocarbons or heavy metals (Tan *et al.* 2019; Khalid *et al.* 2021). The hazards of these potential contaminants were not considered in the experimental work of this thesis, but the different *in vitro* models applied and developed in the framework of this dissertation offer a broad spectrum of powerful tools to investigate a variety of research questions, including the hazard assessment of contaminants associated with micro- and nanoplastics.

However, the area of application is not limited to toxicological research. Pharmaceutical research, for example regarding polymeric particles as drug carriers, could benefit from these models. Furthermore, specific approaches like the inverted model (chapter 4) or the embedding of buoyant particles in agarose (chapter 5) can be extended to any low-density material and are not exclusive to plastics. The presented models can be combined, to answer specific research questions, for example by implementing the THP-1 knockout cell lines (chapter 6) into the inverted triple culture (chapter 4), to investigate the role of NLRP3 or CASP1 in pro-inflammatory reactions induced by PE particles.

As nanotechnology is a rapidly growing field, future inventions and developments are likely to make use of advanced materials. These could include organic/inorganic hybrid particles (e.g. polymer-coated metals or vice-versa), nanocomposites, or nanostructures manufactured by synthetic biology applications. Based on the toxicological knowledge of current engineered nanomaterials and particulate pollutants, the safety of these new materials will have to be assessed prior to application. Especially when applied in the food sector or intended for medical use (e.g. drug delivery via oral route), the *in vitro* models described in this thesis will provide a basic tool kit for early assessment of possible intestinal toxicity.

7.1 References

Baron, L., Gombault, A., Fanny, M., Villeret, B., Savigny, F., Guillou, N., Panek, C., Le Bert, M., Lagente, V., Rassendren, F., Riteau, N., Couillin, I., 2015. The NLRP3 inflammasome is activated by nanoparticles through ATP, ADP and adenosine. Cell Death Dis. 6, e1629. doi:10.1038/cddis.2014.576.

Bauer, C., Duewell, P., Lehr, H.-A., Endres, S., Schnurr, M., 2012. Protective and aggravating effects of Nlrp3 inflammasome activation in IBD models: influence of genetic and environmental factors. Dig. Dis. 30(suppl 1), 82–90. doi:10.1159/000341681.

Hongprasith, N., Kittimethawong, C., Lertluksanaporn, R., Eamchotchawalit, T., Kittipongvises, S., Lohwacharin, J., 2020. IR microspectroscopic identification of microplastics in municipal wastewater treatment plants. Environ. Sci. Pollut. Res. (Environmental Science and Pollution Research) 27 (15), 18557–18564. doi:10.1007/s11356-020-08265-7.

Hou, J., Lei, Z., Cui, L., Hou, Y., Yang, L., An, R., Wang, Q., Li, S., Zhang, H., Zhang, L., 2021. Polystyrene microplastics lead to pyroptosis and apoptosis of ovarian granulosa cells via NLRP3/Caspase-1 signaling pathway in rats. Ecotoxicol. Environ. Saf. 212, 112012. doi:10.1016/j.ecoenv.2021.112012.

Kämpfer, A.A.M., Busch, M., Büttner, V., Bredeck, G., Stahlmecke, B., Hellack, B., Masson, I., Sofranko, A., Albrecht, C., Schins, R.P.F., 2021. Model Complexity as Determining Factor for In Vitro Nanosafety Studies: Effects of Silver and Titanium Dioxide Nanomaterials in Intestinal Models. Small, 2004223. doi:10.1002/smll.202004223.

Kämpfer, A.A.M., Urbán, P., Gioria, S., Kanase, N., Stone, V., Kinsner-Ovaskainen, A., 2017. Development of an in vitro co-culture model to mimic the human intestine in healthy and diseased state. Toxicol. In Vitro 45, 31–43. doi:10.1016/j.tiv.2017.08.011.

Khalid, N., Aqeel, M., Noman, A., Khan, S.M., Akhter, N., 2021. Interactions and effects of microplastics with heavy metals in aquatic and terrestrial environments. Environ. Pollut. 290, 118104. doi:10.1016/j.envpol.2021.118104.

Lei, L., Wu, S., Lu, S., Liu, M., Song, Y., Fu, Z., Shi, H., Raley-Susman, K.M., He, D., 2018. Microplastic particles cause intestinal damage and other adverse effects in zebrafish Danio rerio and nematode Caenorhabditis elegans. Sci. Total Environ. 619-620, 1–8. doi:10.1016/j.scitotenv.2017.11.103.

Li, B., Ding, Y., Cheng, X., Sheng, D., Xu, Z., Rong, Q., Wu, Y., Zhao, H., Ji, X., Zhang, Y., 2019. Polyethylene microplastics affect the distribution of gut microbiota and inflammation development in mice. Chemosphere 244, 125492. doi:10.1016/j.chemosphere.2019.125492.

Liang, B., Zhong, Y., Huang, Y., Lin, X., Liu, J., Lin, L., Hu, M., Jiang, J., Dai, M., Wang, B., Zhang, B., Meng, H., Lelaka, J.J.J., Sui, H., Yang, X., Huang, Z., 2021. Underestimated health risks: polystyrene micro- and nanoplastics jointly induce intestinal barrier dysfunction by ROS-mediated epithelial cell apoptosis. Part. Fibre Toxicol. 18 (1), 20. doi:10.1186/s12989-021-00414-1.

Liu, P., Qian, L., Wang, H., Zhan, X., Lu, K., Gu, C., Gao, S., 2019. New Insights into the Aging Behavior of Microplastics Accelerated by Advanced Oxidation Processes. Environ. Sci. Technol. 53 (7), 3579–3588. doi:10.1021/acs.est.9b00493.

Lunov, O., Syrovets, T., Loos, C., Nienhaus, G. U., Mailänder, V., Landfester, K. *et al.* (2011). Amino-functionalized polystyrene nanoparticles activate the NLRP3 inflammasome in human macrophages. ACS Nano 5, 9648–9657. doi:10.1021/nn203596e.

Mu, Y., Sun, J., Li, Z., Zhang, W., Liu, Z., Li, C., Peng, C., Cui, G., Shao, H., Du, Z., 2021. Activation of pyroptosis and ferroptosis is involved in the hepatotoxicity induced by polystyrene microplastics in mice. Chemosphere 291(Pt 2), 132944. doi:10.1016/j.chemosphere.2021.132944.

Sandys, O., te Velde, A., 2022. Raising the Alarm: Environmental Factors in the Onset and Maintenance of Chronic (Low-Grade) Inflammation in the Gastrointestinal Tract. Dig Dis Sci, 1–14. doi:10.1007/s10620-021-07327-1.

Tan, X., Yu, X., Cai, L., Wang, J., Peng, J., 2019. Microplastics and associated PAHs in surface water from the Feilaixia Reservoir in the Beijiang River, China. Chemosphere 221, 834–840. doi:10.1016/j.chemosphere.2019.01.022.

Wang, W., Zhang, J., Qiu, Z., Cui, Z., Li, N., Li, X., Wang, Y., Zhang, H., Zhao, C., 2022. Effects of polyethylene microplastics on cell membranes: A combined study of experiments and molecular dynamics simulations. J. Hazard. Mater. 429, 128323. doi:10.1016/j.jhazmat.2022.128323.

Wei, J., Wang, X., Liu, Q., Zhou, N., Zhu, S., Li, Z., Li, X., Yao, J., Zhang, L., 2021. The impact of polystyrene microplastics on cardiomyocytes pyroptosis through NLRP3/Caspase-1 signaling pathway and oxidative stress in Wistar rats. Environ. Toxicol., 1–10. doi:10.1002/tox.23095.

Yan, Z., Liu, Y., Zhang, T., Zhang, F., Ren, H., Zhang, Y., 2021. Analysis of Microplastics in Human Feces Reveals a Correlation between Fecal Microplastics and Inflammatory Bowel Disease Status. Environ. Sci. Technol. doi:10.1021/acs.est.1c03924.

Yee, M.S.-L., Hii, L.-W., Looi, C.K., Lim, W.-M., Wong, S.-F., Kok, Y.-Y., Tan, B.-K., Wong, C.-Y., Leong, C.-O., 2021. Impact of Microplastics and Nanoplastics on Human Health. Nanomaterials 11 (2). doi:10.3390/nano11020496.

Zhen, Y., Zhang, H., 2019. NLRP3 Inflammasome and Inflammatory Bowel Disease. Front. Immunol. 10, 276. doi:10.3389/fimmu.2019.00276.

Zheng, H., Wang, J., Wei, X., Le Chang, Liu, S., 2021. Proinflammatory properties and lipid disturbance of polystyrene microplastics in the livers of mice with acute colitis. Sci. Total Environ. 750, 143085. doi:10.1016/j.scitotenv.2020.143085.

Publications

First author papers

Busch, M., Bredeck, G., Kämpfer, A.A.M., Schins, R.P.F., 2021. Investigations of acute effects of polystyrene and polyvinyl chloride micro- and nanoplastics in an advanced *in vitro* triple culture model of the healthy and inflamed intestine. *Environ. Res.* 193, 110536. doi:10.1016/j.envres.2020.110536.

Busch, M., Kämpfer, A.A.M., Schins, R.P.F., 2021. An inverted *in vitro* triple culture model of the healthy and inflamed intestine: Adverse effects of polyethylene particles. *Chemosphere* 284, 131345. doi:10.1016/j.chemosphere.2021.131345.

Busch, M., Bredeck, G., Waag, F., Rahimi, K., Ramachandran, H., Bessel, T., Barcikowski, S., Herrmann, A., Rossi, A., Schins, R.P.F., 2022. NLRP3-proficient and -deficient THP-1 cells as an *in vitro* screening tool for inflammasome activation by micro- and nanoplastics. *Submitted to Toxicology in Vitro.*

Busch, M., Ramachandran, H., Wahle, T., Rossi, A., Schins, R.P.F., 2022. Investigating the role of the NLRP3 inflammasome pathway in acute intestinal inflammation: use of THP-1 knockout cell lines in an advanced triple culture model. *Submitted to Frontiers in Immunology.*

Co-author papers

Kämpfer, A.A.M., **Busch, M.**, Schins, R.P.F., 2020. Advanced *In Vitro* Testing Strategies and Models of the Intestine for Nanosafety Research. *Chem. Res. Toxicol.* 33 (5), 1163–1178. doi:10.1021/acs.chemrestox.0c00079.

Kämpfer, A.A.M., **Busch, M.**, Büttner, V., Bredeck, G., Stahlmecke, B., Hellack, B., Masson, I., Sofranko, A., Albrecht, C., Schins, R.P.F., 2021. Model Complexity as Determining Factor for *In Vitro* Nanosafety Studies: Effects of Silver and Titanium Dioxide Nanomaterials in Intestinal Models. *Small*, 2004223. doi:10.1002/smll.202004223.

Kämpfer, A.A.M., Shah, U.K., Chu, S.L., **Busch, M.**, Büttner, V., Rothen-Rutishauser, B., Schins, R.P.F., Jenkins, G.J., 2022. Interlaboratory comparison of an intestinal triple culture to confirm transferability and reproducibility. *Submitted to In Vitro Models.*

Presentations

Poster presentations

Busch, M., Kämpfer, A., Albrecht, C., Schins, R.P.F. Investigating the toxicological potential of micro- and nanoplastics in a 3D intestinal model. 12th International Particle Toxicology Conference, 11-13 September 2019, Salzburg, Austria.

Busch, M., Kämpfer, A., Albrecht, C., Schins, R.P.F. Investigating the toxicological potential of micro- and nanoplastics in a 3D model of the inflamed intestine. 5th Pharm-Tox Summit, 2-5 March 2020, Leipzig, Germany.

Busch, M., Bredeck, G., Kämpfer, A., Schins, R.P.F. Investigations of acute effects of polystyrene and polyvinyl chloride micro- and nanoplastics in an advanced *in vitro* triple culture model of the healthy and inflamed intestine. 6th Pharm-Tox Summit, 1-3 March 2021, online.

Busch, M., Bredeck, G., Kämpfer, A., Schins, R.P.F. Investigations of acute effects of polystyrene and polyvinyl chloride micro- and nanoplastics in an advanced *in vitro* triple culture model of the healthy and inflamed intestine. NanoTox, 20-22 April 2021, online.

Busch, M., Kämpfer, A., Schins, R.P.F. An inverted *in vitro* triple culture model of the healthy and inflamed intestine: adverse effects of polyethylene particles. 11th World Congress on Alternatives and Animal Use in the Life Sciences, 23 August - 2 September 2021, online.

Busch, M., Bredeck, G., Waag, F., Rahimi, K., Ramachandran, H., Bessel, T., Barcikowski, S., Hermann, A., Rossi, A., Schins, R.P.F. NLRP3-proficient and -deficient THP-1 cells as an *in vitro* screening tool for inflammasome activation by micro- and nanoplastics. 7th Pharm-Tox Summit, 7-10 March 2022, online.

8. Eidesstattliche Erklärung

Ich versichere an Eides Statt, dass die Dissertation von mir selbständig und ohne unzulässige fremde Hilfe unter Beachtung der „Grundsätze zur Sicherung guter wissenschaftlicher Praxis an der Heinrich-Heine-Universität Düsseldorf“ erstellt worden ist. Die vorliegende Arbeit wurde von mir selbständig verfasst und keine anderen als die angegebenen Hilfsmittel verwendet. Alle wörtlich oder inhaltlich übernommenen Stellen habe ich als solche gekennzeichnet. Zudem versichere ich, dass ich die vorliegende Dissertation nur in diesem und keinem anderen Promotionsverfahren eingereicht habe und diesem kein früheres Promotionsverfahren vorausgegangen ist.

Düsseldorf, März 2022

_____

Mathias Busch